QIMI JIANG

SINGULARITY-FREE WORKSPACE ANALYSIS AND GEOMETRIC OPTIMIZATION OF PARALLEL MECHANISMS

Thèse présentée
à la Faculté des études supérieures de l'Université Laval
dans le cadre du programme de doctorat en génie mécanique
pour l'obtention du grade de Philosophiæ Doctor (Ph.D.)

FACULTÉ DES SCIENCES ET DE GÉNIE
UNIVERSITÉ LAVAL
QUÉBEC

2008

Abstract

Parallel mechanisms are widely used as robotic manipulators, motion simulators, parallel machines, etc. However, the closed-loop nature of their architectures limits the motion of the platform and creates complex kinematic singularities inside the workspace. Hence, to maximize the singularity-free workspace of parallel mechanisms is highly desirable in a design context.

This thesis focuses on two kinds of parallel mechanisms. As a typical planar parallel mechanism, the planar 3-$R\underline{P}R$ parallel mechanism is addressed. As a typical spatial parallel mechanism, the Gough-Stewart platform is analyzed.

For each kind of parallel mechanism, a simple form of singularity equation is derived. The principle of the presented derivation is to separate the origin O' of the mobile frame from the considered point P and make O' coincide with a special point of the platform. As a result, the obtained singularity equation about a general point P of the platform contains only a minimal set of geometric parameters. Besides, it is proved that the centres of the workspace circles/spheres lie exactly on the singularity locus. This basic fact and the simplified singularity equation found the solid basis for singularity-free workspace analysis as well as geometric optimization.

For planar 3-$R\underline{P}R$ parallel mechanisms, the singularity-free workspace as well as the corresponding leg length ranges in a prescribed orientation are determined. The optimal architecture that holds the maximal singularity-free workspace is studied.

For Gough-Stewart platforms, this thesis focuses on the minimal simplified symmetric manipulator (MSSM). Since a Gough-Stewart platform has 6 degrees of freedom, its

workspace falls into two classes: position workspace (or simply workspace) and orientation workspace. Based on the simplified singularity equation, a general procedure is firstly developed to determine the maximal singularity-free workspace around a point of interest in a given orientation as well as the corresponding leg length ranges. In order to maximize the orientation-based maximal singularity-free workspace, an algorithm is presented to optimize the three orientation angles. Considering that a platform usually works in a range of orientations, two algorithms are proposed to compute the maximal singularity-free total orientation workspace. Using the Roll–Pitch–Yaw Euler angles (ϕ, θ, ψ), the orientation workspace at a prescribed position can be defined by 12 workspace surfaces. Based on this fact, a numerical algorithm is presented to evaluate and represent the orientation workspace at a prescribed position for given leg length ranges. Then, a procedure is proposed to determine the maximal singularity-free orientation workspace as well as the corresponding leg length ranges. In practice, a platform may work in a position region. Hence, the effect of the working position on the maximal singularity-free orientation workspace is analyzed and two algorithms are proposed to compute the maximal singularity-free orientation workspace over an interesting position region. Finally, an algorithm for optimizing the geometric parameters is developed to determine the optimal architecture for the MSSM Gough-Stewart platform leading to the maximal singularity-free workspace around a point of interest in the reference orientation.

The obtained results can be used for geometric design, parameter (leg length) set up or singularity-free trajectory planning of the considered parallel mechanisms. Besides, the proposed algorithms can also be applied to other types of parallel mechanisms.

Résumé

Les mécanismes parallèles sont fréquemment utilisés comme robots manipulateurs, comme simulateurs de mouvement, comme machines parallèles, etc. Cependant, à cause des chaînes cinématiques fermées qui caractérisent leur architecture, le mouvement de leur plateforme est limité et des singularités cinématiques complexes peuvent apparaître à l'intérieur de leur espace de travail. Par conséquent, une maximisation l'espace de travail libre de singularité pour ce type de mécanismes est souhaitable dans un contexte de conception.

Dans cette thèse, deux types de mécanismes parallèles sont étudiés: les mécanismes parallèles plans —avec, en particulier le 3-$R\underline{P}R$— et les mécanismes spatiaux —avec, en particulier, la plateforme de Gough-Stewart.

Pour chaque type de mécanisme parallèle, une forme simple d'équation de singularité est obtenue. Le principe consiste à séparer l'origine O' du repère mobile du point considéré P et de faire coïncider O' avec un point particulier de la plateforme. L'équation ainsi obtenue est l'équation de singularité du point P de la plateforme qui contient un ensemble minimal de paramètres géométriques. Par ailleurs, il est prouvé que les centres des cercles et sphères définissant l'espace de travail se trouvent exactement sur les lieux de singularité. Cette observation et l'équation de singularité simplifiée constituent les points de départ de l'analyse de l'espace de travail libre de singularité ainsi que de l'optimisation géométrique.

Pour le mécanisme parallèle plan 3-$R\underline{P}R$, l'espace de travail libre de singularité et les limites correspondantes pour la longueur des pattes dans une orientation prescrite

sont déterminés. Ensuite l'architecture optimale qui permet d'obtenir un espace de travail maximal tout en étant libre de singularité est discutée.

En ce qui concerne la plateforme de Gough-Stewart, cette thèse se concentre sur le manipulateur symétrique simplifié minimal (MSSM). Comme une plateforme de Gough-Stewart a 6 degrés de liberté, son espace de travail se divise en deux: l'espace de travail en position (ou simplement espace de travail) et l'espace de travail en orientation. À partir de l'équation de singularité simplifiée, une procédure générale est développée afin de déterminer l'espace de travail libre de singularité maximal autour d'un point particulier dans une orientation donnée, et afin de déterminer les limites correspondantes des longueurs de patte. Dans le but de maximiser l'espace de travail libre de singularité en orientation, un algorithme est présenté qui optimise les trois angles d'orientation. Sachant qu'une plateforme fonctionne habituellement pour une certaine gamme d'orientations, deux algorithmes qui calculent l'espace de travail en orientation libre de singularité maximal sont présentés. En utilisant les angles d'Euler en *roulis*, *tangage* et *lacet* (ϕ, θ, ψ), l'espace de travail en orientation pour une position prescrite peut être défini par 12 surfaces. Basé sur ce fait, un algorithme numérique est présenté qui évalue et représente l'espace de travail en orientation pour une position prescrite dans les limites données de longueur de patte. Ensuite, une procédure est proposée afin de déterminer l'espace de travail en orientation libre singularité maximal ainsi que les limites correspondantes des longueurs de patte. En pratique, une plateforme peut fonctionner dans un ensemble de positions. Ainsi, l'effet de la position de travail sur l'espace de travail en orientation libre de singularité maximal est analysé et deux algorithmes sont proposés pour calculer ce dernier pour tout un ensemble de positions particulières. Finalement, un algorithme qui optimise les paramètres géométriques est développé dans le but de déterminer l'architecture optimale qui permet à la plateforme de MSSM Gough-Stewart d'obtenir l'espace de travail libre singularité maximal autour d'une position particulière pour l'orientation de référence.

Les résultats obtenus peuvent être utilisés pour la conception géométrique, la configuration des paramètres (longueur des pattes) ou la planification de trajectoires libres de singularité des mécanismes parallèles considérés. En outre, les algorithmes proposés peuvent également être appliqués à d'autres types de mécanismes parallèles.

Foreword

This thesis describes my research work in the Robotics Laboratory of Laval University, Quebec, Canada in the past three years.

I would like to express my sincere gratitude to Laval University, the Department of Mechanical Engineering, especially my supervisor Professor Clément Gosselin for providing me a good study opportunity for this PhD program. Many thanks for Professor Gosselin's excellent supervision, full support, continuous encouragement, especially for his careful and patient review of all my paper manuscripts and this thesis manuscript.

Also, I would like to thank the reviewers of this thesis, Professor Marc J. Richard, Professor Ilian A. Bonev and Professor Marc Arsenault, for their precious time and good suggestions. From their comments, I have learned a lot of things, especially some good ideas.

Also, I would like to thank all my colleagues in the robotics laboratory for their support, kindness and friendship. Special thanks for Boris Mayer St-Onge's technical support in computer system.

Finally, I would like to thank my wife, my son and my daughter for their understanding, support and love.

Contents

List of Tables

List of Figures

List of Symbols

$\mathbf{A}$	Jacobian matrix
A_b	Average area of singularity-free workspace for a prescribed orientation range of ϕ (3-$R\underline{P}R$)
A_i	Area of singularity-free workspace at ϕ_i (3-$R\underline{P}R$), or area of workspace section i (*MSSM*)
B_i	Attachment point of leg i and the base $(i = 1, 2, 3)$ (3-$R\underline{P}R$), or $(i = 1, 2, ..., 6)$ (*Gough-Stewart platform*)
$\mathbf{b}_i$	Position vector of B_i in the reference frame
C_i	Centre of workspace circle i (3-$R\underline{P}R$), or workspace sphere i (*MSSM*)
$(x_{ci}, y_{ci}.z_{ci})$	Coordinates of C_i in the Cartesian space $Oxyz$
C_b	Centroid of the base
C_p	Centroid of the platform
$\mathbf{D}$	Jacobian matrix
D	Orientation workspace variable
d	Distance between two points
F	Singularity function

f_i	Coefficients of singularity equation, $(i = 1, 2, ..., 20)$ (*Gough-Stewart platform*)
G_i	Coefficients of singularity equation, $(i = 1, 2, ..., 6)$ (3-$R\underline{P}R$)
h	half height of workspace
k	Size ratio between the platform and the base
N	Number of chosen orientations or positions
O	Origin of the reference frame
O'	Origin of the mobile frame
P	Considered point of the platform
$\mathbf{p}$	Position vector of P in the reference frame
$\mathbf{p}'$	Position vector of P in the mobile frame
P_0	Point of interest in the workspace
P_i	Attachment point of leg i and the platform $(i = 1, 2, 3)$ (3-$R\underline{P}R$), or $(i = 1, 2, ..., 6)$ (*MSSM*)
$\mathbf{p}_i$	Position vector of P_i in the reference frame
$\mathbf{p}'_i$	Position vector of P_i in the mobile frame
$\mathbf{Q}$	Rotation matrix
q_{ij}	Entry of the rotation matrix Q
R	Radius of singularity circle (3-$R\underline{P}R$)
R_i	Radius of workspace circle i (3-$R\underline{P}R$), or workspace sphere i (*MSSM*)
S	Area of triangle $\Delta C_1C_2C_3$ (3-$R\underline{P}R$)
S_b	Area of base triangle $\Delta B_1B_2B_3$ (3-$R\underline{P}R$)
t	Computation time
t_i	Geometric parameter i
V	Volume of position workspace or orientation workspace

$\mathbf{v}$	Velocity vector of platform
ϕ	Orientation angle
θ	Orientation angle
ψ	Orientation angle
$\dot{\boldsymbol{\rho}}$	Actuator velocity vector
ρ_i	Length of leg i $(i = 1, 2, 3)$ (3-$R\underline{P}R$), or $(i = 1, 2, ..., 6)$ (*MSSM*)
$\dot{\rho}_i$	Velocity of actuator i $(i = 1, 2, 3)$ (3-$R\underline{P}R$), or $(i = 1, 2, ..., 6)$ (*MSSM*)
ρ_i^{max}	Maximal Length of leg i $(i = 1, 2, 3)$ (3-$R\underline{P}R$), or $(i = 1, 2, ..., 6)$ (*MSSM*)
ρ_i^{min}	Minimal Length of leg i $(i = 1, 2, 3)$ (3-$R\underline{P}R$), or $(i = 1, 2, ..., 6)$ (*MSSM*)
$\rho_{i,lim}^{max}$	Geometric limited value of the maximal leg length ρ_i^{max} $(i = 1, 2, ..., 6)$ (*MSSM*)
$\rho_{i,lim}^{min}$	Geometric limited value of the minimal leg length ρ_i^{min} $(i = 1, 2, ..., 6)$ (*MSSM*)

Chapter 1

Introduction

This chapter introduces the research background, the research focuses as well as the organization of this thesis.

1.1 Research Background

1.1.1 Robot and Mechanism

So far, there is no common definition for robot. For different people, the word "robot" means different things. Generally speaking, a robot is a mechanical or virtual, artificial

agent. It is usually an electromechanical system, which, by its appearance or movements, conveys a sense that it has intent or agency of its own. The word "robot" can refer to both a physical robot and a virtual software agent, but the latter is usually referred to as a "bot" to differentiate. To be complete, a robot should be the combination of the physical hardware and the virtual software.

According to the physical appearance, a robot can be a mechanical manipulator, a numerically controlled machine, a walking machine or a humanoid of science fiction. In industry, most robots are mechanical manipulators instead of humanoids in appearance. Considering that a mechanical manipulator is a mechanism, the three terms "robot", "manipulator" and "mechanism" often refer to the same thing in the robotics community. So is the case in this thesis.

1.1.2 Parallel Mechanism

According to the kinematic structure, a mechanism can be serial, parallel or hybrid [1]. The kinematic structure of a serial mechanism takes the form of an open-loop chain while a parallel mechanism is made up of a closed-loop chain. In other words, a parallel mechanism is a multi-DOF (degree of freedom) mechanism composed of one moving platform and one base connected by at least two serial kinematic chains in-parallel. These serial kinematic chains are referred to as legs or limbs. If a mechanism consists of both open- and closed-loop chains, it becomes a hybrid mechanism.

Parallel mechanisms possess significant advantages over serial mechanisms in terms of dynamic properties, load-carrying capacity, high accuracy as well as stiffness. This is because parallel mechanisms are characterized by several kinematic chains connecting the base to the end-effector, which allows the actuators to be located on or near the base of the mechanism. Therefore, parallel mechanisms can be used in many applications where these properties are of primary importance while a limited workspace is acceptable.

Gough built the first hexapod to test tires as shown in Fig. 1.1(a) [2]. This parallel mechanism is commonly referred to as "Gough-Stewart platform" and now generally accepted in the robotics and mechanisms community. But the most common application

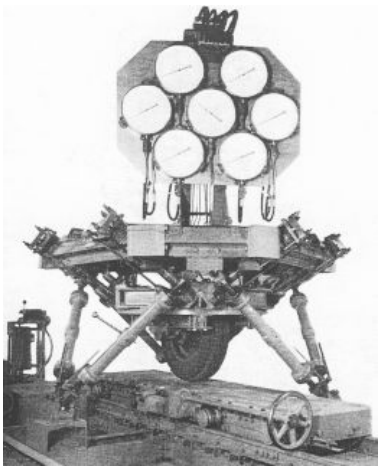

(a) Gough's tire testing machine.

(b) Flight simulator (CAE Electronics Ltd, Canada).

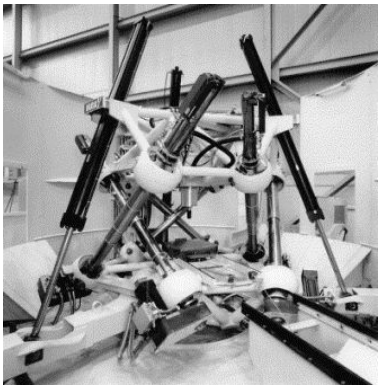

(c) Parallel kinematic machine (Giddings & Lewis).

(d) Delta parallel robot (Humboldt University, Germany).

(e) Agile eye (Robotics Laboratory, Laval University).

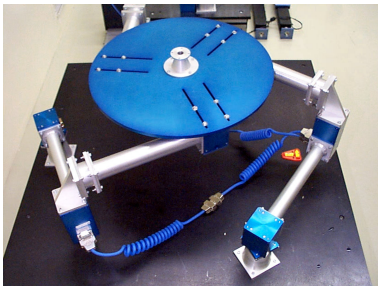

(f) Planar parallel mechanism (Nanyang Technological University).

Figure 1.1: Parallel mechanisms

of parallel mechanisms is undoubtedly in flight simulation (see Fig. 1.1(b)), as originally proposed by Stewart [3]. Although flight simulators have been used for several years, it was only in the 1970s that Hunt introduced the concept of parallel manipulator and suggested, in his book, using this type of mechanism in robotics [4]. Since then, parallel manipulators have been given considerable attention. The number of applications in which parallel mechanisms are used has been steadily increasing and several prototype mechanisms have been built. For instance, parallel mechanisms can also be used as

machine tools (Fig. 1.1(c)) or even for medical purposes (Fig. 1.1(d)). So far, many types of parallel mechanisms have been proposed. Fig. 1.1 shows only a few examples. A comprehensive list is given in [5].

Unfortunately, there are some factors limiting the application of parallel mechanisms. One main factor is that the workspace of parallel mechanisms is quite limited, because the closed-loop nature of parallel mechanisms limits the motion of the platform. The other one is that singular configurations may exist inside the workspace [4], [6–12]. When a parallel mechanism is in a singular configuration, the number of degrees of freedom of the mechanism changes instantaneously. If the mechanism gains one or more degrees of freedom, it becomes uncontrollable. Furthermore, in such a singular configuration, the actuator forces can become very large, which may result in a breakdown of the mechanism.

As the limited workspace is coupled with singularities and the occurrence of singular configurations may be difficult to predict, the kinematic design and the trajectory planning of parallel mechanisms become very difficult problems. Therefore, it is of primary importance to pursue the maximal singularity-free workspace for parallel mechanisms [13], [14].

1.1.3 Workspace

The workspace is the region that can be reached by the end-effector. In this thesis, the end-effector is the considered point P of the platform. For most parallel mechanisms especially for the spatial parallel mechanisms, the platform can translate and rotate. Hence, workspace usually falls into two classes: position workspace and orientation workspace. The position workspace can be classified into several types such as constant orientation workspace (the position workspace in a given orientation) and total orientation workspace (the common region of the position workspaces in all orientations of a given set). Accordingly, the orientation workspace can also be classified into orientation workspace at a given position, orientation workspace over a position region (the common region of the orientation workspaces at all positions in a given set), etc. [15], [16].

Comparatively, the definition of position workspace is simple. Its representation in the position Cartesian space is straightforward and easy to understand. Take the Gough-Stewart platform as a example, the position workspace can be defined by 12 workspace spheres, which are simple surfaces. So far, most research works focus on the analysis of position workspace (constant orientation workspace) [16–28].

However, the definition of orientation workspace is more complex. Its representation has been a challenging task. Especially, the orientation workspace can be defined by numerous parameterization approaches such as the direction cosine matrix (DCM), Euler axis and angle (rotation vector), Euler angles, tilt and torsion angles [29], quaternions [30], Rodrigues parameters as well as Cayley-Klein parameters. Even for Euler angles, there are 12 possible conventions. The most popular convention is the zxz convention. So far, very few works exist on the topic of orientation workspace computation. Some of the relevant works in this area may be found in [15], [16], [27], [28], [35–38].

1.1.4 Singularity

1.1.4.1 Singularity Classification

Kinematic singularity analysis is a very important issue in the design and control of parallel mechanisms. When kinematic singularities occur, the moving platform may lose or gain some DOFs of motion when the inputs are specified. From different perspectives, kinematic singularities can be classified into different types [7–12]. However, from the mathematical point of view and the motion relationship, kinematic singularities can be classified into three basic types, each of which has a different physical interpretation [7]. The first type of singularity, referred to as inverse kinematic singularities, usually occurs at the boundaries of the workspace of a mechanism. When inverse kinematic singularities occur, the moving platform loses one or more DOFs of motion. These singularities lead to simple expressions and can be easily avoided. The second type of singularity, referred to as direct kinematic singularities, occurs when the platform gains instantaneous freedom. This type of singularity is difficult to predict. They can appear inside the workspace of parallel mechanisms. They are difficult to analyze and become a serious concern for robot designers. The third type of singularity is called

architecture singularities and was studied in [8]. This type of singularity can be avoided by choosing proper structural parameters.

The second type of singularity is also called RO (Redundant Output) in [10]. It corresponds to configurations in which the stiffness of the mechanism is locally lost. This type of singularity is the main concern for robot designers.

1.1.4.2 Research on Singularity

Kinematic singularity analysis has received much attention from many researchers over the past two decades [4], [7–12], [39–90]. For serial mechanisms, methods based on damped least squares and singular value decomposition for singularity avoidance can be applied [39], [40], [45]. However, these methods are not directly applicable to parallel mechanisms due to the different nature of the singularities. Hence, researchers have to develop different approaches to address the singularity problem of parallel mechanisms.

Based on the determinant of the manipulator's Jacobian matrices, the singularity problem of parallel mechanisms was touched in [7]. This work has been further refined in [10], where detailed physical interpretations are provided. After that, analytical expressions for the singularity loci of planar and spherical parallel manipulators have been obtained [47], [50], [64], [81].

For the 6-DOF Gough-Stewart platforms, previous studies just focused on a few special cases of singularities. A singularity that occurs when all the lines associated with the prismatic actuators intersect a common line was first pointed out in [4]. Then, it was shown in [41] that a singular configuration occurs when the platform rotates around an axis orthogonal to the base plane by an angle of 90°. A more general approach was then proposed in [43], [44] using Grassmann geometry. Although these analyses can be a major contribution to the subject, results are unfortunately not available for the most general case of Gough-Stewart platforms. Moreover, although it is generally easy to determine the geometric conditions that lead to a singular configuration using Grassmann geometry, it is sometimes difficult to express them mathematically. This is a serious drawback in a context of analysis and design, where it is very useful to obtain analytical expressions for the singularity loci to generate graphical representations in the manipulator's workspace. Other geometric approaches have also been used by some researchers on simplified Gough-Stewart platforms [66], [67].

In order to obtain an analytical expression of the singularity locus of the general Gough-Stewart platform, for the first time, a linear decomposition algorithm was applied in [69] to derive the singularity equation about an arbitrary point of the platform. Actually, this is also a complete singularity equation because the 20 coefficients are functions of the three orientation angles. The obtained analytical expression is useful for better understanding the geometry of the singularity locus, particularly the projection of the five-dimensional manifold (general singularity locus) onto $\mathcal{R}^3$ for a prescribed platform orientation. This expression can also be used to obtain an interactive graphical representation of the singularity locus in the Cartesian space. Later, based on the cascaded expansion of the determinant of the Jacobian matrix, a procedure was developed in [87] to obtain the explicit expressions of the 20 coefficients as functions of the orientation angles.

Unfortunately, the singularity equations obtained in [69] and [87] are very complex because they contain too many geometric parameters. Besides, this derivation lacks flexibility. For different considered points, different mobile frames are used. Hence, the coordinates of the attachment points P_i $(i = 1, 2, ..., 6)$ in the new mobile frame need to be re-determined.

Singularity equations were also derived in [78] and [79] respectively for the 6-3 Gough-Stewart platform and the general Gough-Stewart platform. To obtain the singularity expression, these two works just made the origin O' of the mobile frame coincide with one attachment point (P_1) of the platform. Because of this specific choice, the vector connecting point O' and point P_1 vanishes and the total number of terms of the determinant of the Jacobian matrix reduces from 20 to 10. Otherwise, the number of terms cannot be reduced [69].

Obviously, the singularity equations obtained in [78] and [79] are about the special point P_1. Although a singular position of P_1 represents a singular pose of the platform, this special point is not a point of practical interest. Besides, for all symmetrical Gough-Stewart platforms, this approach cannot make the obtained singularity equations contain only a minimal set of geometric parameters.

Considering that singularity equations are difficult to obtain for mechanisms with more than three degrees of freedom because of the complexity of the determinant of the Jacobian matrices, some numerical algorithms have been developed [49], [51], [65],

[82], [83], [91]. For instance, a fast algorithm was presented in [49] to solve the problem of trajectory validation for a 6-DOF parallel mechanism with respect to its workspace. Numerical methods were used in [51] to study the singularity loci of spatial 5-DOF parallel manipulators. An exact method and an approximate method were proposed in [65] to determine a path which can avoid singularities and remain close to a prescribed path. A numerical technique was presented in [82] for path planning inside the workspace of parallel mechanisms avoiding singularities. The path is modified to avoid the singular configurations by a local routing method based on Grassmann's line geometry. A variational approach was used in [83] for the planning of singularity-free paths for parallel mechanisms. This approach is based on a Lagrangian incorporating both a kinetic energy term and a potential energy term to ensure that the path is short and that the obtained path is singularity-free. The basic principle of the above trajectory planning algorithms is to connect an initial configuration to a final configuration through a singularity-free path, which is a prescribed path for a given task.

1.1.5 Singularity-Free Workspace

The singularity-free workspace is interesting for trajectory planning. However, the singularity-free workspace is very complex and not easy to determine. So far, very few works can be found on this topic. A method was presented in [77] to determine whether there is a singularity in a given region defined in the workspace. The answer is definite and can be used to identify the singularity-free zones inside the workspace. The singularity-free workspace of planar parallel manipulators with prismatic joints was addressed in [92]. Both the base and the platform of the used manipulator are collinear. The singularity problem of planar 3-$R\underline{P}R$ parallel mechanisms was studied in [94]. A maximal singularity-free zone which is a circle for a prescribed point was obtained. The singularity problem of the general Gough-Stewart platform was addressed in [95]. A procedure was presented to determine a maximal singularity-free zone which is a sphere around a point of interest P_0 for a prescribed orientation. This method was also extended to the six-dimensional workspace.

However, in practice, a singularity-free workspace cannot be a circle or sphere. In other works, the real singularity-free workspace as well as the corresponding leg length ranges have not been well addressed.

1.2 Research Focus

The closed-loop nature of parallel mechanisms limits the motion of the platform and creates complex kinematic singularities inside the workspace. Hence, to maximize the singularity-free workspace of parallel mechanisms is highly desirable in a design context. This thesis focuses on two kinds of parallel mechanisms. As a typical planar parallel mechanism, the planar 3-$R\underline{P}R$ parallel mechanism is addressed. As a typical spatial parallel mechanism, the Gough-Stewart platform is analyzed.

1.2.1 Singularity Equation

Deriving the singularity equation is the first and key step for singularity analysis. The singularity equation for planar 3-$R\underline{P}R$ parallel mechanism is available in some references such as [50] while the singularity equation for general Gough-Stewart platform can be found in [69], [87]. However, these singularity equations contain too many geometric parameters and are not convenient for singularity analysis, especially for geometric optimization. Hence, the first focus of this thesis is to derive simple singularity equations using a minimal set of geometric parameters.

1.2.2 Singularity-Free Workspace

The second focus is to determine the maximal singularity-free workspace for a given architecture with a base of unit area. This includes

- Determining the maximal singularity-free workspace around a point of interest P_0 as well as the corresponding leg length ranges for a given orientation.
- Determining the optimal orientation in which the platform holds the maximal "orientation-based maximal singularity-free workspace", i.e., orientation optimization.
- Determining the maximal singularity-free total orientation workspace.

- Determining the maximal singularity-free orientation workspace at a prescribed position.
- Determining the maximal singularity-free orientation workspace over a prescribed position region.

1.2.3 Geometric Optimization

The third focus is geometric optimization, i.e., how to optimize the geometric parameters in order to determine the optimal architecture which maximizes the "architecture-based maximal singularity-free workspace".

1.3 Thesis Organization

The main body of this thesis is divided into two parts. The first part addresses the planar 3-$R\underline{P}R$ parallel mechanism. It contains the following two chapters:

- Chapter 2: Determination of the singularity-free workspace.
- Chapter 3: Geometric design optimization based on singularity-free workspace analysis.

The second part addresses the Gough-Stewart platform. It contains the following eight chapters:

- Chapter 4: Derivation of the singularity equations.
- Chapter 5: Computation of the maximal singularity-free workspace for a given orientation.
- Chapter 6: Orientation optimization.
- Chapter 7: Computation of the maximal singularity-free total orientation workspace.

- Chapter 8: Evaluation and representation of the orientation workspace.
- Chapter 9: Computation of the maximal singularity-free orientation workspace at a given position.
- Chapter 10: Computation of the maximal singularity-free orientation workspace over a given position region.
- Chapter 11: Geometric optimization.

In Chapter 4, the singularity equations which contain only a minimal set of geometric parameters are derived for all typical Gough-Stewart platforms. The followed seven chapters (5 – 11) focus on the MSSM Gough-Stewart platform which is used for the demonstration of the presented algorithms. However, it is very easy to apply the algorithms developed in chapters (5 – 10) to other types of Gough-Stewart platforms.

Finally, conclusions are drawn in Chapter 12.

Chapter 2

Singularity-Free Workspace of the Planar 3-$R\underline{P}R$ Parallel Mechanism

A new approach is presented in this chapter to derive the singularity equation for the planar 3-$R\underline{P}R$ parallel mechanism. The obtained singularity equation for any point P of the platform contains only a minimal set of geometric parameters. The three centres of the workspace circles are proved to lie exactly on the singularity locus. For similar triangular base and platform, the singularity locus is a circle [71]. These observations make it easy to determine the singularity-free workspace as well as the corresponding leg length ranges for this type of planar parallel mechanism. Finally, a procedure for the geometric design is developed in order to avoid singularities inside the workspace.

2.1 Introduction

As a typical planar parallel mechanism, the planar 3-$R\underline{P}R$ parallel mechanism has been studied by several researchers [13], [22], [23], [47], [50], [52], [54], [64], [71], [88], [92], [94], [96–98]. In [22], an algorithm based on the Gauss divergence theorem was presented to compute the workspace of this type of parallel mechanism. In [23], the maximal workspace, also called the inclusive workspace in [16], was analyzed. The singularity problem of the planar 3-$R\underline{P}R$ parallel mechanism with a collinear platform was addressed in [47]. The singularity equation for the planar 3-$R\underline{P}R$ parallel mechanism was derived in [50]. Although the obtained singularity equation is simple, it is only about the attachment point P_1 which is not a general point of the platform. In practice, this special point P_1 cannot represent the performance of the end-effector of the mechanism. The singularity equation for a general point P of the platform was derived in [54] and [94] by choosing the considered point P as the origin O' of the mobile frame. However, the obtained singularity equation cannot contain a minimal set of geometric parameters. In [64], the Clifford algebra was used to perform the singularity analysis of the planar 3-$R\underline{P}R$ parallel mechanism. In [71], it was observed that the singularity locus is a circle for a planar 3-$R\underline{P}R$ parallel mechanism with similar triangular base and platform. In [90], the singular curves in the joint space and the cusp points of the planar 3-$R\underline{P}R$ parallel mechanism were studied. A reliable synthesis method capable of optimally selecting the geometric parameters of the planar 3-$R\underline{P}R$ parallel mechanism was presented in [88]. In [92], the synthesis of the planar 3-$R\underline{P}R$ parallel mechanism with a collinear platform was performed. Besides, two situations in which the forward kinematics of the planar 3-$R\underline{P}R$ parallel mechanism degenerates were investigated in [93].

In order to derive the singularity equation for a general point P of the platform using a minimal set of geometric parameters, this chapter presents a new approach by separating the origin O' of the mobile frame from the considered point P and by making O' coincide with a special point of the platform. The simplified singularity equation can be used for singularity-free workspace determination as well as for geometric design.

2.2 Singularity Analysis

As shown in Fig. 2.1, a planar 3-$R\underline{P}R$ parallel mechanism with actuated prismatic joints consists of a fixed triangle base $\triangle B_1B_2B_3$ and a mobile triangle platform $\triangle P_1P_2P_3$. B_i and P_i are connected via the actuated prismatic joint of variable length $\rho_i (i = 1, 2, 3)$. Passive revolute joints are located at B_i and P_i, and the mechanism has 3 DOFs. The moving platform can translate in the xy plane and rotate with respect to an axis perpendicular to the xy plane.

2.2.1 Singularity Equation

To derive the singularity equation, two coordinate systems are defined as shown in Fig. 2.1. A reference frame Oxy is attached to the base by selecting B_1 as the origin O and B_1B_2 as the x axis. The mobile frame $O'x'y'$ is attached to the platform by selecting P_1 as the origin O' and P_1P_2 as the x' axis. The position of B_i in the fixed frame Oxy is denoted by vector $\mathbf{b}_i = [x_{bi}, y_{bi}]^T (i = 1, 2, 3)$ and the position of P_i in the mobile frame $O'x'y'$ is denoted by vector $\mathbf{p}'_i = [x'_{pi}, y'_{pi}]^T (i = 1, 2, 3)$. $\mathbf{b}_i$ and $\mathbf{p}'_i$ are constant vectors in their respective frames.

Let vector $\mathbf{p}_r = [x_r, y_r]^T$ denote the position of the origin O' of the mobile frame in

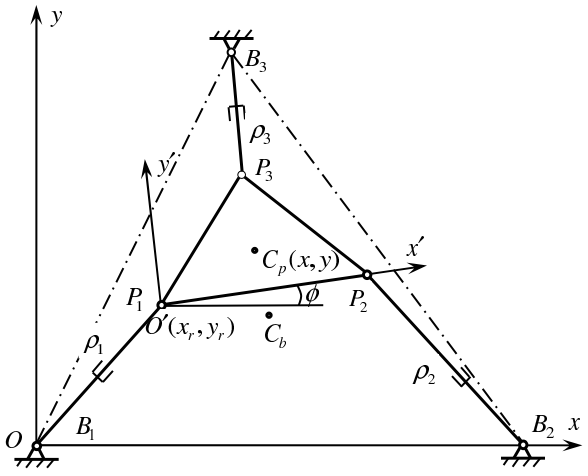

Figure 2.1: Planar 3-$R\underline{P}R$ parallel mechanism.

the fixed frame and $\mathbf{Q}$ be the rotation matrix representing the rotation of the platform from frame Oxy to frame $O'x'y'$ with

$$\mathbf{Q} = \begin{bmatrix} \cos\phi & -\sin\phi \\ \sin\phi & \cos\phi \end{bmatrix}. \tag{2.1}$$

If the position of the considered point P of the platform in the fixed and mobile frames are respectively $\mathbf{p} = [x, y]^T$ and $\mathbf{p}' = [x_p, y_p]^T$, then

$$\mathbf{p} = \mathbf{p}_r + \mathbf{Q}\mathbf{p}' \tag{2.2}$$

or

$$\mathbf{p}_r = \mathbf{p} - \mathbf{Q}\mathbf{p}'. \tag{2.3}$$

Hence, the position of $P_i (i = 1, 2, 3)$ in the fixed frame can be expressed as

$$\mathbf{p}_i = \mathbf{p}_r + \mathbf{Q}\mathbf{p}'_i = \mathbf{p} + \mathbf{Q}(\mathbf{p}'_i - \mathbf{p}'). \tag{2.4}$$

The length of leg i is the distance between B_i and P_i. Hence,

$$\rho_i^2 = (\mathbf{p}_i - \mathbf{b}_i)^T(\mathbf{p}_i - \mathbf{b}_i). \tag{2.5}$$

Differentiating eq.(2.5) with respect to time, one obtains

$$\mathbf{A}\mathbf{v} = \mathbf{D}\dot{\boldsymbol{\rho}} \tag{2.6}$$

where $\dot{\boldsymbol{\rho}} = [\dot{\rho}_1, \dot{\rho}_2, \dot{\rho}_3]^T$ denotes the actuator velocities and $\mathbf{v} = [\dot{x}, \dot{y}, \dot{\phi}]^T$ the Cartesian velocity vector of the platform. $\mathbf{A}$ and $\mathbf{D}$ are two Jacobian matrices.

Referring to Fig. 2.1, suppose, without loss of generality, that the coordinates of B_i in the fixed frame Oxy are actually B_1(0,0), $B_2(t_1,0)$ and $B_3(t_2, t_3)$ and the coordinates of P_i in the mobile frame $O'x'y'$ are P'_1(0,0), $P'_2(t_4, 0)$ and $P'_3(t_5, t_6)$. The condition for the direct kinematic singularity is $\det(\mathbf{A}) = 0$. From this and considering the above coordinates of B_i and P_i $(i = 1, 2, 3)$, the singularity equation can be obtained as follows:

$$G_1x^2 + G_2y^2 + G_3xy + G_4x + G_5y + G_6 = 0 \tag{2.7}$$

where

$$\begin{cases} G_1 = g_1 \sin\phi \\ G_2 = g_2 \sin\phi + g_3 \cos\phi \\ G_3 = -g_3 \sin\phi + g_4 \cos\phi \\ G_4 = g_5 \sin^2\phi + g_6 \cos^2\phi \ + g_7 \sin\phi\cos\phi + g_8 \sin\phi \\ G_5 = g_9 \sin^2\phi + g_{10} \cos^2\phi + g_{11} \sin\phi\cos\phi + g_{12} \sin\phi + g_{13} \cos\phi \\ G_6 = g_{14} \sin\phi + g_{15} \cos\phi + g_{16} \sin^2\phi + g_{17} \cos^2\phi + g_{18} \sin\phi\cos\phi \end{cases} \tag{2.8}$$

and

$$\begin{cases} g_1 = -t_3 t_4 \\ g_2 = -t_1 t_6 \\ g_3 = t_1 t_5 - t_2 t_4 \\ g_4 = t_3 t_4 - t_1 t_6 \\ g_5 = (t_2 - t_1) t_4 t_5 + (t_1 t_5 - t_2 t_4) x_p + t_3 t_4 (t_6 - 2y_p) \\ g_6 = (t_1 t_6 - t_3 t_4) y_p \\ g_7 = t_4 (t_2 t_6 - t_1 t_6 - t_3 t_5) + (t_1 t_6 + t_3 t_4) x_p + (t_1 t_5 - t_2 t_4) y_p) \\ g_8 = t_1 t_3 t_4 \\ g_9 = t_1 t_6 (2x_p - t_4) + (t_2 t_4 - t_1 t_5) y_p \\ g_{10} = t_4 (t_3 t_5 - t_2 t_6) + (t_1 t_6 - t_3 t_4) x_p + 2(t_2 t_4 - t_1 t_5) y_p \\ g_{11} = t_4 (t_1 t_5 - t_2 t_5 - t_3 t_6) + (t_2 t_4 - t_1 t_5) x_p + (t_1 t_6 + t_3 t_4) y_p \\ g_{12} = t_1 (t_2 t_5 - t_2 t_4 + t_3 t_6) \\ g_{13} = t_1 (t_2 t_6 - t_3 t_5) \\ g_{14} = t_1 t_6 x_p (t_4 - x_p) + (t_1 t_5 - t_2 t_4) x_p y_p + (t_2 t_5 + t_3 t_6 - t_1 t_5 - t_3 y_p) t_4 y_p \\ g_{15} = (t_3 t_4 - t_1 t_6) x_p y_p + (t_2 t_6 - t_3 t_5) t_4 y_p + (t_1 t_5 - t_2 t_4) y_p^2 \\ g_{16} = t_1 [(t_2 t_4 - t_2 t_5 - t_3 t_6) x_p + t_3 t_4 y_p] \\ g_{17} = (t_3 t_5 - t_2 t_6) t_1 y_p \\ g_{18} = (t_3 t_5 - t_2 t_6 - t_3 t_4) t_1 x_p + (t_2 t_4 - t_2 t_5 - t_3 t_6) t_1 y_p. \end{cases} \tag{2.9}$$

If P_1 is taken as the considered point P, eq.(2.7) takes exactly the form given in [50].

2.2.2 Singularity Locus

In general, the singularity locus for a given orientation can be a hyperbola or a parabola or an ellipse [50]. Ellipses may degenerate into circles. By observation of eqs.(2.7)–(2.9), it is not difficult to find that if $t_4/t_1 = t_5/t_2 = t_6/t_3 = k$ (k is the size ratio

between the platform and the base), then $g_1 \equiv g_2$ and $g_3 \equiv g_4 \equiv 0$. As a result, $G_1 \equiv G_2$ and $G_3 \equiv 0$. In this case, the base and the platform are similar triangles, and the singularity locus expressed by eq.(2.7) is a circle [71]. The centre $C(x_c, y_c)$ and radius R of the singularity circle can be given as follows:

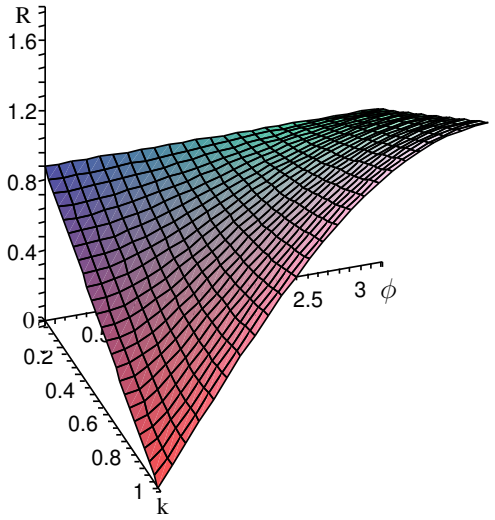

(a) Radius R as a function of k and ϕ

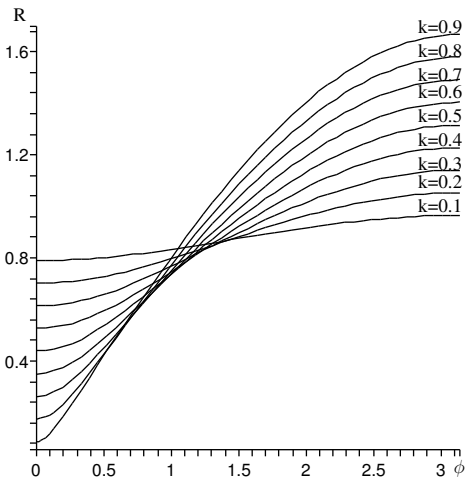

(b) Radius R as a function of ϕ.

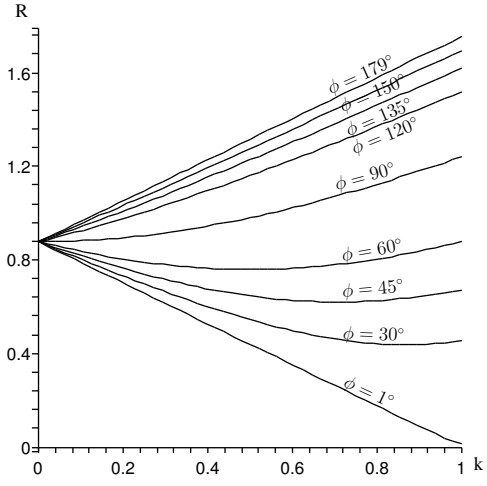

(c) Radius R as a function of k.

Figure 2.2: The evolution of R with respect to k and ϕ ($t_1 = 2/\sqrt[4]{3}$, $t_2 = 1/\sqrt[4]{3}$, $t_3 = \sqrt[4]{3}$).

$$\begin{cases} x_c = \{[k(t_2^2 - t_1t_2 + t_3^2) - 2t_3y_p]\sin\phi + (2x_p - kt_1)t_3\cos\phi + t_1t_3\}/(2t_3) \\ y_c = \{(2x_p - kt_1)t_3\sin\phi + [k(t_1t_2 - t_2^2 - t_3^2) + 2t_3y_p]\cos\phi + t_2^2 - t_1t_2 + t_3^2\}/(2t_3) \\ R = \sqrt{[(t_1 - t_2)^2 + t_3^2](t_2^2 + t_3^2)(k^2 - 2k\cos\phi + 1)}/(2t_3). \end{cases} \tag{2.10}$$

Equation (2.10) shows that for a given orientation $\phi \neq i\pi \ \ (i = 0, 1)$, only the centre of the singularity circle depends on the position of the considered point P. The radius does not. When $\phi = i\pi \ \ (i = 0, 1)$, the whole plane becomes singular. Figs. 2.2(b) and 2.2(c) respectively show the evolution of the radius R of the singularity circle with respect to the orientation angle ϕ and the size ratio k. The geometric parameters are: $t_1 = 2/\sqrt[4]{3}$, $t_2 = 1/\sqrt[4]{3}$, $t_3 = \sqrt[4]{3}$, i.e., the base is an equilateral triangle of unit area.

2.3 Singularity-Free Workspace for a Given Orientation

Referring to [22], the workspace equations of 3-$R\underline{P}R$ parallel mechanisms can be obtained by expanding eq.(2.5) for three legs as follows:

$$\begin{cases} \rho_1^2 = [x - (x_p\cos\phi - y_p\sin\phi)]^2 + [y - (x_p\sin\phi + y_p\cos\phi)]^2 \\ \rho_2^2 = [x - (x_p\cos\phi - y_p\sin\phi - t_4\cos\phi + t_1)]^2 + [y - (x_p\sin\phi + y_p\cos\phi - t_4\sin\phi)]^2 \\ \rho_3^2 = [x - (x_p\cos\phi - y_p\sin\phi - t_5\cos\phi + t_6\sin\phi + t_2)]^2 \\ \qquad +[y - (x_p\sin\phi + y_p\cos\phi - t_5\sin\phi - t_6\cos\phi + t_3)]^2. \end{cases} \tag{2.11}$$

For a given orientation ϕ, these are three circle equations. These circles can be referred to as *workspace circles*, because they can be used to determine the workspace. The three centres $C_i(x_{ci}, y_{ci}) \ \ (i = 1, 2, 3)$ of the workspace circles are

$$\begin{cases} x_{c1} = x_p\cos\phi - y_p\sin\phi \\ y_{c1} = x_p\sin\phi + y_p\cos\phi \\ x_{c2} = x_p\cos\phi - y_p\sin\phi - t_4\cos\phi + t_1 \\ y_{c2} = x_p\sin\phi + y_p\cos\phi - t_4\sin\phi \\ x_{c3} = x_p\cos\phi - y_p\sin\phi - t_5\cos\phi + t_6\sin\phi + t_2 \\ y_{c3} = x_p\sin\phi + y_p\cos\phi - t_5\sin\phi - t_6\cos\phi + t_3. \end{cases} \tag{2.12}$$

For given leg length ranges $[\rho_i^{min}, \rho_i^{max}]$ $(i = 1, 2, 3)$, when the leg lengths respectively take their maximal and minimal values, there will be six workspace circles which define the boundary of the workspace. In other words, the workspace lies inside three circles whose radii are the maximal leg lengths ρ_i^{max} $(i = 1, 2, 3)$ and outside the other three circles whose radii are the minimal leg lengths ρ_i^{min} $(i = 1, 2, 3)$.

By substituting the coordinates (x_{ci}, y_{ci}) of the three centres C_i $(i = 1, 2, 3)$ into the singularity equation eq.(2.7), it can be found that eq.(2.7) is satisfied. This means that all three centres of the workspace circles lie exactly on the singularity locus [75], [76].

If the platform is similar to the base, one obtains

$$\begin{cases} \overline{C_1C_2} = \overline{B_1B_2}\sqrt{k^2 - 2k\cos\phi + 1} \\ \overline{C_2C_3} = \overline{B_2B_3}\sqrt{k^2 - 2k\cos\phi + 1} \\ \overline{C_3C_1} = \overline{B_3B_1}\sqrt{k^2 - 2k\cos\phi + 1}. \end{cases} \tag{2.13}$$

Equation (2.13) shows that triangle $\triangle C_1C_2C_3$ is also similar to the base. Its area is

$$S = (k^2 - 2k\cos\phi + 1)S_b. \tag{2.14}$$

where S_b is the area of the base triangle $\triangle B_1B_2B_3$. For a base of unit area ($S_b = 1$), S is constant for a given orientation ϕ.

In order to determine the singularity-free workspace for a given orientation ϕ, the minimal leg lengths ρ_i^{min} $(i = 1, 2, 3)$ should first be prescribed. As the minimal leg lengths depend on the physical architecture, they can be initially chosen as the same. With this assumption, the maximal leg length ρ_i^{max} $(i = 1, 2, 3)$ can be determined with the following procedure (taking Fig. 2.3(a) as an example):

Step 1: Compute $C(x_c, y_c)$ and R using eq.(2.10) as well as $C_i(x_{ci}, y_{ci})$ $(i = 1, 2, 3)$ using eq.(2.12). To compute C and C_i, it is necessary to provide the coordinates of the considered point P in the mobile frame. For convenience, take the centroid of the platform as the considered point P. Hence, $x_p = (t_4 + t_5)/3, y_p = t_6/3$.

Step 2: The intersections N_i and N_i' $(i = 1, 2, 3)$ of the minimal workspace circles and the singularity circle can be computed with eq.(2.15) as follows:

$$\begin{cases} (x - x_{ci})^2 + (y - y_{ci})^2 = (\rho_i^{min})^2 & (i = 1, 2, 3) \\ (x - x_c)^2 + (y - y_c)^2 = R^2. \end{cases} \tag{2.15}$$

Step 3: Compute ρ_i^{max} $(i = 1, 2, 3)$:

- Compute the distances between the centre C_1 and the two intersections N_3 and N_2': $\overline{C_1N_3}$ and $\overline{C_1N_2'}$. Then, take the shortest of these distances (here $\overline{C_1N_3}$) as ρ_1^{max} in order to avoid singularity inside the workspace.
- Compute the distances between the centre C_2 and the two intersections N_1 and N_3': $\overline{C_2N_1}$ and $\overline{C_2N_3'}$. Then, take the shortest of these distances (here $\overline{C_2N_3'}$) as ρ_2^{max}.
- Compute the distances between the centre C_3 and the two intersections N_2 and N_1': $\overline{C_3N_2}$ and $\overline{C_3N_1'}$. Then, take the shortest of these distances (here $\overline{C_3N_2}$) as ρ_3^{max}.

With the obtained maximal leg lengths, three maximal workspace circles respectively centred at C_i $(i = 1, 2, 3)$ are available. Fig. 2.3(a) shows only the parts of these circles lying inside the singularity circle, i.e., three arcs: M_1N_3, M_2N_3' and M_3N_2. Arc M_1N_3 intersects the second minimal workspace circle at M_4 and arc M_2N_3' intersects arc M_3N_2 at M_5. The hatched region formed by five arcs, $M_4N_3N_3'M_5N_2M_4$, is the singularity-free workspace for the considered case.

For general similar base and platform, the maximal leg lengths ρ_i^{max} $(i = 1, 2, 3)$ may be different from one to another. Besides, Fig. 2.3(a) shows that the minimal length of leg 1 will be $\overline{C_1M_5}$, which is greater than its initially chosen value.

2.4 Case Studies

For a base of unit area , $t_3 = 2/t_1$. Substituting this equation into eq.(2.10), R will be a function of t_1, t_2, k and ϕ. To obtain an extremum of R, the following conditions

should be satisfied:

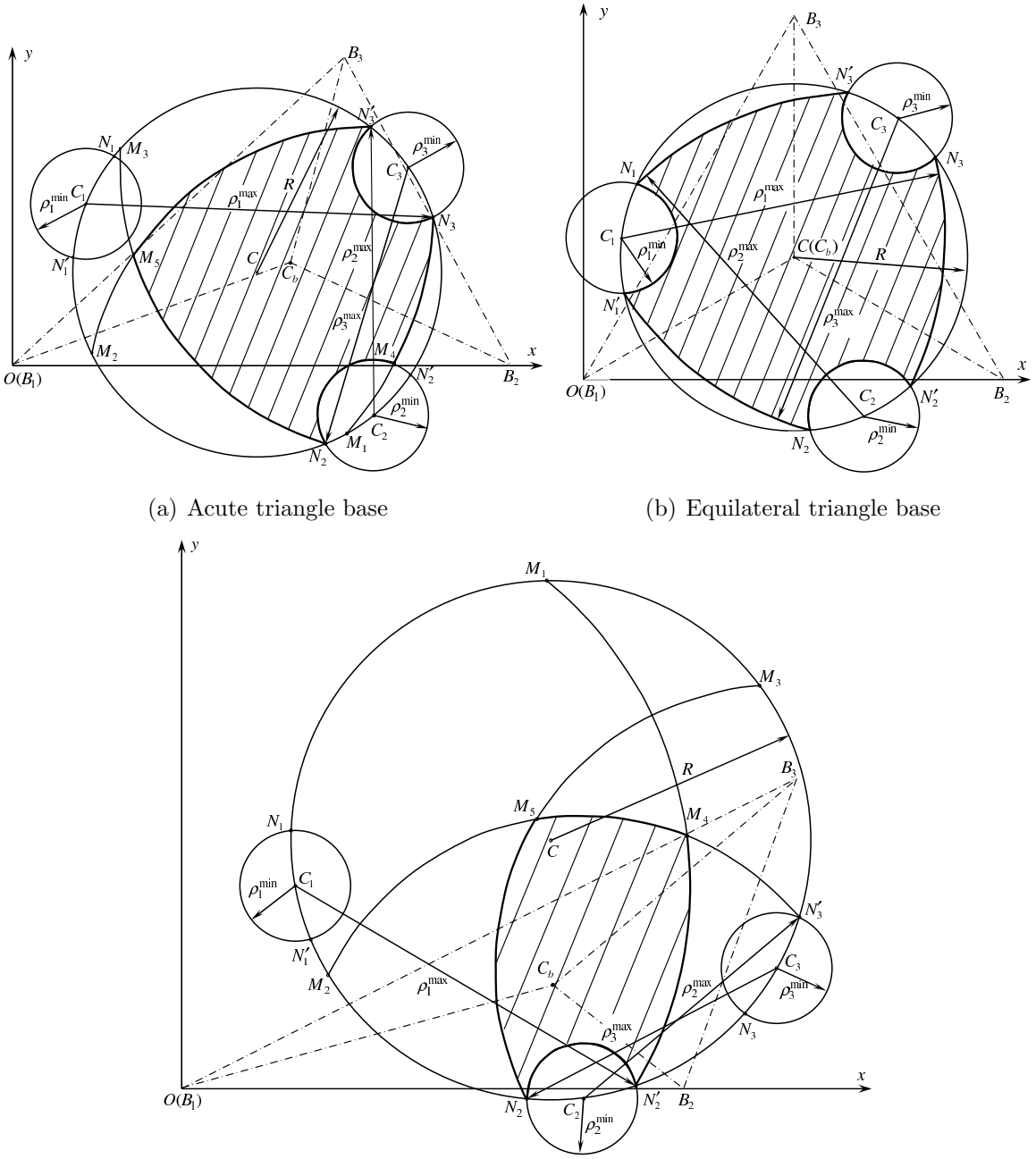

(a) Acute triangle base

(b) Equilateral triangle base

(c) Obtuse triangle base

Figure 2.3: The singularity-free workspace with different triangle bases.

$$\begin{cases} \partial R/\partial t_1 = 0 \\ \partial R/\partial t_2 = 0 \\ \partial R/\partial k = 0 \\ \partial R/\partial \phi = 0. \end{cases} \tag{2.16}$$

Unfortunately, there is no real solution for this equation set. However, for given nonzero k and $\phi \neq i\pi$ $(i = 0, 1)$, a real solution can be obtained from the first two equations of eq.(2.16), i.e., $t_1 = 2/\sqrt[4]{3}$, $t_2 = 1/\sqrt[4]{3}$. As a result, $t_3 = \sqrt[4]{3}$. The obtained base is actually an equilateral triangle. In this case, one has

$$R = 2\sqrt{(k^2 - 2k\cos\phi + 1)/\sqrt{3}} \simeq 0.877\sqrt{k^2 - 2k\cos\phi + 1}. \tag{2.17}$$

Hence, for given k and ϕ, eq.(2.17) provides the extreme radius of the singularity circle for a base of unit area which is obtained when the base and the platform are equilateral triangles. Since triangle $\triangle C_1C_2C_3$ is similar to the base triangle $\triangle B_1B_2B_3$, then triangle $\triangle C_1C_2C_3$ is also equilateral. As a result, the three centres C_i $(i = 1, 2, 3)$ of the workspace circles are evenly distributed on the singularity circle, as shown in Fig. 2.3(b). In this case, both ρ_i^{min} and ρ_i^{max} are equal for $i = 1, 2, 3$, and the obtained singularity-free workspace (the hatched region) occupies most of the region inside the singularity circle.

However, the extreme radius given by eq.(2.17) for given k and ϕ is not a maximum, but a minimum. From eq.(2.14), it can be seen that for given k and ϕ, triangle $\triangle C_1C_2C_3$ has the same area, no matter what its shape is. And the singularity circle is the circumscribed circle of triangle $\triangle C_1C_2C_3$. When triangle $\triangle C_1C_2C_3$ is equilateral, its circumscribed circle becomes minimal. Although the minimal singularity circle occurs when the base and the platform are equilateral triangles, the singularity-free workspace may be maximal. To demonstrate this point, consider the following three case studies.

Case 1: In Fig. 2.3(a), the geometric parameters of the base are: $t_1 = 1.8$, $t_2 = 1.2$, $t_3 = 1.11$, which form an acute triangle of unit area. Substituting the values of t_1, t_2 and t_3 into eq.(2.10), one obtains

$$R \simeq 0.929\sqrt{k^2 - 2k\cos\phi + 1}. \tag{2.18}$$

Case 2: In Fig. 2.3(b), the geometric parameters of the base are: $t_1 = 2/\sqrt[4]{3}$,

$t_2 = 1/\sqrt[4]{3}$, $t_3 = \sqrt[4]{3}$, which form an equilateral triangle of unit area. The radius of the singularity circle is given by eq.(2.17).

Case 3: In Fig. 2.3(c), the geometric parameters of the base are: $t_1 = 1.8$, $t_2 = 2.2$, $t_3 = 1.11$, which form an obtuse triangle of unit area. Substitute the values of t_1, t_2, t_3, into eq.(2.10), one obtains

$$R \simeq 1.310\sqrt{k^2 - 2k\cos\phi + 1}. \tag{2.19}$$

Comparing eq.(2.17) to eq.(2.18) and eq.(2.19), it is easy to find that when the base and platform are equilateral triangles, the singularity circle is minimal. To compare the singularity-free workspace in these three cases, consider for instance the situation with $k = 0.6$, $\phi = 45°$, and ρ_i^{min} is initially chosen as 0.2. The graphics in the same scale are shown in Fig. 2.3. First, compare case 1 to case 2. The radius of the singularity circle in case 1 is 0.665, which is larger than that (0.627) in case 2. But the area of the singularity-free workspace in case 1 is smaller than that in case 2. Then, compare case 3 to case 2. Although the radius of the singularity circle in case 3 is 1.494 times of that in case 2, the singularity-free workspace occupies no more than one-third of the region inside the singularity circle (see Fig. 2.3(c)). Hence, the area of the singularity-free workspace in case 3 is still smaller than that in case 2. The numerical results in these three cases will be given in the next chapter.

The reason for which a robot with a larger singularity circle has a smaller singularity-free workspace is that the centres of the workspace circles, C_i $(i = 1, 2, 3)$, are not evenly distributed on the singularity circle. For given k and ϕ, the area of triangle $\triangle C_1C_2C_3$ does not vary with its shape. It is easy to imagine that for case 3 with an obtuse triangle base, when the obtuse angle becomes larger, the vertices of triangle $\triangle C_1C_2C_3$ will lie on an arc close to a line. Although the singularity circle may be very large, the singularity-free workspace occupies only a small corner of the singularity circle (see Fig. 2.3(c)).

Equation (2.10) shows that the centre of the singularity circle is dependent on the position of the considered point P and the orientation angle ϕ. Take the centroid of the platform as the considered point P, the centre of the singularity circle for case 1 in Fig. 2.3(a) and case 3 in Fig. 2.3(c) is dependent on the orientation angle ϕ, as shown in Figs. 2.4(a) and 2.4(c). In these two cases, the locus of the centre of the singularity

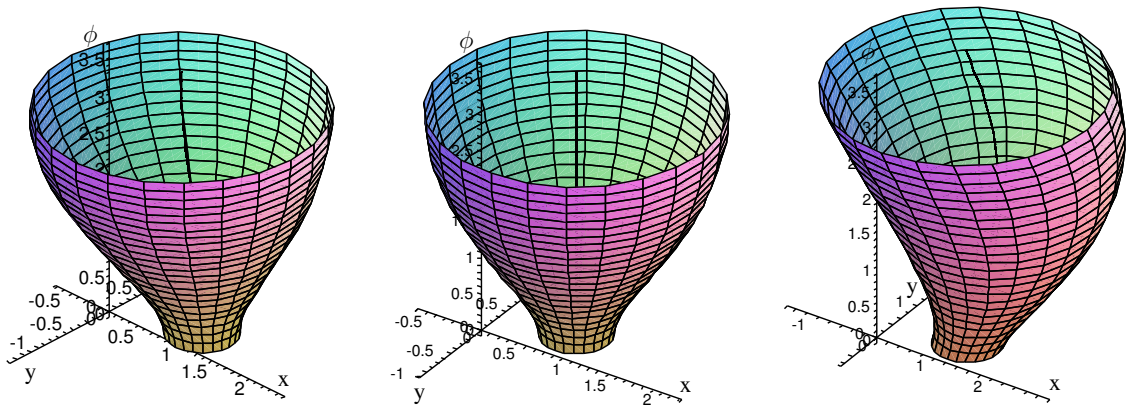

(a) Acute triangle base (b) Equilateral triangle base (c) Obtuse triangle base

Figure 2.4: The evolution of the singularity circle with respect to ϕ ($k = 0.6$).

circle is a curve in the $Oxy\phi$ space. However, the centre of the singularity circle for case 2 in Fig. 2.3(b) always coincides with the centroid C_b of the base. As a result, the locus of the centre of the singularity circle is a straight line in the $Oxy\phi$ space, as shown in Fig. 2.4(b). With this property as well as symmetry, the parallel mechanism with an equilateral triangle base will have better kinematic properties compared to other architectures.

From the analysis of the singularity-free workspace as well as the location of the singularity circle, it can be seen that a planar 3-$R\underline{P}R$ parallel mechanism with an equilateral triangle base is the optimal architecture.

2.5 Application

2.5.1 Design Procedure

In general, after a robot has been designed and manufactured, the size ratio k cannot be changed. But the orientation angle ϕ should cover a working range. Considering this point, the design procedure for 3-$R\underline{P}R$ parallel robots with equilateral triangle base and platform can be generalized as follows:

- Referring to Fig. 2.2(a) and considering the physical architecture, select a proper size ratio k.
- According to the desired function, determine a range of the orientation angle: $[\phi_1, \phi_2]$. Note that $\phi = i\pi \ \ (i = 0, 1)$ should not be included in the prescribed range.
- Referring to Fig. 2.2(a) or Fig. 2.2(b), use eq.(2.17) to compute the corresponding range of the radius of the singularity circle: $[R_1(\phi_1), R_2(\phi_2)]$. $R_1(\phi_1)$ will be used to determine the maximal leg length ranges.
- Considering the physical architecture such as the size of one prismatic joint and two revolute joints on one leg, determine the minimal leg lengths $\rho_i^{min} \ \ (i = 1, 2, 3)$.
- Referring to Fig. 2.3, take the centroid of the platform as the considered point, use the procedure presented in Section 2.3 to compute the maximal leg lengths $\rho_i^{max} \ \ (i = 1, 2, 3)$ in order to determine the maximal leg length ranges.
- Choose a proper leg length range within the computed maximal leg length range for each leg and complete the geometric design.

2.5.2 Example

In order to demonstrate the proposed design procedure, an example is now provided. The parameters of the base are $t_1 = 2/\sqrt[4]{3}$, $t_2 = 1/\sqrt[4]{3}$, $t_3 = \sqrt[4]{3}$. The size ratio k is selected as 0.6 and the desired orientation range of ϕ is $[100°, 165°]$. Taking the minimal leg lengths as 0.2. Then, $\rho_i^{max} \ \ (i = 1, 2, 3)$ is determined as 1.995 by $R_1 \ \ (= 1.099)$. The possible maximal leg length range is $[0.2, 1.995]$ for all three legs. Hence, the leg length ranges can be chosen from this computed maximal leg length range, say $[0.8, 1.5]$. It can be guaranteed that no singularity exists inside the workspace of the designed robot for the prescribed range of orientation.

2.6 Conclusions

By separating the origin O' of the mobile frame from the considered point P and making O' coincide with a special point of the platform, the singularity equation containing only a minimal set of geometric parameters is derived in this chapter for planar 3-$R\underline{P}R$ parallel mechanism. Just as pointed out in [71], for similar triangular base and platform, the singularity locus is a circle. Furthermore, this chapter observes that in the case with similar triangular base and platform, the singularity circle for any considered point of the platform is of the same size. Besides, the three centres C_i $(i = 1, 2, 3)$ of the workspace circles can be verified to lie exactly on the singularity locus [75], [76]. These interesting observations can be used to determine the singularity-free workspace as well as the corresponding leg length ranges.

Three case studies with different triangular bases of unit area are performed. The graphics with the same scale show that the mechanism with an equilateral triangle base and platform may lead to the maximal singularity-free workspace, because the singularity-free workspace in this case occupies most of the region inside the singularity circle. Furthermore, the location of the singularity circle for the centroid of the platform is independent from the orientation angle ϕ.

Considering that symmetric architectures are widely used in practice, a geometric design procedure for planar 3-$R\underline{P}R$ parallel robots with equilateral triangle base and platform is provided. The given example shows that as long as the working ranges of the leg lengths lie within the maximal ranges determined with the presented method and the orientation angle ϕ does not equal $i\pi$ $(i = 0, 1)$, it can be guaranteed that the workspace definitely lies inside the singularity circle. The risk for encountering a singularity inside the workspace can be avoided completely. Therefore, the information provided in this chapter is of great significance for robot designers in practice.

Chapter 3

Optimal Geometric Design of the Planar 3-$R\underline{P}R$ Parallel Mechanism

For a base of unit area, it was conjectured in the preceding chapter that the planar 3-$R\underline{P}R$ parallel robots with equilateral triangle base and platform possess the maximal singularity-free workspace. However, this point is very difficult to prove theoretically. The singularity-free workspace seems to be related to the size of the inscribed circle of triangle $\triangle C_1C_2C_3$. This chapter finds that when the base is an equilateral triangle, the inscribed circle of triangle $\triangle C_1C_2C_3$ is maximal. The numerical analysis of the singularity-free workspace based on the Gauss divergence theorem shows that for a given orientation angle ϕ, there exists an optimal minimal leg length which leads to a corresponding maximal singularity-free workspace. However, for a prescribed working range of ϕ, the optimal minimal leg length may be different from these individual optimal minimal leg lengths.

3.1 Introduction

The singularity locus of planar 3-$R\underline{P}R$ parallel mechanisms with similar triangular base and platform is a circle [71]. In the preceding chapter, the three centres C_i $(i = 1, 2, 3)$ of the workspace circles were shown to lie exactly on the singularity circle. With these useful observations, the singularity-free workspace as well as the corresponding leg length ranges for a given architecture and a given orientation can be determined. Three case studies with different triangular bases of unit area were performed. The plots with the same scale show that the mechanism with an equilateral triangle base and platform leads to the maximal singularity-free workspace, because in this case, the singularity-free workspace occupies most of the region inside the singularity circle. However, as mentioned above, this point is very difficult to prove theoretically.

Fig. 2.3 shows that the singularity-free workspace seems to be related to the size of the inscribed circle of triangle $\triangle C_1C_2C_3$. For a base of unit area, the radius of this inscribed circle can be given as

$$r = r(t_1, t_2, k, \phi). \tag{3.1}$$

For a given value of k and ϕ, the following conditions need to be satisfied in order to obtain a maximum of r:

$$\begin{cases} \partial r/\partial t_1 = 0 \\ \partial r/\partial t_2 = 0 \\ \partial^2 r/\partial t_1^2 < 0 \\ \partial^2 r/\partial t_2^2 < 0. \end{cases} \tag{3.2}$$

For an equilateral triangle base of unit area, $t_1 = 2/\sqrt[4]{3}$, $t_2 = 1/\sqrt[4]{3}$. Substituting these values into eq.(3.2), it can be found that eq.(3.2) is satisfied. This means that when the base is an equilateral triangle, the inscribed circle of triangle $\triangle C_1C_2C_3$ becomes maximal.

Followed will be the numerical investigation of the singularity-free workspace based on the Gauss divergence theorem [22], [99]. This includes the analysis of the effect of the orientation angle ϕ, the analysis of the effect of the minimal leg length as well as the analysis of the effect of the base shape. Considering these factors, the geometric

design procedure proposed in the previous chapter is optimized.

3.2 Numerical Analysis of the Singularity-Free Workspace

The area of the singularity-free workspace can be computed using the Gauss divergence theorem [22], [99], provided that a description of the boundary of the workspace is available. Since the singularity-free workspace can be affected by several factors such as the orientation angle ϕ, the minimal leg length ρ_i^{min} as well as the shape of the base, this section analyzes the effects of these factors.

3.2.1 Computation of the Singularity-Free Workspace

In order to compute the area of the singularity-free workspace, the first and key step is the boundary definition. The boundary of the singularity-free workspace of planar 3-$R\underline{P}R$ parallel mechanisms can be defined with the method mentioned in [22]. Referring to Fig. 2.3, the singularity-free workspace lies inside the singularity circle. In general, the boundary possibly consists of several arcs on six workspace circles, three circles with the minimal leg lengths ρ_i^{min} $(i = 1, 2, 3)$ and the others with the maximal leg lengths ρ_i^{max} $(i = 1, 2, 3)$. The minimal leg lengths ρ_i^{min} should be given first and the maximal leg lengths ρ_i^{max} can be determined using the method proposed in the previous chapter. Hence, the boundary of the singularity-free workspace can be determined as follows:

- For each workspace circle, compute the intersections with the other six circles (including the singularity circle).
- Order the intersections to divide the considered workspace circle into elementary arcs.
- Test each elementary arc to determine whether it belongs to the boundary of the singularity-free workspace. If the considered arc is to belong to the boundary, its

two endpoints and middle point should satisfy the following condition:

$$\rho_i^{min} \leq d_i \leq \rho_i^{max} \qquad (i = 1, 2, 3) \tag{3.3}$$

where d_i is the distance from the endpoints or the middle point of the considered arc to the centre C_i of the workspace circle.

After the boundary has been defined, the area of the singularity-free workspace can be computed using the Gauss divergence theorem [22], [99].

3.2.2 Effect of the Orientation Angle

The three cases presented in Chapter 2 are again used here for demonstration. With the above proposed algorithm, the area A of the singularity-free workspace with respect to the orientation angle ϕ for $\rho_i^{min} = 0.2$ can be computed and shown in Figs. 3.1 and 3.2. Fig. 3.1 shows that for a large range of the orientation angle, the equilateral triangle base holds the maximal singularity-free workspace. But when the orientation angle is small, Fig. 3.2 shows that the obtuse triangle base may yield the maximal singularity-free workspace. The reason will be explained in the following subsection.

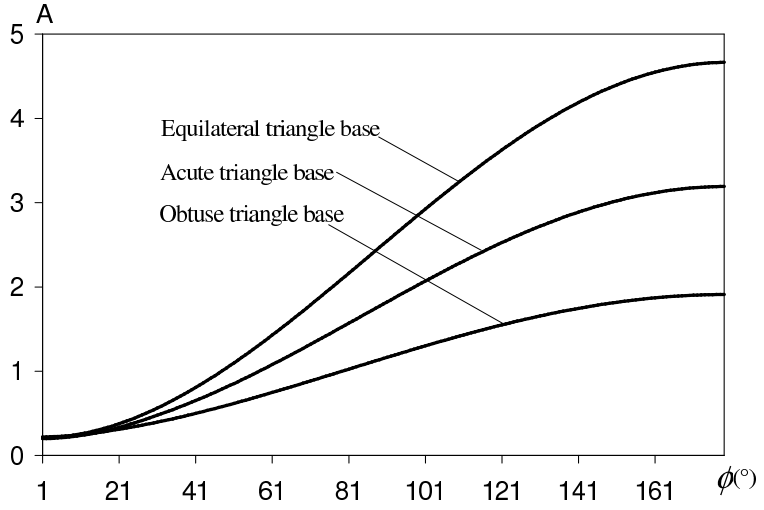

Figure 3.1: The area of the singularity-free workspace with respect to ϕ ($\rho_i^{min} = 0.2$).

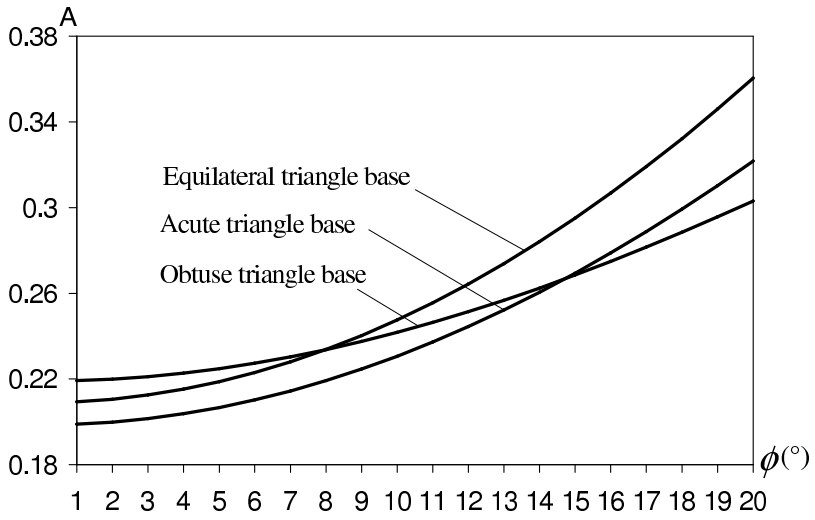

Figure 3.2: The area of the singularity-free workspace with respect to small ϕ ($\rho_i^{min} = 0.2$).

3.2.3 Effect of the Minimal Leg Length

If the minimal leg length ρ_i^{min} is constant for any orientation angle, Fig. 3.2 shows that when the orientation angle is small, the obtuse triangle base may lead to the maximal singularity-free workspace. This is because of the effect of the minimal leg length ρ_i^{min}. To demonstrate this point, the area of the singularity-free workspace with respect to the minimal leg length ρ_i^{min} for $\phi = 45^\circ$ is computed and shown in Fig. 3.3. This figure shows that for each case, there exists an optimal value of ρ_i^{min}, which leads to the corresponding maximal singularity-free workspace. When ϕ is small, the singularity circles also become small. For a constant ρ_i^{min}, this is equivalent to increasing the value of ρ_i^{min} for unchanged singularity circles. As a result, the obtuse triangle base obtains a larger singularity-free workspace than the equilateral triangle base (see Fig. 3.3).

To compare the singularity-free workspaces of the three cases, it seems to be more reasonable to use their respective optimal value of ρ_i^{min} for every ϕ. Fig. 3.4 shows the area of the singularity-free workspace with respect to ϕ with optimal ρ_i^{min}. It can be seen that for any orientation angle ϕ, the equilateral triangle base yields the maximal singularity-free workspace.

Obviously, for different orientation angles, the optimal values of ρ_i^{min} are different. Fig. 3.5 shows the optimal ρ_i^{min} with respect to the orientation angle ϕ. It can be seen

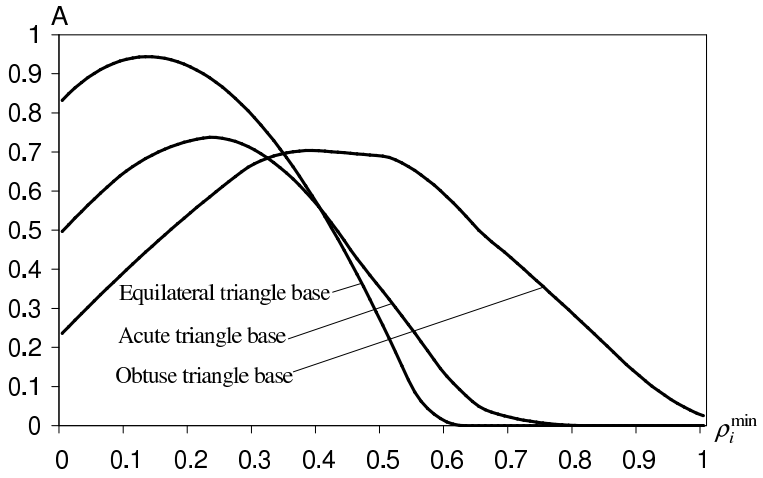

Figure 3.3: The area of the singularity-free workspace with respect to ρ_i^{min} ($\phi = 45°$).

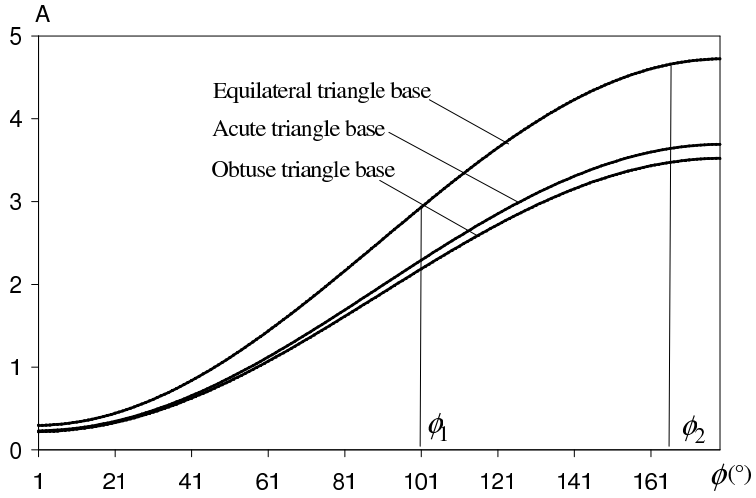

Figure 3.4: The area of the singularity-free workspace with respect to ϕ (optimal ρ_i^{min}).

that the optimal ρ_i^{min} for equilateral triangle base is minimal. This is consistent with Fig. 3.3.

3.2.4 Effect of the Shape of the Base

From the three case studies described in the previous subsections, it seems that when the base is an equilateral triangle, the planar 3-$R\underline{P}R$ parallel robot has the maximal singularity-free workspace. In order to further investigate this issue, consider the ge-

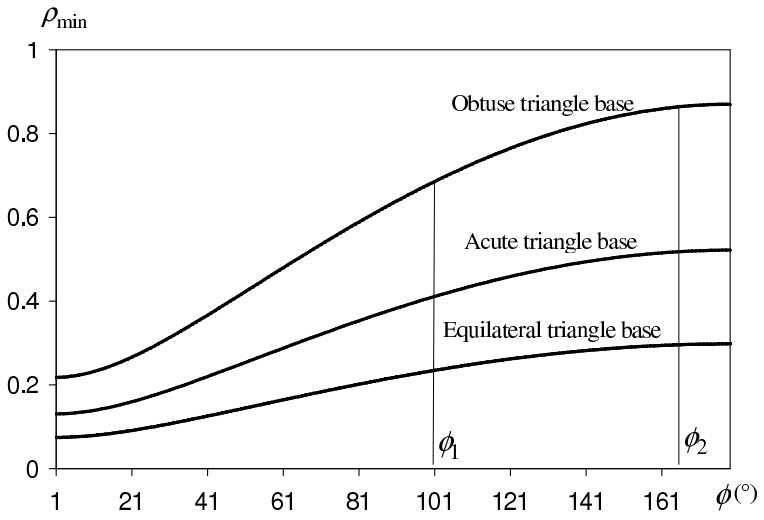

Figure 3.5: The optimal ρ_i^{min} with respect to ϕ.

ometric parameter $t_1 = 2/\sqrt[4]{3}$, which is the side length of an equilateral triangle base of unit area, as a constant. Referring to Fig. 2.1, changing t_2 leads to different base shapes. Starting from -5, with an increase of t_2, the base shape changes as follows: obtuse triangle ($t_2 < 0$) $\rightarrow$ right triangle ($t_2 = 0$) $\rightarrow$ acute triangle ($0 < t_2 < 1/\sqrt[4]{3}$) $\rightarrow$ equilateral triangle ($t_2 = 1/\sqrt[4]{3}$) $\rightarrow$ acute triangle ($1/\sqrt[4]{3} < t_2 < 2/\sqrt[4]{3}$) $\rightarrow$ right triangle ($t_2 = 2/\sqrt[4]{3}$) $\rightarrow$ obtuse triangle ($t_2 > 2/\sqrt[4]{3}$).

The numerical results with several typical orientation angles are shown in Fig. 3.6. This figure shows that when $t_2 = 1/\sqrt[4]{3} \approx 0.76$ (equilateral triangle base), the area of the singularity-free workspace becomes maximal. Although these results do not constitute a formal proof, they strongly support the conjecture that the equilateral shape provides the maximal singularity-free workspace.

3.3 Geometric Design

3.3.1 Optimal ρ_i^{min} for a Prescribed Range of ϕ

In general, after a robot has been designed and manufactured, the size ratio k between the platform and the base cannot be changed. But the orientation angle ϕ should cover

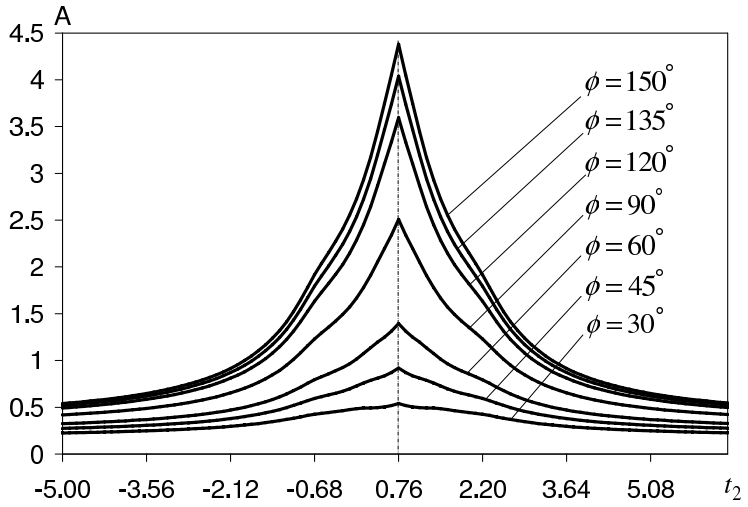

Figure 3.6: The area of the singularity-free workspace with respect to t_2.

a working range. In order to obtain the maximal singularity-free workspace, Fig. 3.5 shows that for every value of ϕ, there exists an optimal value of the minimal leg length ρ_i^{min}. For a prescribed working range $\phi \in [\phi_1, \phi_2]$, Fig. 2.2 shows that the radius of the singularity circle monotonically increases with ϕ. In order to avoid singularities inside the workspace, the maximal leg lengths should be determined by ϕ_1. Fig. 3.7 shows the construction obtained with an equilateral triangle base of unit area. The used minimal leg length is the optimal one at ϕ_1. The hatched region formed by six arcs, $N_1N_1'N_2N_2'N_3N_3'N_1$, is the singularity-free workspace at ϕ_1. However, being limited by the maximal leg length determined by ϕ_1, the singularity-free workspace at ϕ_2 is only the intercross-hatched region formed by three arcs, $M_1M_2M_3M_1$. Obviously, this workspace is much smaller than the workspace at ϕ_1. This situation shows that the optimal values of the minimal leg lengths obtained as shown in Fig. 3.5 are not necessarily optimal for a prescribed working range of ϕ.

To obtain the optimal value of the minimal leg length for a prescribed working range of ϕ, six case studies are now performed. The size ratio k is given by 0.6 and the prescribed working range of ϕ is $[100^\circ, 165^\circ]$, i.e., $\phi_1 = 100^\circ$ and $\phi_2 = 165^\circ$.

Case 1: The minimal leg length is 0.2.

Case 2: The minimal leg length is 0.233276, which is the optimal one at ϕ_1.

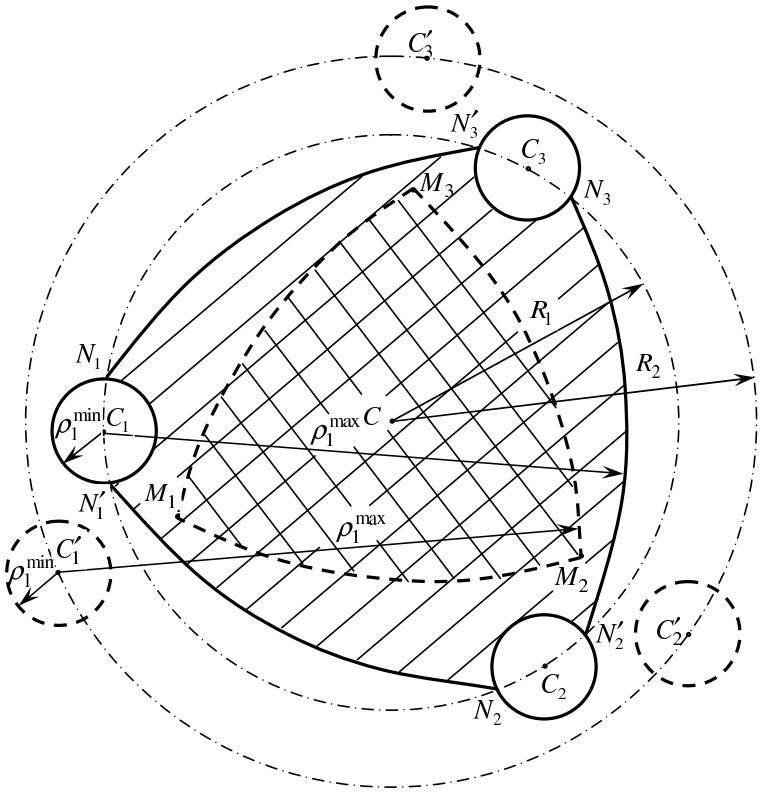

Figure 3.7: The singularity-free workspaces for ϕ_1 and ϕ_2 ($\phi_1 < \phi_2$).

Case 3: The minimal leg length is 0.295636, which is the optimal one at ϕ_2.

Case 4: The minimal leg length is determined by solving the following optimization problem:

$$\max_{\rho_i^{min}} A_a \tag{3.4}$$

where A_a is the average area of the singularity-free workspaces over the prescribed working range of ϕ, which can be expressed as

$$A_a = \frac{1}{\phi_2 - \phi_1} \int_{\phi_1}^{\phi_2} A(\phi) d\phi. \tag{3.5}$$

Case 5: The minimal leg length is determined by minimizing the difference between A_1 and A_2, which are respectively the area of the singularity-free workspaces at ϕ_1 and ϕ_2, i.e.,

$$\min_{\rho_i^{min}} |A_1 - A_2|. \tag{3.6}$$

Table 3.1: Numerical results of the case studies.

$Case$	ρ_i^{min}	ρ_i^{max}	A_1	A_2	$\lvert A_1 - A_2 \rvert$	A_a	ΔA_a
1	0.2	1.995261	2.887449	1.523389	1.364060	2.088205	0.368054
2	0.233276	2.009044	2.894137	1.589744	1.304393	2.146203	0.354989
3	0.295636	2.033677	2.871123	1.711608	1.159515	2.234786	0.314177
4	0.412168	2.075469	2.709505	1.927286	0.782219	2.308779	0.207856
5	0.647965	2.142531	1.957423	1.957423	0	2.012230	0.024850
6	0.656267	2.144448	1.921667	1.947769	0.026102	1.992113	0.024325

Case 6: The minimal leg length is determined by minimizing the fluctuation of the area of the singularity-free workspace, i.e.,

$$\min_{\rho_i^{min}} \Delta A_a \tag{3.7}$$

where ΔA_a is the average difference of the area of the singularity-free workspaces with respect to A_a and given as

$$\Delta A_a = \frac{1}{n} \sum_{i=1}^{n} |A_i - A_a| \tag{3.8}$$

where A_i is the area of the singularity-free workspace at ϕ_i.

If the convergence precision is set to 10^{-6}, n in eq.(3.8) will be greater than 400. The numerical results are shown in Fig. 3.8 and listed in Table 3.1. The results show that for cases 1 – 3, the differences between A_1 and A_2 as well as the values of ΔA_a are quite large. For case 4, the difference between A_1 and A_2 as well as the value of ΔA_a decrease considerably, and A_a reaches the maximum. Hence, if the objective of the designers is to obtain the maximal singularity-free workspace over a prescribed range of ϕ, case 4 is the optimal solution.

For case 5, $A_1 = A_2$ and ΔA_a is only 0.024850, which is quite small. For case 6, the value of ΔA_a reaches the minimum, 0.024325. Fig. 3.8 shows that the curves corresponding to cases 5 and 6 are very close. However, the curve corresponding to case 5 is always above that corresponding to case 6. Hence, the value of A_a in case 5 is larger than that in case 6, while the value of ΔA_a in case 5 is very close to that in case 6. Especially, the difference between A_1 and A_2 in case 5 is 0. Hence, if the objective of the designers is to obtain a singularity-free workspace of almost the same size at every orientation angle in the prescribed range, case 5 is the optimal solution.

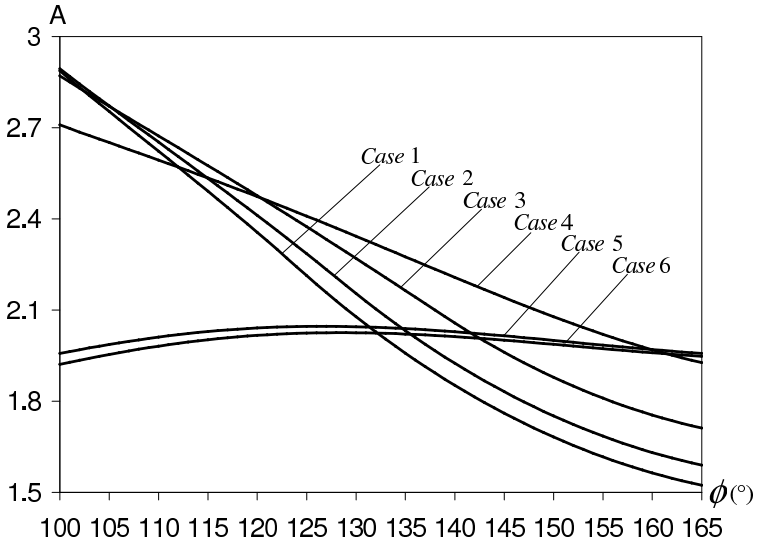

Figure 3.8: The area of the singularity-free workspace with respect to ϕ (with different ρ_i^{min}).

3.3.2 Design Procedure

Considering the effect of the minimal leg length, the design procedure proposed in Chapter 2 can be modified as follows:

- Select a proper size ratio k between the platform and the base.
- According to the desired function, determine a range of the orientation angle: $[\phi_1, \phi_2]$. Note that $\phi = i\pi$ $(i = 0, 1)$ should not be included in the prescribed range since these values correspond to singular orientations.
- Use eq.(3.4) or (3.6) (depending on which design objective is pursued) to compute the optimal minimal leg length. Then, use the procedure described in Chapter 2 to determine the maximal leg length at ϕ_1. To avoid singularities inside the workspace, this determined maximal leg length is also used as the maximal leg length for the whole prescribed range of ϕ.
- Choose a proper leg length range within the computed maximal leg length range for each leg and complete the geometric design.

3.4 Conclusions

In this chapter, it is verified that the inscribed circle of triangle $\triangle C_1C_2C_3$ for an equilateral triangle base is maximal. This indirectly shows that the planar 3-$R\underline{P}R$ parallel robots with an equilateral triangle base possess the maximal singularity-free workspace. In order to demonstrate this point, numerical investigations based on the Gauss divergence theorem are performed. The results show that for every value of ϕ, there is an optimal value of the minimal leg length which leads to the corresponding maximal singularity-free workspace. However, for a prescribed working range of ϕ, these optimal values may not lead to the maximal singularity-free workspaces. Instead, a new optimal minimal leg length should be found by solving eq.(3.4) or eq.(3.6). Considering this factor, the geometric design procedure proposed in Chapter 2 is modified.

Chapter 4

Singularity Equations of Gough-Stewart Platforms

So far, in the derivation of the singularity equations of Gough-Stewart platforms, all research works defined the mobile frame by making its origin O' coincide with the considered point P of the platform. One problem can be that the obtained singularity equations contain too many geometric parameters and are not convenient for singularity analysis, especially not convenient for geometric optimization. Another problem can be that the obtained singularity equations cannot be used directly in practice. To solve these problems, this chapter derives the singularity equations of Gough-Stewart platforms by defining the frames as follows: the origin O' of the mobile frame is separated from the considered point P and chosen to coincide with a special point of the platform in order to minimize the number of geometric parameters of the platform. In the meantime, the fixed frame is also chosen to lie at a special point of the base in order to minimize the number of geometric parameters of the base. As a result, no matter which point of the platform is chosen as the considered point P, the obtained singularity equations contain only a minimal set of geometric parameters.

4.1 Introduction

Singularity equations are difficult to obtain for mechanisms with more than three degrees of freedom because the determinant of the Jacobian matrix becomes very complex. For Gough-Stewart platforms, previous studies just focused on a few special cases of singularities [4], [41], [43], [44], [66], [67]. For the first time, the singularity equation for the general Gough-Stewart platform was derived in [69]. Actually, this is also a complete singularity equation because the 20 coefficients are functions of the 3 orientation angles. Later, based on the cascaded expansion of the determinant of the Jacobian matrix, a procedure was developed in [87] to obtain the explicit expressions of the 20 coefficients as functions of the orientation angles.

Unfortunately, the singularity equations obtained in [69] and [87] are very complex because they contain too many geometric parameters. One of the reasons is that the two frames were defined as shown in Fig. 4.1. The reference frame is attached to the base by choosing an arbitrary point as the origin O. The mobile frame is attached to the platform by choosing the considered point P as the origin O'. As a result, all coordinates of the attachment points B_i and P_i $(i = 1, 2, ..., 6)$ are different from zero. The total number of geometric parameters is 36. This makes the coefficients of the obtained singularity equations very complex and not convenient for singularity analysis, especially not convenient for geometric optimization. For instance, the example used

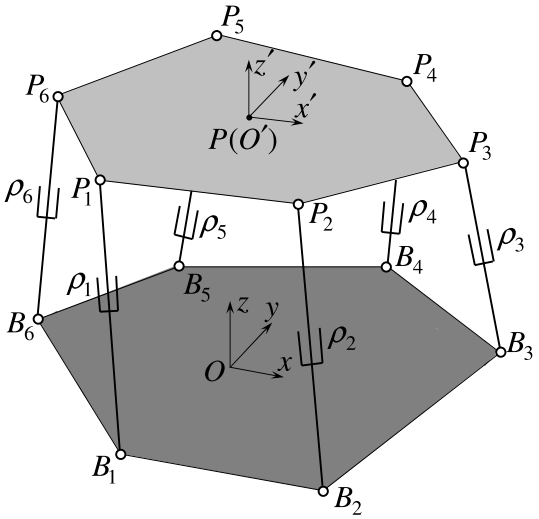

Figure 4.1: General Gough-Stewart platform.

in [69] and [87] — the $INRIA$ prototype — is actually a SSM architecture. Although both the base and the platform are coplanar, the z coordinate of every attachment point of the base and the platform does not vanish. The total number of geometric parameters is still 36.

Besides, this method lacks flexibility because the considered point P is chosen as the origin O' of the mobile frame. Obviously, for different considered points, different mobile frames are used. Hence, the coordinates of the attachment points P_i $(i = 1, 2, ..., 6)$ of the platform in the new mobile frame need to be re-computed.

The singularity equations were also derived in [78] and [79] respectively for the 6-3 Gough-Stewart platform and the general Gough-Stewart platform. To obtain the singularity expression, these two works just made the origin O' of the mobile frame coincide with one attachment point (P_1) of the platform. Because of this specific choice, the vector connecting point O' and point P_1 vanishes and the total number of terms of the determinant of the Jacobian matrix reduces from 20 to 10. Otherwise, the number of terms cannot be reduced [69].

Obviously, the singularity equations obtained in [78] and [79] are for the special point P_1. Although a singular position of P_1 represents a singular pose of the platform, this special point is not a point of practical interest. In practice, a more interesting point may be the centroid C_p of the platform or any other point chosen according to the application. For instance, if we want to determine the maximal singularity-free workspace of the platform, this special point P_1 cannot be used because P_1 is not the suitable position for the end-effector. For this application, the more suitable point may be the centroid of the platform.

For some asymmetrical architectures such as irregular hexagons, the approach used in [78] and [79] may minimize the number of geometric parameters contained in the singularity equation. However, for all symmetrical architectures such as SSM, TSSM and MSSM [69], this approach cannot make the number of geometric parameters minimal. Another interesting point is that the word “explicit" appeared many times in [78] and [79]. Unfortunately, no expression can be found to be a real explicit function of the position coordinates (x, y, z) as well as the orientation coordinates (x_1, x_2, x_3) which were used to denote the Rodrigues parameters. Instead, all expressions are given as products of vectors or matrices.

Now the problem becomes: how to derive the singularity equation about an arbitrary point P of the platform using the minimal set of geometric parameters?

To solve this problem, the principle presented in Chapter 2 is applied, i.e., the origin O' of the mobile frame is separated from the considered point P and chosen to coincide with a special point of the platform in order to minimize the number of geometric parameters of the platform. Similarly, the fixed frame should also be chosen to lie at a special point of the base in order to minimize the number of geometric parameters of the base.

4.2 General Formulation

As shown in Fig. 4.1, a general Gough-Stewart platform consists of a mobile platform $P_1P_2P_3P_4P_5P_6$ and a base $B_1B_2B_3B_4B_5B_6$ connected via six identical UPS legs (B_iP_i, $i = 1, 2, ..., 6$). For a general Gough-Stewart platform, the attachment points B_i ($i = 1, 2, ..., 6$) on the base do not necessarily lie in the same plane, likewise for the attachment points P_i ($i = 1, 2, ..., 6$) on the platform. The mechanism has 6 DOFs and

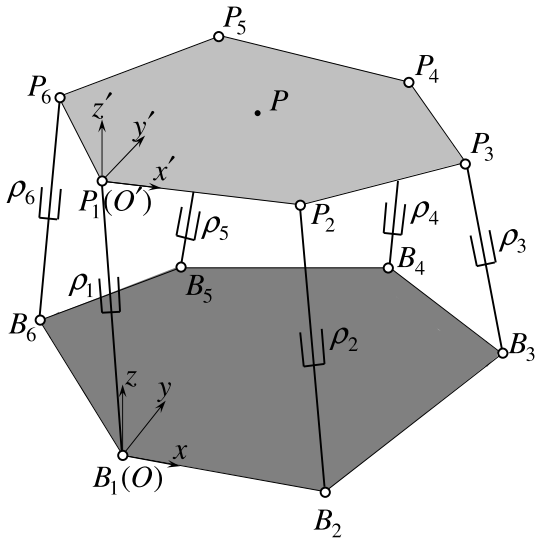

Figure 4.2: General Gough-Stewart platform with new frames definition.

can be controlled by adjusting the lengths of six legs.

To derive the singularity equation, two coordinate systems are defined as shown in Fig. 4.2. The reference frame $Oxyz$ is attached to the base by selecting a convenient point (say B_1) as the origin O and a convenient direction (say B_1B_2) as the x axis. The Oxy plane is chosen such that it contains as many attachment points B_i as possible. The mobile frame $O'x'y'z'$ is attached to the platform by selecting a convenient point (say P_1) as the origin O' and a convenient direction (say P_1P_2) as the x' axis. Similarly, the $O'x'y'$ plane is chosen such that it contains as many attachment points P_i as possible.

The position vector of point B_i $(i = 1, 2, ..., 6)$ in the fixed frame is denoted by $\mathbf{b}_i = [x_{bi}, y_{bi}, z_{bi}]^T$ and the position vectors of point P_i $(i = 1, 2, ..., 6)$ in the fixed and mobile frames are respectively denoted by $\mathbf{p}_i = [x_{pi}, y_{pi}, z_{pi}]^T$ and $\mathbf{p}'_i = [x'_{pi}, y'_{pi}, z'_{pi}]^T$. Obviously, $\mathbf{b}_i$ and $\mathbf{p}'_i$ are constant vectors in their respective frames.

Let $\mathbf{Q}$ denote the rotation matrix representing the rotation of the platform from the fixed frame $Oxyz$ to the mobile frame $O'x'y'z'$ with

$$\mathbf{Q} = \begin{bmatrix} c\theta c\psi & s\phi s\theta c\psi - c\phi s\psi & c\phi s\theta c\psi + s\phi s\psi \\ c\theta s\psi & s\phi s\theta s\psi + c\phi c\psi & c\phi s\theta s\psi - s\phi c\psi \\ -s\theta & s\phi c\theta & c\phi c\theta \end{bmatrix} \tag{4.1}$$

where $c\phi = \cos\phi, s\phi = \sin\phi$, etc., and ϕ, θ, ψ are *Roll-Pitch-Yaw* angles [1], [31–34], [100].

Let vector $\mathbf{p}_r = [x_r, y_r, z_r]^T$ denote the position of the origin O' of the mobile frame in the fixed frame. The position vectors of the considered point P of the platform in the fixed and mobile frames are respectively $\mathbf{p} = [x, y, z]^T$ and $\mathbf{p}' = [x_p, y_p, z_p]^T$. From $\mathbf{p}'$, it can be seen that the considered point P is different from the origin O' of the mobile frame. If $\mathbf{p}' = \mathbf{0}$, the considered point P will coincide with the origin O' of the mobile frame. This shows that this derivation covers the case mentioned in [78] and [79]. The relationship between $\mathbf{p}$ and $\mathbf{p}'$ can be given as

$$\mathbf{p} = \mathbf{p}_r + \mathbf{Q}\mathbf{p}'. \tag{4.2}$$

From eq.(4.2), one obtains

$$\mathbf{p}_r = \mathbf{p} - \mathbf{Q}\mathbf{p}' \tag{4.3}$$

and therefore

$$\mathbf{p}_i = \mathbf{p}_r + \mathbf{Q}\mathbf{p}'_i = \mathbf{p} + \mathbf{Q}(\mathbf{p}'_i - \mathbf{p}'). \tag{4.4}$$

The length ρ_i of leg i is the distance between points B_i and P_i. From this, one obtains

$$\rho_i^2 = (\mathbf{p}_i - \mathbf{b}_i)^T(\mathbf{p}_i - \mathbf{b}_i). \tag{4.5}$$

Differentiating eq.(4.5) with respect to time, one obtains

$$\rho_i\dot{\rho}_i = (\mathbf{p}_i - \mathbf{b}_i)^T\dot{\mathbf{p}} + [\mathbf{Q}(\mathbf{p}'_i - \mathbf{p}') \times (\mathbf{p}_i - \mathbf{b}_i)]^T\boldsymbol{\omega}. \tag{4.6}$$

For all six legs, eq.(4.6) can be re-written as follows:

$$\mathbf{A}\mathbf{v} = \mathbf{D}\dot{\boldsymbol{\rho}} \tag{4.7}$$

where $\dot{\boldsymbol{\rho}} = [\dot{\rho}_1, \dot{\rho}_2, ..., \dot{\rho}_6]^T$ denotes the actuator velocities and $\mathbf{v} = [\dot{\mathbf{p}}^T, \boldsymbol{\omega}^T]^T$ the Cartesian velocity vector of the platform. $\mathbf{A}$ and $\mathbf{D}$ are two Jacobian matrices. $\mathbf{D} = diag(\rho_1, \rho_2, ..., \rho_6)$. From eq.(4.6), the elements in row i of matrix $\mathbf{A}$ are given as

$$[a_{i1}, a_{i2}, ..., a_{i6}] = [(\mathbf{p}_i - \mathbf{b}_i)^T, [\mathbf{Q}(\mathbf{p}'_i - \mathbf{p}') \times (\mathbf{p}_i - \mathbf{b}_i)]^T] \tag{4.8}$$

i.e.

$$\begin{cases} a_{i1} = x + g_i \\ a_{i2} = y + h_i \\ a_{i3} = z + k_i \\ a_{i4} = -n_i y + m_i z + r_i \\ a_{i5} = n_i x - l_i z + s_i \\ a_{i6} = -m_i x + l_i y + u_i \end{cases} \tag{4.9}$$

where

$$\begin{cases} l_i = q_{11}(x'_{pi} - x_p) + q_{12}(y'_{pi} - y_p) + q_{13}(z'_{pi} - z_p) \\ m_i = q_{21}(x'_{pi} - x_p) + q_{22}(y'_{pi} - y_p) + q_{23}(z'_{pi} - z_p) \\ n_i = q_{31}(x'_{pi} - x_p) + q_{32}(y'_{pi} - y_p) + q_{33}(z'_{pi} - z_p) \\ g_i = l_i - x_{bi} \\ h_i = m_i - y_{bi} \\ k_i = n_i - z_{bi} \\ r_i = n_i y_{bi} - m_i z_{bi} \\ s_i = -n_i x_{bi} + l_i z_{bi} \\ u_i = m_i x_{bi} - l_i y_{bi} \end{cases} \tag{4.10}$$

and q_{ij} $(i, j = 1, 2, 3)$ are the entries of rotation matrix $\mathbf{Q}$, which is given by eq.(4.1). Therefore, matrix $\mathbf{A}$ can be written as

$$\begin{aligned} \mathbf{A} = [&\mathbf{e}x + \mathbf{g}, \quad \mathbf{e}y + \mathbf{h}, \quad \mathbf{e}z + \mathbf{k}, \quad -\mathbf{n}y + \mathbf{m}z + \mathbf{r}, \\ &\mathbf{n}x - \mathbf{l}z + \mathbf{s}, \quad -\mathbf{m}x + \mathbf{l}y + \mathbf{u}] \end{aligned} \tag{4.11}$$

where $\mathbf{e} = [1, 1, 1, 1, 1, 1]^T$, $\mathbf{g} = [g_1, g_2, ..., g_6]^T$, $\mathbf{h} = [h_1, h_2, ..., h_6]^T$, $\mathbf{k} = [k_1, k_2, ..., k_6]^T$, $\mathbf{l} = [l_1, l_2, ..., l_6]^T$, $\mathbf{m} = [m_1, m_2, ..., m_6]^T$, $\mathbf{n} = [n_1, n_2, ..., n_6]^T$, $\mathbf{r} = [r_1, r_2, ..., r_6]^T$, $\mathbf{s} = [s_1, s_2, ..., s_6]^T$, $\mathbf{u} = [u_1, u_2, ..., u_6]^T$.

The condition for the direct singularity is $det(\mathbf{A}) = 0$. Similarly to what was done in [69] adn [87], the determinant of matrix $\mathbf{A}$ can be expanded using linear decomposition. The obtained singularity equation takes the following form:

$$\begin{aligned} &f_1x^3 + f_2x^2y + f_3x^2z + f_4x^2 + f_5xy^2 + f_6xyz + f_7xy \\ &+f_8xz^2 + f_9xz + f_{10}x + f_{11}y^3 + f_{12}y^2z + f_{13}y^2 + f_{14}yz^2 \\ &+f_{15}yz + f_{16}y + f_{17}z^3 + f_{18}z^2 + f_{19}z + f_{20} = 0 \end{aligned} \tag{4.12}$$

where the coefficients f_i $(i = 1, 2, ..., 20)$ are functions of the orientation angles (ϕ, θ, ψ), the geometric parameters as well as the coordinates of the considered point P in the mobile frame. These coefficients can be expressed as the following determinants:

$$
\begin{cases}
f_1 = |\mathbf{e\ h\ k\ r\ n\ -m}| \\
f_2 = |\mathbf{e\ h\ k\ -n\ s\ -m}| + |\mathbf{e\ h\ k\ r\ n\ l}| + |\mathbf{g\ e\ k\ r\ n\ -m}| \\
f_3 = |\mathbf{e\ h\ k\ m\ n\ u}| + |\mathbf{e\ h\ k\ r\ -l\ -m}| + |\mathbf{g\ h\ e\ r\ n\ -m}| \\
f_4 = |\mathbf{e\ h\ k\ r\ n\ u}| + |\mathbf{e\ h\ k\ r\ s\ -m}| + |\mathbf{g\ h\ k\ r\ n\ -m}| \\
f_5 = |\mathbf{e\ h\ k\ -n\ s\ l}| + |\mathbf{g\ e\ k\ -n\ s\ -m}| + |\mathbf{g\ e\ k\ r\ n\ l}| \\
f_6 = |\mathbf{e\ h\ k\ -n\ -l\ u}| + |\mathbf{e\ h\ k\ m\ s\ l}| + |\mathbf{g\ e\ k\ m\ n\ u}| \\
\quad + |\mathbf{g\ e\ k\ r\ -l\ -m}| + |\mathbf{g\ h\ e\ -n\ s\ -m}| + |\mathbf{g\ h\ e\ r\ n\ l}| \\
f_7 = |\mathbf{e\ h\ k\ -n\ s\ u}| + |\mathbf{e\ h\ k\ r\ s\ l}| + |\mathbf{g\ e\ k\ r\ n\ u}| \\
\quad + |\mathbf{g\ e\ k\ r\ s\ -m}| + |\mathbf{g\ h\ k\ -n\ s\ -m}| + |\mathbf{g\ h\ k\ r\ n\ l}| \\
f_8 = |\mathbf{e\ h\ k\ m\ -l\ u}| + |\mathbf{g\ h\ e\ m\ n\ u}| + |\mathbf{g\ h\ e\ r\ -l\ -m}| \\
f_9 = |\mathbf{e\ h\ k\ m\ s\ u}| + |\mathbf{e\ h\ k\ r\ -l\ u}| + |\mathbf{g\ h\ e\ r\ n\ u}| \\
\quad + |\mathbf{g\ h\ e\ r\ s\ -m}| + |\mathbf{g\ h\ k\ m\ n\ u}| + |\mathbf{g\ h\ k\ r\ -l\ -m}| \\
f_{10} = |\mathbf{e\ h\ k\ r\ s\ u}| + |\mathbf{g\ h\ k\ r\ n\ u}| + |\mathbf{g\ h\ k\ r\ s\ -m}| \\
f_{11} = |\mathbf{g\ e\ k\ -n\ s\ l}| \\
f_{12} = |\mathbf{g\ e\ k\ -n\ -l\ u}| + |\mathbf{g\ e\ k\ m\ s\ l}| + |\mathbf{g\ h\ e\ -n\ s\ l}| \\
f_{13} = |\mathbf{g\ e\ k\ -n\ s\ u}| + |\mathbf{g\ e\ k\ r\ s\ l}| + |\mathbf{g\ h\ k\ -n\ s\ l}| \\
f_{14} = |\mathbf{g\ e\ k\ m\ -l\ u}| + |\mathbf{g\ h\ e\ -n\ -l\ u}| + |\mathbf{g\ h\ e\ m\ s\ l}| \\
f_{15} = |\mathbf{g\ e\ k\ m\ s\ u}| + |\mathbf{g\ e\ k\ r\ -l\ u}| + |\mathbf{g\ h\ e\ -n\ s\ u}| \\
\quad + |\mathbf{g\ h\ e\ r\ s\ l}| + |\mathbf{g\ h\ k\ -n\ -l\ u}| + |\mathbf{g\ h\ k\ m\ s\ l}| \\
f_{16} = |\mathbf{g\ e\ k\ r\ s\ u}| + |\mathbf{g\ h\ k\ -n\ s\ u}| + |\mathbf{g\ h\ k\ r\ s\ l}| \\
f_{17} = |\mathbf{g\ h\ e\ m\ -l\ u}| \\
f_{18} = |\mathbf{g\ h\ e\ m\ s\ u}| + |\mathbf{g\ h\ e\ r\ -l\ u}| + |\mathbf{g\ h\ k\ m\ -l\ u}| \\
f_{19} = |\mathbf{g\ h\ e\ r\ s\ u}| + |\mathbf{g\ h\ k\ m\ s\ u}| + |\mathbf{g\ h\ k\ r\ -l\ u}| \\
f_{20} = |\mathbf{g\ h\ k\ r\ s\ u}| .
\end{cases}
\tag{4.13}
$$

The singularity equation given by eq.(4.12) as well as the coefficients given by eq.(4.13) are very similar to those given in [69]. However, they are not the same. The main difference comes from eq.(4.2) as well as the expressions of l_i, m_i and n_i ($i = 1, 2, ..., 6$) in eq.(4.10). With eq.(4.2), the origin O' of the mobile frame is separated from the considered point P and the number of geometric parameters can be minimized. As a result, the obtained singularity equations contain only the minimal set of geometric parameters and are simplified greatly. This is the essential difference between this derivation and all previous works because in the past, all researchers defined the mobile frames by selecting the considered point P as the origin O' (see for instance [69], [78], [79], [87]). The following section will illustrate this point by ana-

lyzing the singularity equations of the typical architectures of Gough-Stewart platforms.

4.3 Singularity Equations of Typical Gough-Stewart Platforms

As mentioned above, for Gough-Stewart platforms, if the coordinate frames are defined as in [69] and [87], the total possible number of geometric parameters is 36. This makes the obtained singularity equations very complex. Combining the typical architectures of Gough-Stewart platforms as shown in Fig. 4.3 — which is modified from Fig. 2 in [69] — this section will discuss the number of geometric parameters contained in the singularity equations derived using the above presented method.

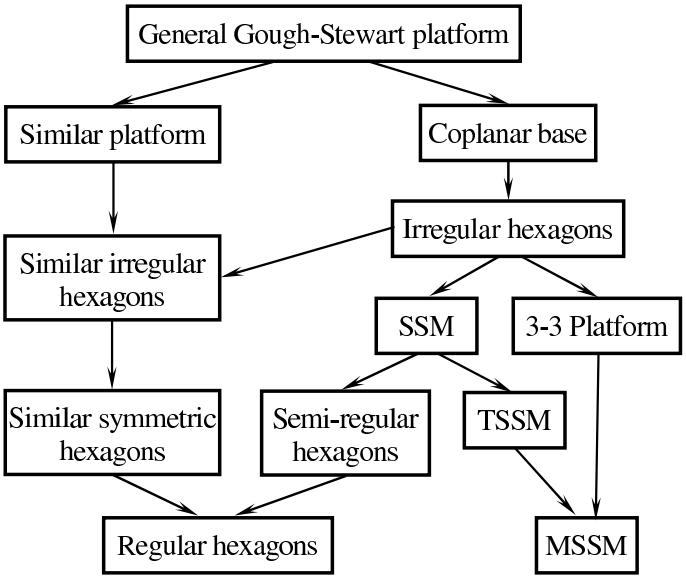

Figure 4.3: Classification of Gough-Stewart platforms.

4.3.1 General and Similar Base and Platform

For the general Gough-Stewart platform as shown in Fig. 4.2, the reference frame $Oxyz$ is attached to the base by selecting B_1 as the origin O and B_1B_2 as the x axis. Besides, the Oxy plane coincides with the plane determined by B_1, B_2, B_3. Hence, the position of B_i $(i = 1, 2, ..., 6)$ in the fixed frame is respectively denoted by vectors $\mathbf{b}_1 = [0, 0, 0]^T$, $\mathbf{b}_2 = [t_1, 0, 0]^T$, $\mathbf{b}_3 = [t_2, t_3, 0]^T$, $\mathbf{b}_4 = [t_4, t_5, t_6]^T$, $\mathbf{b}_5 = [t_7, t_8, t_9]^T$ and $\mathbf{b}_6 = [t_{10}, t_{11}, t_{12}]^T$. The number of geometric parameters defining the base reduces from 18 to 12 because six coordinates of B_1, B_2 and B_3 vanish.

The mobile frame $O'x'y'z'$ is attached to the platform by taking P_1 as the origin O' and P_1P_2 as the x' axis. The $O'x'y'$ plane coincides with the plane determined by P_1, P_2, P_3. Hence, the position of P_i $(i = 1, 2, ..., 6)$ in the mobile frame is respectively denoted by vectors $\mathbf{p}'_1 = [0, 0, 0]^T$, $\mathbf{p}'_2 = [t_{13}, 0, 0]^T$, $\mathbf{p}'_3 = [t_{14}, t_{15}, 0]^T$, $\mathbf{p}'_4 = [t_{16}, t_{17}, t_{18}]^T$, $\mathbf{p}'_5 = [t_{19}, t_{20}, t_{21}]^T$ and $\mathbf{p}'_6 = [t_{22}, t_{23}, t_{24}]^T$. The number of geometric parameters defining the platform also reduces from 18 to 12.

Obviously, the total number of geometric parameters that will be contained in the singularity equations is 24, not 36. The obtained singularity equations will take the form given in eq.(4.12), just as pointed out in [69] .

However, if the base and the platform are similar — assume the size ratio between the platform and the base is k — the total number of geometric parameters will reduce to 13. Because $t_{13}/t_1 = t_{14}/t_2 = t_{15}/t_3 = t_{16}/t_4 = t_{17}/t_5 = t_{18}/t_6 = t_{19}/t_7 = t_{20}/t_8 = t_{21}/t_9 = t_{22}/t_{10} = t_{23}/t_{11} = t_{24}/t_{12} = k$. In this case, the coefficients $f_1, f_2, f_3, f_5, f_6, f_8, f_{11}, f_{12}, f_{14}$ and f_{17} will vanish and the obtained singularity equations will take the following form:

$$f_4x^2 + f_7xy + f_9xz + f_{10}x + f_{13}y^2 + f_{15}yz + f_{16}y + f_{18}z^2 + f_{19}z + f_{20} = 0. \quad (4.14)$$

This form is consistent with the one given in [69].

4.3.2 Coplanar Base, Irregular and Similar Irregular Hexagons

When points B_i $(i = 1, 2, ..., 6)$ on the base are coplanar, the base becomes an irregular hexagon. In this case, the reference frame $Oxyz$ is attached to the base by selecting B_1 as the origin O and B_1B_2 as the x axis. Besides, the Oxy plane coincides with the base plane. Hence, the position of B_i $(i = 1, 2, ..., 6)$ in the fixed frame is respectively denoted by vectors $\mathbf{b}_1 = [0, 0, 0]^T$, $\mathbf{b}_2 = [t_1, 0, 0]^T$, $\mathbf{b}_3 = [t_2, t_3, 0]^T$, $\mathbf{b}_4 = [t_4, t_5, 0]^T$, $\mathbf{b}_5 = [t_6, t_7, 0]^T$ and $\mathbf{b}_6 = [t_8, t_9, 0]^T$. There are 9 geometric parameters defining the base. The mobile frame is still chosen in the same way as in the general Gough-Stewart platforms. Therefore, 12 geometric parameters define the platform and the total number of geometric parameters is 21.

When points P_i $(i = 1, 2, ..., 6)$ on the platform are also coplanar, the platform also becomes an irregular hexagon as shown in Fig. 4.4. In this case, the mobile frame $O'x'y'z'$ is attached to the platform by taking P_1 as the origin O' and P_1P_2 as the x' axis. Besides, the $O'x'y'$ plane coincides with the platform plane. Hence, the position of P_i $(i = 1, 2, ..., 6)$ in the mobile frame is respectively denoted by vectors $\mathbf{p}'_1 = [0, 0, 0]^T$, $\mathbf{p}'_2 = [t_{10}, 0, 0]^T$, $\mathbf{p}'_3 = [t_{11}, t_{12}, 0]^T$, $\mathbf{p}'_4 = [t_{13}, t_{14}, 0]^T$, $\mathbf{p}'_5 = [t_{15}, t_{16}, 0]^T$ and $\mathbf{p}'_6 = [t_{17}, t_{18}, 0]^T$. The number of geometric parameters defining the platform will also reduce to 9 and the total number of geometric parameters will be 18.

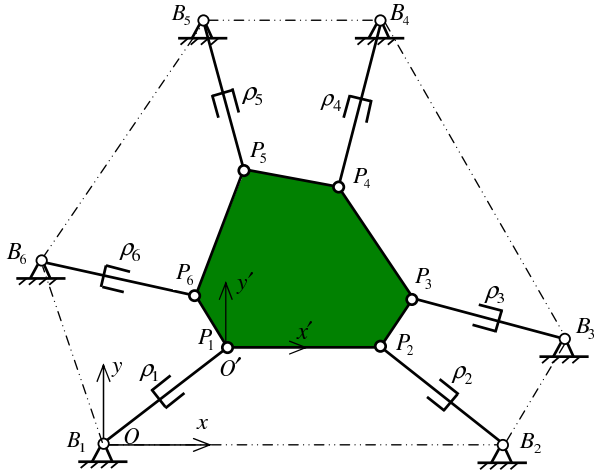

Figure 4.4: Irregular hexagons (top view).

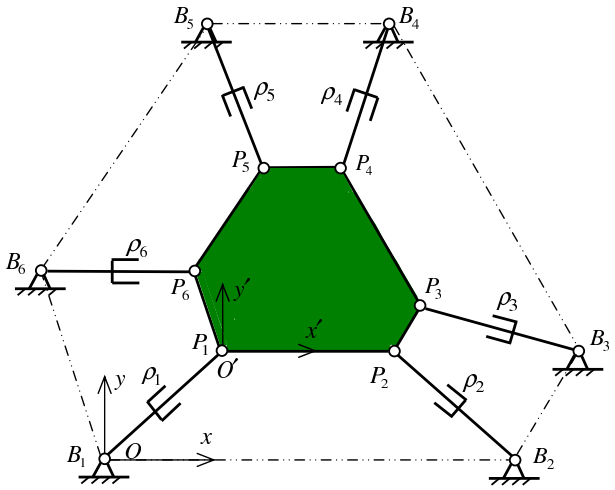

Figure 4.5: Similar irregular hexagons (top view).

For the Gough-Stewart platforms with coplanar base only or irregular hexagonal base and platform, coefficients f_1, f_2, f_5, f_{11} will vanish and the obtained singularity equations will take the following form:

$$\begin{aligned} &f_3x^2z + f_4x^2 + f_6xyz + f_7xy + f_8xz^2 + f_9xz + f_{10}x + f_{12}y^2z \\ &+f_{13}y^2 + f_{14}yz^2 + f_{15}yz + f_{16}y + f_{17}z^3 + f_{18}z^2 + f_{19}z + f_{20} = 0. \end{aligned} \tag{4.15}$$

This form is also consistent with the one given in [69].

For Gough-Stewart platforms with similar irregular hexagons as shown in Fig. 4.5, the total number of geometric parameters will reduce to 10 because $t_{10}/t_1 = t_{11}/t_2 = t_{12}/t_3 = t_{13}/t_4 = t_{14}/t_5 = t_{15}/t_6 = t_{16}/t_7 = t_{17}/t_8 = t_{18}/t_9 = k$. In this case, most coefficients except f_{10}, f_{16}, f_{19} and f_{20} will vanish and the obtained singularity equations will take the following form:

$$f_{10}x + f_{16}y + f_{19}z + f_{20} = 0. \tag{4.16}$$

4.3.3 SSM, TSSM and Semi-regular Hexagons

A SSM — *Simplified Symmetric Manipulator* — is shown in Fig. 4.6. A TSSM — *Triangular Simplified Symmetric Manipulator* — is shown in Fig. 4.7 and the Gough-Stewart platform with semi-regular hexagons is shown in Fig. 4.8. For these

architectures, the reference frame $Oxyz$ is attached to the base by selecting the midpoint of line segment B_1B_2 as the origin O and B_1B_2 as the x axis. The Oxy plane coincides with the base plane. The mobile frame $O'x'y'z'$ is attached to the platform by taking the midpoint of line segment P_1P_2 as the origin O' and P_1P_2 as the x' axis. The $O'x'y'$ plane coincides with the platform plane. Hence, the positions of B_i $(i = 1, 2, ..., 6)$ in the fixed frame are respectively $\mathbf{b}_1 = [-t_1, 0, 0]^T$, $\mathbf{b}_2 = [t_1, 0, 0]^T$, $\mathbf{b}_3 = [t_2, t_3, 0]^T$, $\mathbf{b}_4 = [t_4, t_5, 0]^T$, $\mathbf{b}_5 = [-t_4, t_5, 0]^T$ and $\mathbf{b}_6 = [-t_2, t_3, 0]^T$. The number of geometric parameters defining the base is only 5.

For the SSM and the semi-regular hexagons, the position of P_i $(i = 1, 2, ..., 6)$ in the mobile frame is respectively $\mathbf{p}'_1 = [-t_6, 0, 0]^T$, $\mathbf{p}'_2 = [t_6, 0, 0]^T$, $\mathbf{p}'_3 = [t_7, t_8, 0]^T$, $\mathbf{p}'_4 = [t_9, t_{10}, 0]^T$, $\mathbf{p}'_5 = [-t_9, t_{10}, 0]^T$ and $\mathbf{p}'_6 = [-t_7, t_8, 0]^T$. The number of geometric parameters defining the platform is also 5. For the TSSM, the position of P_i $(i = 1, 2, ..., 6)$ in the mobile frame is respectively $\mathbf{p}'_1 = \mathbf{p}'_6 = [-t_6, 0, 0]^T$, $\mathbf{p}'_2 = \mathbf{p}'_3 = [t_6, 0, 0]^T$ and $\mathbf{p}'_4 = \mathbf{p}'_5 = [0, t_7, 0]^T$. The number of geometric parameters defining the platform is only 2.

Hence, the total number of geometric parameters for the SSM and the semi-regular hexagons is 10 while it is only 7 for the TSSM. The obtained singularity equations for these architectures take the form of eq.(4.15), which are also consistent with those given in [69].

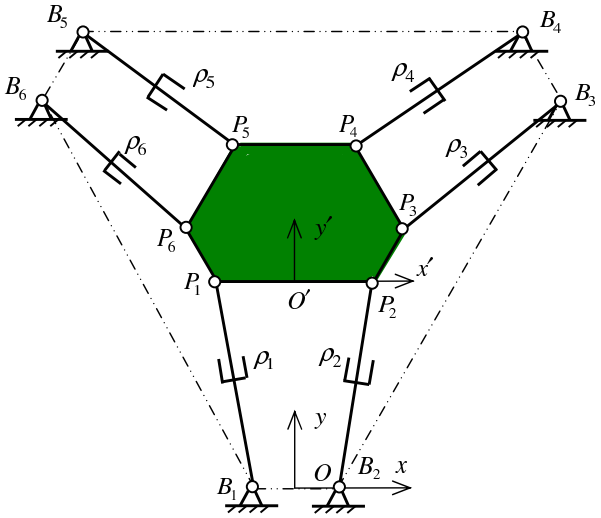

Figure 4.6: SSM architecture (top view).

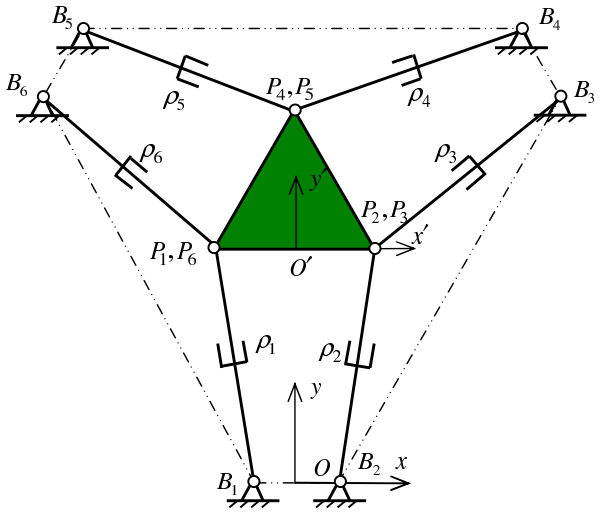

Figure 4.7: TSSM architecture (top view).

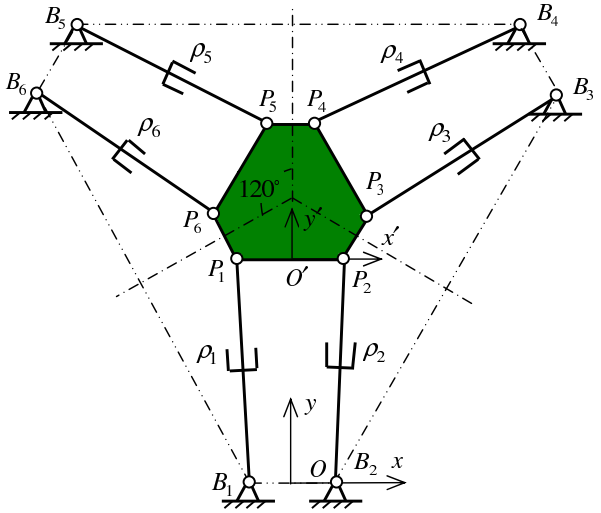

Figure 4.8: Semi-regular hexagons (top view).

4.3.4 Similar Symmetric and Regular Hexagons

For the architectures shown in Figs. 4.9 and 4.10, the base and the platform are not only symmetric, but also similar. The frames can be chosen in the same way as in the SSM. Considering the similarity, for similar symmetric hexagons, the total number of

geometric parameters is 6 (5 for the base and 1 size ratio for the platform). For regular hexagons, the number of geometric parameters defining the base reduces to 1 (the half length of the sides). Therefore, the total number of independent geometric parameters is only 2. For these two architectures, all coefficients of the singularity equations vanish. This means that these two architectures are singular architectures and have no use in practice [8], [69].

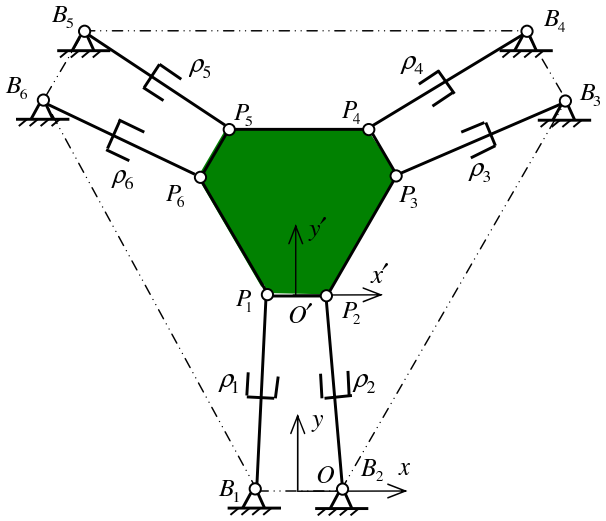

Figure 4.9: Similar symmetric hexagons (top view).

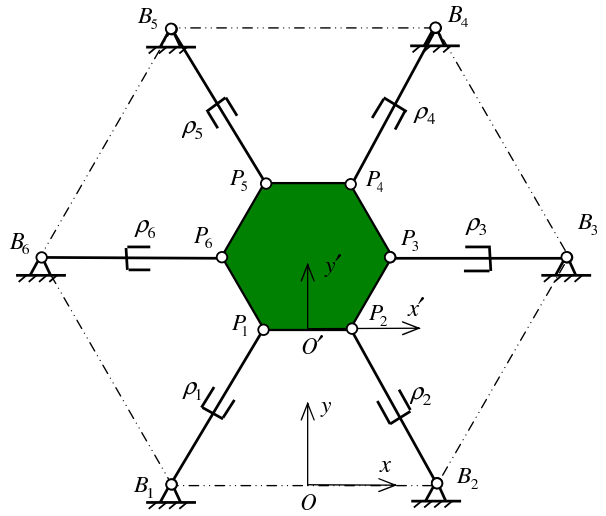

Figure 4.10: Regular hexagons (top view).

4.3.5 General 3-3 Gough-Stewart Platform and MSSM

For the general 3-3 Gough-Stewart platform shown in Fig. 4.11, both the base and the platform are triangles. Hence, the reference frame $Oxyz$ is attached to the base by selecting B_1 as the origin O and B_1B_3 as the x axis. The Oxy plane coincides with the base triangle. The position of B_i $(i = 1, 2, ..., 6)$ in the fixed frame is respectively $\mathbf{b}_1 = \mathbf{b}_2 = [0, 0, 0]^T$, $\mathbf{b}_3 = \mathbf{b}_4 = [t_1, 0, 0]^T$ and $\mathbf{b}_5 = \mathbf{b}_6 = [t_2, t_3, 0]^T$. The number of geometric parameters defining the base is only 3.

The mobile frame $O'x'y'z'$ is attached to the platform by taking P_1 as the origin O' and P_1P_2 as the x' axis. The $O'x'y'$ plane coincides with the platform triangle. Hence, the position of P_i $(i = 1, 2, ..., 6)$ in the mobile frame is respectively $\mathbf{p}'_1 = \mathbf{p}'_6 = [0, 0, 0]^T$, $\mathbf{p}'_2 = \mathbf{p}'_3 = [t_4, 0, 0]^T$ and $\mathbf{p}'_4 = \mathbf{p}'_5 = [t_5, t_6, 0]^T$. The number of geometric parameters defining the platform is also 3. Therefore, the total number of geometric parameters is only 6. The obtained singularity equation takes the form of eq.(4.15).

As shown in Fig. 4.12, the MSSM — *Minimal Simplified Symmetric Manipulator* — architecture can be directly obtained from the general 3-3 Gough-Stewart platforms by making the base and the platform be isosceles triangles. Considering the symmetry, the reference frame $Oxyz$ is attached to the base by selecting $B_1(B_2)$ as the origin O and making the y axis coincide with the symmetric line. The Oxy plane coincides with the base triangle. Hence, the position of B_i $(i = 1, 2, ..., 6)$ in the fixed frame is respectively $\mathbf{b}_1 = \mathbf{b}_2 = [0, 0, 0]^T$, $\mathbf{b}_3 = \mathbf{b}_4 = [t_1, t_2, 0]^T$ and $\mathbf{b}_5 = \mathbf{b}_6 = [-t_1, t_2, 0]^T$. The

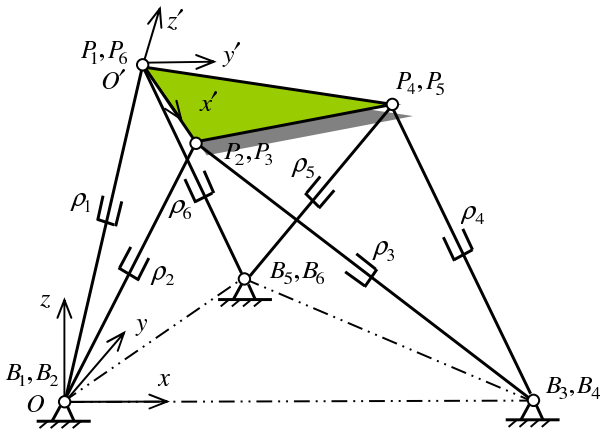

Figure 4.11: General 3-3 Gough-Stewart platform.

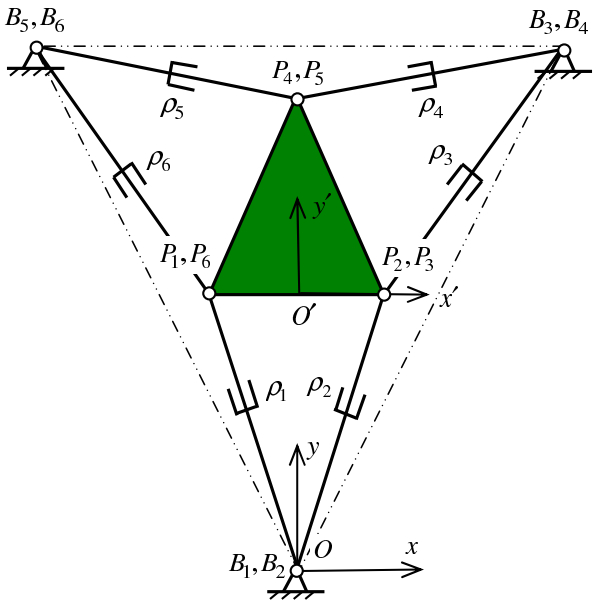

Figure 4.12: MSSM architecture (top view).

number of geometric parameters about the base is only 2.

The mobile frame $O'x'y'z'$ is attached to the platform by taking the midpoint of P_1P_2 as the origin O' and P_1P_2 as the x' axis. The $O'x'y'$ plane coincides with the platform triangle. The position of P_i $(i = 1, 2, ..., 6)$ in the mobile frame is respectively $\mathbf{p}'_1 = \mathbf{p}'_6 = [-t_3, 0, 0]^T$, $\mathbf{p}'_2 = \mathbf{p}'_3 = [t_3, 0, 0]^T$ and $\mathbf{p}'_4 = \mathbf{p}'_5 = [0, t_4, 0]^T$. The number of geometric parameters defining the platform is also 2. Hence, the total number of geometric parameters is only 4. The obtained singularity equations will also take the form of eq.(4.15).

4.3.6 Summary

Some properties of the singularity equations of the typical architectures are summarized in Table 4.1. Compared with Table 1 in [69], the following observations can be made: for every architecture, the number of nonvanishing coefficients is exactly the same as that in [69]. However, the number of geometric parameters contained in the singularity equations was reduced to the minimal independent numbers. And for most architectures, the number of nonvanishing determinants was also reduced. As a re-

sult, the obtained singularity equations can be simplified. For instance, the number of nonvanishing determinants in the case of a coplanar base is 48 in [69], but now only 40. The vanished 24 determinants are f_1, (f_{2-1}, f_{2-2}, f_{2-3}), f_{3-1}, (f_{4-1}, f_{4-3}), (f_{5-1}, f_{5-2}, f_{5-3}), (f_{6-1}, f_{6-3}), (f_{7-1}, f_{7-3}, f_{7-5}, f_{7-6}), f_{9-5}, f_{10-2}, f_{11}, f_{12-1}, (f_{13-1}, f_{13-3}), f_{15-5}, f_{16-2}, where f_{i-j} means the jth determinant of the ith coefficient. For irregular hexagons, SSM, TSSM, semi-regular hexagons, 3-3 and MSSM, the number of nonvanishing determinants is also 48 in [69], but now only 31. The vanished 33 determinants include the above 24 and the following additional 9: f_{3-2}, (f_{6-2}, f_{6-4}), f_{8-1}, f_{9-6}, f_{12-2}, f_{14-1}, f_{15-6}, f_{18-3}. This means that when the platform is also coplanar, the obtained singularity equations can be further simplified.

Table 4.1: Properties of singularity equations.

Architecture	Geometric parameters	Nonvanishing determinants	Nonvanishing coefficients
General case	24	64 (64)	20
Similar platform	13	22 (22)	16
Coplanar base	21	40 (48)	16
Irregular hexagons	18	31 (48)	16
Similar irregular hexagons	10	4 (4)	4
SSM	10	31 (48)	16
TSSM	7	31 (48)	16
Semi-regular hexagons	10	31 (48)	16
Similar symmetric hexagons	6	0	0
Regular hexagons	2	0	0
3-3	6	31 (48)	16
MSSM	4	31 (48)	16

4.4 Example

In practice, the used Gough-Stewart platforms are usually very close to the MSSM architecture for stability and simplicity. Hence, the following seven chapters will focus on analyzing this type of Gough-Stewart platform. Some details about its singularity

equation are given in this section. As mentioned in the previous section, the obtained singularity equation for this architecture takes the form of eq.(4.15). The coefficients can be given in detail as follows:

$$
\begin{cases}
f_3 = 8t_1t_2^2t_3^2t_4q_{31}(q_{21}q_{32}-q_{22}q_{31}) \\
f_4 = \frac{16}{3}t_1t_2^2t_3^2t_4^2q_{31}q_{32}(q_{21}q_{32}-q_{22}q_{31}) \\
f_6 = 8t_1t_2t_3t_4[t_2t_3q_{31}(q_{12}q_{31}-q_{11}q_{32})+t_1t_4q_{32}(q_{21}q_{32}-q_{22}q_{31})] \\
f_7 = \frac{8}{3}t_1t_2t_3t_4[2t_2t_3t_4q_{31}q_{32}(q_{12}q_{31}-q_{11}q_{32})+t_1(3t_3^2q_{31}^2-t_4^2q_{32}^2)(q_{21}q_{32}-q_{22}q_{31})] \\
f_8 = 8t_1t_2t_3t_4[t_1t_4q_{22}(q_{22}q_{31}-q_{21}q_{32})+t_2t_3(2q_{11}q_{22}q_{31}-q_{11}q_{21}q_{32}-q_{12}q_{21}q_{31})] \\
f_9 = \frac{8}{3}t_1t_2t_3t_4[t_2t_3t_4(q_{12}q_{22}q_{31}^2-q_{11}q_{21}q_{32}^2)-t_4^2q_{22}q_{32}(q_{22}q_{31}-q_{21}q_{32}) \\
\quad +3t_2^2t_3q_{31}(q_{11}q_{32}-q_{12}q_{31})+3t_2t_3t_4q_{31}q_{32}(q_{11}q_{22}-q_{12}q_{21}) \\
\quad +3t_1(t_2t_4q_{32}+t_3^2q_{21}q_{31})(q_{22}q_{31}-q_{21}q_{32})] \\
f_{10} = \frac{8}{9}t_1t_2t_3t_4[6t_2^2t_3t_4q_{31}q_{32}(q_{11}q_{32}-q_{12}q_{31})-6t_1t_3^2t_4q_{31}(q_{21}q_{32}-q_{22}q_{31})^2 \\
\quad +3t_1t_2(t_4^2q_{32}^2-3t_3^2q_{31}^2)(q_{21}q_{32}-q_{22}q_{31})+2t_2t_3t_4^2q_{32}(q_{21}q_{32}-q_{22}q_{31})(q_{11}q_{32}-q_{12}q_{31})] \\
f_{12} = 8t_1^2t_2t_3t_4^2q_{32}(q_{12}q_{31}-q_{11}q_{32}) \\
f_{13} = \frac{8}{3}t_1^2t_2t_3t_4(3t_3^2q_{31}^2-t_4^2q_{32}^2)(q_{12}q_{31}-q_{11}q_{32}) \\
f_{14} = 8t_1t_2t_3t_4[t_2t_3q_{11}(q_{11}q_{32}-q_{12}q_{31})+t_1t_4(2q_{11}q_{22}q_{32}-q_{12}q_{22}q_{31}-q_{12}q_{21}q_{32})] \\
f_{15} = \frac{8}{3}t_1t_2t_3t_4[3t_1^2t_3q_{31}(q_{22}q_{31}-q_{21}q_{32})+3t_1t_2t_4q_{32}(q_{11}q_{32}-q_{12}q_{31}) \\
\quad +3t_1t_3^2q_{31}(q_{11}q_{22}q_{31}+q_{11}q_{21}q_{32}-2q_{12}q_{21}q_{31})+t_2t_3t_4(q_{11}q_{32}+q_{12}q_{31})(q_{11}q_{32}-q_{12}q_{31}) \\
\quad +t_1t_4^2q_{32}(q_{12}q_{21}q_{32}+q_{12}q_{22}q_{31}-2q_{11}q_{22}q_{32})] \\
f_{16} = \frac{8}{9}t_1t_2t_3t_4[6t_1^2t_3t_4q_{31}q_{32}(q_{22}q_{31}-q_{21}q_{32})-2t_2t_3t_4^2q_{32}(q_{11}q_{32}-q_{12}q_{31})^2 \\
\quad +3t_1t_2(3t_3^2q_{31}^2-t_4^2q_{32}^2)(q_{11}q_{32}-q_{12}q_{31})+6t_1t_3^2t_4q_{31}(q_{21}q_{32}-q_{22}q_{31})(q_{11}q_{32}-q_{12}q_{31})] \\
f_{17} = 8t_1t_2t_3t_4(t_2t_3q_{11}+t_1t_4q_{22})(q_{12}q_{21}-q_{11}q_{22}) \\
f_{18} = \frac{8}{3}t_1t_2t_3t_4[3t_2^2t_3q_{11}(q_{12}q_{31}-q_{11}q_{32})+3t_1^2t_3q_{21}(q_{21}q_{32}-q_{22}q_{31}) \\
\quad +t_2t_3t_4(q_{11}q_{32}+q_{12}q_{31})(q_{12}q_{21}-q_{11}q_{22})+t_1(3t_2t_4q_{32}+3t_3^2q_{31}-t_4^2q_{32})(q_{12}q_{21}-q_{11}q_{22})] \\
f_{19} = \frac{8}{9}t_1t_2t_3t_4\{3t_1t_2(t_4^2q_{32}^2-3t_3^2q_{31}^2)(q_{11}q_{22}-q_{12}q_{21}) \\
\quad +3t_3t_4[t_2^2(q_{12}^2q_{31}^2-q_{11}^2q_{32}^2)+t_1^2(q_{21}^2q_{32}^2-q_{12}^2q_{31}^2)] \\
\quad +2t_1t_3t_4^2q_{32}(q_{12}q_{21}-q_{11}q_{22})(q_{12}q_{31}-q_{11}q_{32}) \\
\quad +6t_1t_3^2t_4q_{31}(q_{12}q_{21}-q_{11}q_{22})(q_{21}q_{32}-q_{22}q_{31})\} \\
f_{20} = \frac{16}{9}t_1t_2t_3^2t_4^3[t_2^2(q_{12}q_{31}-q_{11}q_{32})^2-t_1^2(q_{22}q_{31}-q_{21}q_{32})^2]q_{32}
\end{cases}
\tag{4.17}
$$

The centroid of the platform is taken here as the considered point P. Hence, the position of the considered point P in the mobile frame is $\mathbf{p}' = [0, t_4/3, 0]^T$. With the obtained singularity equation, the singularity locus in the Cartesian spaces can be plotted. For an equilateral triangle base of unit area, $t_1 = \frac{1}{\sqrt[4]{3}}$ and $t_2 = \sqrt[4]{3}$. Assume that the platform is also an equilateral triangle and take the size ratio k between the

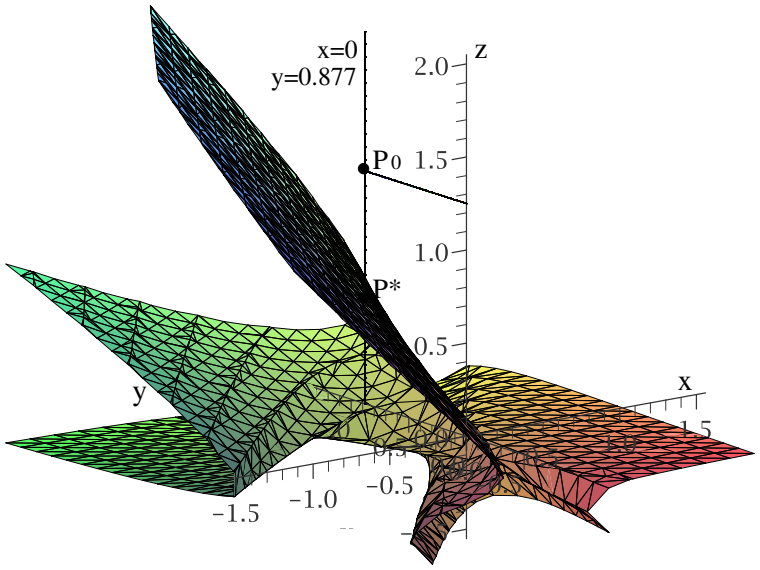

Figure 4.13: Singularity locus in the orientation with $\phi = 30°, \theta = 45°$ and $\psi = 0°$.

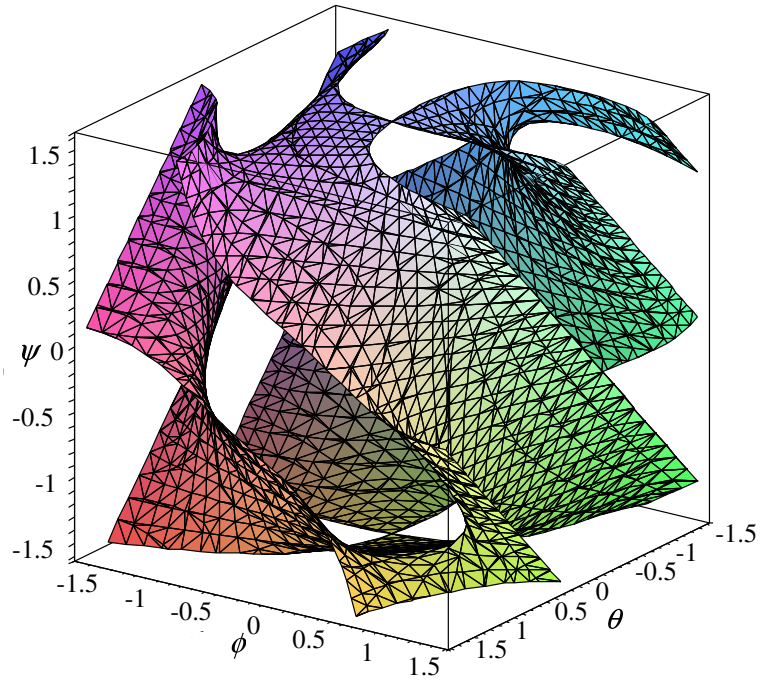

Figure 4.14: Singularity locus at the position $P_0(0, \frac{2\sqrt[4]{3}}{3}, \frac{5}{4})$.

platform and the base be $\frac{3}{5}$. Fig. 4.13 shows the singularity locus in the 3D position Cartesian space in the given orientation with $\phi = 30°, \theta = 45°$ and $\psi = 0°$. Fig. 4.14 shows the singularity locus in the 3D orientation Cartesian space at the given position $P_0(0, \frac{2\sqrt[4]{3}}{3}, \frac{5}{4})$.

Some special orientations need to be pointed out. When $\phi = \theta = 0^\circ$ and $\psi \neq \pm 90^\circ$, all coefficients except f_{17} vanish. In this case, the singularity locus in the 3D Cartesian space ($Oxyz$) is a plane which coincides with the Oxy plane. Another case is: when $\psi = \pm 90^\circ$, all coefficients vanish. In this orientation, every position in the 3D Cartesian space ($Oxyz$) will be singular [41], [69].

4.5 Conclusions

Singularity equations are the basic tool for the singularity analysis of parallel mechanisms. However, the singularity equations of parallel mechanisms with more than three degrees of freedom are difficult to obtain because of the complexity of the Jacobian matrix. Hence, some researchers focused on how to expand the determinant of the Jacobian matrix [69], [78], [79], [87]. Unfortunately, all of them defined the mobile frame by making its origin O' coincide with the considered point P. This makes the obtained singularity equation contain too many geometric parameters or difficult to use in practice. In order to alleviate these problems, this chapter applies the principle presented in chapter 2 to derive the singularity equations of Gough-Stewart platforms. The origin O' of the mobile frame is separated from the considered point P and chosen to coincide with a special point of the platform. Similarly, the fixed frame also lies at a special point of the base. As a result, the singularity equation for any interesting point of the platform contains only the minimal set of geometric parameters. Besides, the geometric parameters do not need to be re-computed for any new considered point once the frames are defined.

In order to demonstrate the proposed method, some properties of the singularity equations of the typical Gough-Stewart platforms are provided. As an example, the singularity equation of the MSSM architecture is given in detail. The example shows that the obtained singularity equation contains only 4 geometric parameters and the coefficients are rather short. With the obtained simple singularity equation, singularity analysis will become more convenient. Especially, the geometric optimization based on singularity analysis will be possible and practical.

Chapter 5

Maximal Singularity-Free Workspace for a Given Orientation

The maximal singularity-free workspace of parallel mechanisms is a desirable criterion in robot design. However, for a 6-DOF parallel mechanism, it is very difficult to find an analytic method to determine the maximal singularity-free workspace around a prescribed point for a given orientation. Hence, a numerical algorithm is presented in this chapter to determine the maximal singularity-free workspace as well as the corresponding leg length ranges of the MSSM Gough-Stewart platform. This algorithm is based on the relationship between the maximal singularity-free workspace and the singularity surface. Case studies with different orientations are performed to demonstrate the presented algorithm. The results obtained can be applied to the geometric design or parameter (leg length) setup of the MSSM parallel robots.

5.1 Introduction

Several researchers addressed the determination of the workspace based on given leg length ranges [15], [16], [18]. When the workspace is determined, the next task is to verify whether any singularity exists inside the workspace. In order to avoid the singularities inside the workspace, different algorithms were presented for the trajectory planning [49], [65], [77], [82], [83]. For instance, a method was presented in [77] to determine whether there is a singularity in a given region defined in the workspace. The answer is definite and can be used to identify the singularity-free zones inside the workspace. Besides, a procedure was presented in [95] to determine a maximal singularity-free sphere around a prescribed point P_0 for a given orientation. This method was also extended to the six-dimensional workspace.

However, it is clear that such a maximal singularity-free sphere does not represent the real maximal singularity-free workspace. The reason is that any practical workspace cannot be a sphere for Gough-Stewart platforms. The difference between the two

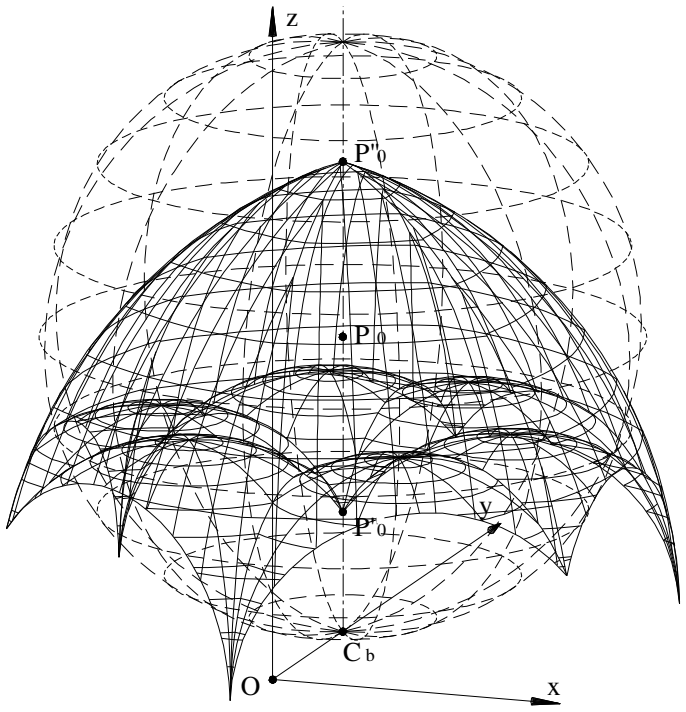

Figure 5.1: The maximal singularity-free workspace (solid) and the maximal singularity-free sphere (dashed) around $P_0(0, \frac{2\sqrt[4]{3}}{3}, \frac{5}{4})$ in the reference orientation.

can be shown in Fig. 5.1, in which the given orientation is the reference orientation with $\phi = \theta = \psi = 0°$. Hence, a more interesting problem may be: How to determine the maximal singularity-free workspace around a prescribed point P_0 as well as the corresponding leg length ranges for a given orientation? If this problem can be solved, the information obtained will be more useful in a practical context.

Unfortunately, the maximal singularity-free workspace in a general orientation as shown in Fig. 5.2 is very complex. It is affected by several factors such as the prescribed point, the given orientation angles as well as the geometric parameters. Hence, it is very difficult to find an analytic method to determine the maximal singularity-free workspace. Instead, a numerical algorithm is presented in this chapter to compute the maximal singularity-free workspace as well as the corresponding leg length ranges of the MSSM Gough-Stewart platform.

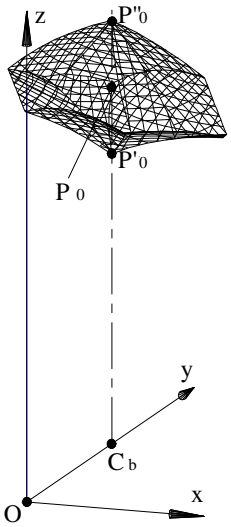

Figure 5.2: The maximal singularity-free workspace around $P_0(0, \frac{2\sqrt[4]{3}}{3}, \frac{5}{4})$ in the orientation with $\phi = 30°$, $\theta = 45°$, $\psi = 0°$.

5.2 Workspace Sphere

As mentioned in Chapter 4, if two frames are defined as shown in Fig. 4.12, the total number of geometric parameters is only 4. Substituting these geometric parameters

into eq.(4.5), one obtains

$$\rho_i^2 = (x - x_{ci})^2 + (y - y_{ci})^2 + (z - z_{ci})^2 \qquad (i = 1, 2, ..., 6) \tag{5.1}$$

where

$$\begin{cases} x_{ci} = x_{bi} - q_{11}(x'_{pi} - x_p) - q_{12}(y'_{pi} - y_p) - q_{13}(z'_{pi} - z_p) \\ y_{ci} = y_{bi} - q_{21}(x'_{pi} - x_p) - q_{22}(y'_{pi} - y_p) - q_{23}(z'_{pi} - z_p) \\ z_{ci} = z_{bi} - q_{31}(x'_{pi} - x_p) - q_{32}(y'_{pi} - y_p) - q_{33}(z'_{pi} - z_p). \end{cases} \tag{5.2}$$

For a given orientation (ϕ, θ, ψ), eq.(5.1) represents six spheres in the 3D Cartesian space $Oxyz$. These spheres can be referred to as *workspace spheres*, because they can be used to determine the workspace [18]. The six centres $C_i(x_{ci}, y_{ci}, z_{ci})$ $(i = 1, 2, ..., 6)$ of the workspace spheres in a general orientation can be listed in Table 5.1. For given leg length ranges $[\rho_i^{min}, \rho_i^{max}]$ $(i = 1, 2, ..., 6)$, when the leg lengths respectively take their maximal and minimal values, there will be 12 workspace spheres which define the boundary of the workspace. In other words, the workspace lies inside 6 spheres whose radii are the maximal leg lengths ρ_i^{max} $(i = 1, 2, ..., 6)$ and outside the other 6 spheres whose radii are the minimal leg lengths ρ_i^{min} $(i = 1, 2, ..., 6)$.

By substituting the coordinates (x_{ci}, y_{ci}, z_{ci}) of the six centres C_i $(i = 1, 2, ..., 6)$ into the singularity equation eq.(4.15), it can be found that eq.(4.15) is satisfied. This means that all six centres of the workspace spheres lie exactly on the singularity locus. Besides, Table 5.1 shows that in a general orientation, C_1 and C_6, C_2 and C_3 as well as C_4 and C_5 respectively lie in three different planes parallel to the base.

Table 5.1: The six centres of the workspace spheres in a general orientation (ϕ, θ, ψ).

C_i	x_{ci}	y_{ci}	z_{ci}
1	$q_{11}t_3 + q_{12}t_4/3$	$q_{21}t_3 + q_{22}t_4/3$	$q_{31}t_3 + q_{32}t_4/3$
2	$-q_{11}t_3 + q_{12}t_4/3$	$-q_{21}t_3 + q_{22}t_4/3$	$-q_{31}t_3 + q_{32}t_4/3$
3	$t_1 - q_{11}t_3 + q_{12}t_4/3$	$t_2 - q_{21}t_3 + q_{22}t_4/3$	$-q_{31}t_3 + q_{32}t_4/3$
4	$t_1 - 2q_{12}t_4/3$	$t_2 - 2q_{22}t_4/3$	$-2q_{32}t_4/3$
5	$-t_1 - 2q_{12}t_4/3$	$t_2 - 2q_{22}t_4/3$	$-2q_{32}t_4/3$
6	$-t_1 + q_{11}t_3 + q_{12}t_4/3$	$t_2 + q_{21}t_3 + q_{22}t_4/3$	$q_{31}t_3 + q_{32}t_4/3$

5.3 Maximal Singularity-Free Workspace

5.3.1 Workspace Around $\mathbf{P}_0$

By strict definition, the workspace around a prescribed point $P_0(x_0, y_0, z_0)$ should be a region:

- which can be reached by the end-effector for given leg length ranges;
- in which P_0 lies exactly at the centroid.

However, such a workspace is very difficult to define in practice because the shape of any practical workspace is very complex. Instead of the strict definition, this chapter defines it as shown in Fig. 5.3. Considering that C_i $(i = 1, 2, ..., 6)$ are the six centres of the workspace spheres, the workspace around a prescribed point P_0 can be defined as a region:

- which can be reached by the end-effector for given leg length ranges;
- in which P_0 lies at the midpoint of the segment $P_0'P_0''$ which is perpendicular to the base and inside the workspace. P_0' and P_0'' respectively lie on the downside and upside boundary of the workspace.

The length of $\overline{P_0'P_0''}$ is referred to as the height of the workspace along this perpendicular line or in short the height of the workspace. Obviously, this height is not necessarily the whole height of the workspace (see Fig. 5.4(a)). But this quantity is very important because it determines the size of the workspace. For convenience, instead of using this quantity directly, the half height denoted by h will be more useful. Obviously, h is the length of $\overline{P_0P_0''}$ $(=\overline{P_0'P_0})$.

As shown in Fig. 5.3, the distance between the centre C_i $(i = 1, 2, ..., 6)$ and the prescribed point P_0 is referred to as the nominal leg length ρ_i^{nom}. When the half height h is given, the maximal and the minimal leg lengths can be determined. Fig. 5.3 shows that the maximal leg length ρ_i^{max} should be equal to $\overline{C_iP_0''}$ and the minimal leg length ρ_i^{min}

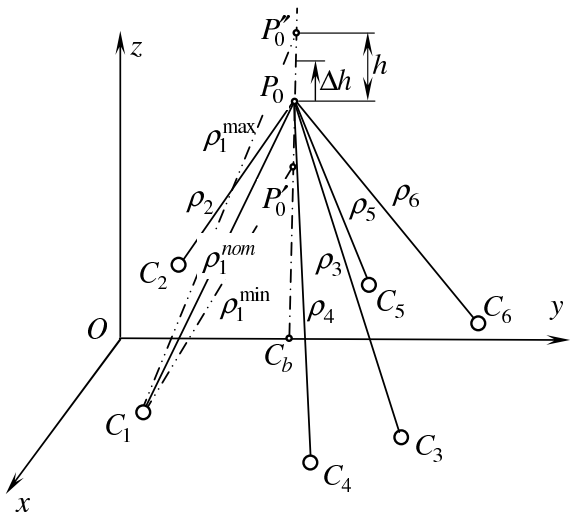

Figure 5.3: Workspace around a prescribed point P_0.

should be equal to $\overline{C_iP_0'}$. However, this is not always the case. In some orientations, the centre C_i may be higher than the prescribed point P_0. In this case, $\overline{C_iP_0'} > \overline{C_iP_0''}$. Hence, the maximal leg length $\rho_i^{max} = \max(\overline{C_iP_0'}, \overline{C_iP_0''})$. For the minimal leg length ρ_i^{min}, if the centre C_i is higher than P_0' and lower than P_0'', ρ_i^{min} will be the perpendicular distance from C_i to the line $P_0'P_0''$. Otherwise, $\rho_i^{min} = \min(\overline{C_iP_0'}, \overline{C_iP_0''})$.

5.3.2 Maximal Singularity-Free Workspace Around $\mathbf{P}_0$

The maximal singularity-free workspace around the prescribed point $P_0(x_0, y_0, z_0)$ is the maximal workspace around this point in which no singular configuration exists. In this case, the half height h reaches its limit value h_{lim} so that the boundary of the workspace just touches the singularity surface at some point(s).

However, there are two cases which make the maximal singularity-free workspace vanish. One case is that the prescribed point P_0 lies exactly on the singularity surface. Another case is that the prescribed point P_0 lies in the Oxy plane, because in practice P_0 should be above the Oxy plane.

5.4 Numerical Algorithm

5.4.1 Basic Principle

The maximal singularity-free workspace can be determined by the limit value h_{lim} of the half height h. However, it is very difficult to determine h_{lim} analytically. Hence, a numerical algorithm is presented to solve this problem. The basic principle of the algorithm can be stated as follows: increase the half height h from 0 until the boundary of the workspace touches the singularity surface. Referring to Fig. 5.3, the general procedure can be described as follows: first, set the half height h to 0. Then, increase h by one step Δh and verify whether any singularity exists inside the obtained workspace. If no singularity exists, continue to increase h using the same step size Δh. Otherwise, the used step size is too large for this step. Then, restore h to its previous value and reduce the step size Δh by one half. Then, increase h using the reduced step size Δh. Repeat this procedure until the half height h converges to its limit value h_{lim}. At this moment, the step size Δh becomes very small and the singularity-free workspace reaches the maximum. The detailed procedure is given in Appendix A.

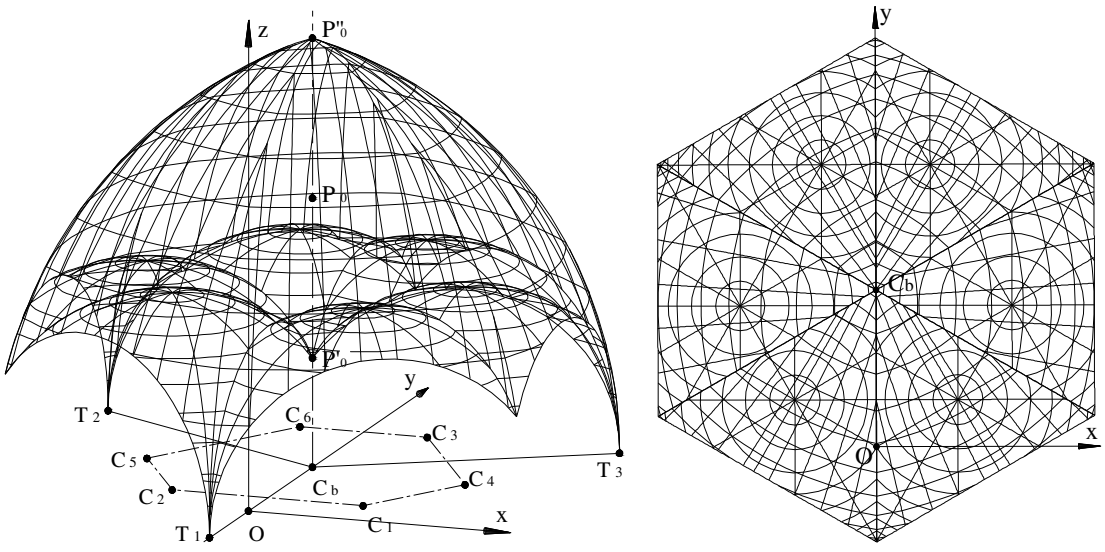

(a) 3D representation (b) Top view

Figure 5.4: The maximal singularity-free workspace around $P_0(0, \frac{2\sqrt[4]{3}}{3}, \frac{5}{4})$ in the reference orientation.

In order to make the above procedure more efficient, the initial value of the step size Δh is not necessarily very small. Actually, it can be chosen as follows (see Fig. 4.13): First, compute the intersection $P^*(x_0, y_0, z^*)$ of the line perpendicular to the base ($x = x_0, y = y_0$) and the singularity surface. If $z_0 > z^*$ as shown in Fig. 4.13, then $\Delta h = z_0 - z^*$. Otherwise, $\Delta h = min\{z_0, (z^* - z_0)\}$.

5.4.2 Workspace Volume

For every given half height h, there exists a workspace. To guarantee no singularity inside the obtained workspace, it is necessary to perform singularity verification. However, in the 3D Cartesian space $Oxyz$, both the workspace and the singularity surface are very complex. To verify the singularity in the 3D Cartesian space $Oxyz$ is not convenient. Comparatively, the singularity verification in a 2D workspace section with a given z is easy. If every workspace section is singularity-free, the entire workspace should be singularity-free.

However, since there are infinitely many workspace sections, it is impossible to verify all of them. One solution to this problem is to verify only a few workspace sections which are used to evaluate the workspace volume. The density of these workspace sections depends on the convergence precision. In other words, when the workspace volume converges to a given precision, the two neighbouring workspace sections can be regarded as sufficiently close. For a given half height h, the workspace volume V can be given as

$$V \approx \sum_{i=0}^{n-1} \frac{(A_i + A_{i+1})\Delta z}{2} \tag{5.3}$$

where A_i $(i = 0, 1, ..., n)$ is the area of the ith workspace section and Δz is the distance between two consecutive workspace sections.

However, the number n is hard to determine because the z coordinates of the highest and the lowest points of the workspace are unknown. Considering that point $P_0(x_0, y_0, z_0)$ always lies inside the workspace, a valid workspace section should exist in the plane with $z = z_0$. Hence, the workspace can be divided into two parts: the upside part with $z \geq z_0$ and the downside part with $z \leq z_0$. Take the upside part as

an example. Its volume V_1 can be given as

$$V_1 \approx \sum_{i=0}^{n_1-1} \frac{(A_i + A_{i+1})\Delta z}{2} \tag{5.4}$$

where A_0 is the area of the workspace section with $z = z_0$. The number n_1 can be determined as follows: for a given step size Δz, n_1 is the maximal number of steps for z to increase from z_0 until a value $(z_0 + n_1\Delta z)$ at which the corresponding workspace section vanishes, i.e., $A_{n_1} = 0$.

The volume V_2 of the downside part can be computed in a similar way. When V_1 and V_2 are available, their sum is the volume V of the entire workspace.

Hence, the computation of the workspace volume is twofold: when the half height h has not reached its limit value h_{lim}, the objective is to perform singularity verification. When h reaches its limit value h_{lim}, the volume of the maximal singularity-free workspace is obtained. Obviously, if h exceeds its limit value h_{lim}, the singularity curve will be found in some workspace section. The computation of the workspace volume will not continue. In this case, h is restored to its previous value and the step size Δh is reduced. Then, the new step size Δh is used to increase the half height h.

5.4.3 Workspace Section

To compute the workspace and verify whether any singularity exists inside the workspace, it is necessary to define the workspace section. If the workspace section exists in the plane with a given z, the sections of the maximal workspace sphere with radius ρ_i^{max} and the minimal workspace sphere with radius ρ_i^{min} are two circles respectively with radii as

$$\begin{cases} r_{iz}^{max} = \sqrt{(\rho_i^{max})^2 - (z - z_{ci})^2} \\ r_{iz}^{min} = \sqrt{(\rho_i^{min})^2 - (z - z_{ci})^2}. \end{cases} \tag{5.5}$$

There is a possible total of 12 circles in a section. Hence, the workspace section should be a region in which any point (x, y) has to satisfy the following condition:

$$r_{iz}^{min} \leq \sqrt{(x - x_{ci})^2 + (y - y_{ci})^2} \leq r_{iz}^{max}. \tag{5.6}$$

The boundary of the workspace section can be defined using the method given in [18].

5.4.4 Singularity Verification

The singularity verification can be implemented in the workspace section. The rationale is as follows: if no singularity exists inside every workspace section, as long as two neighbouring workspace sections are sufficiently close, it can be guaranteed under a given precision that no singularity exists inside the workspace.

In the workspace section plane with a given z, the singularity locus can be given by a quadratic curve as

$$ax^2 + bxy + cy^2 + dx + ey + g = 0 \tag{5.7}$$

where

$$\begin{cases} a = f_1 z + f_2 \\ b = f_3 z + f_4 \\ c = f_8 z + f_9 \\ d = f_5 z^2 + f_6 z + f_7 \\ e = f_{10} z^2 + f_{11} z + f_{12} \\ g = f_{13} z^3 + f_{14} z^2 + f_{15} z + f_{16}. \end{cases} \tag{5.8}$$

The singularity verification can be performed as follows: first, separate the singularity curve into several arcs by computing its intersections with the 12 section circles determined in the previous subsection. Then, verify whether any obtained arc lies inside the workspace section.

The singularity curve given by eq.(5.7) may be an ellipse ($b^2 - 4ac < 0$), a parabola ($b^2 - 4ac = 0$) or a hyperbola ($b^2 - 4ac > 0$). For a general quadratic curve, it is not convenient to compute its intersections with the 12 section circles. Even if all intersections are available, it is still difficult to order them and use them to separate the singularity curve into reasonable arcs. In order to solve this problem, a coordinate transformation is necessary (see Fig. 5.5 in which the case of an ellipse is not shown). The objective is to make the y_1 axis of the new frame Ox_1y_1 parallel to one axis of the ellipse, or the symmetric line of the parabola, or the symmetric line of the hyperbola

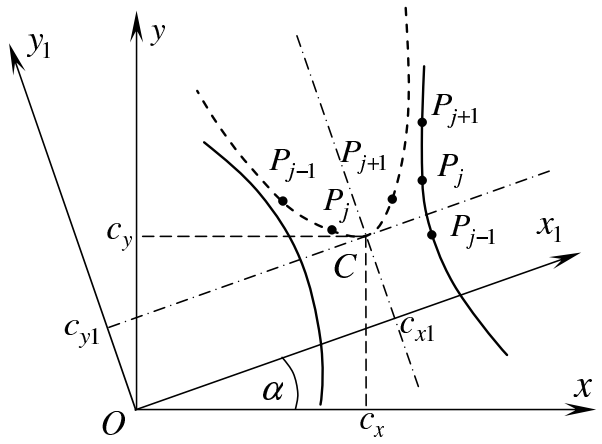

Figure 5.5: Coordinate transformation.

which separates the hyperbola into two independent curves. To achieve this point, the cross term in xy has to vanish.

Suppose the rotation angle is α, the coordinate relationship can be expressed as

$$\begin{cases} x = x_1 \cos\alpha - y_1 \sin\alpha \\ y = x_1 \sin\alpha + y_1 \cos\alpha. \end{cases} \tag{5.9}$$

By substituting eq.(5.9) into eq.(5.7), one obtains

$$a_1 x_1^2 + b_1 x_1 y_1 + c_1 y_1^2 + d_1 x_1 + e_1 y_1 + g = 0 \tag{5.10}$$

where

$$\begin{cases} a_1 = a\cos^2\alpha + b\sin\alpha\cos\alpha + c\sin^2\alpha \\ b_1 = (c-a)\sin 2\alpha + b\cos 2\alpha \\ c_1 = a\sin^2\alpha - b\sin\alpha\cos\alpha + c\cos^2\alpha \\ d_1 = d\cos\alpha + e\sin\alpha \\ e_1 = e\cos\alpha - d\sin\alpha. \end{cases} \tag{5.11}$$

To make the cross term vanish, b_1 should be equal to 0. From this, one obtains

$$\alpha = \frac{\arctan(\frac{b}{a-c})}{2} \qquad \alpha \in (-\pi/2, \pi/2). \tag{5.12}$$

Hence, after a rotation α of the coordinate frame, the singularity curve can be given in the new frame as

$$a_1 x_1^2 + c_1 y_1^2 + d_1 x_1 + e_1 y_1 + g = 0. \tag{5.13}$$

However, the above operation does not guarantee that the objective of the coordinate transformation has been achieved completely. The following cases still need to be addressed:

- $a_1c_1 = 0$:
  The singularity curve is a parabola. If $a_1 \neq 0$, $y_1 = -(a_1x_1^2 + d_1x_1 + g)/e_1$ which is a parabola with the symmetric line parallel to the y_1 axis, just as shown in Fig. 5.5. If $c_1 \neq 0$, the symmetric line will be parallel to the x_1 axis. To make the symmetric line parallel to the y_1 axis, the rotation angle needs to be changed by $\pi/2$. If $\alpha > 0$, reduce α by $\pi/2$. Otherwise, increase α by $\pi/2$.

- $a_1c_1 \neq 0$:
  In this case, eq.(5.13) can be re-written as

$$\frac{(x_1 - c_{x1})^2}{a_0} + \frac{(y_1 - c_{y1})^2}{b_0} = 1 \tag{5.14}$$

  where

$$\begin{cases} c_{x1} = -d_1/(2a_1) \\ c_{y1} = -e_1/(2c_1) \\ a_0 = (d_1^2/a_1 + e_1^2/c_1 - 4g)/(4a_1) \\ b_0 = (d_1^2/a_1 + e_1^2/c_1 - 4g)/(4c_1). \end{cases} \tag{5.15}$$

  If $a_0b_0 > 0$, the singularity curve is an ellipse. Otherwise, the singularity curve is a hyperbola. If $a_0 > 0$ and $b_0 < 0$, the hyperbola is just as shown in Fig. 5.5 and can be decomposed into two independent curves: $x_1 = c_{x1} + \sqrt{a_0[1 - (y_1 - c_{y1})^2/b_0]}$ and $x_1 = c_{x1} - \sqrt{a_0[1 - (y_1 - c_{y1})^2/b_0]}$. If $a_0 < 0$ and $b_0 > 0$, the symmetric line separating the hyperbola into two curves is parallel to the x_1 axis. To make it parallel to the y_1 axis, the rotation angle needs to be changed by $\pi/2$. If $\alpha > 0$, reduce α by $\pi/2$. Otherwise, increase α by $\pi/2$.

Besides, the 12 section circles also need to be transformed into the new frame using eq.(5.9). Then, the intersections of the singularity curve and the 12 section circles can be computed in the new frame Ox_1y_1. When all intersections are available, they can be easily ordered to separate the singularity curve into reasonable arcs. For an ellipse, the ordering operation can be performed using the angle between the line CP_j

and the x_1 axis. For a parabola, the ordering operation can be performed using the x_1 coordinate of every intersection. For a hyperbola, the ordering operation can be performed respectively with its two independent curves using the y_1 coordinate of every intersection. After the singularity curve is separated into several arcs, it is easy to verify whether any of these arcs is inside the workspace section or not.

5.5 Case Studies

In order to demonstrate the proposed algorithm, consider the MSSM architecture used in Chapter 4 Section 4.4, i.e., both the base and the platform are equilateral triangles with a size ratio $k = \frac{3}{5}$. Hence, the geometric parameters are: $t_1 = \frac{1}{\sqrt[4]{3}}$, $t_2 = \sqrt[4]{3}$, $t_3 = \frac{3}{5\sqrt[4]{3}}$ and $t_4 = \frac{3\sqrt[4]{3}}{5}$. Take the centroid of the platform as the considered point (end-effector) P. Its position in the mobile frame $O'x'y'z'$ is given as $\mathbf{p'} = [0, \frac{\sqrt[4]{3}}{5}, 0]^T$.

In practice, the interesting workspace of the end-effector should be located above the base and the most interesting position may be on the perpendicular line through the centroid $C_b(0, \frac{2\sqrt[4]{3}}{3}, 0)$ of the base. This line can be given as

$$\begin{cases} x = 0 \\ y = \frac{2\sqrt[4]{3}}{3} \approx 0.877 \\ z > 0. \end{cases} \tag{5.16}$$

For an equilateral triangle base of unit area, the length of the three sides is $\frac{2}{\sqrt[4]{3}} \approx 1.520$. Hence, the most interesting position for $P_0(x_0, y_0, z_0)$ may be at $(0, \frac{2\sqrt[4]{3}}{3}, \frac{5}{4})$.

5.5.1 Case 1: $\phi = \theta = \psi = 0°$

The given orientation is the reference orientation. In this case, the singularity surface becomes a plane which coincides with the Oxy plane. The six centres of the workspace spheres are listed in Table 5.2. It can be seen that all six centres lie exactly in the Oxy plane.

The determined maximal singularity-free workspace around $P_0(0, \frac{2\sqrt[4]{3}}{3}, \frac{5}{4})$ is represented in Fig. 5.4, which looks like an umbrella and is symmetric about the plane

Table 5.2: The six centres of the workspace spheres in the reference orientation.

C_i	1	2	3	4	5	6
x_{ci}	$\frac{3}{5\sqrt[4]{3}}$	$-\frac{3}{5\sqrt[4]{3}}$	$\frac{2}{5\sqrt[4]{3}}$	$\frac{1}{\sqrt[4]{3}}$	$-\frac{1}{\sqrt[4]{3}}$	$-\frac{2}{5\sqrt[4]{3}}$
y_{ci}	$\frac{\sqrt[4]{3}}{5}$	$\frac{\sqrt[4]{3}}{5}$	$\frac{6\sqrt[4]{3}}{5}$	$\frac{3\sqrt[4]{3}}{5}$	$\frac{3\sqrt[4]{3}}{5}$	$\frac{6\sqrt[4]{3}}{5}$
z_{ci}	0	0	0	0	0	0

Table 5.3: Numerical results in the reference orientation.

V	h_{lim}	Δh	Δz	z_{max}	z_{min}
2.758013	0.742702	1.907349×10^{-5}	1.160473×10^{-4}	1.992702	0.002724

perpendicular to the base through the y axis. The numerical results are listed in Table 5.3. The used initial step sizes are $\Delta h = 1.25$ and $\Delta z = 0.05$. The final step sizes become $\Delta h = 1.907349 \times 10^{-5}$ and $\Delta z = 1.160473 \times 10^{-4}$. The lowest points with $z = 0.002724$ are very close to the singularity surface (the Oxy plane). These points correspond to three of the six tips, not the point P_0' with $z_0' = 0.507298$. In this case, the leg length ranges for all six legs are the same: $[0.917823, 2.134458]$, because of the symmetry. The nominal leg length is $\rho_i^{nom} = 1.465452$ $(i = 1, 2, ..., 6)$.

As the singularity surface in the reference orientation becomes a plane coinciding with the Oxy plane, it is easy to determine the maximal singularity-free sphere around P_0 as shown in Fig. 5.1.

Figs. 5.6 and 5.7 respectively show the evolution of the volume V and the half height h of the maximal singularity-free workspace with respect to the prescribed position along the line given by eq.(5.16). Fig. 5.8 shows the corresponding evolution of the leg lengths. These figures show that there exists an inflexion at $z_0 \approx 0.899$. Besides, Fig. 5.8 shows that the increments of the maximal and minimal leg lengths from this position to the next position are very small. This phenomenon can be explained with Figs. 5.9 and 5.10.

For the six centres C_i $(i = 1, 2, ..., 6)$, Table 5.2 shows that C_1 and C_2, C_3 and C_6, as well as C_4 and C_5 are symmetric about the y axis (see Fig. 5.9). This is consistent with the layout of the six legs as shown in Fig. 4.12. It is easy to verify that the distances from the six centres to the centroid of the base are exactly equal to one

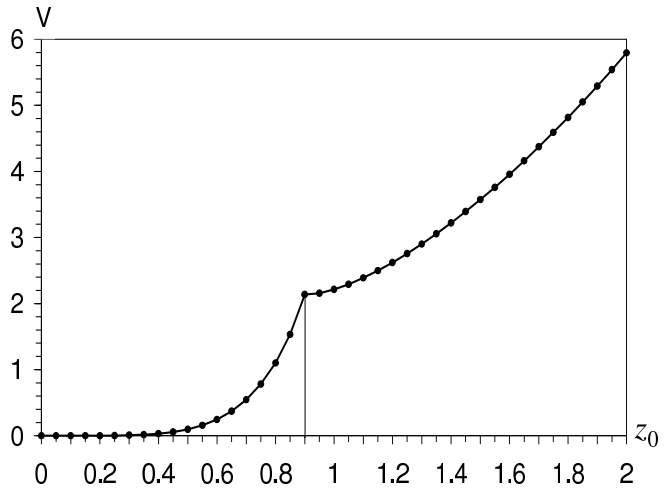

Figure 5.6: The evolution of volume V with respect to z_0 ($\phi = \theta = \psi = 0°$).

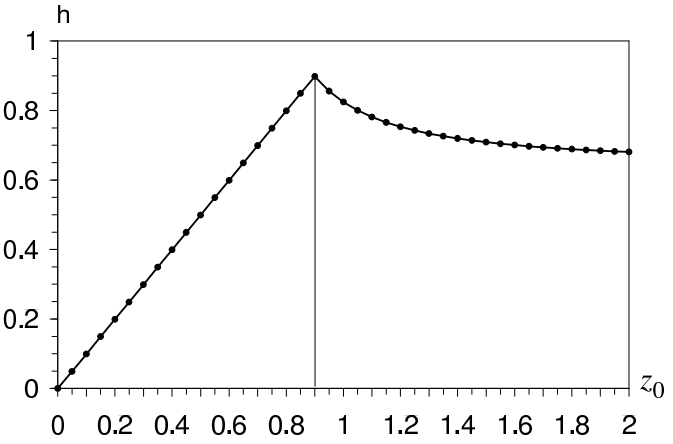

Figure 5.7: The evolution of half height h with respect to z_0 ($\phi = \theta = \psi = 0°$).

another. Hence, the six centres lie on a circle centred at C_b. To make the workspace lie at the upside of the base, the bottom of the workspace should be closed in the Oxy plane. This requires that the minimal leg length $\rho_i^{min} \geq \overline{C_iC_b}$. When the minimal leg length takes $\overline{C_iC_b}$, the minimal workspace sphere centred at C_i will have radius $\overline{C_iC_b}$. The sections of the six minimal workspace spheres in the Oxy plane are six circles which intersect one another at C_b, N_{12}, N_{25}, N_{56}, N_{36}, N_{34} and N_{14}. Hence, the region $N_{12}N_{25}N_{56}N_{36}N_{34}N_{14}N_{12}$ defined by six arcs is a closed region which contains all six minimal circles. Similarly, the sections of the six maximal workspace spheres (taking ρ_i^{max} as their radii) in the Oxy plane are also six circles. Their common region are defined by six arcs $M_{12}M_{25}M_{56}M_{36}M_{34}M_{14}M_{12}$.

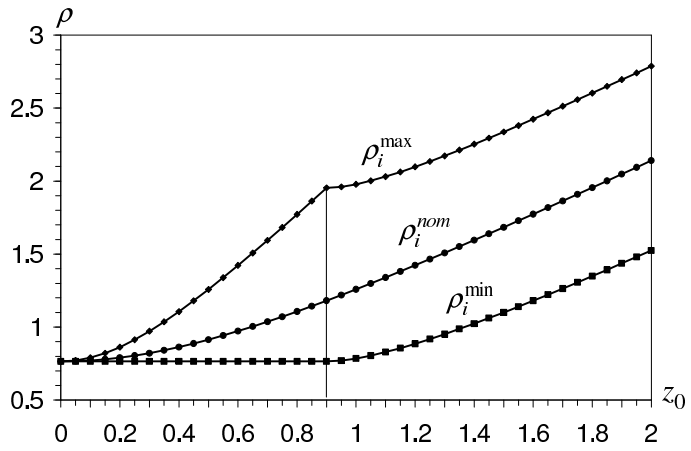

Figure 5.8: The evolution of leg lengths with respect to z_0 ($\phi = \theta = \psi = 0°$).

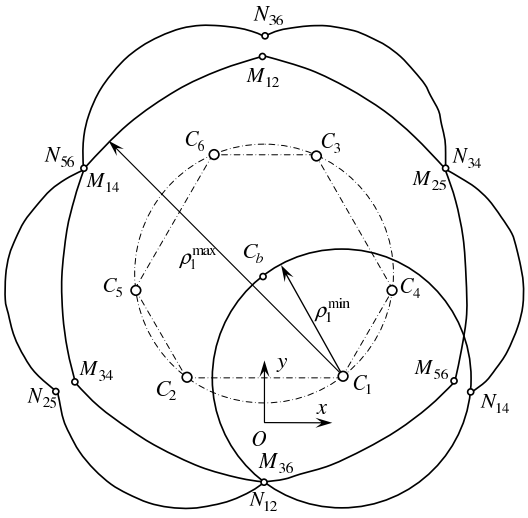

Figure 5.9: Singularity-free workspace analysis.

If the interesting position P_0 is not high, the minimal leg lengths do not need to increase because, in the Oxy plane, the region $M_{12}M_{25}M_{56}M_{36}M_{34}M_{14}M_{12}$ is completely inside the region $N_{12}N_{25}N_{56}N_{36}N_{34}N_{14}N_{12}$. If P_0 goes up and makes the maximal leg length exceed the distance $\overline{C_1N_{56}}$ ($= \overline{C_2N_{34}}$), the minimal leg lengths have to increase. Otherwise, in the Oxy plane, the region $M_{12}M_{25}M_{56}M_{36}M_{34}M_{14}M_{12}$ will not be contained completely by the region $N_{12}N_{25}N_{56}N_{36}N_{34}N_{14}N_{12}$. As a result, part of the obtained workspace will lie below the base.

The distance between C_i and C_b is given by 0.765. Hence, $\overline{C_1N_{56}}$ or $\overline{C_2N_{34}}$ can be computed as 1.954. With this value, the height of point P_0'' can be determined as

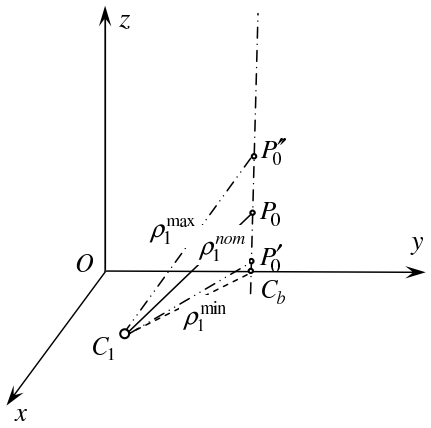

Figure 5.10: Leg length analysis.

1.798. Accordingly, the height (z_0) of P_0 is 0.899 which is exactly the z coordinate of the inflexions in Figs. 5.6–5.8.

Referring to Fig. 5.10, take leg 1 as an example. When P_0 goes up by Δz_0 after it reaches 0.899, the point P_0' begins to go up by $\Delta z_0'$. The increment of the half height h will be Δh ($= \Delta z_0 - \Delta z_0'$). And the increment of the height of point P_0'' will be $\Delta z_0''$ ($= 2\Delta z_0 - \Delta z_0'$). If $\Delta h \geq 0$, i.e., $\Delta z_0 \geq \Delta z_0'$, the maximal leg length ρ_1^{max} will exceed $\overline{C_1 N_{56}}$. However, as the angle $\angle P_0'' C_1 C_b$ is greater than the angle $\angle P_0' C_1 C_b$, the maximal leg length ρ_1^{max} will increase faster than the minimal leg length ρ_1^{min}. To make the leg length ρ_1^{max} be not longer than $\overline{C_1 N_{56}}$, Δh has to be less than 0, i.e., $\Delta z_0 < \Delta z_0'$. This is exactly as shown by Fig. 5.7. As a result, the evolutions of V as well as ρ_i^{max} and ρ_i^{min} increase slowly.

5.5.2 Case 2: $\phi = 30°$, $\theta = 45°$ and $\psi = 0°$

In this case, the singularity surface in the 3D Cartesian space $Oxyz$ is shown in Fig. 4.13. It can be seen that the singularity surface intersects the line given by eq.(5.16) at $z^* \approx 0.577$. The six centres of the workspace spheres are listed in Table 5.4. It can be seen that the six centres do not lie in one plane because they lie on the singularity surface which is no longer a plane. C_1 and C_6, C_4 and C_5 respectively lie in two different planes which are parallel to and lower than the base while C_2 and C_3 lie in another plane which is parallel to and higher than the base.

Table 5.4: The six centres of the workspace spheres in the orientation with $\phi = 30°$, $\theta = 45°$, $\psi = 0°$.

C_i	1	2	3	4	5	6
x_{ci}	0.415	-0.229	0.531	0.574	-0.946	-0.344
y_{ci}	0.228	0.228	1.544	0.860	0.860	1.544
z_{ci}	-0.229	0.415	0.415	-0.186	-0.186	-0.229

Table 5.5: Numerical results in the orientation with $\phi = 30°$, $\theta = 45°$, $\psi = 0°$.

V	h_{lim}	Δh	Δz	z_{max}	z_{min}
0.063893	0.233527	1.192093×10^{-6}	5.838186×10^{-4}	1.483527	1.016473

Table 5.6: Leg lengths in the orientation with $\phi = 30°$, $\theta = 45°$, $\psi = 0°$.

No.	1	2	3	4	5	6
ρ_i^{nom}	1.668144	1.082058	1.192633	1.546573	1.719760	1.658730
ρ_i^{max}	1.878339	1.270895	1.366271	1.765551	1.919077	1.869984
ρ_i^{min}	1.465033	0.914109	1.042650	1.332545	1.530151	1.454304

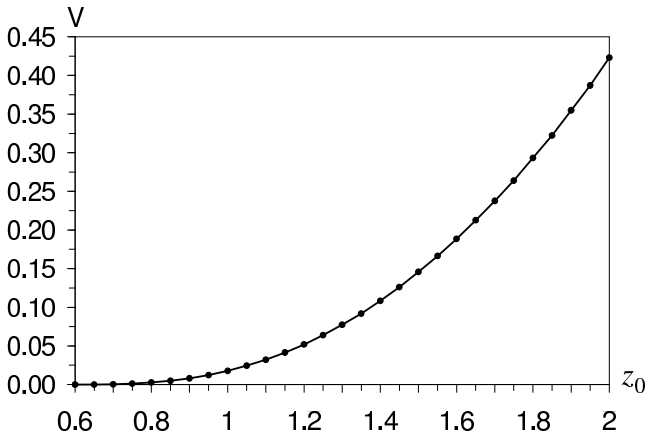

Figure 5.11: The evolution of volume V with respect to z_0 ($\phi = 30°$, $\theta = 45°$, $\psi = 0°$).

The determined maximal singularity-free workspace around $P_0(0, \frac{2\sqrt[4]{3}}{3}, \frac{5}{4})$ is represented in Fig. 5.2, which looks like a diamond and is no longer symmetric. The numerical results are listed in Table 5.5. The used initial step sizes are $\Delta h = \frac{5}{4} - 0.577 = 0.673$ and $\Delta z = 0.05$. The final step sizes become $\Delta h = 1.192093 \times 10^{-6}$ and $\Delta z = 5.838186 \times 10^{-4}$. The leg lengths are listed in Table 5.6. It can be seen that in this

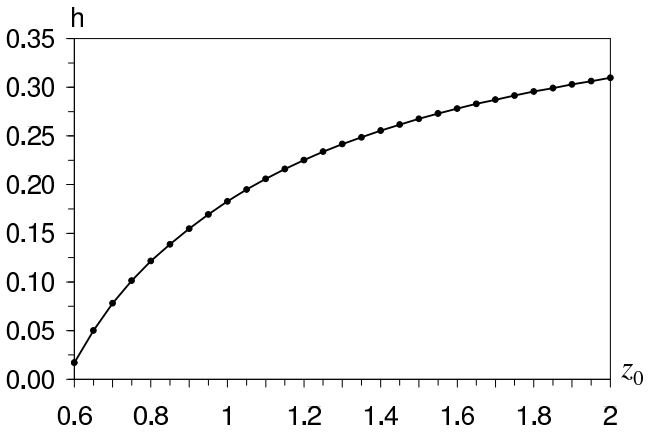

Figure 5.12: The evolution of half height h with respect to z_0 ($\phi = 30°$, $\theta = 45°$, $\psi = 0°$).

case, the leg length ranges for all six legs are different from one to another because of the effect of the orientation. Comparing with Case 1, the volume of the maximal singularity-free workspace around $P_0(0, \frac{2\sqrt[4]{3}}{3}, \frac{5}{4})$ in this case becomes very small.

Considering that the singularity surface intersects the line given by eq.(5.16) at $z^* = 0.577$, the maximal singularity-free workspace around position P_0 with ($z_0 \leq 0.577$) is very small and of less practical interest. Figs. 5.11 and 5.12 respectively show the evolution of the volume and the half height of the maximal singularity-free workspace with respect to the prescribed position with $0.6 \leq z_0 \leq 2$ and Fig. 5.13 shows the corresponding evolution of the leg lengths. These figures show that at the position with $z_0 = 0.6$, the volume V and the half height h of the maximal singularity-free workspace is close to 0 and the maximal and minimal leg lengths for each leg are close to the nominal leg length. The reason is that this position is very close to the intersection P^*.

5.5.3 Computational Cost

The presented algorithm was programmed using Visual C++ 6.0 in a Windows XP environment. The CPU of the used computer is a Pentium IV with 2.4 GHz. The computational time at the given convergence precision, $\varepsilon = 10^{-4}$, is about 4 seconds. If the convergence precision is improved to $\varepsilon = 10^{-5}$, the computational time will be

approximately 7 seconds for case 2, for example. However, the results do not change in the first 6 digits after the decimal point. For instance, the value of h_{lim} will change from

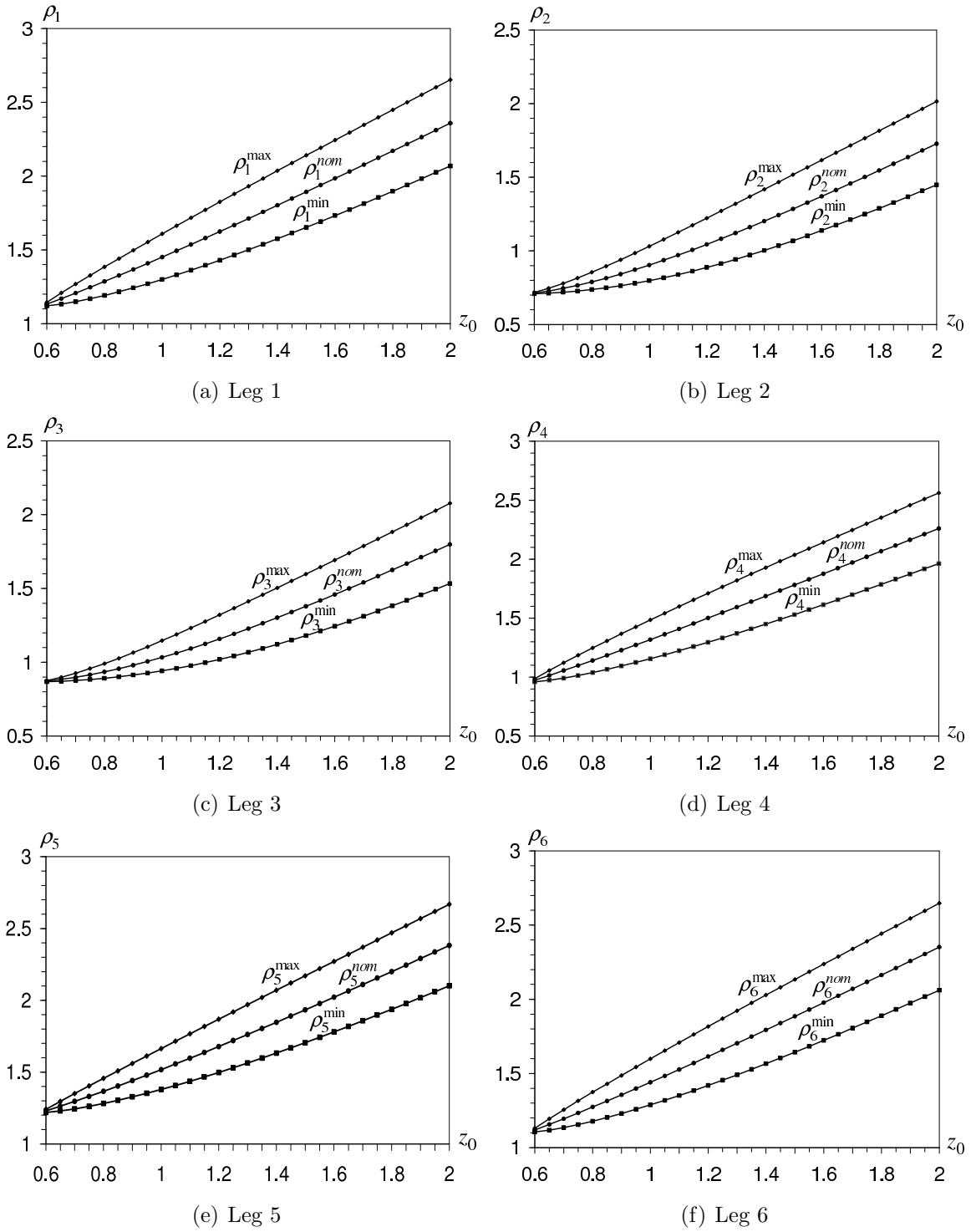

Figure 5.13: The evolution of leg lengths with respect to z_0 ($\phi = 30°$, $\theta = 45°$, $\psi = 0°$).

0.2335274220 to 0.2335274965. The increment is only 7.45×10^{-8}. Hence, $\varepsilon = 10^{-4}$ is already a good convergence precision with an acceptable computational cost.

5.6 Conclusions

This chapter presents a general numerical algorithm to determine the maximal singularity-free workspace around a prescribed point P_0 for a given orientation for the MSSM Gough-Stewart platform. Additionally, the corresponding leg length ranges which lead to the maximal singularity-free workspace can also be determined. Case studies with different orientations are performed to demonstrate the presented algorithm. The obtained results can be applied to the geometric design or parameter (leg length) setup of the MSSM parallel robots.

Chapter 6

Orientation Optimization

Based on a given orientation, Chapter 5 presented a general numerical algorithm to determine the maximal singularity-free workspace around a point of interest for the MSSM Gough-Stewart platform. This chapter focuses on analyzing the effects of the orientation angles on the "orientation-based maximal singularity-free workspace" in order to determine the optimal orientation. Besides the numerical algorithm presented in Chapter 5 and used for general orientations, this chapter presents an analytic algorithm to determine the maximal singularity-free workspace in an orientation with $\phi = \theta = 0^\circ$ and $\psi \neq \pm 90^\circ$, because the singularity surface in these orientations becomes a plane coinciding with the base plane. The results show that the maximal singularity-free workspace in some orientations can be larger than that in the reference orientation ($\phi = \theta = \psi = 0^\circ$). However, the global optimal orientation is difficult to determine. Only an approximate optimal orientation is available.

6.1 Introduction

A general numerical algorithm was presented in Chapter 5 to determine the maximal singularity-free workspace around a prescribed point P_0 as well as the corresponding leg length ranges in a given orientation for the MSSM Gough-Stewart platform. In this context, the term "maximal" means that when the boundary of the singularity-free workspace just touches the singularity surface at some point(s), the singularity-free workspace reaches its maximal status. If the orientation changes, this "maximal" singularity-free workspace changes accordingly. Hence, what is determined in Chapter 5 is actually the "orientation-based maximal singularity-free workspace", because it is based on a given orientation. Obviously, the "orientation-based maximal singularity-free workspace" is a function of the orientation.

This chapter focuses on analyzing the effect of the orientation on the "orientation-based maximal singularity-free workspace" around a point of interest P_0 for the MSSM Gough-Stewart platform. The objective is to determine the optimal orientation that maximizes the "orientation-based maximal singularity-free workspace". Hence, the maximal singularity-free workspace in the optimal orientation is the maximum of the "orientation-based maximal singularity-free workspaces".

In the context of a given orientation, the "orientation-based maximal singularity-free workspace" will be simply referred to as the maximal singularity-free workspace for concise description as long as no confusion exists. However, in the context of orientation optimization, the difference between these two concepts should be highlighted.

6.2 Point of Interest and Considered Architecture

The singularity-free workspace determined in Chapter 5 depends on the prescribed point P_0, the orientation of the platform as well as the geometric parameters. If all these factors are taken into consideration at the same time, the problem becomes too complex to be solved. Obviously, for the problem of orientation optimization, the orientation angles (ϕ, θ, ψ) should be the variables to be optimized. The other factors such as the point of interest P_0 and the geometric parameters of the platform can be

prescribed. Now the problem becomes: which point and which architecture should be chosen for the orientation optimization.

In practice, the most interesting point P_0 should lie above the base and on the perpendicular line through the centroid $C_b(x_{cb}, y_{cb}, 0)$ of the base. Referring to Fig. 4.12, $x_{cb} = 0$ and $y_{cb} = \frac{2}{3}t_2$. For a base of unit area, $\frac{5}{4}$ is a reasonable height for the point of interest P_0. Hence, point P_0 can be chosen as $P_0(0, \frac{2}{3}t_2, \frac{5}{4})$. This choice is arbitrary but reasonable.

The geometric parameters heavily affect the singularity-free workspace. For different architectures, the optimal orientation may be different. However, the highlight in this chapter is the orientation optimization. Hence, any architecture with reasonable geometric parameters can be taken as the considered architecture. In this chapter, the used architecture is the same as that used in Chapter 4 Section 4.4, i.e., both the base and the platform are equilateral triangles with a size ratio $k = \frac{3}{5}$. Hence, the geometric parameters are: $t_1 = \frac{1}{\sqrt[4]{3}}$, $t_2 = \sqrt[4]{3}$, $t_3 = \frac{3}{5\sqrt[4]{3}}$ and $t_4 = \frac{3\sqrt[4]{3}}{5}$. Besides, the centroid of the platform is taken as the considered point P. Its position in the mobile frame $O'x'y'z'$ is given as $\mathbf{p}' = [0, \frac{\sqrt[4]{3}}{5}, 0]^T$.

Therefore, the objective of the orientation optimization problem can be described as follows: *Maximize the "orientation-based maximal singularity-free workspace" around the point of interest P_0 by optimizing the orientation angles of the MSSM Gough-Stewart platform.*

6.3 Effects of the Orientation Angles

6.3.1 Effect of ϕ

In order to investigate the effect of the orientation angle ϕ, set θ and ψ to 0. In this case, the singularity equation given by eq.(4.15) becomes

$$f_{12}y^2z + f_{13}y^2 + f_{14}yz^2 + f_{15}yz + f_{16}y + f_{17}z^3 + f_{18}z^2 + f_{19}z + f_{20} = 0 \qquad (6.1)$$

where $f_i = f_i(\phi)$ $(i = 12, 13, ..., 20)$ are given as follows:

$$\begin{cases} f_{12} = -8t_1^2 t_2 t_3 t_4^2 s^2\phi \\ f_{13} = \frac{8}{3} t_1^2 t_2 t_3 t_4^3 s^3\phi \\ f_{14} = 8t_1 t_2 t_3 t_4 s\phi(2t_1 t_4 c\phi + t_2 t_3) \\ f_{15} = -\frac{8}{3} t_1 t_2 t_3 t_4^2 s^2\phi(2t_1 t_4 c\phi - 3t_1 t_2 - t_2 t_3) \\ f_{16} = -\frac{8}{9} t_1 t_2^2 t_3 t_4^3 s^3\phi(3t_1 + 2t_3) \\ f_{17} = -8t_1 t_2 t_3 t_4 c\phi(t_1 t_4 c\phi + t_2 t_3) \\ f_{18} = \frac{8}{3} t_1 t_2 t_3 t_4 s\phi[t_1 t_4^2 c^2\phi - 3t_2^2 t_3 - t_2 t_4(3t_1 + t_3)c\phi] \\ f_{19} = \frac{8}{9} t_1 t_2^2 t_3 t_4^2 s^2\phi(3t_1 t_4 c\phi + 2t_3 t_4 c\phi - 3t_2 t_3) \\ f_{20} = \frac{16}{3} t_1 t_2^3 t_3^2 t_4^3 s^3\phi. \end{cases} \tag{6.2}$$

For a given ϕ, eq.(6.1) describes a singularity surface in the 3D Cartesian space $Oxyz$. Since there is no term in x, the singularity surface is a ruled surface with a generator parallel to the x axis as shown in Fig. 6.1(a). The six centres of the workspace spheres are listed in Table 6.1. From this table, it can be seen that in an orientation with $\theta = \psi = 0°$, four centres C_1, C_2, C_3 and C_6 lie on the same plane parallel to the base and two centres C_4 and C_5 lie on the other parallel plane, see Fig. 6.1(b).

Using the algorithm developed in Chapter 5, the evolution of the volume V of the "orientation-based maximal singularity-free workspace" as a function of ϕ is shown

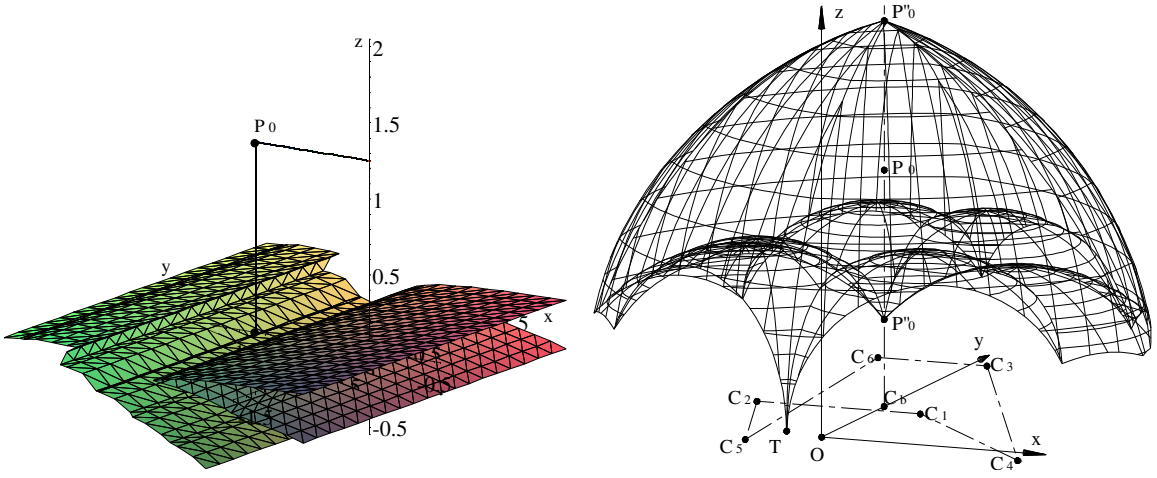

(a) Singularity surface (b) Maximal singularity-free workspace

Figure 6.1: The singularity surface and maximal singularity-free workspace in the orientation with $\phi = 25.084°$ and $\theta = \psi = 0°$.

Table 6.1: The six centres of the workspace spheres in an orientation with $\theta = \psi = 0°$.

C_i	x_{ci}	y_{ci}	z_{ci}
1	t_3	$t_4c\phi/3$	$t_4s\phi/3$
2	$-t_3$	$t_4c\phi/3$	$t_4s\phi/3$
3	$t_1 - t_3$	$t_2 + t_4c\phi/3$	$t_4s\phi/3$
4	t_1	$t_2 - 2t_4c\phi/3$	$-2t_4s\phi/3$
5	$-t_1$	$t_2 - 2t_4c\phi/3$	$-2t_4s\phi/3$
6	$-(t_1 - t_3)$	$t_2 + t_4c\phi/3$	$t_4s\phi/3$

in Fig. 6.2. From this figure, it can be seen that for some values of ϕ, the maximal singularity-free workspace can be larger than that in the reference orientation ($\phi = \theta = \psi = 0°$). When $\phi \approx 25.084°$ (this point can be determined using a one-dimensional optimization algorithm, e.g. the golden section search), the "orientation-based maximal singularity-free workspace" reaches a maximum (3.154371) as shown in Fig. 6.1(b).

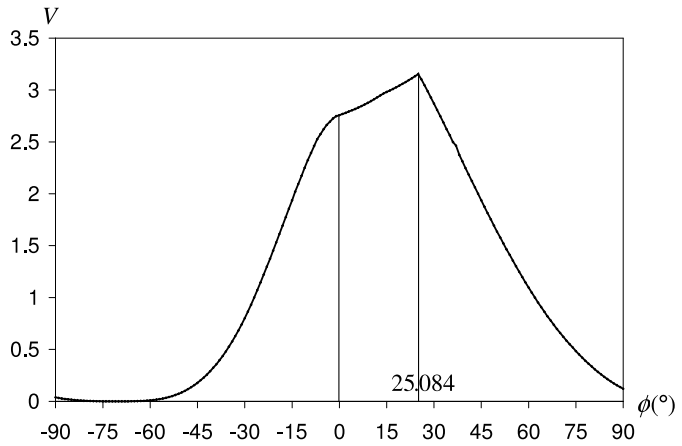

Figure 6.2: Volume V as a function of ϕ ($\theta = \psi = 0°$).

6.3.2 Effect of θ

In order to investigate the effect of the orientation angle θ, set ϕ and ψ to 0. In this case, the singularity equation given by eq.(4.15) becomes

$$f_3x^2z + f_7xy + f_8xz^2 + f_{10}x + f_{15}yz + f_{17}z^3 + f_{19}z = 0 \tag{6.3}$$

where $f_i = f_i(\theta)$ $(i = 3, 7, 8, 10, 15, 17, 19)$ are given as follows:

$$\begin{cases} f_3 = -8t_1t_2^2t_3^2t_4s^2\theta \\ f_7 = 8t_1^2t_2t_3^3t_4s^3\theta \\ f_8 = -8t_1t_2t_3t_4s\theta(t_1t_4 + 2t_2t_3c\theta) \\ f_{10} = -\frac{8}{3}t_1^2t_2t_3^3t_4s^3\theta(3t_2 - 2t_4) \\ f_{15} = 8t_1^2t_2t_3^2t_4s^2\theta(t_1 + t_3c\theta) \\ f_{17} = -8t_1t_2t_3t_4c\theta(t_1t_4 + t_2t_3c\theta) \\ f_{19} = -\frac{8}{3}t_1^2t_2t_3^2t_4s^2\theta[t_1t_4 + (3t_2 - 2t_4)t_3c\theta]. \end{cases} \tag{6.4}$$

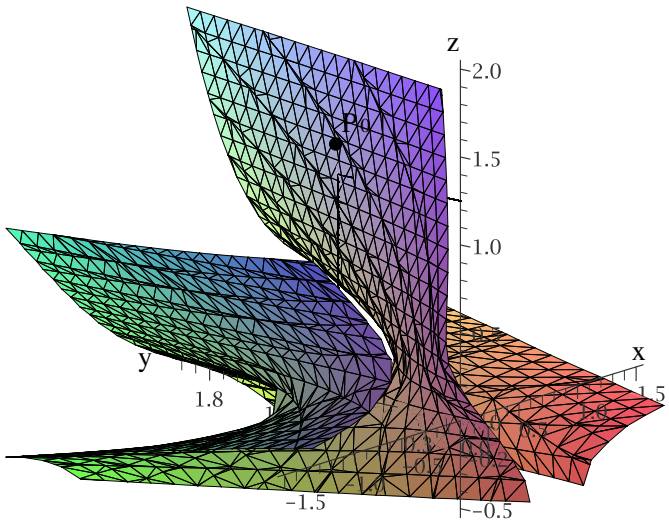

Figure 6.3: The singularity surface in the orientation with $\theta = 81.442°$ and $\phi = \psi = 0°$.

Table 6.2: The six centres of the workspace spheres in an orientation with $\phi = \psi = 0°$.

C_i	x_{ci}	y_{ci}	z_{ci}
1	$t_3c\theta$	$t_4/3$	$-t_3s\theta$
2	$-t_3c\theta$	$t_4/3$	$t_3s\theta$
3	$t_1 - t_3c\theta$	$t_2 + t_4/3$	$t_3s\theta$
4	t_1	$t_2 - 2t_4/3$	0
5	$-t_1$	$t_2 - 2t_4/3$	0
6	$-(t_1 - t_3c\theta)$	$t_2 + t_4/3$	$-t_3s\theta$

For a given θ, eq.(6.3) describes a singularity surface in the 3D Cartesian space $Oxyz$

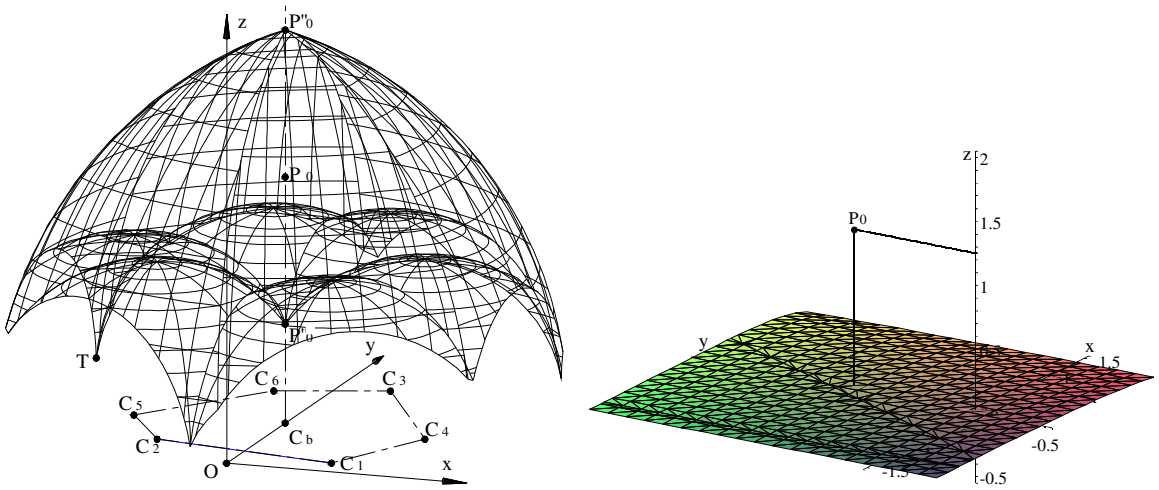

(a) Maximal singularity-free workspace (b) Singularity surface

Figure 6.4: The maximal singularity-free workspace and singularity surface in the orientation with $\theta = 3.042^\circ$ and $\phi = \psi = 0^\circ$.

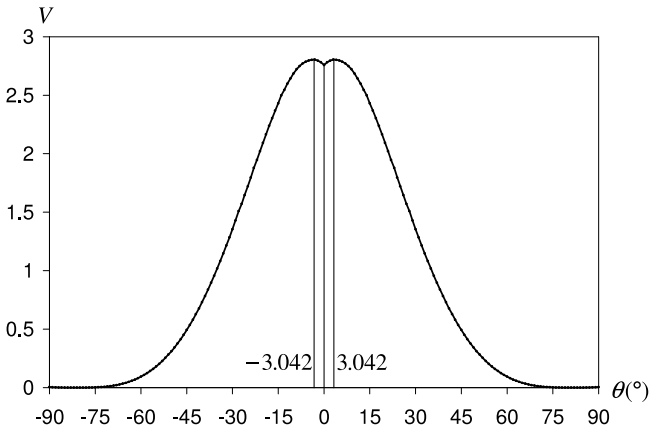

Figure 6.5: Volume V as a function of θ ($\phi = \psi = 0^\circ$).

as shown in Fig. 6.3. The six centres of the workspace spheres are listed in Table 6.2. From this table, it can be seen that in an orientation with $\phi = \psi = 0^\circ$, C_1 and C_6, C_2 and C_3 respectively lie on two different planes which are parallel to the base and the other two centres C_4 and C_5 lie on the base plane, see Fig. 6.4(a).

Using the algorithm developed in Chapter 5, the evolution of the volume V of the "orientation-based maximal singularity-free workspace" as a function of θ is shown in Fig. 6.5. From this figure, it can be seen that the obtained curve is symmetric about $\theta = 0^\circ$. This phenomenon is not difficult to understand because the MSSM Gough-

Stewart platform is symmetric about the y axis, see Fig. 4.12. When $\theta \approx \pm 3.042°$, the "orientation-based maximal singularity-free workspace" reaches a maximum (2.800493). Figs. 6.4(a) and 6.4(b) respectively show the maximal singularity-free workspace and singularity surface in the orientation with $\theta = 3.042°$ and $\phi = \psi = 0°$. When $\theta \approx \pm 81.442°$, the singularity-free workspace vanishes. This means that in these two orientations, the singularity surface passes through the prescribed point P_0, see Fig. 6.3.

6.3.3 Effect of ψ

In general, the singularity surface is very complex, as shown in Figs. 4.13, 6.1(a) and 6.3. It is very difficult to find an analytic approach to determine the contact point(s) between the boundary of the singularity-free workspace and the singularity surface in order to determine the maximal singularity-free workspace in a given orientation. This is why a general numerical search algorithm was presented in Chapter 5.

However, in the orientations with $\phi = \theta = 0°$ and $\psi \neq \pm 90°$, the singularity surface becomes a plane coinciding with the base plane. The coordinates of the six centres of the workspace spheres are listed in Table 6.3. From this table, it can be seen that the six centres of the workspace spheres lie on the base plane as shown in Fig. 6.6. It is therefore possible to develop an analytic method to determine the maximal singularity-free workspace in any of these orientations.

In order to determine the contact point(s) between the boundary of the singularity-

Table 6.3: The six centres of the workspace spheres in an orientation with $\phi = \theta = 0°$ and $\psi \neq \pm 90°$.

C_i	x_{ci}	y_{ci}	z_{ci}
1	$t_3 c\psi - t_4 s\psi/3$	$t_3 s\psi + t_4 c\psi/3$	0
2	$-t_3 c\psi - t_4 s\psi/3$	$-t_3 s\psi + t_4 c\psi/3$	0
3	$t_1 - t_3 c\psi - t_4 s\psi/3$	$t_2 - t_3 s\psi + t_4 c\psi/3$	0
4	$t_1 + 2t_4 s\psi/3$	$t_2 - 2t_4 c\psi/3$	0
5	$-t_1 + 2t_4 s\psi/3$	$t_2 - 2t_4 c\psi/3$	0
6	$-t_1 + t_3 c\psi - t_4 s\psi/3$	$t_2 + t_3 s\psi + t_4 c\psi/3$	0

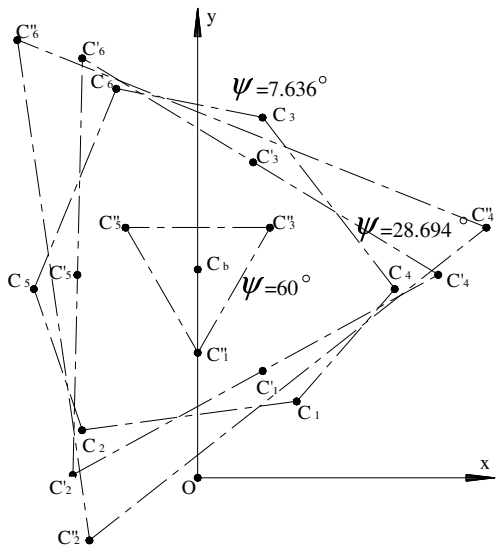

Figure 6.6: The six centres of the workspace spheres for three different values of ψ with $\phi = \theta = 0°$.

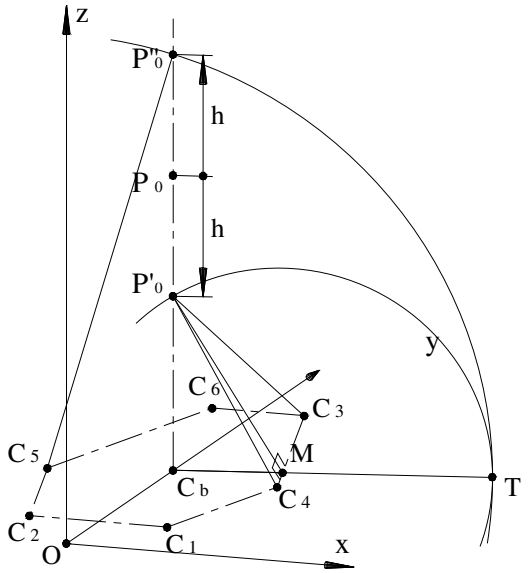

Figure 6.7: Determination of the contact point(s).

free workspace and the singularity surface, it is necessary to consider the distribution of the six centres. Referring to Fig. 6.6, for different values of ψ, the distributions of the six centres can be different. If the six centres form a convex hexagon as shown in Fig. 6.7, the contact point T can be determined by the minimal workspace spheres respectively centred at the two ends of one side and the maximal workspace sphere centred at another vertex of the convex hexagon, see Figs. 6.7 and 6.8(a). If the six centres do not

form a convex hexagon ($C_1'C_2'C_5'C_6'C_3'C_4'$ and $C_1''C_2''C_5''C_6''C_3''C_4''$ in Fig. 6.6), the contact point(s) will depend on the maximal convex polygon formed by some of the six centres, see Figs. 6.8(b) and 6.8(c). Hence, the maximal convex polygon should be determined first as follows:

- Compute the centroid C^0 of the six centres:

$$\begin{cases} x_c^0 = \frac{1}{6}\sum_{i=1}^{6} x_{ci} \\ y_c^0 = \frac{1}{6}\sum_{i=1}^{6} y_{ci}. \end{cases} \tag{6.5}$$

- Compute the distance from every centre C_i to C^0:

$$d_i = \sqrt{(x_{ci} - x_c^0)^2 + (y_{ci} - y_c^0)^2}. \tag{6.6}$$

- Select the three centres (say $C_4C_6C_2$ in Fig. 6.6) with the longest distances to form a triangle because the convex polygon should consist of at least three vertices. Then, compute the centroid C^Δ of this initial triangle $\Delta C_4C_6C_2$:

$$\begin{cases} x_c^\Delta = (x_{c2} + x_{c4} + x_{c6})/3 \\ y_c^\Delta = (y_{c2} + y_{c4} + y_{c6})/3. \end{cases} \tag{6.7}$$

- Check whether the other three centres lie outside the initial triangle or not. If yes, the number of the vertices of the convex polygon increases by one. For instance, C_3 and C^Δ lie on the different sides of $\overline{C_4C_6}$. Hence, C_3 should be a new vertex. The vertices of the new formed polygon can be ordered by the orientation angle α_i of every vertex with respect to the new centroid. For instance, after C_3 is added, the new formed convex hexagon should be $C_4C_3C_6C_2$.

For the considered architecture (the platform is similar to the base), the maximal convex polygon may be a hexagon or a triangle. But when the platform is not similar to the base, the number of the vertices of the maximal convex polygon may be 4 or 5.

After the maximal convex polygon formed by N ($3 \leq N \leq 6$) centres is determined, the maximal singularity-free workspace in a given orientation with $\phi = \theta = 0^\circ$ and $\psi \neq \pm 90^\circ$ can be determined by the following algorithm.

As the contact point lies on the singularity plane, its z coordinate vanishes. Suppose the contact point $T(x, y, 0)$ is the intersection of the singularity plane and two minimal

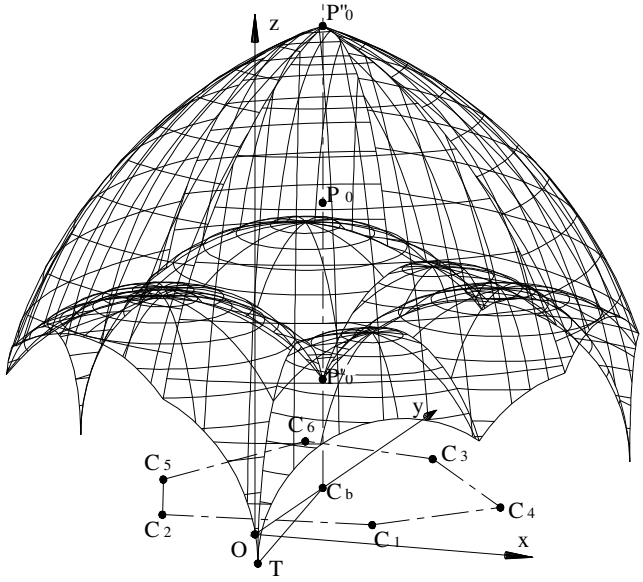

(a) $\psi = 7.636°$ and $\phi = \theta = 0°$.

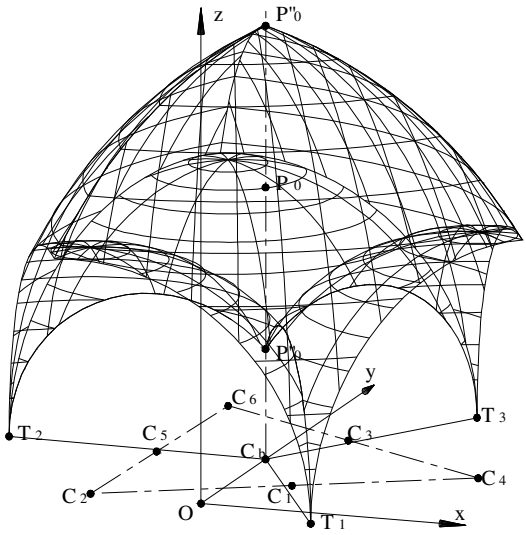

(b) $\psi = 28.69°$ and $\phi = \theta = 0°$.

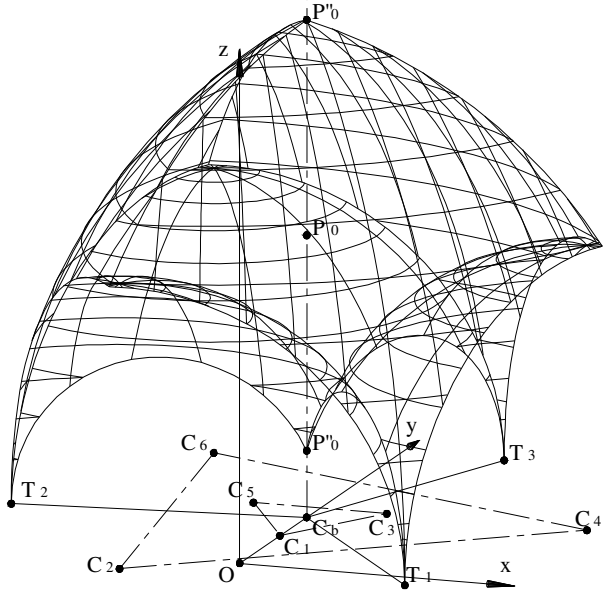

(c) $\psi = 60°$ and $\phi = \theta = 0°$.

Figure 6.8: The maximal singularity-free workspaces in three different orientations.

workspace spheres respectively centred at two neighbouring vertices C_i and C_j of the maximal convex polygon (In the case of Fig. 6.7, these two centres are respectively C_3 and C_4). Considering the minimal workspace sphere centred at C_i, its radius ρ_i^{min} should satisfy the condition, $\rho_i^{min} = \overline{C_i P_0'} = \overline{C_i T}$. From this, one obtains

$$x_{ci}^2 + (y_{cb} - y_{ci})^2 + (z_0 - h)^2 = (x - x_{ci})^2 + (y - y_{ci})^2 \tag{6.8}$$

where h is the half height of the singularity-free workspace.

Similarly, for the minimal workspace sphere centred at C_j, $\rho_j^{min} = \overline{C_jP_0'} = \overline{C_jT}$. One obtains

$$x_{cj}^2 + (y_{cb} - y_{cj})^2 + (z_0 - h)^2 = (x - x_{cj})^2 + (y - y_{cj})^2. \tag{6.9}$$

On the other hand, $T(x, y, 0)$ should also lie on one of the maximal workspace spheres, say one centred at vertex C_k of the maximal convex polygon (In the case of Fig. 6.7, C_k is C_5.) Hence, the radius ρ_k^{max} should satisfy the condition, $\rho_k^{max} = \overline{C_kP_0''} = \overline{C_kT}$. From this, one obtains

$$x_{ck}^2 + (y_{cb} - y_{ck})^2 + (z_0 + h)^2 = (x - x_{ck})^2 + (y - y_{ck})^2. \tag{6.10}$$

There are three unknowns (x, y, h) in eqs.(6.8), (6.9) and (6.10). Subtracting eq.(6.9) from eq.(6.8), one obtains

$$x = my + n \tag{6.11}$$

where

$$\begin{cases} m = \frac{y_{cj} - y_{ci}}{x_{ci} - x_{cj}} \\ n = \frac{y_{ci} - y_{cj}}{x_{ci} - x_{cj}} y_{cb}. \end{cases} \tag{6.12}$$

Subtracting eq.(6.10) from eq.(6.8), the half height h can be expressed as

$$h = \frac{(x_{ci} - x_{ck})x + (y_{ci} - y_{ck})y}{2z_0} + \frac{(y_{ck} - y_{ci})y_{cb}}{2z_0}. \tag{6.13}$$

Substituting eq.(6.11) into eq.(6.13), one obtains

$$h = uy + v \tag{6.14}$$

where

$$\begin{cases} u = [(x_{ci} - x_{ck})m + (y_{ci} - y_{ck})]/(2z_0) \\ v = [(x_{ci} - x_{ck})m + (y_{ck} - y_{ci})y_{cb}]/(2z_0). \end{cases} \tag{6.15}$$

Substituting eqs.(6.11) and (6.14) into eq.(6.8), one obtains

$$ay^2 + by + c = 0 \tag{6.16}$$

where

$$\begin{cases} a = 1 + m^2 - u^2 \\ b = 2m(n - x_{ci}) - y_{ci} - u(v - z_0) \\ c = (n - x_{ci})^2 - (v - z_0)^2 - x_{ci}^2. \end{cases} \tag{6.17}$$

Equation (6.16) can then be solved for y. The solution is then back substituted into eq.(6.11) to obtain x and into eq.(6.14) to obtain h. If the value obtained for h is real and positive and the solution (x, y, h) satisfies the condition, $\overline{C_l P_0''} \geq \overline{C_l T} (l \neq i, j, k)$, then the obtained point $T(x, y, 0)$ is a possible candidate point. However, it may not be the lowest point of the workspace. To find the lowest point of the workspace lying on the singularity plane, every side of the maximal convex polygon should be considered. Up to N solutions can be obtained for h. Then, the smallest one is the desired half height h which corresponds to the lowest point just touching the singularity plane.

In general, there is only one contact point T between the boundary of the singularity-free workspace and the singularity plane, see Fig. 6.8(a). However, for some special cases, there may be two, three or even six contact points, see Figs. 6.8(b) and 6.8(c).

Using the developed analytic algorithm, the exact maximal singularity-free workspace in an orientation with $\phi = \theta = 0^\circ$ and $\psi \neq \pm 90^\circ$ can be effectively determined. To investigate the effect of the orientation angle ψ on the "orientation-based maximal singularity-free workspace", set ϕ and θ to 0. The evolution of the volume V of the "orientation-based maximal singularity-free workspace" as a function of ψ is shown in

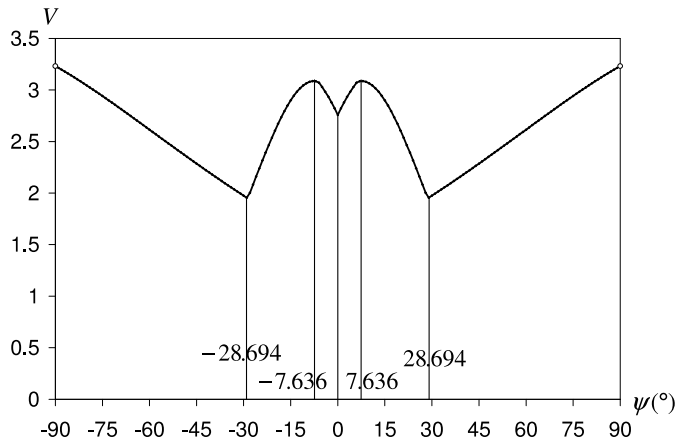

Figure 6.9: Volume V as a function of ψ ($\phi = \theta = 0^\circ$).

Fig. 6.9. From this figure, it can be seen that the obtained curve is symmetric about $\psi = 0°$. This is because the MSSM Gough-Stewart platform is symmetric about the y axis, see Fig. 4.12. When $\psi \approx \pm 7.636°$, the "orientation-based maximal singularity-free workspace" reaches a local maximum (3.086536). Fig. 6.8(a) shows the maximal singularity-free workspace in the orientation with $\psi = 7.636°$ and $\phi = \theta = 0°$.

However, when $\psi \approx \pm 28.694°$, the "orientation-based maximal singularity-free workspace" has a local minimum. In these two orientations, the six centres of the workspace spheres form one triangle, see $C'_1C'_2C'_5C'_6C'_3C'_4$ in Fig. 6.6. When the absolute value of ψ increases, the volume of the "orientation-based maximal singularity-free workspace" also increases. The six centres of the workspace spheres respectively form two triangles, $\Delta C''_1C''_3C''_5$ and $\Delta C''_2C''_4C''_6$ as shown in Fig. 6.6. However, when $\psi = \pm 90°$, the singularity-free workspace vanishes because these are two singular orientations.

6.4 Orientation Optimization

In the preceding section, the effect of each of the three orientation angles on the "orientation-based maximal singularity-free workspace" is analyzed by setting the other two to 0. Referring to Figs. 6.2, 6.5 and 6.9, the orientation with $\phi = 25.084°$, $\theta = 3.042°$ and $\psi = 7.636°$ should be a good orientation. However, in this orientation, the volume of the maximal singularity-free workspace as shown in Fig. 6.10(a) is only 2.277666, which is smaller than those in the corresponding optimal orientations in the above three figures. The reason is that in this orientation, every orientation angle is no longer 0. As a result, the singularity surface becomes more complex than those orientations with two orientation angles being 0, comparing Fig. 6.10(b) with Fig. 6.1(a) and Fig. 6.4(b).

Now the problem becomes: how to determine the optimal orientation in which the "orientation-based maximal singularity-free workspace" reaches its maximal status. Actually, this is a three-dimensional optimization problem which can be formulated as follows:

$$\min_{\phi,\theta,\psi}(-V) \tag{6.18}$$

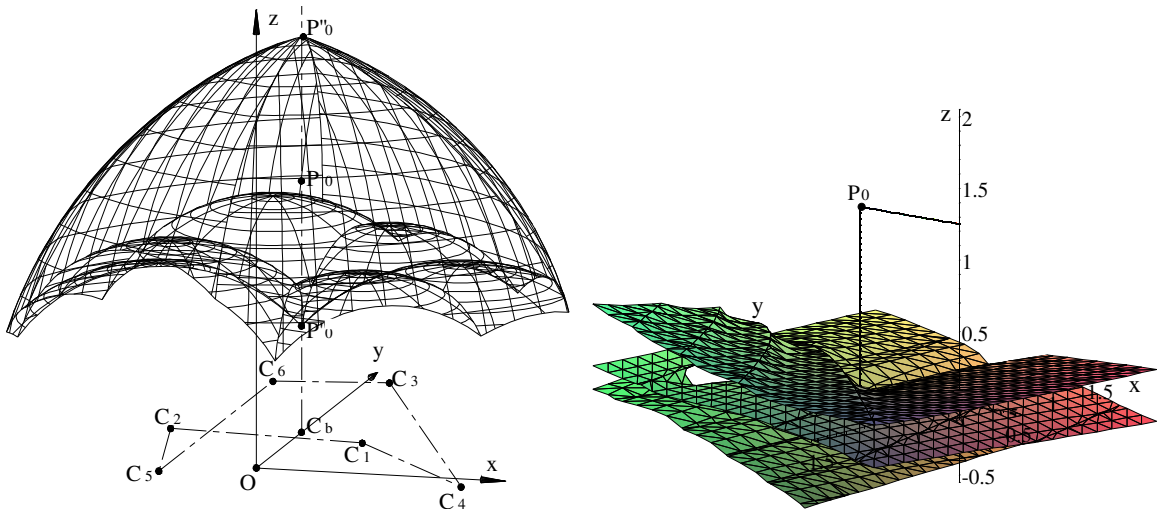

(a) Maximal singularity-free workspace. (b) Singularity surface.

Figure 6.10: The maximal singularity-free workspace and singularity surface in the orientation with $\phi = 25.084°$, $\theta = 3.042°$ and $\psi = 7.639°$.

$$
\begin{aligned}
& s.t. \\
& \qquad -90° < \phi < 90°, \\
& \qquad -90° < \theta < 90°, \\
& \qquad -90° < \psi < 90°.
\end{aligned}
$$

where V is the volume of the "orientation-based maximal singularity-free workspace" which is a function of ϕ, θ and ψ. In practice, the three orientation angles should be in a range given by $(-90°, 90°)$.

To solve the above optimization problem, Powell's search method [101] is used. In order to find the global optimal solution, 27 different initial orientations $(\phi_0, \theta_0, \psi_0)$ are taken for analysis. The distribution of these initial orientations is shown in Fig. 6.11. The centroid numbered 14 represents the reference orientation, i.e., $\phi_0 = \theta_0 = \psi_0 = 0$. The other initial nodes can be obtained in the following way: in the ϕ axis, take 0 as the central value and respectively offset 0.5 on both sides. Hence, three values $(-0.5, 0, 0.5)$ for ϕ_0 are available. Similarly, three values $(-0.5, 0, 0.5)$ for θ_0 and three values $(-0.5, 0, 0.5)$ for ψ_0 can be obtained. Therefore, the total number of combinations is 27.

The computation results are listed in Appendix B. From Appendix B, it can be

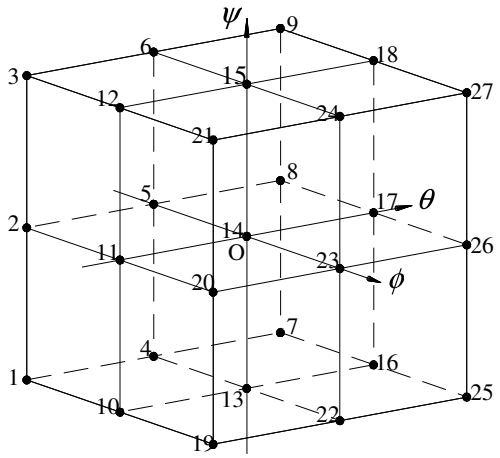

Figure 6.11: The distribution of the initial orientations.

seen that for different initial values, the three orientation angles cannot converge at one single point. However, the orientation $(-0.245146, 0.348268, -0.119460)$ or $(-14.046°, 19.954°, -6.845°)$ at which converged from the initial values $(-0.5, 0.5, -0.5)$ leads to the largest local $V_{max} = 3.510794$. The corresponding maximal singularity-free workspace and the singularity surface in this orientation is shown in Fig. 6.12. This orientation can be regarded as the approximate global optimal orientation. The leg length ranges for determining the maximal singularity-free workspace in this orientation are listed in Table 6.4.

Appendix B also shows that for several sets of initial values, the orientation angles at which the procedure converges are very close to the two limited orientations as shown in Fig. 6.9. For instance, the initial values $(-0.5, -0.5, -0.5)$ make the three orientation angles converge at $(0.001100,\ -0.001553,\ -1.565352)$ or $(0.063°, -0.089°, -89.687°)$. The obtained local $V_{max} = 3.221893$. The maximal singularity-free workspace and singularity surface in this orientation is shown in Fig. 6.13. The leg length ranges for determining the maximal singularity-free workspace in this orientation are listed in

Table 6.4: The leg length ranges for determining the maximal singularity-free workspace in the orientation with $\phi = -14.046°$, $\theta = 19.954°$ and $\psi = -6.845°$.

No.	1	2	3	4	5	6
ρ_i^{min}	1.030137	0.782654	0.887634	0.808829	0.841195	0.970039
ρ_i^{max}	2.419000	2.094247	2.135700	2.085011	2.097779	2.394024

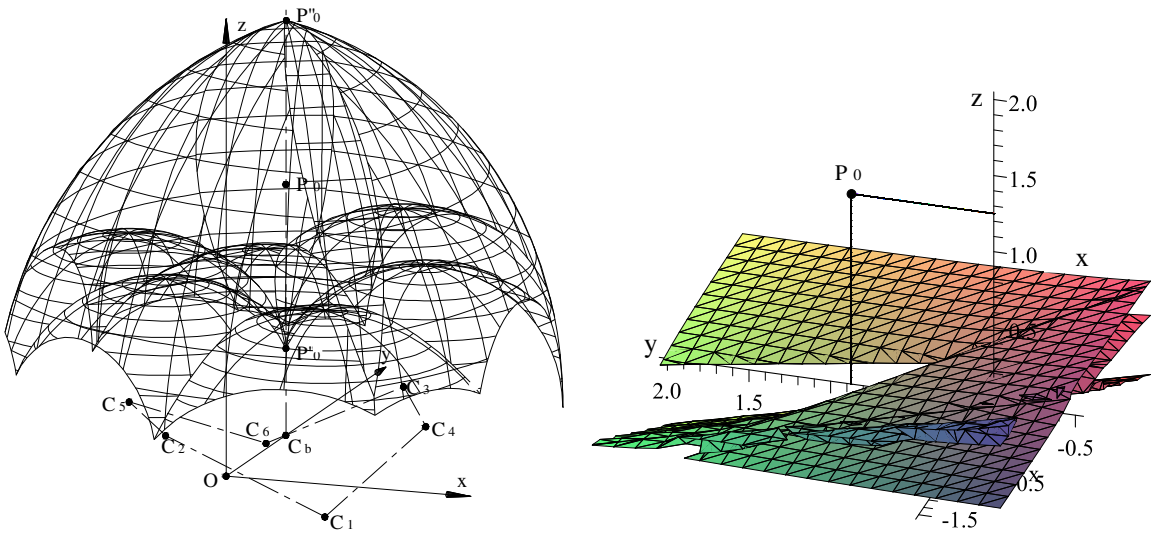

(a) Maximal singularity-free workspace. (b) Singularity surface.

Figure 6.12: The maximal singularity-free workspace and singularity surface in the orientation with $\phi = -14.046°$, $\theta = 19.954°$ and $\psi = -6.845°$.

Table 6.5.

Although the maximal singularity-free workspace in this orientation is quite large, this orientation is not a good orientation because of the following two reasons: first, this orientation is close to the singular orientation with $\phi = \theta = 0°$ and $\psi = -90°$. Second, Table 6.5 shows that the leg length ranges among the six legs are quite different.

Another interesting set of initial values is the reference orientation $(0, 0, 0)$. This set of initial values makes the three orientation angles converge to (0.442719, 0.022472, -0.063686) or $(25.366°, 1.288°, -3.649°)$ which is very close to the optimal orientation $(25.084°, 0°, 0°)$ in Fig. 6.2.

Table 6.5: The leg length ranges for determining the maximal singularity-free workspace in the orientation with $\phi = 0.063°$, $\theta = -0.089°$ and $\psi = 89.687°$.

No.	1	2	3	4	5	6
ρ_i^{min}	1.364515	0.512158	1.364654	0.512199	1.364670	0.511790
ρ_i^{max}	2.727771	2.418152	2.728999	2.418309	2.729138	2.416766

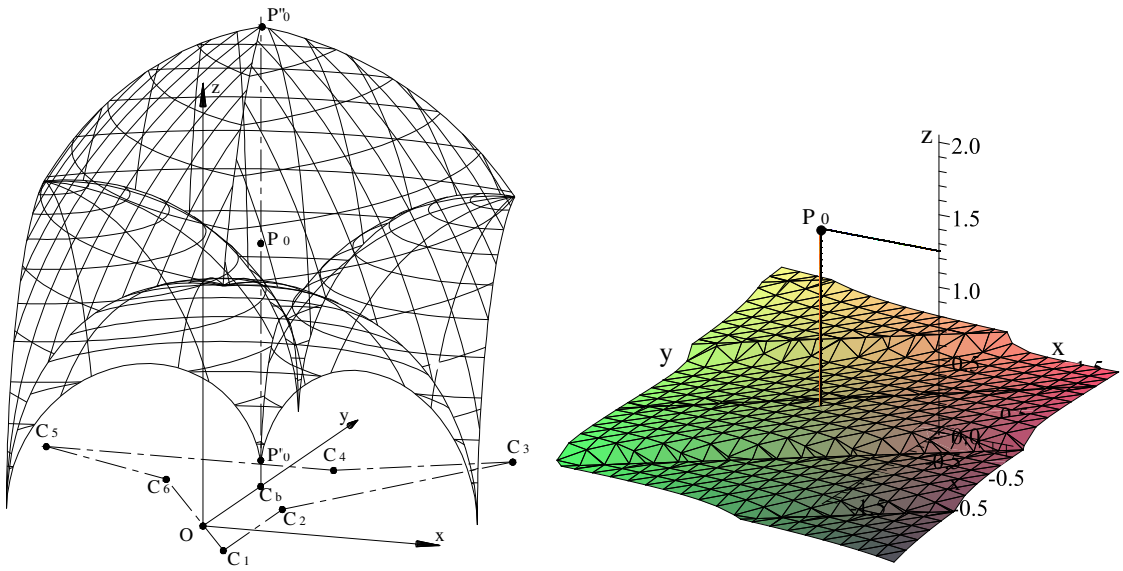

(a) Maximal singularity-free workspace.

(b) Singularity surface.

Figure 6.13: The maximal singularity-free workspace and singularity surface in the orientation with $\phi = 0.063°$, $\theta = -0.089°$ and $\psi = -89.687°$.

6.5 Computational Cost

The presented algorithm was programmed using Visual C++ 6.0 in a Windows XP environment. The CPU of the computer is a Pentium IV with 2.4 GHz. If the convergence precision is given as $\varepsilon = 10^{-5}$, the average time used for the optimization computation with one set of initial values is about 8 minutes.

Besides, the newly developed analytic algorithm used to determine the maximal singularity-free workspace in an orientations with $\phi = \theta = 0°$ and $\psi \neq \pm 90°$ can speed up the computation. For instance, at the given precision of $\varepsilon = 10^{-5}$, the time used by the new algorithm is about 4 seconds and the time used by the numerical search algorithm given in Chapter 5 is about 7 seconds.

6.6 Conclusions

This chapter focuses on analyzing the effect of the orientation on the "orientation-based maximal singularity-free workspace" in order to determine the optimal orientation for a given MSSM architecture. To speed up the computation in an orientation with $\phi = \theta = 0^\circ$ and $\psi \neq \pm 90^\circ$, an analytic algorithm is developed for determining the corresponding maximal singularity-free workspace. The results show that the maximal singularity-free workspace in some orientations can be larger than that in the reference orientation ($\phi = \theta = \psi = 0^\circ$). Although the global optimal orientation is difficult to determine, an approximate optimal orientation is available which provides very useful information for this kind of manipulator in a practical context.

Chapter 7

Maximal Singularity-Free Total Orientation Workspace

In practice, the maximal singularity-free total orientation workspace is interesting because a parallel mechanism often works in a range of orientations. Two algorithms are presented in this chapter to compute the maximal singularity-free total orientation workspace for the MSSM Gough-Stewart platform. The given example shows that to obtain the maximal singularity-free total orientation workspace is a time-consuming process even when using the relatively efficient modified algorithm. The example also shows that only a few orientations among the discretized orientations have a contribution to the boundary of the maximal singularity-free total orientation workspace.

7.1 Introduction

The constant orientation workspace is the workspace in a given orientation, i.e., the orientation is constant. This is the most interesting workspace in practice. In Chapter 5, a general numerical algorithm was presented to determine the maximal singularity-free workspace as well as the corresponding leg length ranges in a given orientation for the MSSM Gough-Stewart platform. For a given orientation with $\phi = \theta = 0°$ and $\psi \neq \pm 90°$, an analytic algorithm was developed in Chapter 6.

Besides the constant orientation workspace, the total orientation workspace may also be interesting in practice because a parallel mechanism often works in a range of orientations. In [15], an algorithm was presented to determine the total orientation workspace for given leg length ranges. However, so far nobody has touched the maximal singularity-free total orientation workspace. This chapter will develop two algorithms to determine the maximal singularity-free total orientation workspace in a given range of orientations for the MSSM Gough-Stewart platform.

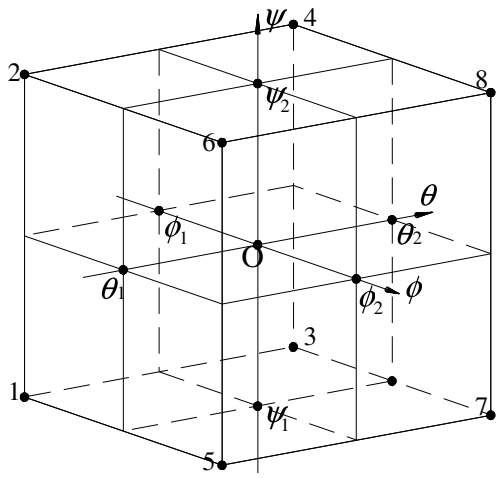

Figure 7.1: A set of orientations defined by $\phi \in [\phi_1, \phi_2]$, $\theta \in [\theta_1, \theta_2]$ and $\psi \in [\psi_1, \psi_2]$.

7.2 Definitions

7.2.1 Total Orientation Workspace

According to [15], the total orientation workspace is a region which can be reached by the end-effector of the platform with any orientation in a set defined by three ranges for the orientation angles. In other words, the total orientation workspace is the intersection of the workspaces for a given set of orientations. The given set of orientations can be represented by a parallelepiped in the Cartesian orientation space $O\phi\theta\psi$ as shown in Fig. 7.1 in which $\phi \in [\phi_1, \phi_2]$, $\theta \in [\theta_1, \theta_2]$ and $\psi \in [\psi_1, \psi_2]$.

7.2.2 Maximal Singularity-Free Total Orientation Workspace

Similarly, the maximal singularity-free total orientation workspace can be defined as the maximal singularity-free workspace which can be reached by the end-effector of the platform with any orientation in a set defined by three ranges for the orientation angles.

Referring to chapter 5, in every orientation, there exists a maximal singularity-free workspace. Hence, the maximal singularity-free total orientation workspace can be defined as the intersection of the maximal singularity-free workspaces for a given set of orientations.

7.3 Computational Algorithms

According to the definition given in the previous section, the maximal singularity-free total orientation workspace is the intersection of the maximal singularity-free workspaces in all orientations in a given set. However, for a given set of orientations as shown in Fig. 7.1, there are infinitely many orientations. In practice, it is impossible to compute the maximal singularity-free workspace in every individual orientation. One solution is to use the intersection of the maximal singularity-free workspaces for a finite

number of orientations to approach the real maximal singularity-free total orientation workspace under a given convergence precision. The finite number of orientations can be chosen as follows: if the range of every orientation angle is evenly divided into n ($n \geq 1$) parts, the total number of obtained orientations will be $N = (n+1)^3$. For instance, if $n = 1$, the total number of obtained orientations is 8 as shown in Fig. 7.1.

7.3.1 Basic Algorithm

The basic algorithm to determine the maximal singularity-free total orientation workspace can be described as follows: first, compute the maximal singularity-free workspace in every chosen orientation using the algorithms presented in the two preceding chapters. Then, determine their intersection which should satisfy the following condition:

$$\rho_{im}^{min} \leq d \leq \rho_{im}^{max} \tag{7.1}$$

where ρ_{im}^{max} and ρ_{im}^{min} ($i = 1, 2, ..., 6;\ m = 1, 2, ..., N$) are respectively the maximal and minimal leg lengths for leg i in orientation m, and d is the distance from any point (x, y, z) in the maximal singularity-free total orientation workspace to the workspace sphere centre $C_{im}(x_{cim}, y_{cim}, z_{cim})$, i.e., $d = \sqrt{(x - x_{cim})^2 + (y - y_{cim})^2 + (z - z_{cim})^2}$.

The volume V of the maximal singularity-free total orientation workspace can then be given as

$$V \approx \sum_{k=0}^{M-1} \frac{(A_k + A_{k+1})\Delta z}{2} \tag{7.2}$$

where A_k ($k = 0, 1, ..., M$) is the area of the common workspace section at z_k.

Now the focus becomes: how to compute the area of the common workspace section at a given z. For a given orientation m, there are six maximal workspace spheres with radii ρ_{im}^{max} and six minimal workspace spheres with radii ρ_{im}^{min}, which respectively centred at six workspace centres C_{im} ($i = 1, 2, ..., 6$). On the plane with a given z, the sections of these workspace spheres are circles with radii as follows:

$$\begin{cases} r_{zim}^{max} = \sqrt{(\rho_{im}^{max})^2 - (z - z_{cim})^2} \\ r_{zim}^{min} = \sqrt{(\rho_{im}^{min})^2 - (z - z_{cim})^2}. \end{cases} \tag{7.3}$$

For a given orientation m, there is a possible total of 12 workspace section circles. Hence, the possible total number of workspace section circles for all N orientations is $12N$. As a result, the common workspace section should be a region in which any point (x, y) has to satisfy the following condition:

$$r_{zim}^{min} \leq \sqrt{(x - x_{cim})^2 + (y - y_{cim})^2} \leq r_{zim}^{max} \quad (i = 1, 2, ..., 6; \quad m = 1, 2, ..., N). \tag{7.4}$$

The area A of the common workspace section at a given z can be computed by accumulating the contribution of every workspace section circle using the Gauss divergence theorem [22], [99]. The contribution of every workspace section circle can be computed as follows:

- Step 1: Compute the possible intersections of the considered workspace section circle and other $(12N - 2)$ workspace section circles.
- Step 2: Order the obtained intersections to separate the considered workspace section circle into several arcs.
- Step 3: Judge every arc to see whether it satisfies eq.(7.4) or not. If yes, its contribution can be computed using the Gauss divergence theorem [22], [99].

7.3.2 Modified Algorithm

In theory, the above presented algorithm is correct. However, there are two drawbacks in practice. One is that this algorithm consumes too much computer memory. The other is that the computation can be too slow or even breaks down. The reason for the first drawback is that too many variables are needed to store the intermediate results. For every orientation, there are six workspace centres and every centre has three coordinates. Hence, the number of variables used to keep the centres information is 18. Besides, 12 variables are needed to keep the maximal and minimal leg lengths which lead to the platform holding the maximal singularity-free workspace in the prescribed orientation. Furthermore, another 12 variables are also needed to save the radii of the workspace section circles. Hence, the total number of variables needed to save these basic data for every individual orientation is 42. For N orientations, the number of

needed variables is $42N$. For instance, if $N = 27000$ and the data type is double, the needed memory just for saving these basic data is about 9 Mbytes.

Besides these basic data, there are other intermediate results that must also be kept during the computation. When the memory used to save all these intermediate results increases, the memory used for running the computation program decreases. As a result, the computation slows down. When the number of orientations increases to some degree, the computation even breaks down.

Another reason for which the computation slows down is that when the number of orientations increases to some degree, the main computation time is spent on computing the area of the common workspace section. For instance, to compute the contribution of every workspace section circle, it is necessary to compute its intersections with other $(12N - 2)$ workspace section circles. Hence, the total number of the intersections to compute is $[12N(12N-2)]$. This shows that with an increasing number of orientations, the time just for computing the intersections increases by a factor of $[12N(12N - 2)]$. Of course, some workspace section circles may not exist on the considered section plane, and for some workspace section circles, there are no intersections between them. However, some computations are still needed to verify these situations.

To overcome the above drawbacks, the presented basic algorithm is modified. Considering that the maximal singularity-free workspaces for the eight orientations corresponding to the eight vertices of the parallelepiped as shown in Fig. 7.1 are relatively small and that their shapes are quite different from one to another, it can be inferred that the possibility for these eight workspaces to contribute to the boundary of the maximal singularity-free total orientation workspace may be relatively high. Hence, these eight orientations can be taken as the basic group. The intersection of these eight workspaces can be determined using the procedure mentioned in the basic algorithm. If some workspace has no contribution to the boundary of their intersection, it is discarded. The remaining orientations forms the valid group, which may contain only K orientations. When the maximal singularity-free workspace in a new orientation is available, the new one will be added into the valid group to form a new group. Similarly, by determining the intersection of the maximal singularity-free workspaces corresponding to the new group and discarding those without contribution to the boundary, a new valid group will be formed. Repeating this procedure until all chosen orientations are considered, the final obtained intersection of the maximal singularity-free workspaces

corresponding to the last valid group is also the intersection of the maximal singularity-free workspaces in all considered orientations.

As the number of orientations contained in every group is small, only a few variables are needed to keep the intermediate results. Hence, less memory is occupied. Every time a new orientation is added, the valid group needs to be updated. However, the required computation time is still significantly reduced because of the small number of orientations contained in each group.

7.4 Example

In order to demonstrate the presented algorithms, consider the MSSM architecture used in Chapter 4 Section 4.4, i.e., both the base and the platform are equilateral triangles with a size ratio $k = \frac{3}{5}$. Hence, the geometric parameters are: $t_1 = \frac{1}{\sqrt[4]{3}}$, $t_2 = \sqrt[4]{3}$, $t_3 = \frac{3}{5\sqrt[4]{3}}$ and $t_4 = \frac{3\sqrt[4]{3}}{5}$. Take the centroid of the platform as the considered point P. Its position in the mobile frame $O'x'y'z'$ is given as $\mathbf{p}' = [0, \frac{\sqrt[4]{3}}{5}, 0]^T$. Besides, the position of interest P_0 is taken at $(0, \frac{2\sqrt[4]{3}}{3}, \frac{5}{4})$.

The given set of orientations can be defined by three ranges for the orientation angles as follows: $\phi \in [-15°, 15°]$, $\theta \in [-15°, 15°]$ and $\psi \in [-15°, 15°]$. Figs. 7.2(a) – 7.2(h) respectively show the maximal singularity-free workspaces in the 8 orientations in the basic group. Their intersection is given in Fig. 7.2(i). The computation shows that the maximal singularity-free workspaces in two of the orientations $(-15°, -15°, 15°)$ and $(-15°, 15°, -15°)$ have no contribution to the boundary of this intersection. These two orientations correspond to vertices 2 and 3 of the parallelepiped in Fig. 7.1. In other words, the maximal singularity-free workspaces as shown in Figs. 7.2(b) and 7.2(c) completely contain the intersection as shown in Fig. 7.2(i).

In order to make the intersection approach the maximal singularity-free total orientation workspace, more orientations inside the given set should be used. Fig. 7.3 shows the evolution of the volume V of the intersection as a function of the number N of the chosen orientations. This evolution graph looks like a damped vibration. For instance, when every range of three orientation angles is evenly divided into 3 parts ($n = 3$ and $N = 4^3$), the volume of the intersection is $V = 0.904399$. When every

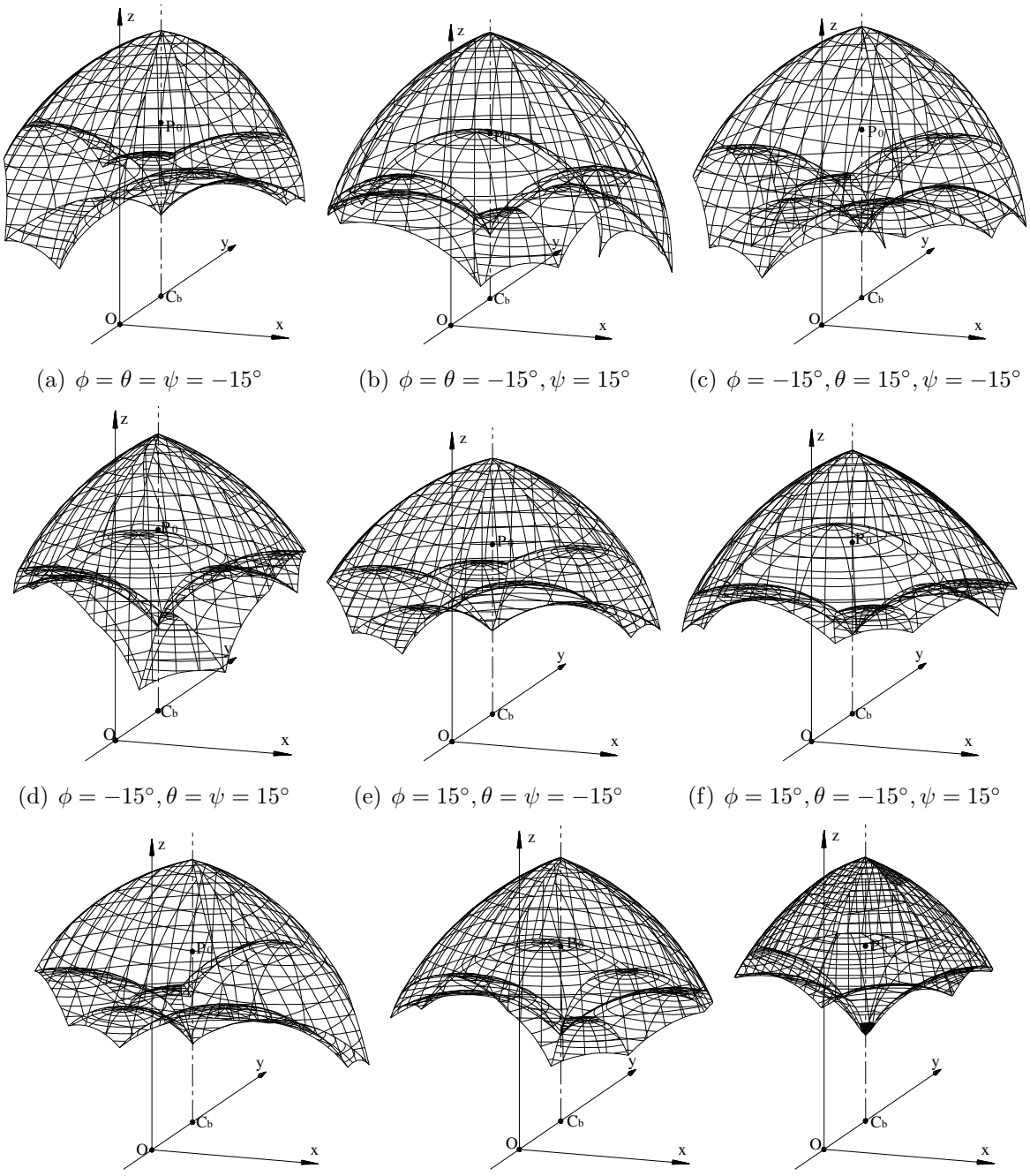

(a) $\phi = \theta = \psi = -15°$ (b) $\phi = \theta = -15°, \psi = 15°$ (c) $\phi = -15°, \theta = 15°, \psi = -15°$

(d) $\phi = -15°, \theta = \psi = 15°$ (e) $\phi = 15°, \theta = \psi = -15°$ (f) $\phi = 15°, \theta = -15°, \psi = 15°$

(g) $\phi = \theta = 15°, \psi = -15°$ (h) $\phi = \theta = \psi = 15°$ (i) Intersection of (a) – (h)

Figure 7.2: The maximal singularity-free workspaces in eight basic orientations as well as their intersection.

range of three orientation angles is evenly divided into 4 parts ($n = 4$ and $N = 5^3$), the volume of the intersection should decrease. However, the computation shows that this is not the case. Instead of decreasing, the volume of the intersection increases a little to

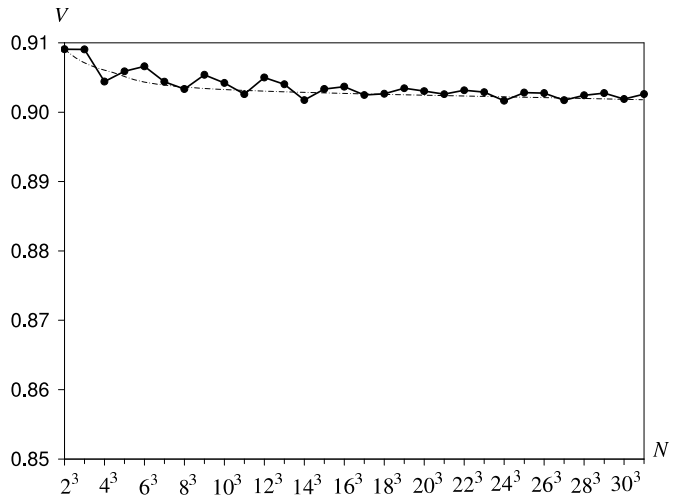

Figure 7.3: Volume V as a function of N.

$V = 0.905886$. The corresponding final valid groups of orientations in these two cases are respectively listed in Table 7.1 and Table 7.2, where V_i denotes the corresponding maximal singularity-free workspace. These two tables show that both of their valid groups contain eight orientations and the first six orientations are exactly the same. The only difference between these two cases is their last two valid orientations.

The reason for which the intersection in the case with $n = 4$ and $N = 5^3$ increases a little is because the last two valid orientations contribute less to the boundary of the intersection. However, when the number of the chosen orientations increases, the network of the given set as shown in Fig. 7.1 becomes denser. As a result, the general trend of the evolution of the intersection decreases with respect to N. The fluctuation becomes progressively smaller until the intersection converges at the maximal singularity-free total orientation workspace. When $n = 30$ and $N = 31^3$, the volume of the intersection is $V = 0.902604$. If the convergence precision is set to 10^{-4}, this intersection is already a very good approximation of the maximal singularity-free total orientation workspace.

Table 7.1 and Table 7.2 show that the first six orientations contained in the final valid groups of the above two cases are exactly the same as those forming the valid group of orientations in the case with $n = 1$ and $N = 8$ as shown in Fig. 7.1. Actually, no matter how many parts each range of three orientation angles is divided into, these six orientations are always contained in the final valid group. For instance, Table 7.3

Table 7.1: The final valid group of orientations for $N = 4^3$.

i	$\phi(^\circ)$	$\theta(^\circ)$	$\psi(^\circ)$	V_i
1	**-15**	**-15**	**-15**	**1.641922**
2	**-15**	**15**	**15**	**1.641922**
3	**15**	**-15**	**-15**	**1.504150**
4	**15**	**-15**	**15**	**1.701075**
5	**15**	**15**	**-15**	**1.701075**
6	**15**	**15**	**15**	**1.504150**
7	-15	-15	-5	1.511631
8	15	15	5	1.511631

Table 7.2: The final valid group of orientations for $N = 5^3$.

i	$\phi(^\circ)$	$\theta(^\circ)$	$\psi(^\circ)$	V_i
1	**-15**	**-15**	**-15**	**1.641922**
2	**-15**	**15**	**15**	**1.641922**
3	**15**	**-15**	**-15**	**1.504150**
4	**15**	**-15**	**15**	**1.701075**
5	**15**	**15**	**-15**	**1.701075**
6	**15**	**15**	**15**	**1.504150**
7	-15	-15	-7.5	1.504649
8	15	15	0	1.697334

shows the case with $n = 29$ and $N = 30^3$.

Another interesting observation is that the number of valid orientations is small. Table 7.3 shows that even if the number of chosen orientations becomes very large (say 27000), the total number of valid orientations is only 10. This shows that the maximal singularity-free workspaces in most orientations have no contribution to the boundary of the intersection. However, it is very difficult to accurately judge whether an orientation has a contribution before performing some necessary computations. To obtain a good approximation for the maximal singularity-free total orientation workspace, the only way is to increase the number of chosen orientations, i.e., to densify the network of the given set as shown in Fig. 7.1.

Table 7.3: The final valid group of orientations for $N = 30^3$.

i	$\phi(^\circ)$	$\theta(^\circ)$	$\psi(^\circ)$	V_i
1	**-15**	**-15**	**-15**	**1.641922**
2	**-15**	**15**	**15**	**1.641922**
3	**15**	**-15**	**-15**	**1.504150**
4	**15**	**-15**	**15**	**1.701075**
5	**15**	**15**	**-15**	**1.701075**
6	**15**	**15**	**15**	**1.504150**
7	-15	-15	-13.965517	1.653930
8	-15	15	13.965517	1.653930
9	15	-15	-5.689655	1.479307
10	15	15	5.689655	1.479307

7.5 Computational Cost

The presented algorithms were programmed using C++ 6.0 in a Linux environment (Fedora 7, Kernel 2.6.22.1-41, 64 bits). The computer used has a dual core CPU with 2.2 GHz. If the convergence precision is given as $\varepsilon = 10^{-4}$, using the modified algorithm, the evolution of the needed time t for computing the volume V of the intersection as a function of the number N of chosen orientations is shown in Fig. 7.4. It can be seen that the used time increases very quickly with the number of orientations. Obviously, it is a time-consuming process to obtain a very good approximation for the maximal singularity-free total orientation workspace. For instance, the intersection at $N = 31^3$ can be regarded as a very good approximation. However, the used time is 7374 minutes.

In some applications, such a precise result may be not necessary. In this situation, the intersection at $N = 8$ as shown in Fig. 7.2(i) can be regarded as a good estimation for the maximal singularity-free total orientation workspace. Actually, the difference between the volume at $N = 8$ and that at $N = 31^3$ is only 0.006464. The error is only 0.716%. But the computation time at $N = 8$ is around 1 minute, only 1/7374 of that at $N = 31^3$.

In order to compare the modified algorithm with the basic algorithm, Fig. 7.5 shows the evolution of the computation time with respect to the number of chosen orientations respectively using the two algorithms. This figure shows that when N is large, the time used by the basic algorithm is much longer than that used by the modified algorithm. For instance, when $N = 21^3$, the time used by the basic algorithm is 6084 minutes while the time used by the modified algorithm is only 2256 minutes. The latter is about 1/3 of the former. This result demonstrates the analysis made in Section 7.3.

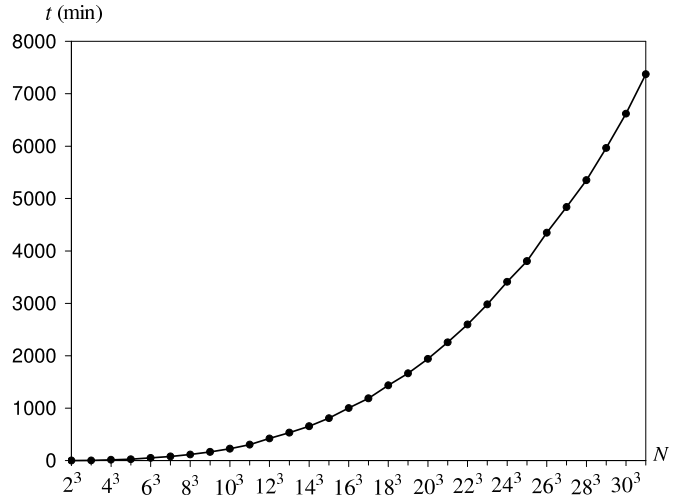

Figure 7.4: Computation time t as a function of N.

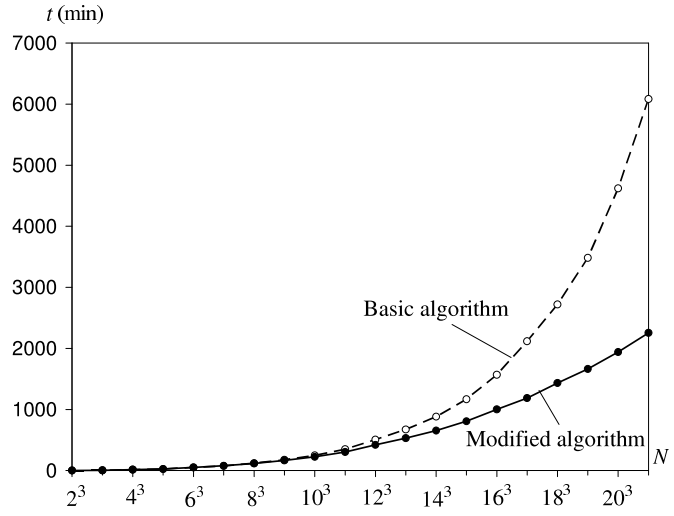

Figure 7.5: Efficiency comparison betwen the two algorithms.

7.6 Conclusions

So far, most research works focused on determining the constant orientation workspace. The maximal singularity-free total orientation workspace is left unaddressed. In practice, this type of workspace may also be interesting because a parallel mechanism often works in a range of orientations. This chapter presents two algorithms to compute the maximal singularity-free total orientation workspace for the MSSM Gough-Stewart platform.

The given example shows that to obtain the maximal singularity-free total orientation workspace is a time-consuming process even when the relatively efficient modified algorithm is used. Besides, the example also shows that only a few orientations among the discretized orientations have a contribution to the boundary of the maximal singularity-free total orientation workspace. Unfortunately, it is very difficult to identify these valid orientations before performing some necessary computations.

In some applications, the exact maximal singularity-free total orientation workspace may not be necessary. The intersection at $N = 8$ as shown in Fig. 7.2(i) can be regarded as a good estimation.

Chapter 8

Evaluation and Representation of the Orientation Workspace

The evaluation and representation of the orientation workspace of robotic manipulators is a challenging task. This chapter focuses on the determination of the orientation workspace of the MSSM Gough-Stewart platform with given leg length ranges $[\rho_i^{min},\ \rho_i^{max}]$. By use of the *Roll–Pitch–Yaw* angles (ϕ, θ, ψ), the orientation workspace at a prescribed position can be defined by 12 workspace surfaces. The obtained orientation workspace is a region in the 3D Cartesian orientation space $O\phi\theta\psi$. As all rotations $\mathbf{R}(x, \phi)$, $\mathbf{R}(y, \theta)$ and $\mathbf{R}(z, \psi)$ take place with respect to the fixed frame, any point of the orientation workspace provides a clear measure for the platform to respectively rotate in order around the (x, y, z) axes of the fixed frame. Also, as the shape of the 3D orientation workspace is very complex, a numerical algorithm is presented to compute its volume.

8.1 Introduction

As mentioned in Chapter 1, compared to the position workspace, the definition of the orientation workspace is more complex. Its representation is a challenging task. Especially, the orientation workspace can be defined by numerous parameterization approaches [29]. So far, very few works exist on the topic of orientation workspace computation.

Considering the complexity of the orientation workspace, only two of the three possible rotations of the end-effector of Gough-Stewart platforms were computed and represented in [35] and [36]. In [35], the rotation around the unit normal of the platform was set to 0. Hence, the remaining 2D rotations of the platform lead to the locus of the unit normal of the platform being an inverted hollow pyramid. This pyramid was referred to as the orientation pyramid. Then, the area of all the facets of the orientation pyramid was used as the measure of the orientation workspace.

Similarly, a unit link on the platform was used in [36] to describe the orientation workspace. One end of the chosen unit link is the fixed point. When the platform rotates around the fixed point, the locus of the other end of the chosen unit link is a patch of spherical surface. Then the area of the obtained patch of spherical surface was used as the measure of the orientation workspace. Just as argued in [36], this algorithm is able to determine only two of the three possible rotations of the end-effector. Obviously, the rotation around the chosen unit link was neglected.

Later, a method was presented in [37] to represent the orientation workspace of a general parallel manipulator (GPM) in a cylindrical coordinate system. A pencil of rays from the origin was used in [16] to compute the orientation workspace. Obviously, the computation precision depends on the density of the used rays and details about this point were not provided. However, the main drawback can be that with this approach, it is difficult to obtain the complete boundary of the real orientation workspace because the shape of the orientation workspace in most cases is very complex. Besides, some information on the effect of geometric parameters on the orientation angles was provided in [27]. Some numerical analysis of the orientation workspace of spherical manipulators with different parameterization methods was performed in [38].

This chapter focuses on the determination of the 3D orientation workspace of the MSSM Gough–Stewart platform. Referring to Chapter 4, the *Roll–Pitch–Yaw* angles (ϕ, θ, ψ) are used in this thesis. The advantage of this parameterization approach is that all rotations $\mathbf{R}(x, \phi)$, $\mathbf{R}(y, \theta)$ and $\mathbf{R}(z, \psi)$ take place with respect to the fixed frame. Hence, the defined orientation workspace can be easily represented in a 3D Cartesian orientation space. The obtained orientation can be given as

$$\mathbf{Q} = \mathbf{R}(z, \psi)\mathbf{R}(y, \theta)\mathbf{R}(x, \phi). \tag{8.1}$$

Equation (8.1) is equivalent to the zyx convention of the Euler angles. Hence, the three angles (ψ, θ, ϕ) used in the above rotation matrix $\mathbf{Q}$ were also referred to as the Euler angles in [54], [87]. As pointed out in [29], the Euler angles have numerous possible conventions and multiple interpretations. For every convention, the Euler angles usually present the rotation measure with respect to the mobile frame which is fixed to the platform. In order to avoid unnecessary confusion, this thesis does not use the term *Euler angles*. Instead, the *Roll–Pitch–Yaw* angles are used.

So far, the *Roll–Pitch–Yaw* angles are widely used in aviation, image navigation, computer vision as well as robotics [31–34]. They have already become a standard convention in practice. Hence, when an engineer reads eq.(8.1), he/she always realizes that the orientation is obtained by the following process: the platform rotates by a angle ϕ around the x axis of the fixed frame; then rotates by a angle θ around the y axis of the fixed frame and finally rotates by a angle ψ around the z axis of the fixed frame. If the orientation workspace in the 3D Cartesian orientation space $O\phi\theta\psi$ is determined, any point inside the workspace provides a clear measure for the platform to respectively rotate in order around the (x, y, z) axes of the fixed frame. Although the volume of the 3D orientation workspace is not straightforward and easy to understand [28], it can be used as the measure of the 3D orientation workspace. Hence, a numerical algorithm is presented to evaluate the volume of the 3D orientation workspace.

8.2 Orientation Workspace

Referring to Fig. 4.12 and taking the centroid C_p of the platform as the end-effector P, then the position of P in the mobile frame will be $\mathbf{p}' = [0, t_4/3, 0]^T$. Substituting $\mathbf{p}$, $\mathbf{p}'$,

$\mathbf{p}'_i$ and $\mathbf{b}_i$ into eq.(4.5), the following equations can be obtained for six legs:

$$\begin{cases}
\rho_1^2 = [\frac{2}{3}t_4(xc\phi - ys\phi s\theta) - 2t_3yc\theta]s\psi - [2t_3xc\theta + \frac{2}{3}t_4(xs\phi s\theta + yc\phi)]c\psi \\
\quad +2t_3zs\theta - \frac{2}{3}t_4zs\phi c\theta + t_3^2 + \frac{1}{9}t_4^2 + x^2 + y^2 + z^2 \\
\rho_2^2 = [\frac{2}{3}t_4(xc\phi - ys\phi s\theta) + 2t_3yc\theta]s\psi + [2t_3xc\theta - \frac{2}{3}t_4(xs\phi s\theta + yc\phi)]c\psi \\
\quad -2t_3zs\theta - \frac{2}{3}t_4zs\phi c\theta + t_3^2 + \frac{1}{9}t_4^2 + x^2 + y^2 + z^2 \\
\rho_3^2 = [\frac{2}{3}t_4c\phi(x - t_1) + (\frac{2}{3}t_4s\phi s\theta - 2t_3c\theta)(t_2 - y)]s\psi \\
\quad +[(\frac{2}{3}t_4s\phi s\theta - 2t_3c\theta)(t_1 - x) + \frac{2}{3}t_4c\phi(t_2 - y)]c\psi \\
\quad -2t_3zs\theta - \frac{2}{3}t_4zs\phi c\theta + t_1^2 + t_2^2 + t_3^2 + \frac{1}{9}t_4^2 - 2t_1x - 2t_2y + x^2 + y^2 + z^2 \\
\rho_4^2 = \frac{4}{3}t_4[s\phi s\theta(y - t_2) + c\phi(t_1 - x)]s\psi + \frac{4}{3}t_4[s\phi s\theta(x - t_1) + c\phi(y - t_2)]c\psi \\
\quad +\frac{4}{3}t_4zs\phi c\theta + t_1^2 + t_2^2 + \frac{4}{9}t_4^2 - 2t_1x - 2t_2y + x^2 + y^2 + z^2 \\
\rho_5^2 = \frac{4}{3}t_4[s\phi s\theta(y - t_2) - c\phi(t_1 + x)]s\psi + \frac{4}{3}t_4[s\phi s\theta(x - t_1) + c\phi(y - t_2)]c\psi \\
\quad +\frac{4}{3}t_4zs\phi c\theta + t_1^2 + t_2^2 + \frac{4}{9}t_4^2 + 2t_1x - 2t_2y + x^2 + y^2 + z^2 \\
\rho_6^2 = [\frac{2}{3}t_4c\phi(x + t_1) + (\frac{2}{3}t_4s\phi s\theta + 2t_3c\theta)(t_2 - y)]s\psi \\
\quad -[(\frac{2}{3}t_4s\phi s\theta - 2t_3c\theta)(t_1 + x) - \frac{2}{3}t_4c\phi(t_2 - y)]c\psi \\
\quad +2t_3zs\theta - \frac{2}{3}t_4zs\phi c\theta + t_1^2 + t_2^2 + t_3^2 + \frac{1}{9}t_4^2 + 2t_1x - 2t_2y + x^2 + y^2 + z^2.
\end{cases} \tag{8.2}$$

When the position of the end-effector P is taking the position of P_0, its three coordinates (x, y, z) become three constants (x_0, y_0, z_0). If ϕ, θ and ψ become variables, the leg length is a function of only ϕ, θ and ψ. In this case, the above equations can be rewritten as follows:

$$\rho_i = \rho_i(\phi, \theta, \psi) \qquad (i = 1, 2, ..., 6). \tag{8.3}$$

If the leg length is given, eq.(8.3) describes a surface in the 3D Cartesian orientation space $O\phi\theta\psi$. If the leg length respectively takes its maximal and minimal values, the corresponding two workspace surfaces will define the potential boundaries of the orientation workspace, see Fig. 8.1. In this figure, the left surface conresponds to the minimal leg length ρ_i^{min} and the right surface corresponds to the maximal leg length ρ_i^{max}. These surfaces can be referred to as the orientation workspace surfaces or simply workspace surfaces. If the leg length takes a value between the maximal and minimal leg lengths, the corresponding surface should lie in between the left one and the right one.

For six legs, if the leg length ranges are given, there are up to twelve workspace surfaces: six corresponding to the maximal leg lengths and six corresponding to the

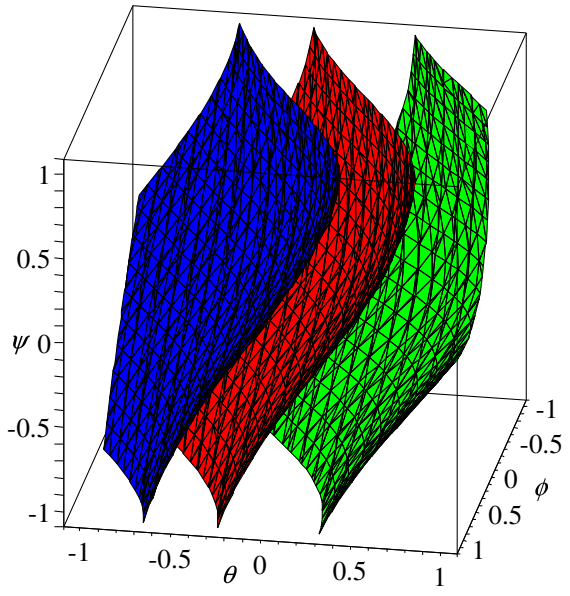

Figure 8.1: Orientation workspace surfaces.

minimal leg lengths. Pieces of these 12 workspace surfaces will define the entire boundary of the orientation workspace, as shown in Fig. 8.2.

However, the maximal and minimal leg lengths cannot be given arbitrarily. Actually, there are geometric limitations as shown in Fig. 8.3. Suppose the prescribed position of the platform is $P_0(x_0, y_0, z_0)$. When the attachment points B_i, P_i and the centroid C_p (taken as the end-effector P) of the platform lie on one line, the extreme leg lengths can be determined as follows:

$$\begin{cases} \rho_{i,lim}^{max} = \sqrt{(x_0 - x_{bi})^2 + (y_0 - y_{bi})^2 + (z_0 - z_{bi})^2} + e \\ \rho_{i,lim}^{min} = \sqrt{(x_0 - x_{bi})^2 + (y_0 - y_{bi})^2 + (z_0 - z_{bi})^2} - e \end{cases} \tag{8.4}$$

where $e = \overline{C_pP_i} = \overline{C_pP_i'}$, the coordinates (x_{bi}, y_{bi}, z_{bi}) of B_i in the fixed frame $Oxyz$ are given by vector $\mathbf{b}_i (i = 1, 2, ..., 6)$. Fig. 8.3 shows that the maximal leg length ρ_i^{max} cannot be greater than $\rho_{i,lim}^{max}$ and the minimal leg length ρ_i^{min} cannot be less than $\rho_{i,lim}^{min}$. When the leg length takes one of the extreme leg lengths $\rho_{i,lim}^{max}$ or $\rho_{i,lim}^{min}$, there will be only one point on the corresponding workspace surface which belongs to the orientation workspace. Hence, to define the boundary of the orientation workspace efficiently, the maximal and the minimal leg lengths should take reasonable values in the interval $[\rho_{i,lim}^{min},\ \rho_{i,lim}^{max}]$. In other words, the maximal and minimal extensions of the legs should be compatible with the geometric constraints.

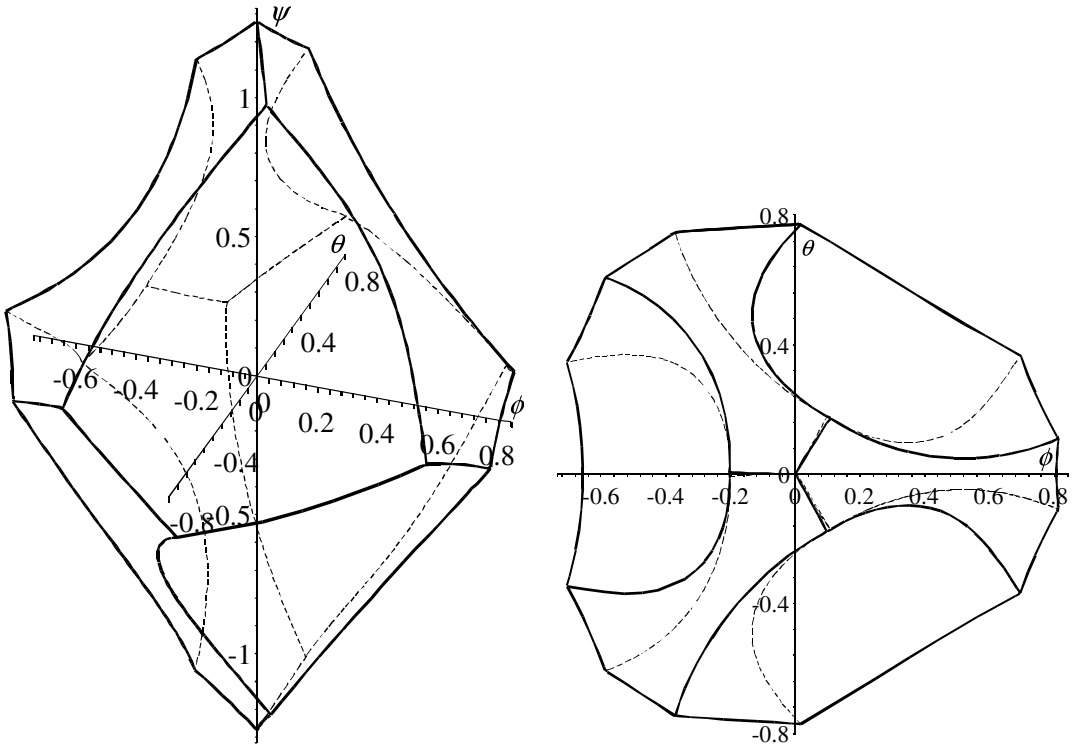

(a) 3D representation (b) Top view

Figure 8.2: Orientation workspace.

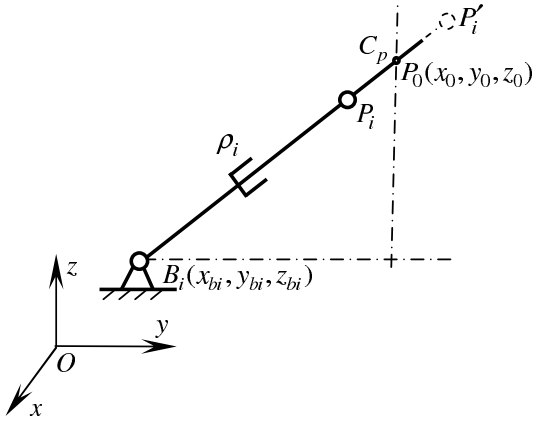

Figure 8.3: Geometric limitation of leg length.

8.3 Numerical Algorithm

As mentioned in the previous section, if the leg length ranges $[\rho_i^{min},\ \rho_i^{max}]$ $(i = 1, 2, ..., 6)$ are given, the orientation workspace can be defined by 12 workspace surfaces. However,

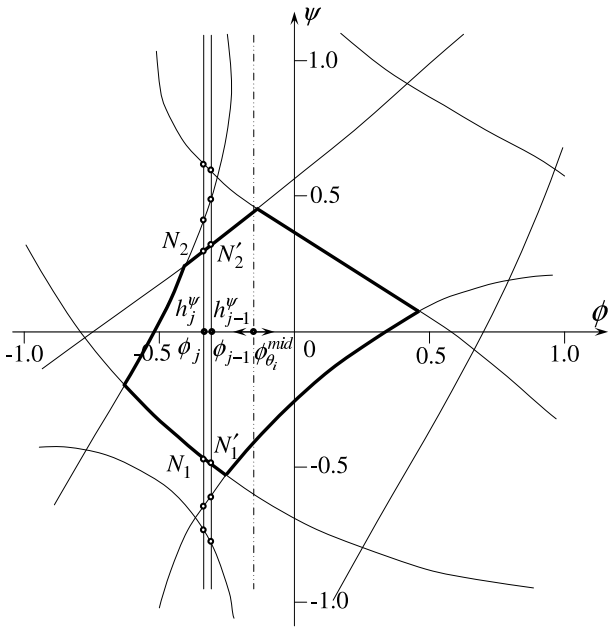

Figure 8.4: The workspace section on the plane with $\theta = \theta_i$.

the shape of the orientation workspace is very complex. Although it is possible to determine the portions of the surfaces that are actual boundaries of the workspace (see Fig. 8.2), it is impossible to find an analytic formula to evaluate the volume of the orientation workspace. Thus, a numerical algorithm is presented in this section to solve this problem.

The basic idea of the presented algorithm is as follows: for a given valid θ_i which is inside the orientation workspace, there should exist a workspace section on the plane with $\theta = \theta_i$ — which is parallel to the $O\phi\psi$ plane — as shown in Fig. 8.4. If the area of every workspace section is available, the volume V of the orientation workspace can be given by the following equation:

$$V \approx \sum_{i=1}^{n} \frac{(A_{i-1} + A_i)\Delta\theta}{2} \tag{8.5}$$

where A_i $(i = 0, 1, ..., n)$ is the area of the workspace section with $\theta = \theta_i$.

However, the number n is hard to determine because the maximal and minimal θ coordinates of the orientation workspace are unknown. Considering that the reference orientation $(0, 0, 0)$ always exists inside the orientation workspace, a valid workspace section should exist on the plane with $\theta = 0$ even if it shrinks to one point in some special case. Hence, the orientation workspace can be divided into two parts: one with

$\theta \leq 0$ and the other one with $\theta \geq 0$. Take the part with $\theta \leq 0$ as an example, its volume V_1 can be given as:

$$V_1 \approx \sum_{i=1}^{n_1} \frac{(A_{i-1} + A_i)\Delta\theta}{2} \tag{8.6}$$

where A_0 is the area of the workspace section with $\theta = 0$. The number n_1 can be determined as follows: for a given step size $\Delta\theta$, n_1 is the maximal number of steps for θ to decrease from 0 until a value $(-n_1\Delta\theta)$ at which the corresponding workspace section vanishes, i.e., $A_{n_1} = 0$.

The volume V_2 of the other part with $\theta \geq 0$ can be computed in a similar way. When V_1 and V_2 are available, their sum is the volume V of the entire workspace.

For programming convenience, A_{i-1} and A_i in eq.(8.6) are respectively denoted by A_0 and A, see Appendix C.

8.3.1 Workspace Section

In order to compute the volume of the orientation workspace, it is necessary to define the workspace section. Referring to Fig. 8.4, for any point inside the workspace section, if its coordinates (ϕ, θ_i, ψ) are substituted into eq.(8.3), the obtained leg length should satisfy the following condition:

$$\rho_i^{min} \leq \rho_i \leq \rho_i^{max} \qquad (i = 1, 2, ..., 6). \tag{8.7}$$

The area A_i of the workspace section with $\theta = \theta_i$ can be given as

$$A_i \approx \sum_{j=1}^{m} \frac{(h_{j-1}^{\psi} + h_j^{\psi})\Delta\phi}{2} \tag{8.8}$$

where h_j^{ψ} $(j = 0, 1, ..., m)$ is the height of the workspace section in the ψ direction at ϕ_j, see Fig. 8.4.

However, the number m is also hard to determine because the maximal and minimal ϕ coordinates of the workspace section are unknown. Considering that two neighbouring workspace sections are very close, the workspace section can be divided into two parts

by $\phi_{\theta_i}^{mid}$: one part with $\phi \leq \phi_{\theta_i}^{mid}$ and the other part with $\phi \geq \phi_{\theta_i}^{mid}$. Here, $\phi_{\theta_i}^{mid}$ is the average value of the maximal and minimal valid ϕ values of previous workspace section, i.e., $\phi_{\theta_i}^{mid} = (\phi_{\theta_{i-1}}^{max} + \phi_{\theta_{i-1}}^{min})/2$. When $\theta = 0$, ϕ_0^{mid} is equal to 0 which is the ϕ coordinate of the reference orientation $(0, 0, 0)$. Take the part with $\phi \leq \phi_{\theta_i}^{mid}$ as an example, its area A_{i1} can be given as

$$A_{i1} \approx \sum_{j=1}^{m_1} \frac{(h_{j-1}^{\psi} + h_j^{\psi})\Delta\phi}{2} \tag{8.9}$$

where h_0^{ψ} is the height of the workspace section at $\phi = \phi_{\theta_i}^{mid}$. The number m_1 can be determined as follows: for a given step size $\Delta\phi$, m_1 is the maximal number of steps for ϕ to decrease from $\phi_{\theta_i}^{mid}$ until a value $(\phi_{\theta_i}^{mid} - m_1\Delta\phi)$ at which the corresponding workspace height vanishes, i.e., $h_{m_1}^{\psi} = 0$.

The area A_{i2} of the other part with $\phi \geq \phi_{\theta_i}^{mid}$ can be computed in a similar way. When A_{i1} and A_{i2} are available, their sum is the area A_i of the entire workspace section with $\theta = \theta_i$.

For programming convenience, A_{i1} and A_{i2} are respectively denoted by A_1 and A_2; h_{j-1}^{ψ} and h_j^{ψ} are respectively denoted by h_0^{ψ} and h^{ψ}, see Appendix C.

8.3.2 Computation of h^{ψ}

In order to compute the area of the workspace section with $\theta = \theta_i$, it is necessary to compute the height h_j^{ψ} of the workspace section in the ψ direction at a given ϕ_j, see Fig. 8.4. In the plane with $\theta = \theta_i$, every workspace surface given by eq.(8.3) becomes a curve, which can be referred to as the workspace curve. For given leg length ranges, the total number of the workspace curves is 12: six correspond to the maximal leg lengths and six correspond to the minimal leg lengths. Fig. 8.4 shows that there are only 8 workspace curves close to the workspace section in the considered case. The other 4 workspace curves do not appear in the region as shown in this figure.

To compute the possible intersections of each workspace curve and the line $\phi = \phi_j$ on the workspace section plane, substitute ϕ by ϕ_j into eq.(8.2), a single variable equation in ψ can be obtained as follows:

$$a_i \sin\psi + b_i \cos\psi + c_i = 0 \qquad (i = 1, 2, ..., 12). \tag{8.10}$$

From eq.(8.10), one obtains

$$\psi = 2tan^{-1}(\frac{-a_i \pm \sqrt{\Delta}}{c_i - b_i}) \qquad (i = 1, 2, ..., 12) \tag{8.11}$$

where $\Delta = a_i^2 + b_i^2 - c_i^2$. If $\Delta > 0$, eq.(8.11) leads to two real solutions for eq.(8.10) in the range $[-\pi, \pi]$; if $\Delta = 0$, eq.(8.11) gives only one real solution in the range $[-\pi, \pi]$; and if $\Delta < 0$, there is no real solution for eq.(8.10). In other words, if $\Delta > 0$, there are two intersections of the considered workspace curve and the line $\phi = \phi_j$; if $\Delta = 0$, there is only one intersection; and if $\Delta < 0$, there is no intersection.

When all intersections are available, then select those lying on the boundary of the workspace section using the condition of eq.(8.7). Then, order the intersections on the boundary by use of their ψ coordinates. For two neighbouring intersections, say N_1 and N_2 in Fig. 8.4, if any arbitrary point on the line segment $\overline{N_1N_2}$ also satisfies eq.(8.7), $\overline{N_1N_2}$ is a contribution of h_j^{ψ}. Summing up all the contributions, the height h_j^{ψ} at the given valid ϕ_j can be obtained. In general, there is only one such segment for the h_j^{ψ}, see Fig. 8.4.

8.3.3 Computation Procedure

The volume V of the orientation workspace can be obtained by respectively computing the two parts of the orientation workspace with $\theta \leq 0$ and $\theta \geq 0$. Appendix C provides a detailed procedure for computing the volume V_1 of the orientation workspace with $\theta \leq 0$. The procedure for computing the volume V_2 of the orientation workspace with $\theta \geq 0$ is similar to that given in Appendix C. When V_1 and V_2 are available, put the sum of V_1 and V_2 to V. The volume V of the entire orientation workspace will be obtained.

8.4 Example

In order to demonstrate the presented algorithm, consider the MSSM architecture used in Chapter 4 Section 4.4, i.e., both the base and the platform are equilateral triangles with a size ratio $k = \frac{3}{5}$. Hence, the geometric parameters are: $t_1 = \frac{1}{\sqrt[4]{3}}$, $t_2 = \sqrt[4]{3}$,

$t_3 = \frac{3}{5\sqrt[4]{3}}$ and $t_4 = \frac{3\sqrt[4]{3}}{5}$. Take the centroid of the platform as the considered point P. Its position in the mobile frame $O'x'y'z'$ is given as $\mathbf{p}' = [0, \frac{\sqrt[4]{3}}{5}, 0]^T$. Besides, the position of interest P_0 is taken at $(0, \frac{2\sqrt[4]{3}}{3}, \frac{5}{4})$, which lies on the perpendicular line through the centroid $C_b(0, \frac{2\sqrt[4]{3}}{3}, 0)$ of the base. The maximal and minimal leg lengths are $\rho_i^{max} = 1.8$, $\rho_i^{min} = 1.2$ $(i = 1, 2, ..., 6)$. The initial step sizes $\Delta\theta = \Delta\phi = 0.01$. The convergence precision is given as $\varepsilon = 10^{-4}$. According to eq.(8.4), $\rho_{i,lim}^{max} \approx 2.053617$ and $\rho_{i,lim}^{min} \approx 1.000757$ $(i = 1, 2, ..., 6)$. Hence, the above chosen maximal and minimal leg lengths $(\rho_i^{max},\ \rho_i^{min})$ lie in the interval $[\rho_{i,lim}^{min},\ \rho_{i,lim}^{max}]$.

Using the above presented algorithm, the volume of the orientation workspace is computed as $V \approx 1.374979$. The final step sizes at the given convergence precision are $\Delta\theta = 0.00125$ and $\Delta\phi = 0.00125$. The determined orientation workspace is represented in Fig. 8.2. This orientation workspace is symmetric about the ϕ axis in the 3D Cartesian orientation space, but not symmetric about the $O\phi\psi$ plane. This point is easy to understand because the MSSM platform is symmetric about the y axis, see Fig. 4.12.

8.5 Computational Cost

The presented algorithm is programmed with Visual C++ 6.0 in a Windows XP environment. The CPU of the used computer is a Pentium IV with 2.4 GHz. If the convergence precision is set to $\varepsilon = 10^{-4}$, the computation time is about 29 seconds. If the convergence precision is improved to $\varepsilon = 10^{-5}$, the computation time is about 80 seconds. But the computed volume V of the orientation workspace changes only slightly. Hence, $\varepsilon = 10^{-4}$ is already a good convergence precision with a reasonable computation time. It is not necessary to increase the convergence precision further.

8.6 Conclusions

Unlike the position workspace, the orientation workspace of a 6-DOF parallel manipulator is not straightforward to determine and represent. Especially, the orientation workspace can be defined by numerous parameterization approaches. Hence, to represent the orientation workspace understandably is a challenging task.

This work presents a numerical algorithm to analyze the orientation workspace of the MSSM Gough-Stewart platform. For given leg length ranges, the orientation workspace of the platform at a prescribed position P_0 can be defined by 12 workspace surfaces. The obtained orientation workspace is a region in the 3D Cartesian orientation space $O\phi\theta\psi$. As the used parameterization approach is the *Roll–Pitch–Yaw* angles, all rotations $R(x, \phi)$, $R(y, \theta)$ and $R(z, \psi)$ take place with respect to the fixed frame. Hence, any point of the orientation workspace provides a clear measure for the platform to respectively rotate in order around the (x, y, z) axes of the fixed frame. An example with an equilateral triangle base and platform is provided to demonstate the presented algorithm.

Chapter 9

Maximal Singularity-Free Orientation Workspace at a Given Position

This chapter addresses the determination of the maximal singularity-free orientation workspace at a prescribed position of the MSSM Gough-Stewart platform. Referring to Chapter 8, the orientation workspace at a prescribed position can be defined by 12 workspace surfaces. This chapter will develop a numerical algorithm to determine these 12 workspace surfaces in order to obtain the maximal singularity-free orientation workspace. Besides, to compare the maximal singularity-free orientation workspace with the maximal singularity-free sphere, an iterative algorithm for determining the maximal singularity-free sphere is also provided.

9.1 Introduction

To the best of the author's knowledge, the maximal singularity-free orientation workspace has not yet addressed because of its complexity. Instead, a maximal singularity-free sphere was used in [95] as a measure of the maximal singularity-free orientation workspace. However, any orientation workspace cannot be a sphere in practice. This point has been demonstrated in Chapter 8, see Fig. 8.2.

This chapter presents an efficient numerical algorithm to determine the maximal singularity-free orientation workspace at a prescribed position of the MSSM Gough-Stewart platform. Additionally, the leg length ranges $[\rho_i^{min},\ \rho_i^{max}]$ $(i = 1, 2, ..., 6)$ which lead to the maximal singularity-free orientation workspace can also be determined.

9.2 Maximal Singularity-Free Orientation Workspace

9.2.1 Singularity Locus

At a given position $P_0(x_0, y_0, z_0)$, the singularity locus given by eq.(4.15) in the 3D Cartesian orientation space $O\phi\theta\psi$ is a surface as shown in Fig. 4.14.

9.2.2 Definition

As mentioned in Chapter 8, the orientation workspace can be defined by 12 workspace surfaces that depend on the maximal and minimal leg lengths of each leg. Hence, the total number of variables is 12. Fig. 9.1 shows the case with the maximal and minimal leg lengths: $\rho_i^{max} = 1.75$ and $\rho_i^{min} = 1.30$. The position is taken at $P_0(0, \frac{2\sqrt[4]{3}}{3}, \frac{5}{4})$. The used MSSM architecture is the same as that used in Chapter 4 Section 4.4, i.e., $t_1 = \frac{1}{\sqrt[4]{3}}$, $t_2 = \sqrt[4]{3}$, $t_3 = \frac{3}{5\sqrt[4]{3}}$ and $t_4 = \frac{3\sqrt[4]{3}}{5}$. If the leg length in the reference orientation $(0, 0, 0)$ is referred to as the nominal leg length ρ_i^{nom}, the nominal leg length in this case is

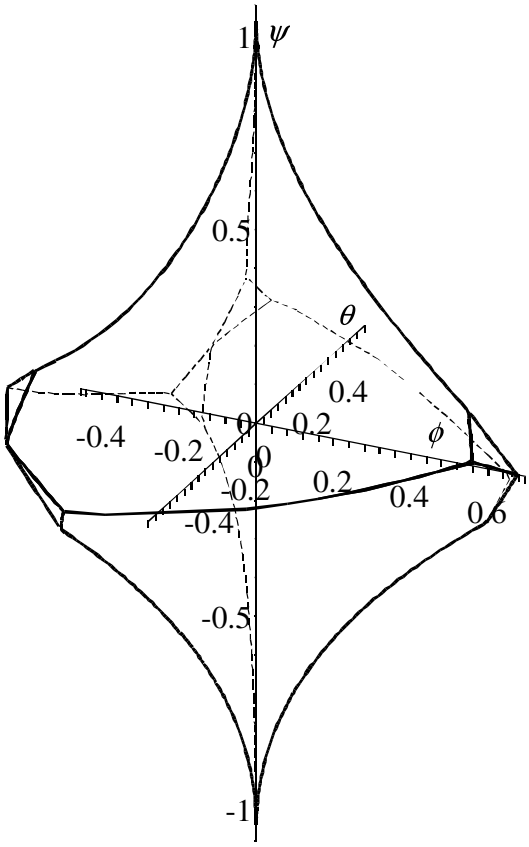

Figure 9.1: The orientation workspace at $P_0(0, \frac{2\sqrt[4]{3}}{3}, \frac{5}{4})$ with $\rho_i^{max} = 1.75$, $\rho_i^{min} = 1.30$.

$\rho_i^{nom} = 1.465452$ $(i = 1, 2, ..., 6)$. It is easy to find that the minimal leg length ρ_i^{min} is closer to the nominal leg length ρ_i^{nom} than the maximal leg length ρ_i^{max}. In Fig. 9.1, the minimal leg lengths correspond to the six small patches of workspace boundary and the maximal leg lengths correspond to the six large patches of workspace boundary. To balance these 12 patches of workspace boundary, one idea is to make the difference between the minimal leg length and the nominal leg length be equal to that between the maximal leg length and the nominal leg length, i.e.,

$$D = \left|\rho_i^{min} - \rho_i^{nom}\right| = |\rho_i^{max} - \rho_i^{nom}| \quad (i = 1, 2, ..., 6). \tag{9.1}$$

As a result, the orientation workspace is determined by only one variable D, which is referred to as the orientation workspace variable. If D changes, the shape and the size of the orientation workspace changes accordingly. When D takes its limit value D_{lim}, the boundary of the orientation workspace just touches the singularity surface at some point(s). In this context, the singularity-free orientation workspace becomes the maximum. In other words, the maximal singularity-free orientation workspace is

determined by D_{lim}.

9.2.3 Computational Algorithm

Although the maximal singularity-free orientation workspace is determined by D_{lim}, it is very difficult to determine D_{lim} analytically because the shape of the orientation workspace is very complex. Hence, a numerical algorithm is presented to solve this problem. The basic idea is to increase D from 0 until the boundary of the orientation workspace touches the singularity surface. The general procedure can be described as follows: First, set the orientation workspace variable D to 0. Then, increase D by one step ΔD and verify whether any singularity exists inside the obtained orientation workspace. If no singularity exists, continue to increase D using the same step size ΔD. Otherwise, the used step size is too large for this step. In this case, restore D to its previous value and reduce the step size ΔD by one half. Then, increase D by the reduced step size ΔD. Repeat this procedure until D converges to its limit value D_{lim}. At this moment, the step size ΔD becomes very small and the singularity-free workspace reaches the maximum. In order to make the procedure more efficient, the initial value of the step size ΔD is not necessarily very small.

In the above general procedure, for every reasonable value of the orientation workspace variable D, there exists an orientation workspace in the 3D Cartesian orientation space $O\phi\theta\psi$. This corresponding orientation workspace can be computed using the method given in Chapter 8.

In order to guarantee no singularity inside the orientation workspace, it is necessary to perform singularity verification. However, in the 3D Cartesian orientation space $O\phi\theta\psi$, both the orientation workspace and the singularity surface are very complex. To directly determine whether any singularity exists inside the 3D orientation space is not convenient. Comparatively, the singularity verification in a 2D workspace section at a given θ is easy. Moreover, if every workspace section is singularity-free, the entire workspace should be singularity-free.

However, there are infinitely many workspace sections and hence it is impossible to verify every one. One solution to this problem is to verify only a few workspace sections

which are used to evaluate the workspace volume. The density of these workspace sections depends on the convergence precision. In other words, when the workspace volume converges at a given precision, two neighbouring workspace sections can be regarded as sufficiently close.

Hence, the computation of the workspace volume is twofold: when D has not reached its limit value D_{lim}, the objective is just to perform singularity verification. When D reaches its limit value D_{lim}, the volume of the maximal singularity-free orientation workspace is obtained. Obviously, if D exceeds its limit value D_{lim}, the workspace intersects the singularity surface. In this case, the computation of the workspace volume cannot continue. Instead, restore D to its previous value and reduce the step size ΔD by one half. Then, use the new step size ΔD to increase D in order to obtain a new singularity-free orientation workspace.

The details of singularity verification performed in every workspace section can be described using Fig. 8.4. If every small quadrilateral $(N_1N_2N_2'N_1')$ between ϕ_j and ϕ_{j-1} is singularity-free, the entire workspace section is singularity-free. To verify whether any singularity exists inside this small quadrilateral, substitute the coordinates of the four vertices (N_1, N_2, N_2', N_1') into the singularity expression (the left hand side of eq.(4.15)), thereby obtaining four function values (F_1, F_2, F_2', F_1'). If all these function values have the same sign, there is no side of the small quadrilateral $(N_1N_2N_2'N_1')$ intersecting the singularity curve. The reason is: when the area of the workspace section converges, the step size $\Delta\phi = |\phi_j - \phi_{j-1}|$ becomes very small. If $F_1F_1' > 0$, there is no intersection between the boundary arc N_1N_1' of the workspace section and the singularity curve. Similarly, if $F_2F_2' > 0$, there is no intersection between the boundary arc N_2N_2' of the workspace section and the singularity curve. And if there is no intersection between the boundary of workspace section and the singularity curve, it is impossible for any line segment (say N_1N_2 or $N_1'N_2'$) inside the workspace section to intersect the singularity curve. Hence, the function values (F_1, F_2, F_2', F_1') should have the same sign. If not, the small quadrilateral $(N_1N_2N_2'N_1')$ will contain part of the singularity curve.

9.2.4 Computational Procedure

The detailed procedure for determining the maximal singularity-free orientation workspace is given in Appendix D.

9.3 Maximal Singularity-Free Sphere

To compare the maximal singularity-free orientation workspace and the maximal singularity-free sphere, an iterative algorithm for determining the maximal singularity-free sphere is presented in this section. The problem consists in finding the point on the singularity surface which is the closest to the reference orientation $(0, 0, 0)$. The formulation can be given as follows:

$$\min_{(\phi,\theta,\psi)} d \tag{9.2}$$

where

$$d = \phi^2 + \theta^2 + \psi^2 + \lambda F \tag{9.3}$$

where λ is the Lagrange multiplier used to transform the constrained problem into an unconstrained one. F is the singularity expression, i.e., the left hand side of eq.(4.15). To obtain the extremum of d, the following condition should be satisfied:

$$\begin{cases} \frac{\partial d}{\partial \phi} = 2\phi + \lambda \frac{\partial F}{\partial \phi} = 0 \\ \frac{\partial d}{\partial \theta} = 2\theta + \lambda \frac{\partial F}{\partial \theta} = 0 \\ \frac{\partial d}{\partial \psi} = 2\psi + \lambda \frac{\partial F}{\partial \psi} = 0 \\ \frac{\partial d}{\partial \lambda} = F = 0. \end{cases} \tag{9.4}$$

Eliminating λ from eq.(9.4), one obtains

$$\theta = \phi \frac{\partial F/\partial \theta}{\partial F/\partial \phi} \tag{9.5}$$

$$\psi = \phi \frac{\partial F/\partial \psi}{\partial F/\partial \phi} \tag{9.6}$$

$$F = 0. \tag{9.7}$$

Instead of the resultant method used in [95], an iterative algorithm is used to solve eqs.(9.5 — 9.7). The procedure is as follows: start from a chosen initial orientation

$(\phi_0, \theta_0, \psi_0)$. From eq.(9.5), a new value θ_1 can be obtained. And from eq.(9.6), a new value ψ_1 can be obtained. Substitute θ_1 and ψ_1 into eq.(9.7), a new value ϕ_1 can be obtained in the interval $[-\pi/2, \pi/2]$ by numerically solving eq.(9.7). Then, use the obtained new orientation $(\phi_1, \theta_1, \psi_1)$ to obtain another new orientation $(\phi_2, \theta_2, \psi_2)$. Repeat the procedure until the following convergence condition is satisfied:

$$\sqrt{(\phi_i - \phi_{i-1})^2 + (\theta_i - \theta_{i-1})^2 + (\psi_i - \psi_{i-1})^2} \leq \varepsilon. \tag{9.8}$$

If the obtained extremum d_e of d is the global minimal distance from the reference orientation $(0, 0, 0)$ to the singularity surface, d_e will be taken as the radius r of the maximal singularity-free sphere, i.e., $r = d_e$. However, to be sure that the obtained d_e is the global minimal distance, singularity verification is necessary. The singularity verification can be performed in the section with $\psi = \psi_i$ ($\psi_i \in [-r, r]$) of the sphere with a radius $r = d_e$. The number of the used sections is determined by the numerical computation of the volume of the sphere. In other words, when the volume of the sphere computed by the numerical algorithm converges to the volume computed by the analytical formula $V = \frac{4\pi r^3}{3}$, two neighbouring sections can be regarded as sufficiently close. The following example shows that the singularity verification is unnecessary.

9.4 Example

To demonstrate the procedure proposed above, consider the MSSM architecture used in Chapter 4 Section 4.4, i.e., both the base and the platform are equilateral triangles with a size ratio $k = \frac{3}{5}$. Hence, the geometric parameters are: $t_1 = \frac{1}{\sqrt[4]{3}}$, $t_2 = \sqrt[4]{3}$, $t_3 = \frac{3}{5\sqrt[4]{3}}$ and $t_4 = \frac{3\sqrt[4]{3}}{5}$. Take the centroid C_p of the platform as the end-effector P. Its position in the mobile frame $O'x'y'z'$ is $\mathbf{p}' = [0, \frac{\sqrt[4]{3}}{5}, 0]^T$. Suppose the prescribed position of the platform is $P_0(0, \frac{2\sqrt[4]{3}}{3}, \frac{5}{4})$, which lies on the perpendicular line through the centroid $C_b(0, \frac{2\sqrt[4]{3}}{3}, 0)$ of the base. The initial step sizes are chosen as $\Delta D = 0.1$, $\Delta\theta = \Delta\phi = 0.01$. The convergence precision is set to $\varepsilon = 10^{-4}$.

9.4.1 Computational Results

Applying the algorithm presented in section 9.2, the determined maximal singularity-free orientation workspace with a volume $V_{max} \approx 2.967244$ is shown as Fig. 9.2. The limit value of the orientation workspace variable is $D_{lim} \approx 0.363330$. As the nominal leg length is $\rho_i^{nom} \approx 1.465452$, the maximal and the minimal leg lengths are $\rho_i^{max} \approx 1.828782$, $\rho_i^{min} \approx 1.102122$ $(i = 1, 2, ..., 6)$. The final step sizes are $\Delta D \approx 4.882813 \times 10^{-5}$, $\Delta\theta = \Delta\phi = 0.0025$.

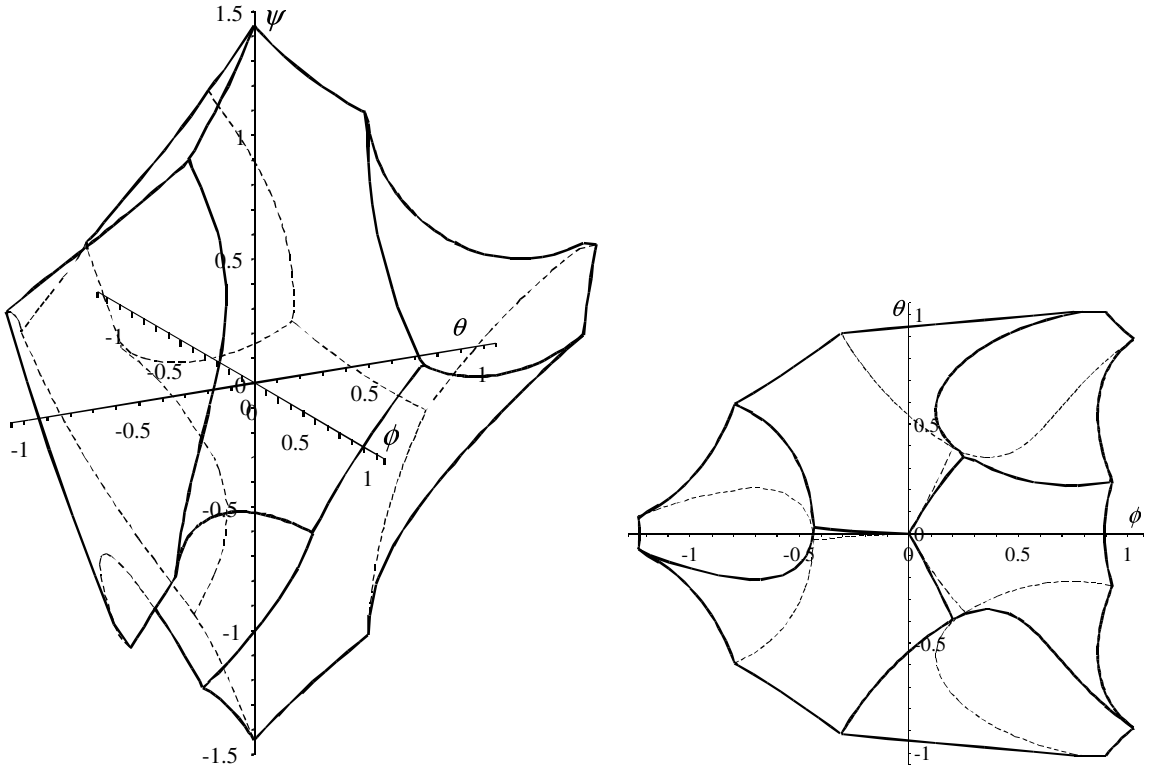

(a) 3D representation (b) Top view

Figure 9.2: The maximal singularity-free orientation workspace at $P_0(0, \frac{2\sqrt[4]{3}}{3}, \frac{5}{4})$.

Applying the iterative algorithm presented in the preceding section, the maximal singularity-free sphere centred in the reference orientation $(0, 0, 0)$ is determined as shown in Fig. 9.3. The computation results show that no matter which orientation $(\phi_0, \theta_0, \psi_0)$ is taken as the starting point, the converged point is always close to $(-1.233272, 0, 0)$. For instance, if $(0, 0, 0)$ is taken as the starting point, the converged point is exactly the point $(-1.233272, 0, 0)$. If $(1, 1, 1)$ is taken as the starting point,

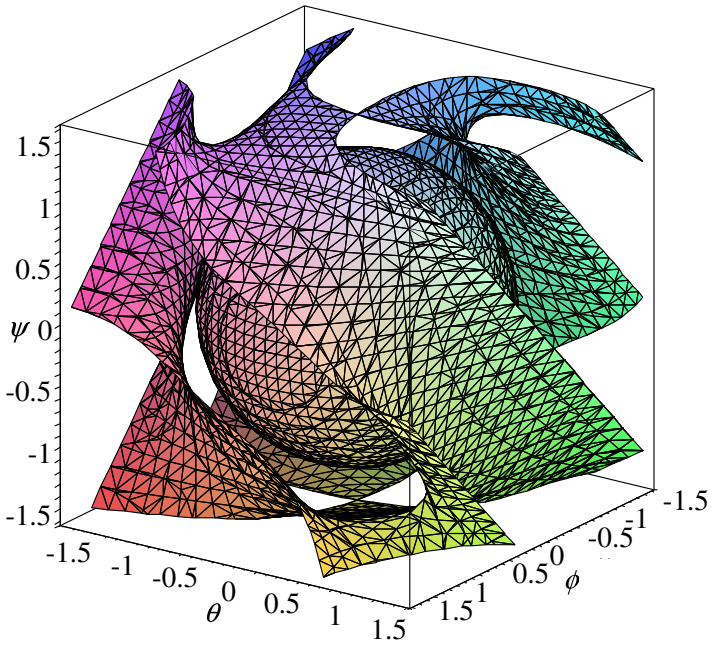

Figure 9.3: The maximal singularity-free sphere.

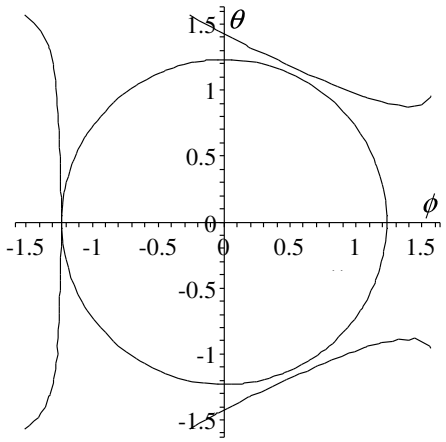

Figure 9.4: The maximal singularity-free circle on the plane with $\psi = 0$.

the converged point is $(-1.233272, 3.118987 \times 10^{-7}, 3.328697 \times 10^{-7})$. Hence, the distance between point $(-1.233272, 0, 0)$ and the reference orientation $(0, 0, 0)$ should be the global minimal distance. The section circle of the maximal singularity-free sphere in the plane with $\psi = 0$ is shown in Fig. 9.4.

In order to compare the maximal singularity-free orientation workspace and the maximal singularity-free sphere, these two regions are superimposed in Fig. 9.5. It can

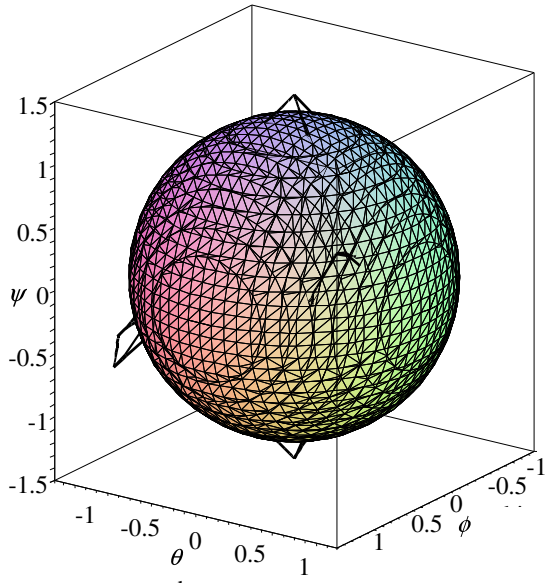

Figure 9.5: The maximal singularity-free orientation workspace and the maximal singularity-free sphere.

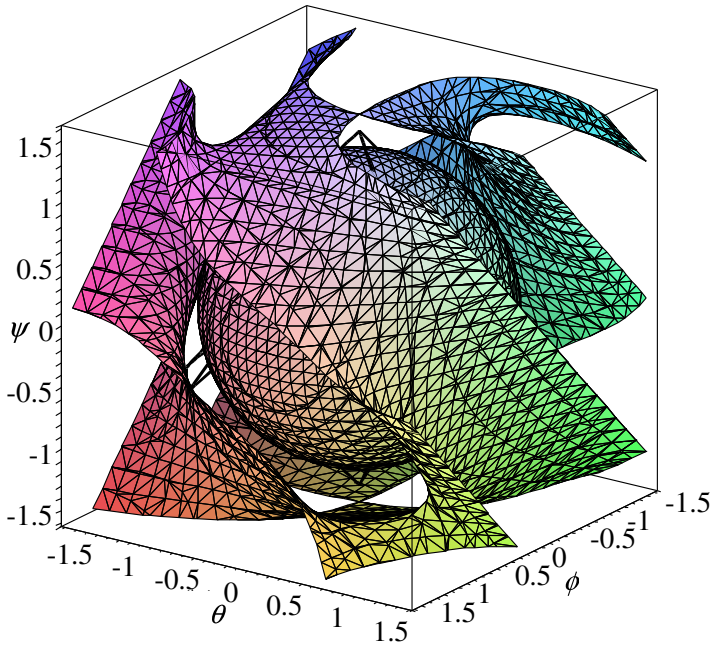

Figure 9.6: The maximal singularity-free orientation workspace, the maximal singularity-free sphere as well as the singularity surface.

be seen that the maximal singularity-free sphere cannot cover the maximal singularity-free orientation workspace completely, though its volume (7.857153) is 2.649209 times

of that (2.967244) of the maximal singularity-free orientation workspace. Fig. 9.6 shows that both the maximal singularity-free orientation workspace and the maximal singularity-free sphere do not intersect the singularity surface.

9.4.2 Computational Cost

The presented algorithm is programmed using Visual C++ 6.0 in a Windows XP environment. The CPU of the used computer is a Pentium IV with 2.4 GHz. The computation for determining the maximal singularity-free sphere is very fast. The computation time at the convergence precision $\varepsilon = 10^{-6}$ is no more than 1 second.

However, the computation time for determining the maximal singularity-free orientation workspace is much longer. If the convergence precision is set to $\varepsilon = 10^{-4}$, the computation time is about 165 seconds. The volume of the maximal singularity-free orientation workspace is $V_{max} = 2.965441$ and the final step size ΔD is 4.882813×10^{-5}, which is already very small. If the convergence precision is improved to $\varepsilon = 10^{-5}$, the computation time is around 345 seconds. The volume of the maximal singularity-free orientation workspace changes to $V_{max} = 2.965849$ and the final step size ΔD changes to 6.103516×10^{-6}. The difference between the computed volumes is only 0.000408. Hence, $\varepsilon = 10^{-4}$ is already a good convergence precision with a reasonable computation time. It is not necessary to increase the convergence precision further.

9.5 Conclusions

This chapter addresses the determination of the maximal singularity-free orientation workspace at a prescribed position for the MSSM Gough-Stewart platform. Using the *Roll–Pitch–Yaw* angles (ϕ, θ, ψ), the orientation workspace at a prescribed position can be defined by 12 workspace surfaces. However, it is very difficult to analytically determine these 12 workspace surfaces in order to obtain the maximal singularity-free orientation workspace. Instead, a numerical algorithm is developed to solve this problem. The presented algorithm is able to determine the maximal singularity-free orientation workspace as well as the corresponding leg length ranges $[\rho_i^{min},\ \rho_i^{max}]$ $(i =$

$1, 2, ..., 6$). In order to compare the maximal singularity-free orientation workspace with the maximal singularity-free sphere, an iterative algorithm for determining the maximal singularity-free sphere is also provided. An example with an equilateral triangle base and platform is used to demonstate the presented algorithms. The results obtained can be applied to the geometric design or parameter (leg length) setup of the MSSM parallel robots.

Chapter 10

Maximal Singularity-Free Orientation Workspace Over a Position Region

The maximal singularity-free orientation workspace at a given position was addressed in Chapter 9. In practice, a parallel mechanism usually works in a range of positions. Hence, the maximal singularity-free orientation workspace over a position region is also interesting. Unfortunately, so far nobody has touched this topic. This chapter will present two algorithms to compute the maximal singularity-free orientation workspace over an interesting position region for the MSSM Gough-Stewart platform.

10.1 Introduction

To the best of the author's knowledge, the determination of the maximal singularity-free orientation workspace over a position region has not yet been addressed because of its complexity. In Chapter 9, the maximal singularity-free orientation workspace at a prescribed position was defined as one with its boundary just touching the singularity surface at some point(s). When the singularity-free orientation workspace reaches its maximal status, the six leg lengths are in the ranges $[\rho_i^{min},\ \rho_i^{max}]$ $(i = 1, 2, ..., 6)$. To determine the maximal singularity-free orientation workspace at a prescribed position, a procedure was developed. Obviously, what is determined in Chapter 9 is the "position-based maximal singularity-free orientation workspace", because this "maximal" singularity-free orientation workspace depends on the prescribed position. In other words, this "maximal" singularity-free orientation workspace is a function of the three coordinates (x, y, z) which define a position.

In this chapter, the effects of the three coordinates (x, y, z) on the "position-based maximal singularity-free orientation workspace" are analyzed first. Then, the definition and computation of the maximal singularity-free orientation workspace over an interesting position region are addressed for the MSSM Gough-Stewart platform.

10.2 Effect of the Considered Position

Consider the MSSM architecture used in Chapter 4 Section 4.4, i.e., both the base and the platform are equilateral triangles with a size ratio $k = \frac{3}{5}$. The geometric parameters are: $t_1 = \frac{1}{\sqrt[4]{3}}$, $t_2 = \sqrt[4]{3}$, $t_3 = \frac{3}{5\sqrt[4]{3}}$ and $t_4 = \frac{3\sqrt[4]{3}}{5}$. Take the centroid C_p of the platform as the end-effector P. Its position in the mobile frame $O'x'y'z'$ is $\mathbf{p}' = [0, \frac{\sqrt[4]{3}}{5}, 0]^T$.

10.2.1 Effect of the x Coordinate

The evolution of the volume V_i of the "position-based maximal singularity-free orientation workspace" as a function of the x coordinate for $y = \frac{2\sqrt[4]{3}}{3}$ and $z = \frac{5}{4}$ is shown in Fig. 10.1. An interesting observation is that when $x = 0$, V_i reaches a maximum.

As $(0, \frac{2\sqrt[4]{3}}{3}, 0)$ is exactly the centroid C_b of the base triangle, one concludes that if the considered position is chosen from the perpendicular line through the centroid C_b of the base, a maximal "position-based maximal singularity-free orientation workspace" can be obtained.

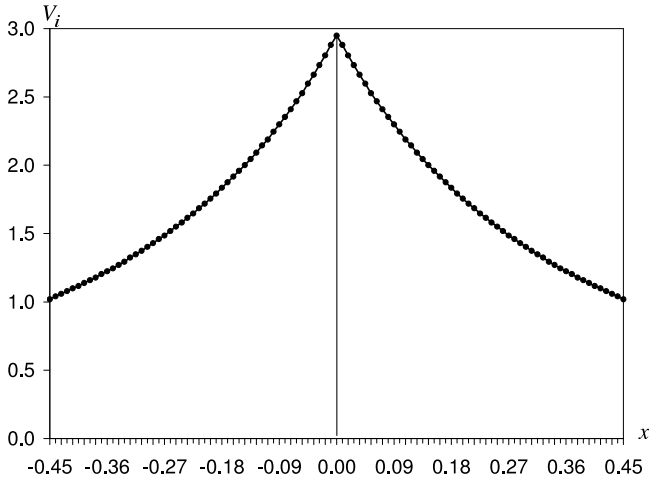

Figure 10.1: Volume V_i as a function of x ($y = \frac{2\sqrt[4]{3}}{3}$, $z = \frac{5}{4}$).

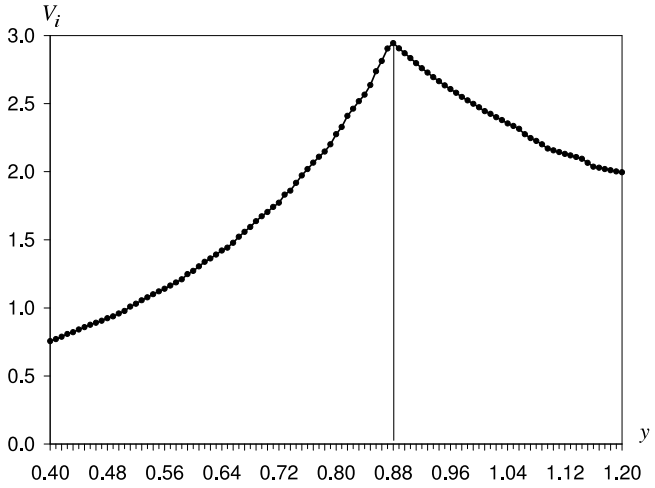

Figure 10.2: Volume V_i as a function of y ($x = 0$, $z = \frac{5}{4}$).

10.2.2 Effect of the y Coordinate

The evolution of the volume V_i of the "position-based maximal singularity-free orientation workspace" as a function of the y coordinate for $x = 0$ and $z = \frac{5}{4}$ is shown in Fig. 10.2. It can be seen that when $y = 0.88$, V_i reaches a maximum. As $0.88 \approx \frac{2\sqrt[4]{3}}{3}$, a conclusion similar to that of the above subsection can be made: when the considered point is chosen from the perpendicular line through the centroid C_b of the base, a maximal "position-based maximal singularity-free orientation workspace" can be obtained.

10.2.3 Effect of the z Coordinate

The evolution of the volume V_i of the "position-based maximal singularity-free orientation workspace" as a function of the z coordinate for $x = 0$ and $y = \frac{2\sqrt[4]{3}}{3}$ is shown in Fig. 10.3. It can be seen that when z is about 1.3, V_i reaches a maximum.

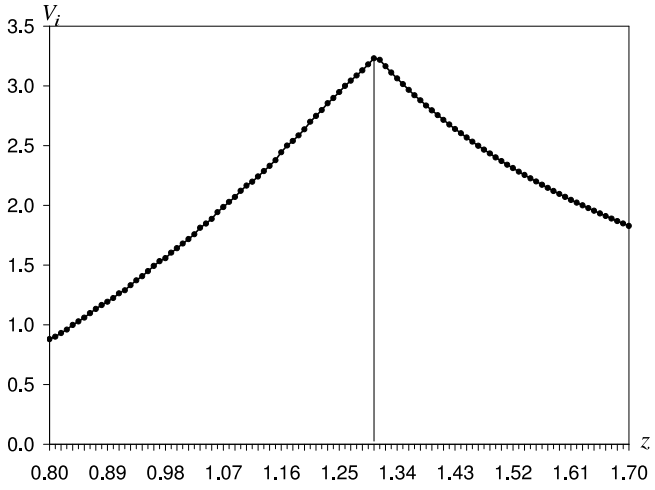

Figure 10.3: Volume V_i as a function of z ($x = 0$, $y = \frac{2\sqrt[4]{3}}{3}$).

10.2.4 Optimal Position

The results obtained in the above subsections show that the point $(0, \frac{2\sqrt[4]{3}}{3}, 1.3)$ seems to be the optimal position at which the "position-based maximal singularity-free orientation workspace" reaches a maximum 3.230874. To verify whether this conclusion is true, consider the following three-dimensional optimization problem:

$$\min_{x,y,z}(-V_i) \tag{10.1}$$

$$s.t. \qquad z > 0.$$

To solve the above optimization problem, Powell's search method [101] is used. Although it is difficult to find the global optimal solution, a solution with $x = 0$, $y = 0.881221$ and $z = 1.308381$ which leads to $V_i^{max} = 3.291199$ seems to be a good approximation of the global optimal solution. It can be seen that this optimal position is not exactly on the perpendicular line through the centroid C_b of the base because $0.881221 > \frac{2\sqrt[4]{3}}{3} (\approx 0.877383)$.

10.3 Singularity-Free Orientation Workspace over a Position Region

Similar to the definition of the total orientation workspace given in [15], the orientation workspace over a position region can be defined as the intersection of the orientation workspaces at all positions in the prescribed position region. The prescribed position region can be represented by a parallelepiped in the Cartesian space $Oxyz$ as shown in Fig. 10.4 in which $x \in [x_1, x_2]$, $y \in [y_1, y_2]$ and $z \in [z_1, z_2]$.

From Chapter 9, it is clear that at every prescribed position, there exists a maximal singularity-free orientation workspace. Hence, the maximal singularity-free orientation workspace over a position region can be defined as the intersection of the maximal singularity-free orientation workspaces at all positions in the prescribed position region.

10.4 Computational Algorithm

According to the definition given in the preceding section, in order to determine the maximal singularity-free orientation workspace over a position region, it is necessary to determine the maximal singularity-free orientation workspaces at all positions in the prescribed position region. However, for a prescribed position region as shown in Fig. 10.4, there are infinitely many positions. In practice, it is impossible to compute the maximal singularity-free orientation workspace at every individual position. One solution is to use the intersection of the maximal singularity-free orientation workspaces at a finite number of positions to approach the real maximal singularity-free orientation workspace over the prescribed position region under a given convergence precision. The finite number of positions can be chosen as follows: if the range of every dimension is evenly divided into n ($n \geq 1$) parts, the total number of obtained positions is $N =$

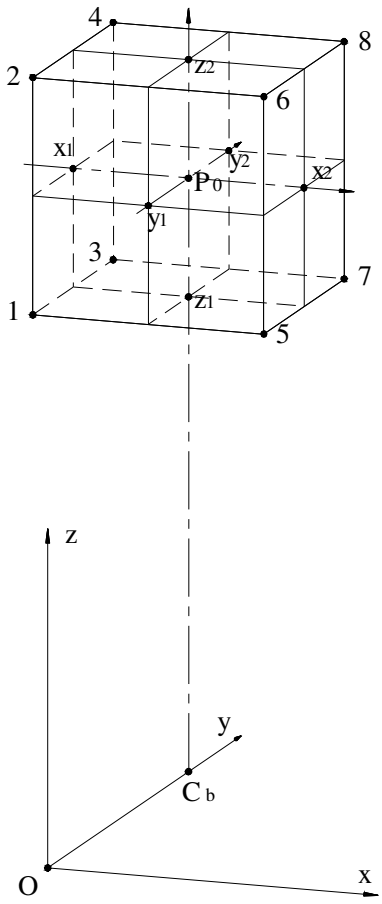

Figure 10.4: A position region defined by $x \in [x_1, x_2]$, $y \in [y_1, y_2]$ and $z \in [z_1, z_2]$.

$(n+1)^3$. For instance, if $n = 1$, the total number of obtained positions is 8 as shown in Fig. 10.4.

10.4.1 Basic Algorithm

In order to determine the maximal singularity-free orientation workspace over a prescribed position region, the following procedure can be used: first, compute the maximal singularity-free orientation workspace at every chosen position using the algorithm presented in Chapter 9. Then, determine their intersection which should satisfy the following condition:

$$\rho_{im}^{min} \leq \rho_{im} \leq \rho_{im}^{max} \quad (i = 1, 2, ..., 6; \quad m = 1, 2, ..., N) \tag{10.2}$$

where ρ_{im} is the leg length of leg i $(i = 1, 2, ..., 6)$ at position m $(m = 1, 2, ..., N)$, obtained for any orientation (ϕ, θ, ψ) inside the maximal singularity-free orientation workspace over the prescribed position region to be substituted into eq.(8.3).

The volume V of the maximal singularity-free orientation workspace over the prescribed position region can be given as

$$V \approx \sum_{k=0}^{M-1} \frac{(A_k + A_{k+1})\Delta\theta}{2} \tag{10.3}$$

where A_k $(k = 0, 1, ..., M)$ is the area of the common workspace section at θ_k. A_k can be computed using the method of Chapter 8 (see Fig. 8.4). The only difference is to make sure that every orientation (ϕ, θ, ψ) in the determined common workspace section satisfies eq.(10.2).

10.4.2 Modified Algorithm

In theory, the above presented basic algorithm is correct. However, this basic algorithm is not efficient in practice. When the number N of chosen positions is large enough, this algorithm consumes too much computer memory and becomes very slow or even breaks down. For instance, at every position, 12 variables are needed to keep the maximal and minimal leg lengths which lead to the platform holding the corresponding maximal

singularity-free orientation workspace. For N positions, the number of needed variables will be $12N$. When the number N is large enough, the main computation time is spent on determining the area of the common workspace section. To compute the height h_j^{ψ} of the common workspace section in the ψ direction at every given ϕ_j (see Fig. 8.4), it is necessary to compute all intersections of the line $\phi = \phi_j$ and $12N$ workspace section curves. To keep these intersections, a large number of variables is needed. When all intersections are available, it is necessary to order them using their ψ coordinates in order to separate the line $\phi = \phi_j$ into several segments. Then apply the condition of eq.(10.2) to determine those having contributions to h_j^{ψ}. To make the computed area of the common workspace section converge at a given precision, the above procedure needs to be repeated several times. Hence, the computation of the common workspace section is a time-consuming process.

To make the computation more efficient, the above basic algorithm is modified. Considering that the maximal singularity-free orientation workspaces at the eight vertices of the parallelepiped shown in Fig. 10.4 are relatively small and that their shapes are quite different from one to another, the possibility for these eight workspaces to contribute to the boundary of the maximal singularity-free orientation workspace over the prescribed position region may be relatively high. Hence, these eight positions are taken as the basic group. The intersection of these eight workspaces can be determined using the procedure mentioned in the basic algorithm. If some workspace has no contribution to the boundary of their intersection, it is discarded. The remaining positions will form the valid group, which may contain only K positions. When the maximal singularity-free orientation workspace at a new position is available, the new one will be added into the valid group to form a new group. Similarly, by determining the intersection of the maximal singularity-free orientation workspaces corresponding to the new group and discarding those without contribution to the boundary, a new valid group will be formed. This procedure is repeated until all chosen positions are considered. The final obtained intersection of the maximal singularity-free orientation workspaces corresponding to the last valid group is also the intersection of the maximal singularity-free orientation workspaces at all considered positions.

As the number of positions contained in every group is small, only a few variables are needed to keep the intermediate results. Hence, less memory is occupied. Obviously, every time after a new position is added, the valid group needs to be updated. But the required computation time is significantly reduced because of the small number of

positions contained in each group.

10.5 Example

In order to demonstrate the presented algorithms, consider the MSSM architecture used in Section 10.2. Take the point $(0, \frac{2\sqrt[4]{3}}{3}, \frac{5}{4})$ as the centroid P_0 of the prescribed position region. Suppose the offset from P_0 to both sides in every dimension is 0.25. Therefore, the prescribed position region can be defined by three ranges as follows: $x \in [-0.25, 0.25]$, $y \in [0.627383, 1.127383]$ and $z \in [1, 1.5]$.

Fig. 10.5 shows the evolution of the volume V of the intersection as a function of the number N of chosen positions. This graph has some fluctuations, especially when N is small. In other words, the intersection does not decrease monotonically with respect to the number of chosen positions. For instance, when every range of three dimensions is evenly divided into two parts ($n = 2$ and $N = 3^3$), the volume of the intersection is $V \approx 0.443978$. When every range of three dimensions is evenly divided into three parts ($n = 3$ and $N = 4^3$), the volume of the intersection should decrease. However, the computation shows that this is not the case. Instead of decreasing, the volume of the intersection increases slightly to $V \approx 0.444180$. The corresponding final valid groups of positions in these two cases are respectively listed in Table 10.1 and Table 10.2, where V_i denotes the corresponding maximal singularity-free orientation workspace. These two tables show that the first four positions are exactly the same. Actually, these are the four positions that form the valid group with $n = 1$ and $N = 8$. However, the fifth valid position in Table 10.1 is different from the fifth valid position in Table 10.2. Besides, Table 10.2 has one more valid position.

Although the number of valid positions in the case with $n = 3$ and $N = 4^3$ is larger than that in the case with $n = 2$ and $N = 3^3$, the fifth and the sixth valid positions in Table 10.2 contribute less to the boundary of the intersection than the fifth valid position in Table 10.1. As a result, the intersection in the case with $n = 3$ and $N = 4^3$ goes up a little as shown in Fig. 10.5. However, with an increase of the number of chosen positions, the network of the prescribed position region as shown in Fig. 10.4 becomes denser. The general trend of the evolution of the intersection decreases with respect to N. The fluctuation becomes progressively smaller until the

intersection converges at the maximal singularity-free orientation workspace over the prescribed position region. When $n = 20$ and $N = 21^3$, the volume of the intersection is $V \approx 0.443731$. If the convergence precision is given as 10^{-4}, this intersection is already a very good approximation of the maximal singularity-free orientation workspace over the prescribed position region.

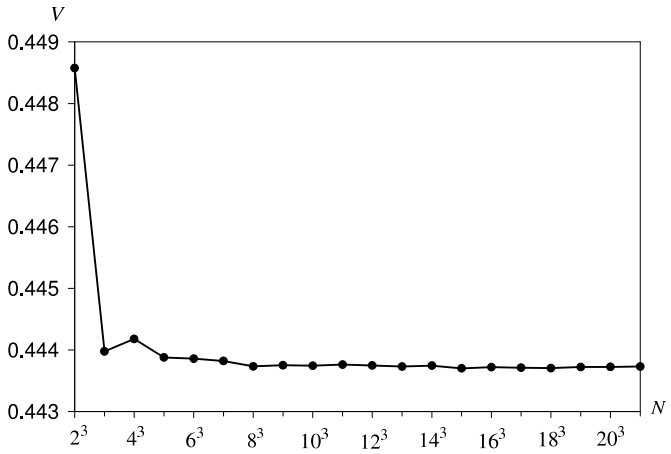

Figure 10.5: Volume V as a function of N.

Table 10.1: The final valid group of positions for $N = 3^3$.

i	x	y	z	V_i
1	**-0.25**	**0.627383**	**1**	**0.781083**
2	**-0.25**	**1.127383**	**1**	**0.543827**
3	**0.25**	**0.627383**	**1**	**0.781083**
4	**0.25**	**1.127383**	**1**	**0.543827**
5	0	0.627383	1	0.706455

Table 10.1 and Table 10.2 show that the first four positions are exactly the same as those forming the valid group of positions in the case with $n = 1$ and $N = 8$. Actually, no matter how many parts each range of the three dimensions is divided into, these four positions are always contained in the final valid group. For instance, Table 10.3 shows the case with $n = 20$ and $N = 21^3$.

Another interesting observation is that the number of valid positions is small. Table 10.3 shows that even if the number of chosen positions becomes very large (say

Table 10.2: The final valid group of positions for $N = 4^3$.

i	x	y	z	V_i
1	**-0.25**	**0.627383**	**1**	**0.781083**
2	**-0.25**	**1.127383**	**1**	**0.543827**
3	**0.25**	**0.627383**	**1**	**0.781083**
4	**0.25**	**1.127383**	**1**	**0.543827**
5	-0.083333	0.627383	1	0.715892
6	0.083333	0.627383	1	0.715892

Table 10.3: The final valid group of positions for $N = 21^3$.

i	x	y	z	V_i
1	**-0.25**	**0.627383**	**1**	**0.781083**
2	**-0.25**	**1.127383**	**1**	**0.543827**
3	**0.25**	**0.627383**	**1**	**0.781083**
4	**0.25**	**1.127383**	**1**	**0.543827**
5	-0.175	0.627383	1	0.746916
6	-0.125	0.627383	1	0.727315
7	-0.1	0.627383	1	0.719813
8	-0.075	0.627383	1	0.713755
9	-0.05	0.627383	1	0.709907
10	-0.025	0.627383	1	0.707139
11	0	0.627383	1	0.706455
12	0.025	0.627383	1	0.707139
13	0.05	0.627383	1	0.709907
14	0.075	0.627383	1	0.713755
15	0.1	0.627383	1	0.719813
16	0.125	0.627383	1	0.727315
17	0.175	0.627383	1	0.746916

9261), the total number of valid positions is only 17. This shows that the maximal singularity-free orientation workspaces at most positions have no contribution to the boundary of the intersection. However, it is very difficult to accurately judge whether a position has a contribution before performing some necessary computations. To obtain a good approximation for the maximal singularity-free orientation workspace over the

prescribed position region, the only way is to increase the number of chosen positions, i.e., to make the network of the prescribed position region as shown in Fig. 10.4 denser.

Besides, Table 10.3 also shows that if the chosen positions lie on the segment $1-5$, the corresponding maximal singularity-free orientation workspaces have a contribution to the boundary of the intersection because they are small.

10.6 Computational Cost

The presented algorithms were programmed using C++ 6.0 in a Linux environment (Fedora 7, Kernel 2.6.22.1-41, 64 bits). The computer used has a dual core CPU with 2.2 GHz. If the convergence precision is given as $\varepsilon = 10^{-4}$, using the modified algorithm, the evolution of the time t needed for computing the volume V of the intersection as a function of the number N of chosen positions is shown in Fig. 10.6. It can be seen that the time used increases very quickly with the number of positions. Obviously, obtaining a very good approximation for the maximal singularity-free orientation workspace over the prescribed position region under a given convergence precision is a time-consuming process. For instance, the intersection at $N = 21^3$ can be regarded as a very good approximation. However, its computation requires 1002 minutes.

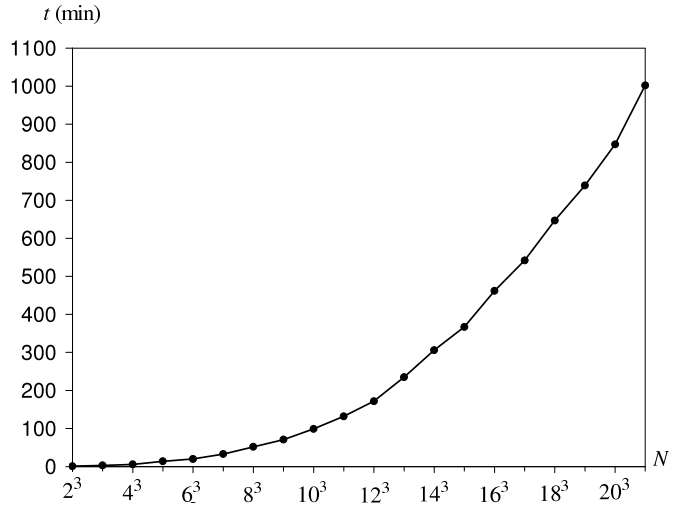

Figure 10.6: Computation time t as a function of N.

In some applications, such a precise result may not be necessary. In this situation, the intersection with $N = 8$ can be regarded as a good estimation for the maximal singularity-free orientation workspace over the prescribed position region. Actually, the difference between the volume at $N = 8$ and that at $N = 21^3$ is only 0.004845. The error is only 1.092%. But the computational time at $N = 8$ is around 1 minute, only 1/1002 of that at $N = 21^3$.

10.7 Conclusions

So far, no work has been found to address the maximal singularity-free orientation workspace over a position region. In practice, this type of workspace is also interesting because a mechanism often works at a range of positions. This chapter presents two algorithms to compute the maximal singularity-free orientation workspace over an interesting position region for the MSSM Gough-Stewart platform.

The given example shows that obtaining the maximal singularity-free orientation workspace over a prescribed position region is a time-consuming process. Besides, the example also shows that only a few positions among the discretized positions have contributions to the boundary of the maximal singularity-free orientation workspace over the prescribed position region. Unfortunately, it is very difficult to identify these valid positions before performing some necessary computations.

In some applications, the exact maximal singularity-free orientation workspace over a prescribed position region may not be necessary. The intersection at $N = 8$ can be regarded as a good estimation.

Chapter 11

Geometric Optimization

This chapter focuses on analyzing the effects of the geometric parameters on the singularity-free workspace in order to determine the optimal architecture for the MSSM Gough-Stewart platform. To this end, the reference orientation is taken as the considered orientation because it is an impartial orientation. In this orientation, the singularity surface becomes a plane coinciding with the base plane. Hence, the analytic algorithm developed in Chapter 6 can be used to determine the "architecture-based maximal singularity-free workspace". The analysis results show that: (1) for similar isosceles triangle base and platform, the optimal architecture is one for which both the base and the platform are equilateral triangles and the size ratio between the platform and the base is $\frac{1}{2}$; (2) if the base and the platform are not similar triangles, the global optimal architecture is difficult to determine. Only an approximate optimal architecture is available.

11.1 Introduction

In the preceding six chapters, the analysis of both the position singularity-free workspace and the orientation singularity-free workspace is based on a MSSM with a given architecture, i.e., the geometric parameters (t_1, t_2, t_3, t_4) are constants. Equation (4.15) shows that the singularity expression is a function of the geometric parameters. For different sets of geometric parameters, the singularity loci are different. Hence, the singularity-free workspace should change accordingly.

Referring to Chapter 5, when the boundary of the singularity-free workspace just touches the singularity surface at some point(s), the singularity-free workspace based on the given architecture reaches its maximal status. For different architectures (corresponding to different geometric parameters), such "maximal" singularity-free workspaces should be different. Hence, what is determined in Chapter 5 is actually the "architecture-based maximal singularity-free workspace", because it is based on a given architecture.

This chapter focuses on analyzing the effects of the geometric parameters on the "architecture-based maximal singularity-free workspace" around a point of interest P_0 in an impartial orientation for the MSSM Gough-Stewart platform. The objective is to determine the optimal architecture that maximizes the "architecture-based maximal singularity-free workspace". Hence, the maximal singularity-free workspace mentioned in this chapter is the maximum of the "architecture-based maximal singularity-free workspace".

In the context of a given architecture, the "architecture-based maximal singularity-free workspace" will be simply referred to as the maximal singularity-free workspace for concise description as long as no confusion exists. However, in the context of geometric optimization, the difference between these two concepts should be highlighted.

11.2 Point of Interest and Impartial Orientation

The maximal singularity-free workspace determined in Chapter 5 depends on the prescribed point P_0, the orientation of the platform as well as the geometric parameters.

If all these factors are taken into consideration at the same time, the problem becomes too complex to be solved. Obviously, for the problem of geometric optimization, the geometric parameters should be the variables to be optimized. The other factors such as the point of interest P_0 and the orientation of the platform can be prescribed. Now the problem becomes: which point and which orientation should be chosen for the geometric optimization.

In practice, the most interesting point P_0 should lie above the base and on the perpendicular line through the centroid $C_b(x_{cb}, y_{cb}, 0)$ of the base. Referring to Fig. 4.12, $x_{cb} = 0$ and $y_{cb} = \frac{2}{3}t_2$. For a base of unit area, $\frac{5}{4}$ is a reasonable height for the point of interest P_0. Hence, point P_0 can be chosen as $P_0(0, \frac{2}{3}t_2, \frac{5}{4})$. This choice is arbitrary but reasonable.

The orientation strongly affects the singularity-free workspace. In a general orientation, the singularity surface changes with the geometric parameters. The singularity surface of a good architecture may pass through point P_0. According to the definition given in Chapter 5, the singularity-free workspace around point P_0 will then vanish. For instance, the base in Fig. 11.1(a) is an equilateral triangle of unit area and the base in Fig. 11.1(b) is not an equilateral triangle of unit area. The size ratios between the platform and the base in these two cases are $\frac{3}{5}$. If the orientation is given by $\phi = -0.527351$ and $\theta = \psi = -1.054701$, the singularity surface in Fig. 11.1(a) passes through the point of interest P_0. As a result, the singularity-free workspace around P_0 vanishes. But the singularity-free workspace around P_0 in Fig. 11.1(b) is not 0. It seems that the architecture in Fig. 11.1(b) is better than that in Fig. 11.1(a). However, the situation in other orientations, say the reference orientation, is quite different (see Fig. 11.2). This shows that the chosen orientation with $\phi = -0.527351$ and $\theta = \psi = -1.054701$ is a partial one which cannot be used for geometric optimization.

The above case study shows that in order to optimize the geometric parameters, an impartial orientation should be used. Considering that the singularity surface in the reference orientation is a plane that coincides with the base plane, for any reasonable point P_0 which is above the base, there always exists a singularity-free workspace. Hence, the reference orientation can be considered as an impartial orientation. On the other hand, in practice, the platform usually translates to the desired position P_0 in the reference orientation first. Then, it rotates to the desired orientation (desired pose). Hence, the "architecture-based maximal singularity-free workspace" in the reference

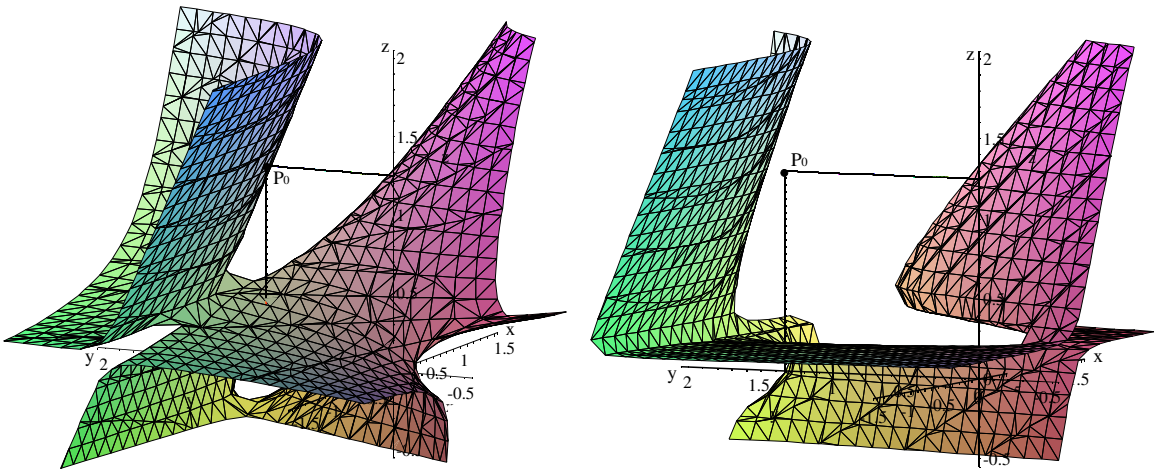

(a) $t_1 = \frac{1}{\sqrt[4]{3}}$, $t_2 = \sqrt[4]{3}$, $k = \frac{3}{5}$. (b) $t_1 = 0.5$, $t_2 = 2$, $k = \frac{3}{5}$.

Figure 11.1: The singularity surfaces for different architectures in the orientation with $\phi = -0.527351$, $\theta = \psi = -1.054701$.

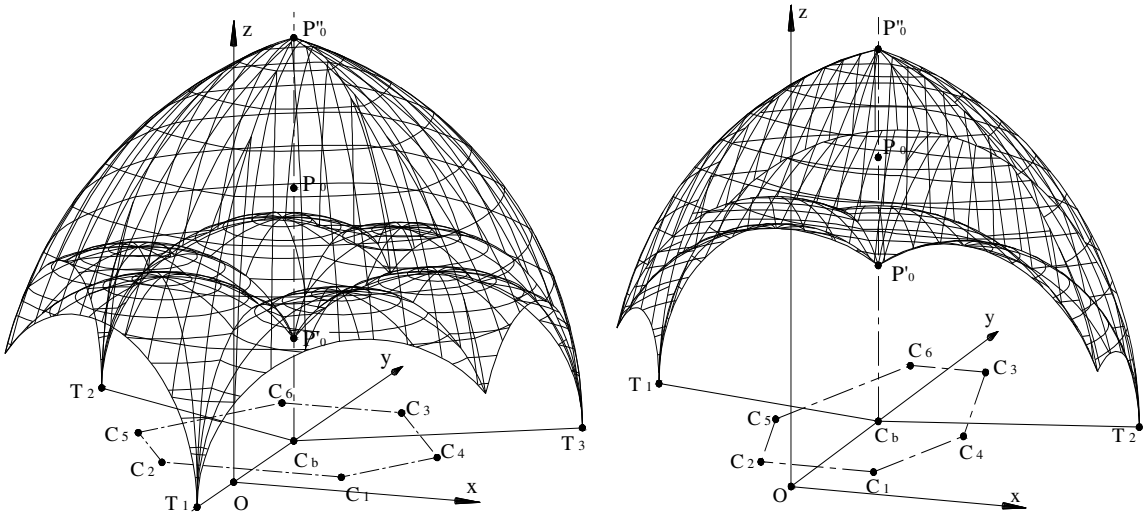

(a) $t_1 = \frac{1}{\sqrt[4]{3}}$, $t_2 = \sqrt[4]{3}$, $k = \frac{3}{5}$. (b) $t_1 = 0.5$, $t_2 = 2$, $k = \frac{3}{5}$.

Figure 11.2: The maximal singularity-free workspaces for different architectures in the reference orientation ($\phi = \theta = \psi = 0$).

orientation becomes an index of practical interest. This chapter will take the reference orientation as the considered orientation. Therefore, the objective of the geometric optimization problem can be described as follows: *Maximize the "architecture-based maximal singularity-free workspace" around the point of interest P_0 in the reference orientation by optimizing the geometric parameters of the MSSM Gough-Stewart plat-*

form.

11.3 Singularity-Free Workspace in the Reference Orientation

In the reference orientation, the singularity surface becomes a plane coinciding with the base plane. As shown in Chapter 5, the six centres of the workspace spheres lie on the singularity surface, i.e., C_i $(i = 1, 2, ..., 6)$ lie on the base plane, see Table 11.1. Hence, the analytic algorithm presented in Chapter 6 can be used to determine the maximal singularity-free workspace around the point of interest P_0 in the reference orientation for any given MSSM architecture.

Table 11.1: The six centres of the workspace spheres in the reference orientation.

C_i	x_{ci}	y_{ci}	z_{ci}
1	t_3	$t_4/3$	0
2	$-t_3$	$t_4/3$	0
3	$t_1 - t_3$	$t_2 + t_4/3$	0
4	t_1	$t_2 - 2t_4/3$	0
5	$-t_1$	$t_2 - 2t_4/3$	0
6	$-t_1 + t_3$	$t_2 + t_4/3$	0

11.4 Effect of the Geometric Parameters

This section analyzes the effects of the geometric parameters on the "architecture-based maximal singularity-free workspace" around the point of interest P_0 in the reference orientation.

For a base of unit area, one independent geometric parameter t_1 is enough to define the base. If the platform is similar to the base, the platform can be described by the size ratio k between the platform and the base. Hence, the total number of

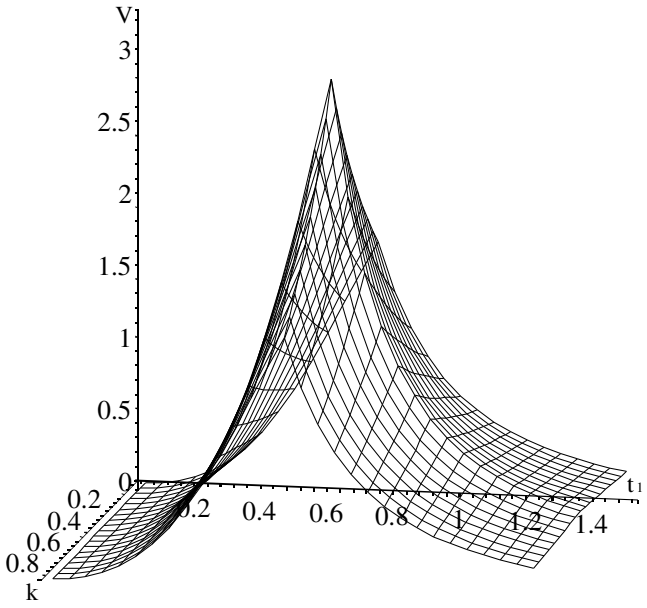

Figure 11.3: Volume V as a function of t_1 and k.

independent geometric parameters is only two. The evolution of the volume V of the "architecture-based maximal singularity-free workspace" as a function of t_1 and k is shown in Fig. 11.3.

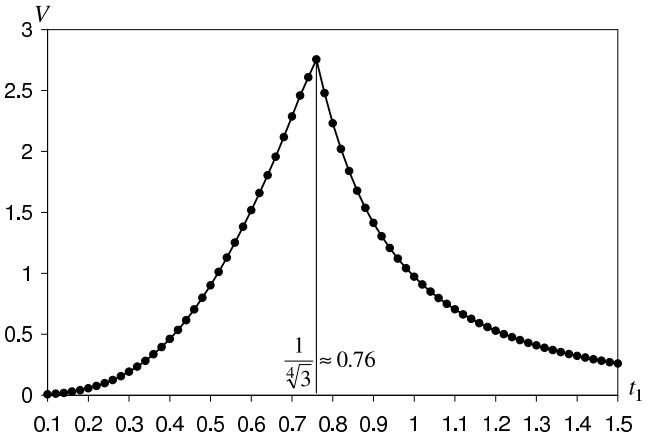

Figure 11.4: Volume V as a function of t_1 ($k = 0.6$).

For a given size ratio k, the "architecture-based maximal singularity-free workspace" is a function of t_1. The evolution of the volume V of the "architecture-based maximal singularity-free workspace" as a function of t_1 for $k = 0.6$ is shown in Fig. 11.4. It can be seen that when the base becomes an equilateral triangle (corresponding to

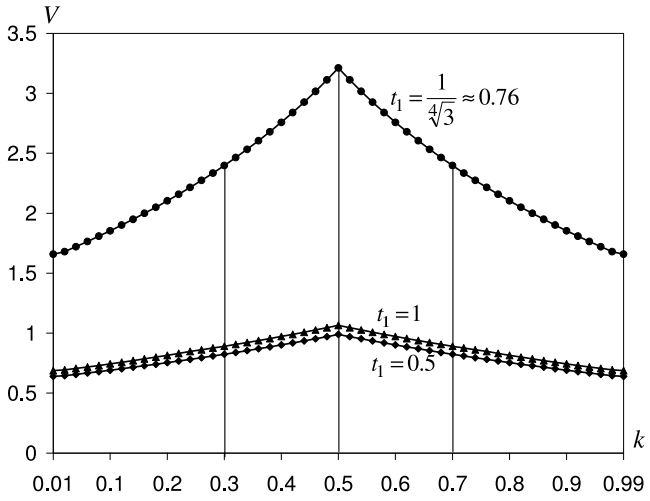

Figure 11.5: Volume V as a function of k for given t_1.

$t_1 = \frac{1}{\sqrt[4]{3}} \approx 0.76$), V reaches a maximum. In other words, for a given size ratio k, when the base is an equilateral triangle, the "architecture-based maximal singularity-free workspace" reaches a maximum.

Now, consider the effect of the size ratio k on the "architecture-based maximal singularity-free workspace". Fig. 11.5 shows three cases respectively with $t_1 = 0.5$, $t_1 = \frac{1}{\sqrt[4]{3}} \approx 0.76$ and $t_1 = 1$. It can be seen that, for every size ratio, the volume V in the case with $t_1 = \frac{1}{\sqrt[4]{3}} \approx 0.76$ is the largest compared to the other two cases. A more interesting point is that when the size ratio is equal to $\frac{1}{2}$, the volume V in all three cases reaches a maximum. Furthermore, the three curves are symmetric about the size ratio $k = \frac{1}{2}$. This observation can be proved as follows:

For a base of unit area, $t_2 = 1/t_1$. When the size ratio k is given, $t_3 = kt_1$ and $t_4 = k/t_1$. The area S of the hexagon $C_1C_2C_5C_6C_3C_4$ as shown in Fig. 11.6 can be given as follows:

$$S = 1 + 2k - 2k^2. \tag{11.1}$$

Equation (11.1) shows that the area S of the hexagon $C_1C_2C_5C_6C_3C_4$ is independent from t_1 and only a function of the size ratio k. When $k = \frac{1}{2}$, S reaches a maximum. Referring to Table 11.1, in this case, $y_{c4} = y_{c5} = x_{cb} = \frac{2}{3t_1}$, $\overline{C_2C_1} = \overline{C_6C_3} = t_1$ and $(y_{c3} - y_{c4}) = (y_{c4} - y_{c1}) = \frac{1}{2t_1}$. Hence, the hexagon $C_1C_2C_5C_6C_3C_4$ is symmetric about the line parallel to the x axis and through the centroid C_b of the base.

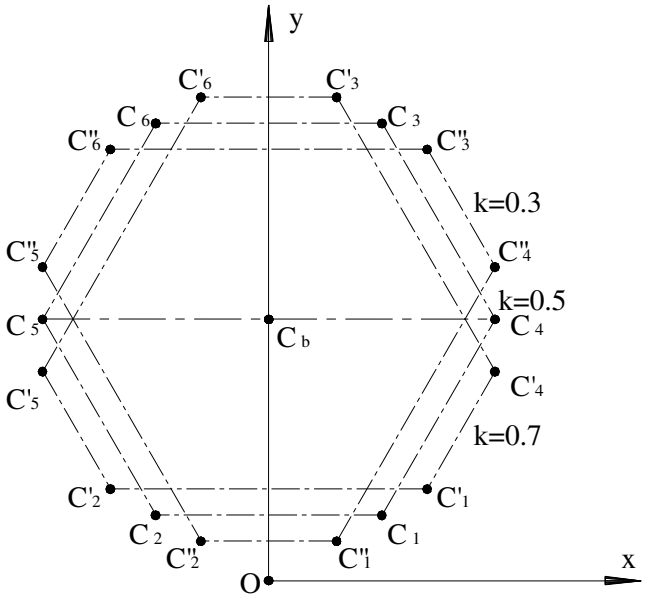

Figure 11.6: The six centres of the workspace spheres with $t_1 = \frac{1}{\sqrt[4]{3}}$ and $k = 0.3,\ \frac{1}{2},\ 0.7$.

Table 11.2: The six centres of the workspace spheres with $k = \frac{1}{2} + \Delta$.

C_i	x_{ci}	y_{ci}	z_{ci}
1	$(1/2+\Delta)t_1$	$(1/2+\Delta)/(3t_1)$	0
2	$-(1/2+\Delta)t_1$	$(1/2+\Delta)/(3t_1)$	0
3	$(1/2-\Delta)t_1$	$(7/2+\Delta)/(3t_1)$	0
4	t_1	$2(1-\Delta)/(3t_1)$	0
5	$-t_1$	$2(1-\Delta)/(3t_1)$	0
6	$-(1/2-\Delta)t_1$	$(7/2+\Delta)/(3t_1)$	0

Table 11.3: The six centres of the workspace spheres with $k = \frac{1}{2} - \Delta$.

C_i	x_{ci}	y_{ci}	z_{ci}
1	$(1/2-\Delta)t_1$	$(1/2-\Delta)/(3t_1)$	0
2	$-(1/2-\Delta)t_1$	$(1/2-\Delta)/(3t_1)$	0
3	$(1/2+\Delta)t_1$	$(7/2-\Delta)/(3t_1)$	0
4	t_1	$2(1+\Delta)/(3t_1)$	0
5	$-t_1$	$2(1+\Delta)/(3t_1)$	0
6	$-(1/2+\Delta)t_1$	$(7/2-\Delta)/(3t_1)$	0

When $k = \frac{1}{2} \pm \Delta$ (Δ is a increment in k), the coordinates of C_i ($i = 1, 2, ..., 6$) are respectively listed in Table 11.2 and Table 11.3. The corresponding hexagons are $C'_1C'_2C'_5C'_6C'_3C'_4$ and $C'''_1C'''_2C'''_5C'''_6C'''_3C'''_4$. Comparing Table 11.2 with Table 11.3, it can be found that the two hexagons $C'_1C'_2C'_5C'_6C'_3C'_4$ and $C'''_1C'''_2C'''_5C'''_6C'''_3C'''_4$ are symmetric about the line parallel to the x axis and through the centroid C_b of the base. Hence, their corresponding maximal singularity-free workspaces are the same. The only difference between them is their orientation, see Fig. 11.7. Actually, the hexagon $C'''_1C'''_2C'''_5C'''_6C'''_3C'''_4$ can be obtained by rotating the hexagon $C'_1C'_2C'_5C'_6C'_3C'_4$ by 180° around C_b.

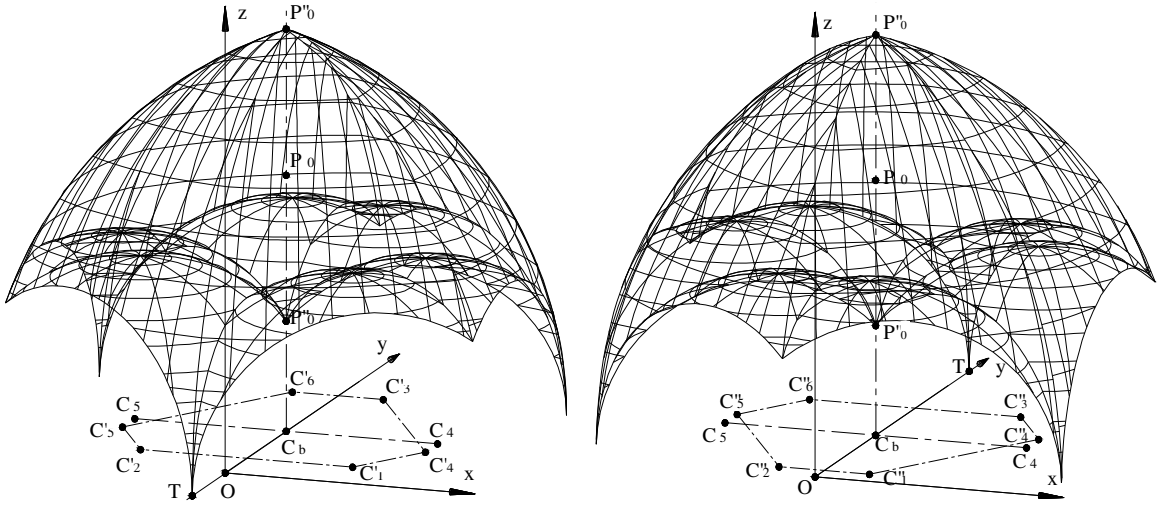

(a) $t_1 = \frac{1}{\sqrt[4]{3}}$ and $k = 0.7$ (b) $t_1 = \frac{1}{\sqrt[4]{3}}$ and $k = 0.3$.

Figure 11.7: The maximal singularity-free workspace with different size ratios.

11.5 Geometric Optimization

11.5.1 2D Optimization

For a base of unit area, $t_2 = 1/t_1$. The only independent geometric parameter to define the base is t_1. If the platform is similar to the base, the size ratio k is enough to describe the platform. Hence, for similar base and platform, the independent geometric parameters used to define the mechanism are only two: t_1 and k. In this case, the geometric optimization problem is a two-dimensional problem which can be formulated

as follows:

$$\min_{t_1,k}(-V) \tag{11.2}$$

$$s.t.$$

$$t_1 > 0,$$
$$0 < k < 1.$$

where V is the volume of the "architecture-based maximal singularity-free workspace" which is a function of t_1 and k. The constraints are $t_1 > 0$ and $0 < k < 1$.

To solve the above optimization problem, Powell's search method [101] is used. The optimization results with different sets of initial values (t_1^0, k^0) are listed in Table 11.4. The distribution of the initial values is shown as Fig. 11.8. From Table 11.4, it can be seen that for any set of reasonable initial values, the two independent geometric parameters (t_1, k) always converge at $(\frac{1}{\sqrt[4]{3}} \approx 0.759836, \frac{1}{2})$. The volume of the corresponding maximal singularity-free workspace as shown in Fig. 11.9 is 3.211712. In other words, it can be reasonably conjectured that $(\frac{1}{\sqrt[4]{3}}, \frac{1}{2})$ is the global solution for this two-dimensional geometric optimization problem. When $t_1 = \frac{1}{\sqrt[4]{3}}$, the base is an equilateral triangle of unit area. Hence, the optimal architecture obtained is one for which both the base and the platform are equilateral triangles with a size ratio $\frac{1}{2}$. This result is consistent with the analysis performed in the previous section.

Table 11.4: Results of the 2D optimization

No.	t_1^0	k^0	t_1	k	V_{max}
1	0.509836	0.25	0.759059	0.499957	3.203626
2	0.509836	0.50	0.759059	0.500000	3.203770
3	0.509836	0.75	0.759059	0.500043	3.203626
4	0.759836	0.25	0.759836	0.499957	3.211567
5	0.759836	0.50	0.759836	0.500000	3.211712
6	0.759836	0.75	0.759836	0.500043	3.211567
7	1.009836	0.25	0.759772	0.499957	3.210869
8	1.009836	0.50	0.759772	0.500000	3.211013
9	1.009836	0.75	0.759772	0.500043	3.210869

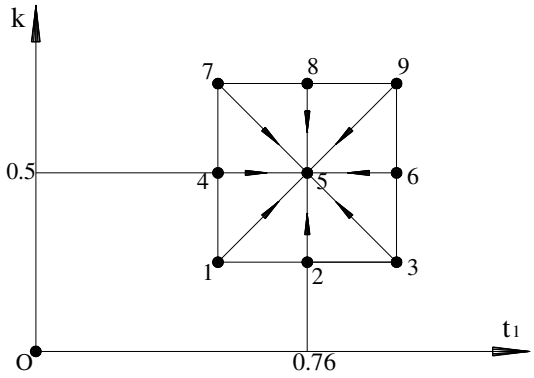

Figure 11.8: Distribution of the initial values for the 2D optimization.

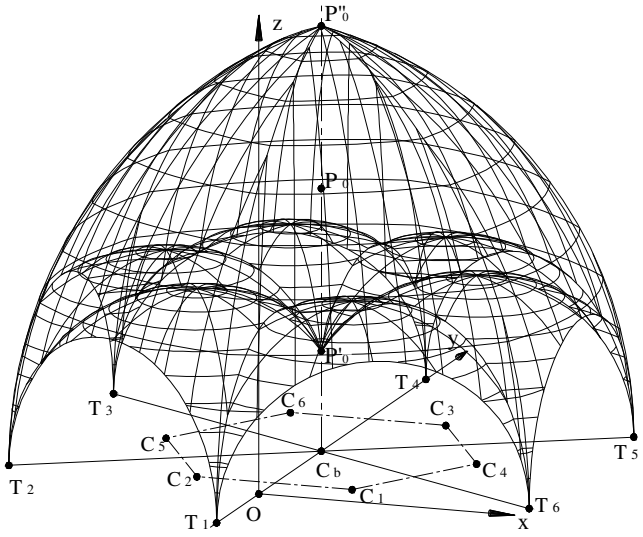

Figure 11.9: The maximal singularity-free workspace for similar base and platform with $t_1 = \frac{1}{\sqrt[4]{3}}$, $t_2 = \sqrt[4]{3}$ and $k = \frac{1}{2}$.

11.5.2 3D Optimization

When the platform is not similar to the base, the number of independent geometric parameters used to completely define the mechanism increases to three: t_1, t_3 and t_4. Now the problem becomes: how to find the optimal set of t_1, t_3 and t_4 in order to maximize the "architecture-based maximal singularity-free workspace". Obviously, in this case, the geometric optimization problem becomes a three-dimensional problem which can be formulated as follows:

$$\min_{t_1,t_3,t_4} (-V) \tag{11.3}$$

$$
\begin{aligned}
&s.t.\\
&\quad 0 < t_3 < t_1,\\
&\quad 0 < t_4 < t_2 (= 1/t_1).
\end{aligned}
$$

where V is the volume of the "architecture-based maximal singularity-free workspace" which is now a function of t_1, t_3 and t_4. The constraints become $0 < t_3 < t_1$ and $0 < t_4 < 1/t_1$.

To solve the above optimization problem, again Powell's search method [101] is used. In order to find the global optimal solution, 125 different sets of initial values (t_1^0, t_3^0, t_4^0) are taken for analysis. The distribution of these initial values is shown in Fig. 11.10. The centroid numbered 63 takes the optimal solution with similar base and platform, i.e., $t_1^0 = \frac{1}{\sqrt[4]{3}}$, $t_3^0 = \frac{1}{2\sqrt[4]{3}}$ and $t_4^0 = \frac{\sqrt[4]{3}}{2}$. The other initial nodes can be obtained by the following rule: in the t_1 axis, take $\frac{1}{\sqrt[4]{3}}$ as the central value and respectively offset 0.25 and 0.5 on both sides. Hence, five values $(0.259836, 0.509836, \frac{1}{\sqrt[4]{3}} \approx 0.759836, 1.009836, 1.259836)$ for t_1^0 are available. In the t_3 axis, take $\frac{1}{2\sqrt[4]{3}}$ as the central value and respectively offset 0.15 and 0.3 on both sides. Hence, five values $(0.079918, 0.229918, \frac{1}{2\sqrt[4]{3}} \approx 0.379918, 0.529918, 0.679918)$ for t_3^0 are available. Finally, in the t_4 axis, take $\frac{\sqrt[4]{3}}{2}$ as the central value and respectively offset 0.25 and 0.5 on both sides. Five values $(0.158037, 0.408037, \frac{\sqrt[4]{3}}{2} \approx 0.658037, 0.908037, 1.158037)$ for t_4^0 are available. Therefore, the total number of combinations is 125.

Unfortunately, for different initial values (t_1^0, t_3^0, t_4^0), these three geometric parameters may not converge at one single point as in the case of the 2D optimization problem. The evolution of the local V_{max} as a function of the 125 sets of initial values are shown in Fig. 11.11. From this figure, it can be seen that starting from the initial values at node 85, the obtained local $V_{max} \approx 3.366039$ is the largest one compared to the other nodes. This local V_{max} can be regarded as the approximate global maximal singularity-free workspace as shown in Fig. 11.12. From the obtained optimal geometric parameters listed in Table 11.5, the platform is an isosceles triangle with $\angle P_1P_4P_2 = 74.3°$ and a area of 0.243215. The base is also an isosceles triangle of unit area with $\angle B_5B_1B_3 = 55.7°$.

Besides, there are 10 other sets (numbers 6, 25, 31, 50, 56, 75, 81, 100, 106, 125) of initial values that lead to a local V_{max} value that is almost the same and close to 3.366039. Actually, starting from these nodes, the three geometric parameters converge

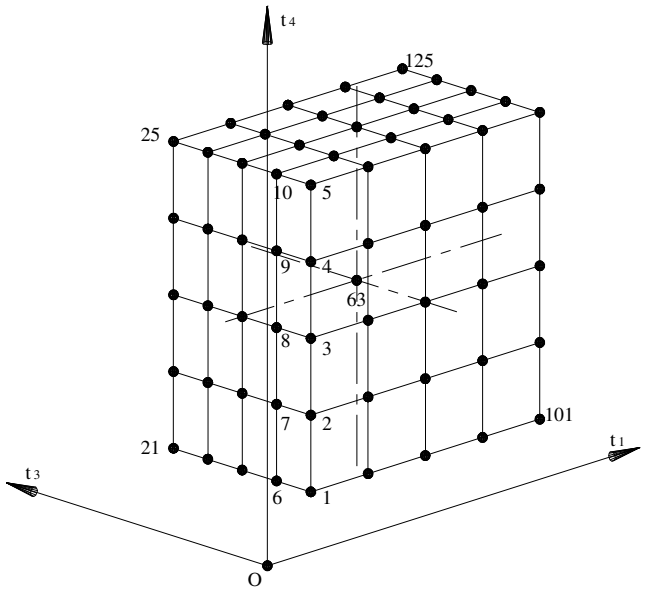

Figure 11.10: Distribution of the initial values for the 3D optimization.

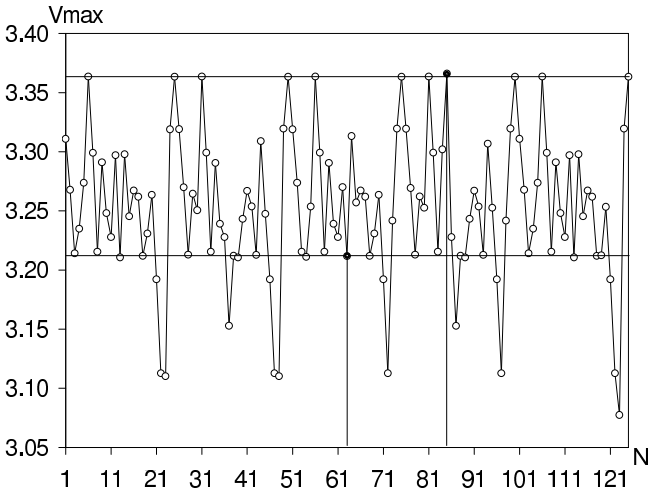

Figure 11.11: The local V_{max} as a function of the initial nodes.

at almost the same point, see Table 11.5. The obtained mechanisms hold the following characteristics: the platforms are isosceles triangles with $\angle P_1P_4P_2$ close to 38.4° and an area of approximately 0.235738. The bases are also isosceles triangles of unit area with $\angle B_5B_1B_3$ close to 55.3°. Hence, the obtained bases are close to that obtained by using node 85 as the initial values. But the platforms are quite different.

Furthermore, Fig. 11.11 shows that the local V_{max} values by using the initial values

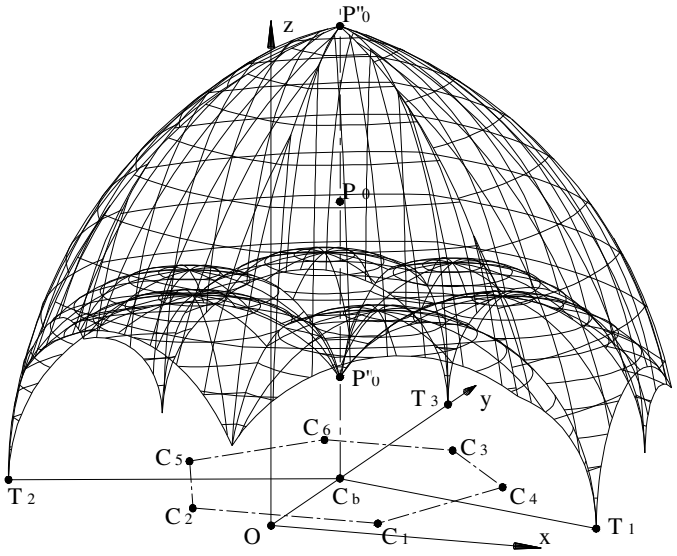

Figure 11.12: The approximate global maximal singularity-free workspace.

at the other 24 nodes (numbers 3, 8, 13, 18, 28, 33, 38, 39, 43, 53, 54, 58, 63, 68, 78, 83, 88, 89, 93, 103, 108, 113, 118 and 119) are very close to 3.211712 which is the global V_{max} for the case with similar base and platform. Also, there are 13 nodes that lead to local V_{max} values smaller than 3.211712. The remaining 81 nodes lead to local V_{max} values between 3.211712 and 3.366039.

Table 11.5: Partial results of the 3D optimization

No.	t_1^0	t_3^0	t_4^0	t_1	t_3	t_4	V_{max}
6	0.259836	0.229918	0.158037	0.724003	0.286678	0.822308	3.363599
25	0.259836	0.679918	1.158037	0.723843	0.286035	0.823057	3.363499
31	0.509836	0.229918	0.158037	0.724003	0.286676	0.822310	3.363600
50	0.509836	0.679918	1.158037	0.723874	0.286157	0.822915	3.363411
56	0.759836	0.229918	0.158037	0.724003	0.286676	0.822310	3.363600
75	0.759836	0.679918	1.158037	0.723869	0.286137	0.822938	3.363426
81	1.009836	0.229918	0.158037	0.724004	0.286682	0.822303	3.363596
85	1.009836	0.229918	1.158037	0.726748	0.429369	0.566447	3.366039
100	1.009836	0.679918	1.158037	0.723876	0.286166	0.822904	3.363405
106	1.259836	0.229918	0.158037	0.724003	0.286678	0.822307	3.363599
125	1.259836	0.679918	1.158037	0.723870	0.286140	0.822934	3.363423

11.5.3 Computational Cost

The presented algorithm was programmed using Visual C++ 6.0 in a Windows XP environment. The CPU of the computer is a Pentium IV with 2.4 GHz. If the convergence precision is given as $\varepsilon = 10^{-5}$, the time used for the 2D optimization computation with one set of initial values is about 145 seconds and the time used for the 3D optimization computation with one set of initial values is about 316 seconds.

11.6 Conclusions

The singularity-free workspace can be affected by several factors such as the prescribed point of interest P_0, the orientation of the platform as well as the geometric parameters. This chapter focuses on analyzing the effects of the geometric parameters on the "architecture-based maximal singularity-free workspace" in order to determine the optimal architecture for the MSSM Gough-Stewart platform. To this end, a point of interest P_0 is selected from the perpendicular line through the centroid C_b of the base. Moreover, the reference orientation is taken as the considered orientation because it is an impartial orientation. In this orientation, the singularity surface becomes a plane coinciding with the base plane. Hence, the analytic algorithm developed in Chapter 6 is used to determine the "architecture-based maximal singularity-free workspace", which makes the computation much faster than the general numerical algorithm presented in Chapter 5. For the MSSM with similar base and platform, the analysis results of the effects of geometric parameters on the "architecture-based maximal singularity-free workspace" as well as the 2D optimization show that the optimal architecture is: both the base and the platform are equilateral triangles and the size ratio between the platform and the base is $\frac{1}{2}$. However, if the platform is not similar to the base, the global optimal architecture is more difficult to determine. Only an approximate optimal architecture is available as shown in Fig. 11.12.

Chapter 12

Conclusions

12.1 Main Contributions

This thesis focuses on the singularity-free workspace analysis and geometric optimization of two typical parallel mechanisms. As a typical planar parallel mechanism, the planar 3-$R\underline{P}R$ parallel mechanism is addressed. As a typical spatial parallel mechanism, the Gough-Stewart platform is analyzed. The main contributions can be summarized as follows:

- A new method is presented to derive the singularity equation by separating the origin O' of the mobile frame from the considered point P and making O' coincide with a special point of the platform. As a result, the obtained singularity equations about a general point P of the platform is simplified, because it contains only a minimal set of geometric parameters.

- For the planar 3-$R\underline{P}R$ parallel mechanism, an algorithm is presented to determine the singularity-free workspace as well as the corresponding leg length ranges in a prescribed orientation. Besides, the optimal architecture which holds the maximal singularity-free workspace is determined.

- For the Gough-Stewart platform, this thesis focuses on the minimal simplified symmetric manipulator (MSSM) [5].

  - The six centres of the workspace spheres are proved to lie exactly on the singularity locus. This basic fact and the simplified singularity equation form the solid basis for the singularity-free workspace analysis as well as geometric optimization.

  - The definition of the workspace around a prescribed position in a given orientation is given first. Based on the relationship between the maximal singularity-free workspace and the singularity surface, a general numerical algorithm is developed to determine the maximal singularity-free workspace as well as the corresponding leg length ranges. For a given orientation with $\phi = \theta = 0^\circ$ and $\psi \neq \pm 90^\circ$, an analytic algorithm is developed.

  - To maximize the "orientation-based maximal singularity-free workspace", an approximate optimal orientation is determined.

  - In practice, a platform usually works in a range of orientations. Hence, two algorithms are presented to compute the maximal singularity-free total orientation workspace in a given set of orientations.

  - Using the *Roll–Pitch–Yaw* angles (ϕ, θ, ψ), the orientation workspace at a prescribed position can be defined by 12 workspace surfaces. A numerical approach is presented to evaluate and represent the orientation workspace for given leg length ranges.

  - Based on the relationship between the maximal singularity-free orientation workspace and the singularity surface, a numerical algorithm is presented to determine the maximal singularity-free orientation workspace as well as the corresponding leg length ranges.

  - The effect of the working position on the "position-based maximal singularity-free orientation workspace" is analyzed. An approximate optimal position is determined. Besides, two algorithms are presented to compute the maximal singularity-free orientation workspace over an interesting position region.

– Finally, an algorithm for optimizing the geometric parameters is developed to determine the optimal architecture for the MSSM Gough-Stewart platform to obtain the maximal singularity-free workspace around a position of interest in the reference orientation.

Although the algorithms presented in Chapter 5 to Chapter 10 are based on the MSSM Gough-Stewart platform, they can be applied to other types of Gough-Stewart platforms or other spatial parallel mechanisms.

12.2 Discussion and Future Work

Although the above contributions have been made to the analysis and optimization of the Gough-Stewart platform, the following points remaining for the future work are still challenging:

- The practical useful maximal singularity-free workspace:
  The maximal position or orientation singularity-free workspace determined in this thesis is one whose boundary just touches the singularity locus at some point(s). Obviously, a contact point represents a singular configuration. In theory, the points close to the contact point(s) represent nonsingular configurations. However, these theoretically nonsingular configurations are as perilous as singular configurations. To avoid this type of configurations, a general principle presented in Chapter 3 is that the practical leg length ranges can be chosen from the determined maximal leg length ranges. However, what is the optimal choice for obtaining the practical useful maximal singularity-free workspace?

  As mentioned in Chapter 1, when a direct kinematic singularity occurs, the platform gains instantaneous freedom. This means that the corresponding constraint vanishes. In other words, the corresponding force/torque in the passive joints which is needed to maintain the desired configuration vanishes or becomes very small. Hence, a proper index to maintain a configuration can be the minimal necessary force/torque. This index can be used to determine the practical useful maximal singularity-free workspace. To this end, a static force analysis will be necessary.

- The objective of the geometric optimization problem:
  In Chapter 11, the objective of the geometric optimization problem is to pursue the maximal singularity-free workspace around a point of interest P_0 in the reference orientation. In practice, probably there are other objectives. For instance, the objective can be to obtain the maximal singularity-free orientation workspace at a given point P_0. The above two objectives can also be combined to be one for the geometric optimization problem. Obviously, for different objectives, the obtained solutions will be different.

- The geometric optimization problem for other types of Gough-Stewart platforms:
  In theory, the optimization problem with multi-variables has been a challenging task. Although this thesis has addressed the geometric optimization problem of the MSSM Gough-Stewart platform, the geometric problem for other types of Gough-Stewart platform is left unaddressed.

- The six-dimensional maximal singularity-free workspace:
  A six-dimensional singularity-free hyper-sphere centred at a prescribed point in the six-dimensional space $xyz - \phi\theta\psi$ was determined in [95]. However, the corresponding leg length ranges were not determined. Actually, it is impossible to determine such corresponding leg length ranges to obtain a maximal singularity-free hyper-sphere, because the six-dimensional workspace for any given leg length ranges cannot be a hyper-sphere. Now the problem becomes: how to determine the maximal leg length ranges to obtain the six-dimensional maximal singularity-free workspace around a point of interest $P_0(x_0, x_0, x_0, \phi_0, \theta_0, \psi_0)$ in the six-dimensional space? To solve this problem, the following two points have to been considered: (1) How to define and compute the size of a six-dimensional workspace? (2) Which metric combination of the position workspace and the orientation workspace is used? The position workspace can be defined by different metrics, say, metre, centimetre, millimetre, etc. The orientation workspace can also be defined by numerous parameterization approaches [29]. Hence, there are many metric combinations between these two types of workspace. Of course, for different metric combinations, the obtained six-dimensional singularity-free workspace will be different.

Bibliography

[1] Tsai, L. W., 1999, *Robot Analysis: the Mechanics of Serial and Parallel Manipulators*, A Wiley-Interscience Publication.

[2] Gough, V. E., 1956–1957, "Contribution to Discussion to Papers on Research in Automobile Stability and Control and in Tyre Performance", *Proceedings of the Auto. Div. Instn mech. Engrs*, p.392, by Cornell staff.

[3] Stewart, D., 1965, "A Platform with Six Degrees of Freedom", *Proceedings of the Institution of Mechanical Engineers*, Vol.180, pp.371–378.

[4] Hunt, K. H., 1978, *Kinematic Geometry of Mechanisms*, Oxford, UK: Oxford University Press.

[5] Merlet, J.-P., 2002, *Parallel Robots*, Kluwer Academic Publishers, Dordrecht.

[6] Hunt, K. H., 1983, "Structural Kinematics of In-Parallel-Actuated Robot Arms", *ASME Journal of Mechanisms, Transmissions and Automation in Design*, Vol.105, No.4, pp.705–712.

[7] Gosselin, C., and Angeles, J., 1990, "Singularity Analysis of Closed-Loop Kinematic Chains", *IEEE Transactions on Robotics and Automation*, Vol.6, No.3, pp.281–290.

[8] Ma, O., and Angeles, J., 1991, "Architecture Singularities of Platform Manipulator", *IEEE Int. Conf. on Robotics and Automation*, Sacramento, California, USA, pp.1542–1547.

[9] Zlatanov, D., Fenton, R. G. and Benhabib, B., 1994, "Analysis of the Instantaneous Kinematics and Singular Configurations of Hybrid Chain Manipulators", *Proceedings of the 1994 ASME Design Technical Conferences*, Minneapolis, MN, DE, Vol.72, pp.467–476.

[10] Zlatanov, D., Fenton, R. G., and Behhabid, B., 1994, "Singularity Analysis of Mechanisms and Robots via a Velocity-Equation Model of the Instantaneous Kinematics", *Proceedings of the IEEE International conference on Robotics and Automation*, San Diego, CA, USA, pp.986–991.

[11] Park, F. C., and Kim, J. M., 1999, "Singularity Analysis of Closed Kinematic Chains", *ASME Journal of Mechanical Design*, Vol.121, No.1, pp.32–38.

[12] Zlatanov, D., Bonev, I. A., and Gosselin, C., 2002, "Constraint Singularities of Parallel mechanisms", *Proceedings of the 2002 IEEE International Conference on Robotics and Automation*, Washington, DC, USA, pp.496-502.

[13] Jiang, Q., and Gosselin, C., 2006, "The Maximal Singularity-Free Workspace of Planar 3-$R\underline{P}R$ Parallel Mechanisms", *Proceedings of IEEE ICMA 2006*, Luoyang, China, June 25-28.

[14] Jiang, Q., and Gosselin, C., 2007, "Computation of the Maximal Singularity-Free Workspace of the MSSM for a Given Orientation", *Proceedings of the ASME 2007 International Design Engineering Technical Conferences & Computers and Information in Engineering Conference*, September 4–7, Las Vegas, Nevada, USA.

[15] Merlet, J.-P., 1999, "Determination of 6D Workspace of Gough-Type Parallel Manipulator and Comparison between Different Geometries", *The International Journal of Robotics Research*, Vol.18, No.9, pp.902–916.

[16] Pernkopf, F., and Husty, M., 2006, "Workspace Analysis of Stewart-Gough-Type Parallel Manipulators", *Proceedings of the I MECH E Part C Journal of Mechanical Engineering Science*, Vol.220, No.7, pp.1019–1032.

[17] Jo, D. Y., and Haug, E. J., 1989, "Workspace Analysis of Closed Loop Mechanisms with Unilateral Constraints", *Proceedings of ASME Design Automation Conference*, September 17-20, Montréal, Canada.

[18] Gosselin, C., 1990, "Determination of the Workspace of 6-DOF Parallel Manipulators", *ASME Journal of Mechanical Design*, Vol.112, No.3, pp.331–336.

[19] Gosselin, C., Lavoie, E., and Toutant, P., 1992, "An Efficient Algorithm for the Graphical Representation of the Three-Dimensional workspace of Parallel Manipulators", *Proceedings of the 22nd ASME Mechanisms Conference*, Scottsdale, September 13–16, Vol.1, pp.323–332.

[20] Gosselin, C., Laverdière, S., and Côté, J., 1992, "SIMA: A Graphic Simulation for the CAD of Parallel Manipulators", *ASME Computers in Engineering*, Vol.1, pp.465–471.

[21] Masory, O., Wang, J., and Zhuang, H., 1993, "On the Accuracy of a Stewart Platform — Part II: Kinematic Calibration and Compensation", *Proceedings of the IEEE International Conference on Robotics and Automation*, May 2-6, Atlanta, GA, USA.

[22] Gosselin, C., and Jean, M., 1996, "Determination of the Workspace of Planar Parallel Manipulators with Joint Limits", *Robotics and Autonomous Systems*, Vol.17, pp.129–138.

[23] Merlet, J.-P., Gosselin, C., and Mouly, N., 1998, "Workspaces of Planar Parallel Manipulators", *Mechanism and Machine Theory*, Vol.33, pp.7–20.

[24] Liu, X.-J., Wang, J., and Gao, F., 2000, "Performance Atlases of the Workspace for Planar 3-DOF Parallel Manipulators", *Robotica*, Vol.18, pp.563–568.

[25] Bonev, I. A., and Gosselin, C., 2002, "A Geometric Algorithm for the Computation of the Constant-Orientation Workspace of 6-RUS Parallel Manipulators", *Proceedings of ASME 2002, Montreal, Canada, DETC2002/MECH-34257*.

[26] Pernkopf, F., and Husty, M., 2002, "Workspace Analysis of Stewart-Gough Manipulators Using Orientation Plots", *Proceedings of MUSME 2002, the International Symposium on Multibody Systems and Mechatronics*, Mexico City, September 12–14, Paper No. M33.

[27] Lee, S. H., Song, J. B., Choi, W. C., and Hong, D., 2002, "Workspace and Force-Moment Transmission of A Variable Arm Type Parallel Manipulator", *Proceedings of the 2002 IEEE International Conference on Robotics 8 Automation*, Washington, DC, pp.3666–3671.

[28] Yang, G. L., Ho, H. L., Lin, W., and Chen, I. M., 2004, "A Differential Geometry Approach for the Workspace Analysis of Spherical Parallel Manipulators", *11th World Congress in Mechanism and Machine Science*, Tianjin, China, 1-4 April, Vol.4, pp.2060-2065.

[29] Bonev, I. A., Zlatanov, D., and Gosselin, C., 2002, "Advantages of the Modified Euler Angles in the Design and Control of PKMs", *Proceeding of the 3rd Chemnitz Parallel Kinematics Seminar, Parallel Kinematic Machines International Conference*, Chemnitz, Germany, April 23–25, pp.171–187.98

[30] Spring, K. W., 1986, "Euler Parameters and the Use of Quaternion Algebra in the Manipulation of Finite Rotations: A Review", *Mechanism and Machine Theory*, Vol.21, No.5, pp.365–373.

[31] Chen, C.-Y, and Fu, L.-C, 1999, "5D Target Trajectory Detection via Intelligent Monocular Visual Tracking System in Real-Time with Air-Target Orientation Recognition", *Proceedings of the American Control Conference*, San Diego, California, June, pp.363–367.

[32] Rosborough, G., Baldwin, D., and Emery, W., 1994, "Precise AVHRR Image Navigation", *IEEE Transactions on Geoscience and Remote Sensing*, Vol.32, No. 3, pp.644–657.

[33] Martinez-de Dios, J. R., Arrue, B. C., Ollero, A., Merino, L., Gomez-Rodriguez, F., 2008, "Computer Vision Techniques for Forest Fire Perception", *Image and Vision Computing*, Vol. 26, pp.550–562.

[34] Kim, D., and Chung, W., 1999, "Analytic Singularity Equation and Analysis of Six-DOF Parallel Manipulators Using Local Structurization Method", *IEEE Transactions on Robotics and Automation*, Vol.15, No.4, pp.612–622.

[35] Romdhane, L., 1994, "Orientation Workspace of Fully Parallel Mechanisms", *European Journal of Mechanics (A/Solids)*, Vol.13, No.4, pp.541–553.

[36] Merlet, J.-P., 1995, "Determination of the Orientation Workspace of Parallel Manipulators", *Journal of Intelligent and Robotic Systems*, Vol.13, pp.143–160.

[37] Bonev, I. A., and Ryu, J., 2001, "A New Approach to Orientation Workspace Analysis of 6-DOF Parallel Manipulators", *Mechanism and Machine Theory*, Vol.36, pp.15–28.

[38] Yang, G., Lin, W., Mustafa, S. K., Chen, I. M., and Yeo, S. H., 2006, "Numerical Orientation Workspace Analysis with Different Parameterization Methods", *IEEE Conference on Robotics, Automation and Mechatronics*, Bangkok, Thailand.

[39] Nakamura, Y., and Hanafusa, H., 1986, "Inverse Kinematic Solutions with Singularity Robustness for Robot Manipulator Control", *Transactions of the ASME Journal of Dynamic systems, Measurement and Control*, Vol.168, pp.163–171.

[40] Wampler, C. W., 1986, "Manipulator Inverse Kinematic Solutions Based on Vector Formulations and Damped Least-Squares Methods", *IEEE Transactions on System, Man., Cybernetics*, Vol.SMC-16, No.1, pp.93–101.

[41] Fichter, E. F., 1986, "A Stewart Platform-Based Manipulator: General Theory and Practical Construction", *The International Journal of Robotics Research*, Vol.5, No.2, pp.157–182.

[42] Suginoto, K., 1987, "Kinematics and Dynamics Analysis of Parallel Manipulators by Means of Motor Algebra", *ASME Journal of Mechanisms, Transmissions and Automation in Design*, Vol.109, pp.3–7.

[43] Merlet, J.-P., 1988, 'Parallel Manipulators Part 2: Singular Configurations and Grassmann Geometry', Technical Report, INRIA, Sophia Antipolis, France.

[44] Merlet, J.-P., 1989, "Singular Configurations of Parallel Manipulators and Grassmann Geometry", *The International Journal of Robotics Research*, Vol.8, No.5, pp.45–56.

[45] Maciejewski, A. A., and Klein, C. A., 1989, "The Singular Value Decomposition: Computation and Applications to Robotics", *International Journal of Robotics Research*, Vol.8, No.6, pp.63–79.

[46] Shi, X., and Fenton, R. G., 1992, "Structural Instabilities of in Platform Type Parallel Manipulators due to Singular Configurations", *Proceedings of the 1992 ASME Design Technical Conferences*, Scottsdale, AZ, DE, Vol.45, pp.347–352.

[47] Sefrioui, J., and Gosselin, C., 1992, "Singularity Analysis and Representation of Planar Parallel Manipulators", *Journal of Robotics and Autonomous System*, Vol.10, pp.209–224.

[48] Collins, C. L., and Long, G. L., 1994, "Line Geometry and the Singularity Analysis of an In-parallel Hand Controller for Force-Reflected Teleoperation", *Proceedings of the 1994 ASME Design Technical Conferences*, Minneapolis, MN, DE, Vol.72, pp.361–369.

[49] Merlet, J.-P., 1994, "Trajectory Verification in the Workspace for Parallel Manipulator", *International Journal of Robotics Research*, Vol.13, No.4, pp.326–333.

[50] Sefrioui, J., and Gosselin, C., 1995, "On the Quadratic Nature of the Singularity Curves of Planar Three-Degree-of-Freedom Parallel Manipulators", *Mechanism and Machine Theory*, Vol.30, No.4, pp.533–551.

[51] Gosselin, C., and Wang, J., 1995, "Singularity Loci of Planar Parallel Manipulators", *Ninth World Congress on the Theory of Machines and Mechanisms*, Milano, Italy, 1982–1986.

[52] Daniali H.R.M., Zsombor-Murray P.J., and Angeles J., 1995, "Singularity Analysis of Planar Parallel Manipulators", *Mechanism and Machine Theory*, Vol.30, No.5, pp.665–678.

[53] Merlet, J.-P., 1997, "Determination of the Presence of Singularities in a Workspace Volume of a Parallel Manipulator", *Computational methods in mechanisms, STS. Konstantin and Elena Resort*, June 16–28, Varna, Bulgaria.

[54] Mayer St-Onge, B. and Gosselin, C., 1997, *Probleme Geometrique Direct et Lieux de Singularite des Manipulateurs Paralleles Plans a Trois Degrees de Liberte*, Research Report of Département de Génie Mécanique, Université Laval, Québec, Canada.

[55] Wang, J., and Gosselin, C., 1997, "Singularity Loci of Planar Parallel Manipulators with Revolute Actuators", *Robotics and Autonomous Systems*, Vol.21, pp.377–398.

[56] Basu, D., and Ghosal, A., 1997, "Singularity analysis of platform-type multi-loop spatial mechanisms", *Mechanism and Machine Theory*, Vol.32, No.3, pp.375–389.

[57] Karger, A., and Husty, M., 1997, "Singularities and Self-Motions of Stewart-Gough Platforms", *Proceedings of the NATO Advanced Study Institute on Computational Methods in Mechanisms*, Varna, Bulgaria, June 16–28, II, pp.279–288.

[58] Roschel, O., and Mick, S., 1998, "Characterization of Architecturally Shaky Platforms", *Advances in Robotic Kinematics: Analysis and Control*, Kluwer Academic Publishers, pp.465–474.

[59] Kong, X., 1998, "Generation of Singular 6-SPS Parallel Manipulators", *Proceedings of the 1998 ASME Design Engineering Technical Conferences*, Atlanta, GA, Sept.13–16, DETC98/MECH-5952.

[60] Innocenti, C., and Parenti-Castelli, V., 1998, "Singularity-Free Evolution from one Configuration to another in Serial and Fully-Parallel Manipulators", *ASME Journal of Mechanical Design*, Vol.120, No.1, pp.73–79.

[61] Karger, A., and Husty, M., 1998, "Architecture Singular Parallel Manipulators", *Advances in Robotic Kinematics: Analysis and Control*, Kluwer Academic Publishers, pp.445–454.

[62] Wang, J., and Gosselin C., 1998, "Kinematic Analysis and Singularity Loci of Spatial Four-Degree-of-Freedom Parallel Manipulators Using a Vector Formulation", *Journal of Mechanical Design*, Vol.120, pp.555–558.

[63] Dasgupta, B., and Mruthyunjaya, T. S., 1998, "Singularity-Free Path Planning for the Stewart Platform Manipulator", *Mechanism and Machine Theory*, Vol.33, No.6, pp.711–725.

[64] Collins, C. L., and McCarthy, J. M., 1998, "The Quartic Singularity Surfaces of Planar Platforms in the Clifford Algebra of the Projective Plane", *Mechanism and Machine Theory*, Vol.33, No.7, pp.931–944.

[65] Bhattacharya, S., Hatwal, H., and Ghosh, A., 1998, "Comparison of an Exact and an Approximate Method of Singularity Avoidance in Platform Type Parallel Manipulators", *Mechanism and Machine Theory*, Vol.33, No.7, pp.965–974.

[66] Hunt, K. H., and McAree, P. R., 1998, "The Octahedral Manipulator: Geometry and Mobility", *The International Journal of Robotics Research*, Vo.17, No.8, pp.868–885.

[67] McAree, P. R., and Daniel, R. W., 1999, "An Explanation of Never-Special Assembly Changing Motions for 3-3 Parallel Manipulators", *The International Journal of Robotics Research*, Vol.18, No.6, pp.556–574.

[68] Huang, Z., Zhao, Y., Wang, J., and Yu, J., 1999, "Kinematic Principle and Geometrical Condition of General-Linear-Complex Special Configuration of Parallel Manipulators", *Mechanism and Machine Theory*, Vol.34, No.8, pp.1171–1186.

[69] Mayer St-Onge, B., and Gosselin, C., 2000, "Singularity Analysis and Representation of the General Gough-Stewart Platform", *International Journal of Robotics Research*, Vol.19, No.3, pp.271–288.

[70] Ebert-Uphoff, I., Lee, J. K., and Lipkin, H., 2000, "Characteristic Tetrahedron of Wrench Singularities for Parallel Manipulators with Three Legs", *Proceedings of a Symposium Commemorating the Legacy, Works, and Life of Sir Robert Stawell Ball upon the 100th Anniversary of A Treatise on theory of Screws*, Cambridge, UK, July 9–11.

[71] Kong, X., and Gosselin, C., 2000, "Determination of the Uniqueness Domains of 3-*R*<u>*P*</u>*R* Planar Parallel Manipulators with Similar Platforms", *Proceedings of ASME 2000 Design Engineering Technical Conferences and Computers and Information in Engineering Conference*, Baltimore, Maryland, September 10-13.

[72] Karger, A., and Husty, M., 2000, "Self-Motions of Griffis-Duffy Type Parallel Manipulators", *Proceedings of the 2000 IEEE International Conference on Robotics and Automation*, San Francisco, CA, April 24–28, Vol.2, pp.7–12.

[73] Angeles, J., Yang, G., and Chen, I. M., 2001, "Singularity analysis of Three-legged, Six-DOF Platform Manipulators with RRRS Legs", *Proceedings of the 2001 IEEE/ASME International Conference on Advanced Intelligent Mechatronics*, Como, Italy, July 8–12, pp.32–36.

[74] Yang, G., Chen, I. M., Lin, W., and Angeles, J., 2001, "Singularity Analysis of Three Legged Parallel Robots Based on the Passive-Joint Velocities", *Proceedings of the 2001 IEEE International Conference on Robotics and Automation*, Seoul, Korea, May 21–26, pp.2407–2412.

[75] Bonev, I. A., and Gosselin, C., 2001, "Singularity Loci of Planar Parallel Manipulators with Revolute Joints", 2nd Workshop on Computational Kinematics, Seoul, Korea, pp.291–299.

[76] Bonev, I. A., Zlatanov, D., and Gosselin, C., 2003, "Singularity Analysis of 3-DOF Planar Parallel Mechanisms via Screw Theory", *Journal of Mechanical Design*, Vol.125, No.3, pp.537–581.

[77] Merlet, J.-P., and Daney, D., 2001, "A Formal-Numerical Approach to Determine the Presence of Singularity within the Workspace of A Parallel Robot", *Proceedings of the International Workshop on Computational Kinematics*, pp.167–176, Seoul, May 20-22.

[78] Di Gregorio, R., 2001, "Analytic Formulation of the 6-3 Fully-Parallel Manipulator's Singularity Determination", *Robotica*, Vol.19, No.6, pp.663–667.

[79] Di Gregorio, R., 2002, "Singularity-Locus Expression of A Class of Parallel Mechanisms", *Robotica*, Vol.20, No.3, pp.323–328.

[80] Wohlhart, K., 2002, "Synthesis of Architecturally Mobile Double-Planar Platforms", *Advances in Robot Kinematics – Theory and Applications*, Kluwer Academic Publishers, pp.473–483.

[81] Gosselin, C., and Wang, J., 2002, "Singularity Loci of a Special Class of Spherical Three-Degree-of-Freedom Parallel Mechanisms with Revolute Actuators", *The International Journal of Robotics Research*, Vol. 21, No. 7, pp.649–659.

[82] Dash, A. K., Chen, I. M., Yeo, S. H., and Yang G., 2003, "Singularity-Free Path Planning of Parallel Manipulators Using Clustering Algorithm and Line Geometry", ICRA-2003.

[83] Sen, S., Dasgupta, B., and Mallik, A. K., 2003, "Variational Approach for Singularity-Free Path-Planning of Parallel Manipulators", *Mechanism and Machine Theory*, Vol.38, No.11, pp.1165–1183.

[84] Huang, Z., Chen, L., Li, Y., 2003, "The Singularity Principle and Property of Stewart Parallel Manipulator", *Journal of Robotic Systems*, Vol.20, pp.163–176.

[85] Huang, Z., Cao, Y., 2005, "Property Identification of the Singularity Loci of a Class of Gough- Stewart Manipulators", *The International Journal of Robotics Research*, Vol.24, pp.675–685.

[86] Huang, Z., Cao, Y., Li, Y., and Chen, L., 2006, "Structure and Property of the Singularity Loci of the 3/6-Stewart-Gough Platform for General Orientations", *Robotica*, Vol.24, pp.75–84.

[87] Li, H., Gosselin, C., Richard, M., and Mayer-St-Onge, B., 2006, "Analytic Form of the Six-Dimensional Singularity Locus of the General Gough-Stewart Platform", *ASME Journal of Mechanical Design* , Vol.128, No.1, pp.279–287.

[88] Arsenault, M., and Boudreau, R., 2006, "Synthesis of Planar Parallel Mechanisms While Considering Workspace, Dexterity, Stiffness and Singularity Avoidance", *ASME Journal of Mechanical Design*, Vol.128, No.1, pp.69–78.

[89] Jiang, Q., and Gosselin, C., 2007, "Singularity Equations of Gough-Stewart Platforms Using A Minimal Set of Geometric Parameter", *Proceedings of the ASME 2007 International Design Engineering Technical Conferences & Computers and Information in Engineering Conference*, September 4–7, Las Vegas, Nevada, USA.

[90] Zein, M., Wenger, p., and Chablat, D., 2007, "Singular curves in the joint space and cusp points of 3-$R\underline{P}R$ parallel manipulators", *Robotica*, Vol.25, pp.717–724.

[91] Tsai, K. Y., and Kohli, D., 1993, "Trajectory Planning in Task Space for General Manipulators", *Journal of Mechanical Design*, Vol.115, pp.915–921.

[92] Gallant, M., and Boudreau, R., 2002, "The Synthesis of Planar Parallel Manipulators with Prismatic Joints for an Optimal, Singularity-Free Workspace", *Journal of Robotics Systems*, Vol.19, No.1, pp.13–24.

[93] Wenger, p., Chablat, D., and Zein, M., 2007, "Degeneracy study of the forward kinematics of planar 3-$R\underline{P}R$ parallel manipulators", *ASME journal of Mechanical Design*, Vol.129, No.12, pp.1265–1268.

[94] Li, H., Gosselin, C., and Richard, M., 2006, "Determination of maximal singularity-free zones in the workspace of planar three-degree-of-freedom parallel mechanisms", *Mechanism and Machine Theory*, Vol.41, No.10, pp.1157–1167.

[95] Li, H., Gosselin, C., and Richard, M., 2007, "Determination of the Maximal Singularity-Free Zones in the Six-Dimensional Workspace of The General Gough-Stewart Platform", *Mechanism and Machine Theory*, Vol.42, No.4, pp. 497–511.

[96] Gosselin, C., and Angeles, J., 1988, "The Optimum Kinematic Design of a Planar Three-Degree-of-Freedom Parallel Manipulator", *Journal of Mechanisms, Transmissions, and Automation in Design*, Vol.110, pp.35–41.

[97] Merlet, J.-P., 1996, "Direct Kinematics of Planar Parallel Manipulators", *Proceedings of the IEEE International Conference on Robotics and Automation*, April 22-28, pp.3744–3749.

[98] Gosselin, C., Sefrioui, J., and Richard, M., 1992, "Solutions Polynomiales au Probleme de la Cinematique Directe des Manipulateurs Paralleles Plans a Trois Degres de Liberte", *Mechanism and Machine Theory*, Vol.27, No.2, pp.107–119.

[99] Gosselin, C., Guillot, M., 1991, "The Synthesis of Manipulators With Prescribed Workspace", *ASME Journal of Mechanical Design*, Vol.113, pp.451–455.

[100] Hughes, P. C., 1986, *Spacecraft Attitude Dynamics*, New York: John Wiley.

[101] Press, W.H., Teukolsky, S.A., Vetterling, W.T., and Flannery, B.P., 1992, *Numerical Recipes in C: the Art of Scientific Computing*, Second Edition, Cambridge University Press, New York.

Appendix A

Procedure for Computing the Maximal Singularity-Free Workspace for a Given Orientation

The procedure for computing the maximal singularity-free workspace around a prescribed point for a given orientation is given in Fig.A.1. The big dashed rectangular frame represents the computation of the volume V of the singularity-free workspace for a given half height h. It contains two small dashed rectangular frames. The left one is for computing the upside part of the singularity-free workspace, V_1, and the right one is for computing the downside part of the singularity-free workspace, V_2. When h converges to its limit value h_{lim}, V reaches the maximum. Details are given as follows:

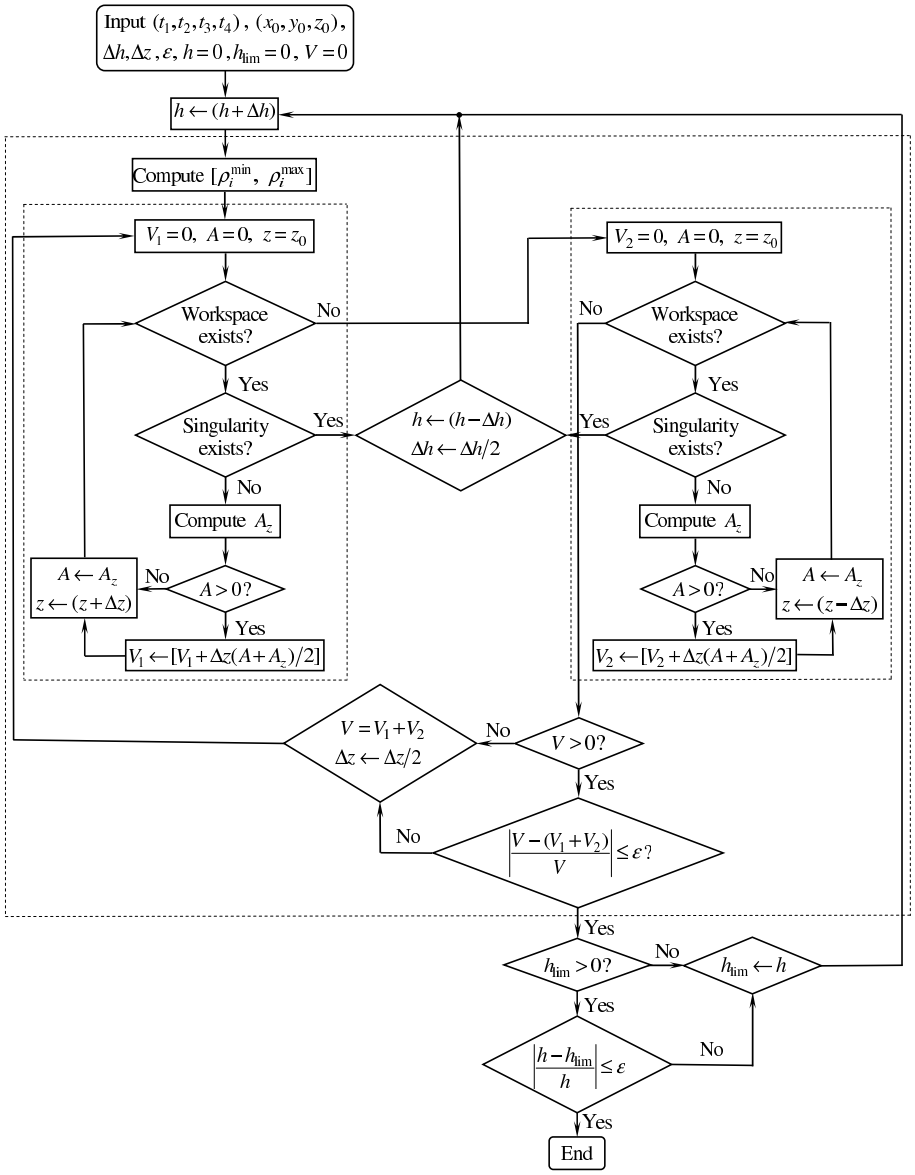

Figure A.1: Procedure for determining the maximal singularity-free workspace.

- Step 1: Input the geometric parameters (t_1, t_2, t_3, t_4), the coordinates (x_0, y_0, z_0) of the prescribed point P_0, the step sizes Δh (for determining h_{lim}) and Δz (for computing V), the convergence precision ε. Set the initial values of h, h_{lim} and V to 0.
- Step 2: Increase h by Δh and compute the leg length ranges $[\rho_i^{min}, \rho_i^{max}]$ $(i = 1, 2, ..., 6)$.
- Step 3: Compute V_1:
  - Step 3.1: Set the initial values of V_1 and A to 0. Here, A denotes the area

of the workspace section at $(z - \Delta z)$. Make z be z_0, which means that the computation starts from the workspace section at $z = z_0$.

- Step 3.2: Determine the workspace section at z using the approach mentioned in Section 5.4.3. If the workspace section does not exist, go to Step 4.
- Step 3.3: Perform singularity verification using the approach mentioned in Section 5.4.4. If a singularity exists inside the workspace section, restore the previous value of h and reduce the step size Δh by one half, then go to Step 2.
- Step 3.4: Compute the area A_z of the workspace section using Gauss divergence theorem [18, 22, 99].
- Step 3.5: If $A > 0$, increase the volume V_1 by $\Delta z(A + A_z)/2$.
- Step 3.6: Give the value of A_z to A and increase z by Δz. Then, go to Step 3.2.

- Step 4: Compute the downside part of the singularity-free workspace, V_2, using the similar procedure given in the right dashed rectangular frame.
- Step 5: If $V > 0$, verify the convergence condition. If V has already reached the desired precision, go to Step 7.
- Step 6: Put the sum of V_1 and V_2 in V. Then, reduce the step size Δz by one half in order to improve the precision and go to Step 3.
- Step 7: If $h_{lim} > 0$, verify the convergence condition. If the convergence condition is satisfied, output the results and end the computation.
- Step 8: Set the value of h to h_{lim} and go to Step 2.

The above procedure shows that the workspace is determined by the half height h. If there is no singularity inside the workspace, continue to increase h using the same step size Δh. Otherwise, restore h to its previous value. Then, reduce the step size Δh by one half and increase h by the new step size. Repeat this procedure until h converges to its limit value h_{lim}.

To guarantee no singularity inside the workspace determined by a given h, the distance Δz between two neighbouring sections should also be sufficiently small. And this is controlled by the convergence condition of the workspace volume V. In other words, the convergence condition for V serves two purposes: make the computed V to achieve the desired precision and guarantee a singularity-free workspace.

Appendix B

Results of Orientation Optimization

For the three-dimensional orientation optimization problem, it is difficult to obtain the global optimal solution, because different initial orientations may lead to different solutions. The computation results based on the 27 different initial orientations as shown in Fig.6.11 are listed in Table B.1.

Table B.1: The optimization results with different initial values (angles in radian).

No.	ϕ_0	θ_0	ψ_0	ϕ	θ	ψ	V_{max}
1	-0.5	-0.5	-0.5	0.001100	-0.001553	-1.565325	3.221893
2	-0.5	-0.5	0	-0.292509	0.499827	0.000000	3.254740
3	-0.5	-0.5	0.5	-0.244911	-0.355576	0.095224	3.412033
4	-0.5	0	-0.5	0.000087	0.000000	-1.568884	3.228725
5	-0.5	0	0	0.431116	0.021286	-0.060407	3.472872
6	-0.5	0	0.5	-0.000367	-0.000000	1.568884	3.228420
7	**-0.5**	**0.5**	**-0.5**	**-0.245146**	**0.348268**	**-0.119460**	**3.510794**
8	-0.5	0.5	0	-0.291883	0.500000	0.000000	3.247484
9	-0.5	0.5	0.5	0.001100	0.001553	1.565325	3.221893
10	0	-0.5	-0.5	0.000173	0.000087	-1.568884	3.228725
11	0	-0.5	0	-0.292595	0.500000	0.000000	3.254562
12	0	-0.5	0.5	1.115748	-0.279073	0.209670	2.174594
13	0	0	-0.5	0.000000	0.000000	1.570070	3.230303
14	0	0	0	0.442719	0.022472	-0.063686	3.456243
15	0	0	0.5	0.002958	-0.005025	1.552622	3.202606
16	0	0.5	-0.5	1.115748	0.279073	-0.209670	2.174594
17	0	0.5	0	-0.292595	0.500000	0.000000	3.254562
18	0	0.5	0.5	0.003839	0.006578	1.547597	3.193827
19	0.5	-0.5	-0.5	0.001100	-0.001553	-1.565325	3.221893
20	0.5	-0.5	0	-0.292509	0.499827	0.000000	3.254740
21	0.5	-0.5	0.5	0.000087	0.000820	1.570070	3.228422
22	0.5	0	-0.5	0.000087	0.000000	-1.568884	3.228725
23	0.5	0	0	0.431116	0.021286	-0.060407	3.472872
24	0.5	0	0.5	-0.000367	-0.000000	1.568884	3.228420
25	0.5	0.5	-0.5	1.067051	0.287991	-0.280311	2.097126
26	0.5	0.5	0	-0.292616	0.500000	-0.000041	3.254094
27	0.5	0.5	0.5	0.001273	0.002406	1.560753	3.216558

Appendix C

Procedure for Computing the Orientation Workspace with Given Leg Length Ranges

The volume V of the orientation workspace can be obtained by respectively computing the two parts of the orientation workspace with $\theta \leq 0$ and $\theta \geq 0$. Fig.C.1 shows the procedure for computing the volume V_1 of the orientation workspace with $\theta \leq 0$. Details are illustrated as follows:

- Step 1: Input the geometric parameters (t_1, t_2, t_3, t_4), the coordinates (x_0, y_0, z_0) of the prescribed position P_0 of the platform, the maximal and minimal leg lengths $(\rho_i^{max}, \rho_i^{min})$, the initial step sizes $(\Delta\theta, \Delta\phi)$ as well as the convergence precision ε.

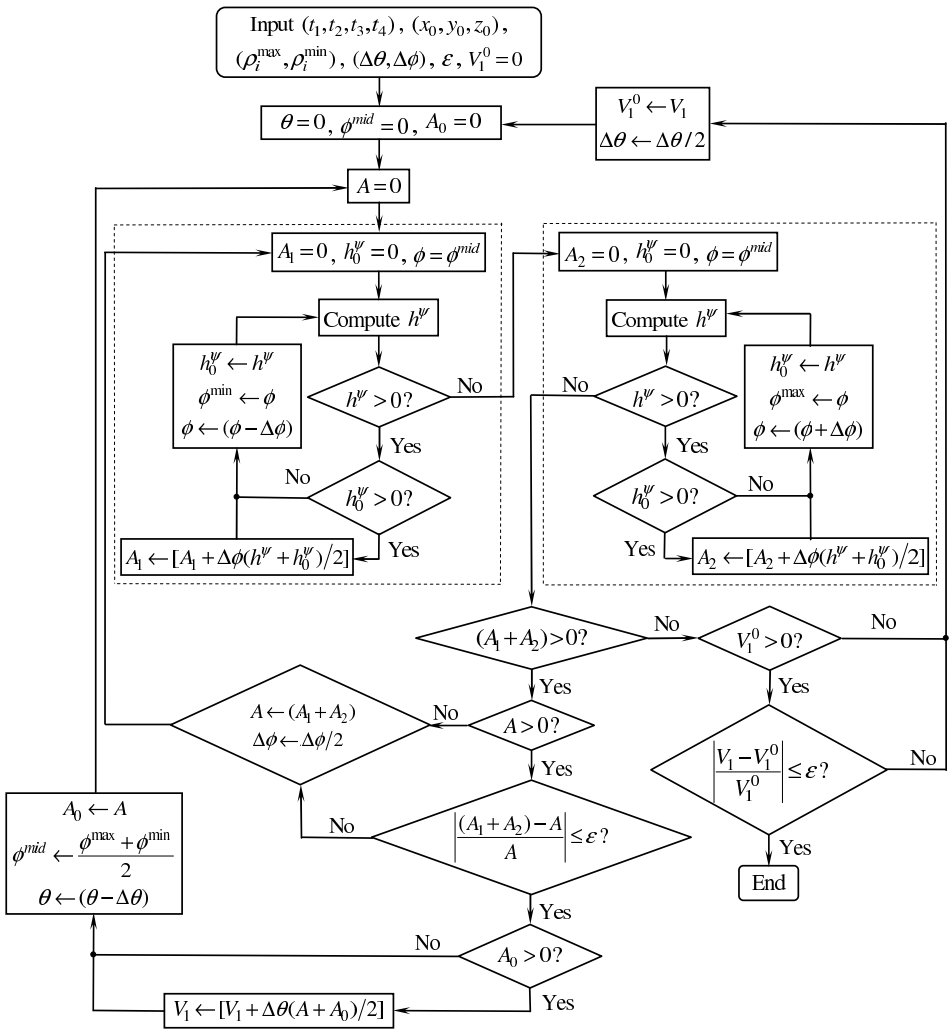

Figure C.1: Procedure for computing the volume V_1 of the orientation workspace with $\theta \leq 0$.

Set V_1^0 to 0. V_1^0 denotes the computed volume of the orientation workspace with $\theta \leq 0$ using a larger step size $\Delta\theta$.

- Step 2: Set the initial values of θ, ϕ^{mid}, A_0 and V_1 to 0. V_1 denotes the computed volume of the orientation workspace with $\theta \leq 0$ using a smaller step size $\Delta\theta$. This step means that the computation starts from the workspace section with $\theta = 0$.
- Step 3: Set A to 0.
- Step 4: Compute the area A_1 of the workspace section with $\phi \leq \phi^{mid}$. The computation procedure of A_1 is given by the left dashed rectangular frame in Fig.C.1, which can be described as follows:
  - Step 4.1: Set A_1 and h_0^{ψ} to 0. Let ϕ equal to ϕ^{mid}. This means the computation

starts from $\phi = \phi^{mid}$.

- Step 4.2: Compute h^{ψ} using the method described in Section 8.3.2. If $h^{\psi} > 0$, continue. Otherwise, go to Step 5.
- Step 4.3: If $h_0^{\psi} > 0$, increase A_1 by $\Delta\phi(h^{\psi} + h_0^{\psi})/2$.
- Step 4.4: Give the value of h^{ψ} to h_0^{ψ} and the value of ϕ to ϕ_{min}, which denotes the minimal valid ϕ in the considered workspace section. Then, reduce ϕ by one step $\Delta\phi$ and go to Step 4.2.

- Step 5: Compute the area A_2 of the workspace section with $\phi \geq \phi^{mid}$ in a similar procedure which is given by the right dashed rectangular frame in Fig.C.1.
- Step 6: If $(A_1 + A_2) > 0$, continue. Otherwise, go to Step 12.
- Step 7: If $A > 0$ (the area of the workspace section computed with a larger step size $\Delta\phi$), continue. Otherwise, go to Step 9.
- Step 8: Check the convergence condition. If A has already reached the desired precision, go to Step 10.
- Step 9: Put the sum of A_1 and A_2 to A, reduce the step size $\Delta\phi$ by one half in order to improve the precision and go to Step 4.1.
- Step 10: If $A_0 > 0$, increase V_1 by $\Delta\theta(A + A_0)/2$.
- Step 11: Give the value of A to A_0 and the result of $(\phi^{max} + \phi^{min})/2$ to ϕ^{mid}, reduce θ by one step $\Delta\theta$ and go to step 3.
- Step 12: If $V_1^0 > 0$, continue. Otherwise, go to Step 14.
- Step 13: Check the convergence condition. If V_1 has already reached the desired precision, output the results and end the computation.
- Step 14: Give the value of V_1 to V_1^0 and reduce the step size $\Delta\theta$ by one half in order to improve the precision. Then, go to Step 2.

Appendix D

Procedure for Computing the Maximal Singularity-Free Orientation Workspace at a Given Position

The procedure for determining the maximal singularity-free orientation workspace at a given position is shown in Fig.D.1. Details are illustrated as follows:

- Step 1: Input the geometric parameters (t_1, t_2, t_3, t_4), the coordinates (x_0, y_0, z_0) of the prescribed position P_0 of the platform, the initial step sizes $(\Delta D, \Delta\theta, \Delta\phi)$ as well as the convergence precision ε. Set D and D_{lim} to 0.

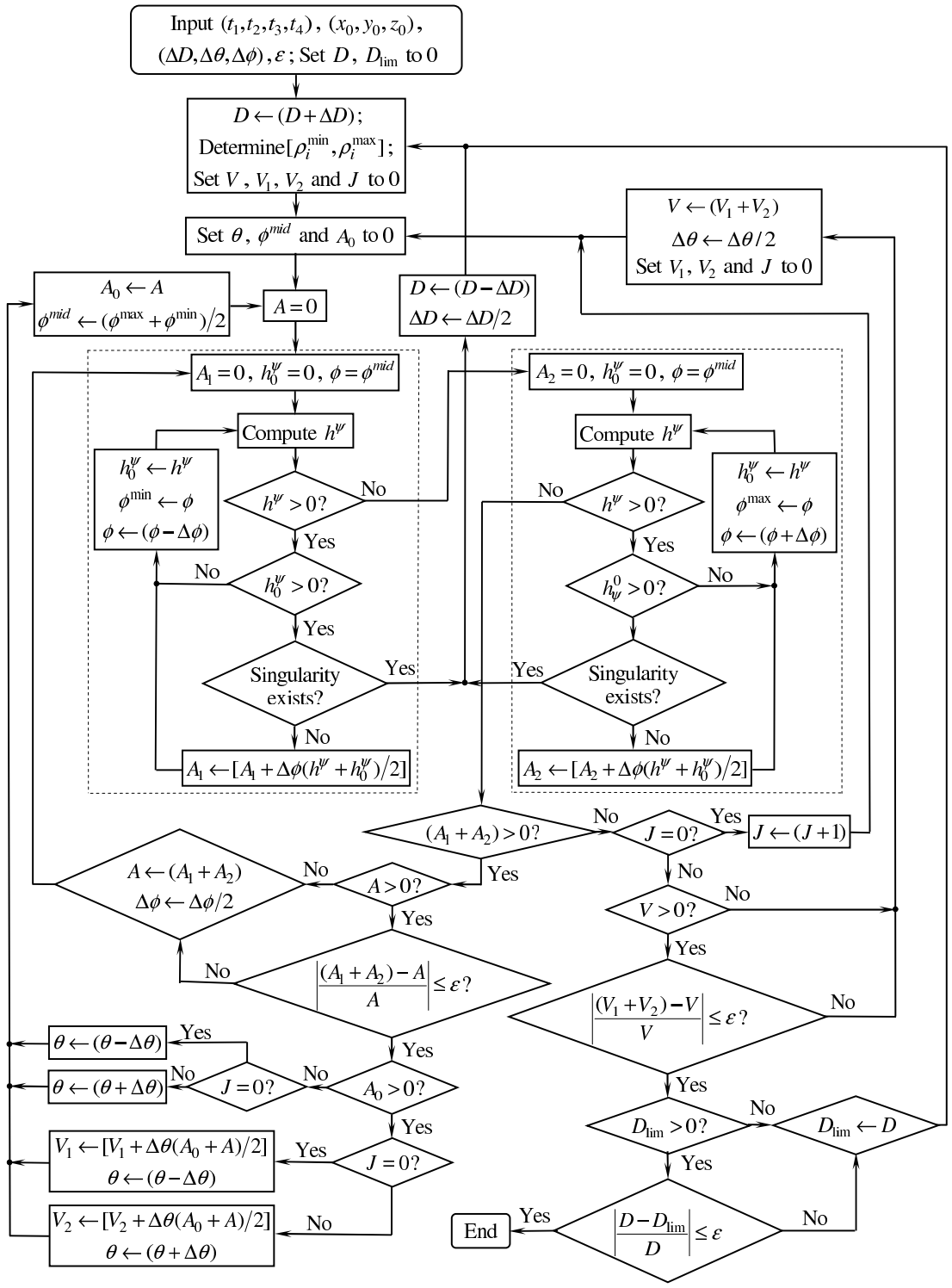

Figure D.1: Procedure for determining the maximal singularity-free orientation workspace.

- Step 2: Increase D by ΔD and compute the leg length ranges $[\rho_i^{min}, \rho_i^{max}]$ $(i = 1, 2, ..., 6)$. Set V, V_1, V_2 and J to 0. If $J = 0$, compute the volume V_1 of the orientation workspace with $\theta \leq 0$. Else if $J = 1$, compute the volume V_2 of the orientation workspace with $\theta \geq 0$.
- Step 3: Set θ, ϕ^{mid} and A_0 to 0. This means that the computation starts from the workspace section with $\theta = 0$.
- Step 4: Set A to 0.
- Step 5: Compute the area A_1 of the workspace section with $\phi \leq \phi^{mid}$. The computation procedure for A_1 is given by the left dashed rectangular frame in Fig.D.1, which can be described as follows:
  - Step 5.1: Set the initial values of A_1 and h_0^{ψ} to 0. Let ϕ equal to ϕ^{mid}. This means that the computation starts from $\phi = \phi^{mid}$.
  - Step 5.2: Compute h^{ψ} using the method described in Section 8.3.2. If $h^{\psi} > 0$, continue. Otherwise, go to Step 6.
  - Step 5.3: If $h_0^{\psi} > 0$, continue. Otherwise, go to Step 5.6
  - Step 5.4: Perform singularity verification using the approach mentioned in Section 9.2.3. If a singularity exists inside the workspace section, restore the previous value of D and reduce the step size ΔD by one half, then go to Step 2.
  - Step 5.5: Increase A_1 by $\Delta\phi(h^{\psi} + h_0^{\psi})/2$.
  - Step 5.6: Give the value of h^{ψ} to h_0^{ψ} and the value of ϕ to ϕ^{min}, which denotes the minimal valid ϕ in the considered workspace section. Then, reduce ϕ by one step $\Delta\phi$ and go to Step 5.2.
- Step 6: Compute the area A_2 of the workspace section with $\phi \geq \phi^{mid}$ using a similar procedure which is given by the right dashed rectangular frame in Fig.D.1.
- Step 7: If $(A_1 + A_2) > 0$, continue. Otherwise, go to Step 15.
- Step 8: If $A > 0$ (the area of the workspace section computed with a larger step size $\Delta\phi$), continue. Otherwise, go to Step 10.
- Step 9: Check the convergence condition. If A has already reached the desired precision, go to Step 11.
- Step 10: Put the sum of A_1 and A_2 to A, reduce the step size $\Delta\phi$ by one half in order to improve the precision and go to Step 5.1.
- Step 11: If $A_0 > 0$, continue. Otherwise, go to Step 13.

- Step 12: If $J = 0$, increase V_1 by $\Delta\theta(A + A_0)/2$ and reduce θ by one step $\Delta\theta$. Else, increase V_2 by $\Delta\theta(A + A_0)/2$ and increase θ by one step $\Delta\theta$. Then, go to Step 14.
- Step 13: If $J = 0$, reduce θ by one step $\Delta\theta$. Else, increase θ by one step $\Delta\theta$.
- Step 14: Set the value of A to A_0 and the result of $(\phi^{max} + \phi^{min})/2$ to ϕ^{mid}. Then, go to Step 4.
- Step 15: If $J = 0$, increase J by 1 and go to Step 3.
- Step 16: If $V > 0$ (the volume of the orientation workspace computed with a larger step size $\Delta\theta$), continue. Otherwise, go to Step 18.
- Step 17: Check the convergence condition. If V has already reached the desired precision, go to Step 19.
- Step 18: Put the sum of V_1 and V_2 to V, reduce the step size $\Delta\theta$ by one half in order to improve the precision and set V_1, V_2 and J to 0. Then, go to Step 3.
- Step 19: If $D_{lim} > 0$, continue. Otherwise, go to Step 21.
- Step 20: Check the convergence condition. If D has already reached its limit value D_{lim}, output the results and end the computation.
- Step 21: Put the value of D to D_{lim} and go to Step 2.